

---

Electronic Thesis and Dissertation Repository

---

4-19-2017 12:00 AM


## Functionalization of Peptide Nucleic Acids via post-synthetic click chemistry

Xiaoxiao Wang  
*The University of Western Ontario*

Supervisor  
Professor Robert H. E. Hudson  
*The University of Western Ontario*

Graduate Program in Chemistry  
A thesis submitted in partial fulfillment of the requirements for the degree in Doctor of Philosophy  
© Xiaoxiao Wang 2017

Follow this and additional works at: <https://ir.lib.uwo.ca/etd>

 Part of the [Amino Acids, Peptides, and Proteins Commons](#), [Nanomedicine Commons](#), [Nucleic Acids, Nucleotides, and Nucleosides Commons](#), and the [Organic Chemicals Commons](#)

---

### Recommended Citation

Wang, Xiaoxiao, "Functionalization of Peptide Nucleic Acids via post-synthetic click chemistry" (2017). *Electronic Thesis and Dissertation Repository*. 4478.  
<https://ir.lib.uwo.ca/etd/4478>

This Dissertation/Thesis is brought to you for free and open access by Scholarship@Western. It has been accepted for inclusion in Electronic Thesis and Dissertation Repository by an authorized administrator of Scholarship@Western. For more information, please contact [wlsadmin@uwo.ca](mailto:wlsadmin@uwo.ca).

## Abstract

Peptide Nucleic Acid (PNA) has shown great potential in molecular diagnostics, antisense/antigene therapy and nanotechnology. Like other synthetic nucleic acids and artificial analogues, PNA has been extensively modified to achieve better performance in these applications. To efficiently develop PNA probes for molecular diagnosis, this thesis is focused on versatile functionalization of PNA via post-synthetic click chemistry.

Chapter 2 presents the synthesis of quencher-free PNA molecular beacons (MBs) targeting a cystic fibrosis transmembrane conductance regulator (CFTR) sequence mutation. To avoid the tedious synthesis of functionalized PNA monomers for probe development, a simple approach to modify PNA oligomers by post-synthetic on-resin click chemistry was developed. Precursor PNA MBs were prepared by incorporation of an Fmoc azide monomer into the oligomer by automatic solid-phase peptide synthesis and subsequent derivatization with pyrene moieties by copper-catalyzed azide-alkyne cycloaddition (CuAAC) produced the functional MBs. Two pyrene-based quencher-free PNA molecular beacons, a stemless MB and one possessing a stem-loop structure, both targeting a portion of the cystic fibrosis gene, were successfully synthesized by this method. Fluorescence studies showed that the stem-loop MB exhibited better discrimination of changes in excimer/monomer ratios as compared to the stemless MB construct and showed promise as MB for detection of this CFTR mutation.

Chapter 3 reports the synthesis of PNA MBs targeting CFTR mutation via a “click-couple-click” method. Unlike the well-known synthetic procedure of conventional PNA MBs that requires different protection strategies on the sites where fluorophores and quenchers are attached, an on-resin “click-couple-click” approach that includes microwave-assisted on-

resin CuAAC of a quencher to PNA, coupling of an azide-containing PNA monomer and another on-resin CuAAC of a fluorophore without the need of protection. By using this method, various PNA MBs have been successfully synthesized and characterized.

Chapter 4 discloses the simultaneous, multiple conjugations of alkynyl-(Gd(III)-DOTA) to a PNA oligomer possessing azide residues in a single post-synthetic CuAAC reaction. The resulting probe, (Gd(III)-DOTA)<sub>4</sub>-PNA, has potential as a MRI contrast agent. Conceptually by binding to the target, poly(rA) tail of mRNA, Gd ions would be significantly loaded to a localized microenvironment, which may improve the enhancement of contrast in MR images. The *in vitro* MR characteristics of this probe is presented.

With the interest in the conjugation of gold nanoparticles (AuNPs) to PNA for the development of targeted contrast agents for CT imaging, preliminary studies have been carried out by conjugation of an oligopeptide to AuNPs. Chapter 5 introduces a new method combining an interfacial strain-promoted azide-alkyne cycloaddition and post assembly deprotection (SPAAC-PAD) for the well-defined functionalization of small, water-soluble gold nanoparticles with oligopeptides. This approach will enable the fabrication of gold nanoparticles with a high degree of complexity with biomolecules for a variety of applications in targeted cancer diagnosis and therapies.

### **Keywords**

Peptide Nucleic Acids, click chemistry, on-resin, molecular beacon, post-synthetic modification, magnetic resonance imaging, contrast agent, poly(rA) tail, gold nanoparticles, peptide.

## Co-Authorship Statement

**Chapter 1** was written by myself with input and final revision by my supervisor, Professor Robert Hudson.

**Chapter 2** has been published as a research paper. I performed all the experimental work and wrote the draft of the manuscript with final revision by my supervisor, Professor Hudson. The final submission was prepared by Professor Hudson.

**Chapter 3** is currently in preparation to be published. Ms. Christie Ettles synthesized the alkynyl reporters. I synthesized the azide PNA monomer. I prepared, functionalized and characterized all PNA oligomers.

**Chapter 4** is currently in preparation to be published. Dr. Mark Milne synthesized the Gd chelator. I prepared, functionalized and characterized the PNA oligomer. Dr. Francisco Martínez supervised by Professor Timothy J. Scholl performed NMRD studies and analyzed the profiles. I wrote the manuscript with input by Dr. Mark Milne and final revision by Professor Hudson.

**Chapter 5** has been published as a research paper. Dr. Pierangelo Gobbo supervised by Professor Mark Workentin, and I contributed equally to this work. I synthesized and characterized the peptides. Dr. Mojmir Suchy prepared the DBCO acid. Dr. Gobbo synthesized and characterized the azide-AuNPs. Dr. Gobbo and I performed peptide-AuNPs conjugation and characterization together. I wrote the manuscript with input by Dr. Gobbo and revision by Professor Workentin and Professor Hudson. The final submission was prepared by Professor Hudson.

## **Acknowledgements**

Foremost, I would like to express my sincere gratitude to my supervisor Professor Robert H. E. Hudson for his continuous guidance, support and inspiration during my Ph.D. pursuit. I appreciate all his contributions of time, ideas and funding to make my experience at Western productive, stimulating and joyful. His broad knowledge and enthusiasm of research on nucleic acids has been being contagious to me throughout the past five years and will deeply influence my future career. He is also willing to share his life experience in the areas beyond research to help me develop a capability on time and personal management.

I would like to thank Professor Elizabeth Gillies, Professor Ken Yeung, Professor Murray Junop and Professor Jean-Paul Desaulniers for taking time to read my thesis and providing with me helpful feedbacks.

All the past and present members of Hudson group have been immensely helpful to my study, research and personal life at Western. I would like to acknowledge Dr. Mojmír Suchý who was always ready to give good advice when I had hard time with my projects. I am especially thankful to Dr. Mark Milne for being a great workmate, collaborator and a great friend, Dr. Augusto Matarazzo for sticking it out in graduate school and sharing all ups and downs with me, as well as my fantastic collaborators, Professor Workentin and Dr. Pierangelo Gobbo for all coffee meetings and inspiring discussions. I would also like to thank André St. Amant for teaching me peptide synthesis, Dr. Melissa Lewis, Kirby Chicas, Christie Ettles, Kelly Firth, Adam Elmeriki and McKenry Charles and for great memories, Gyeongsu (David) Park, Atefeh Rouhi, Dr. Sung Ju Cho and Timothy John Martin-Chan for all your help and support.

Finally, I would like to thank my husband who is also my best friend, Jinqiang (James) Hou, for coming all the way from Australia to support me. As a scientist, he always gives me useful advice and inspires me. As a husband, he supported me with love and encouragement. I could not have made it without him by my side. I am also grateful to my lovely son, Nelson Hou, for curing my insomnia and bringing so much happiness and joy to our life.

## Table of Content

Abstract .....	ii
Co-Authorship Statement.....	iv
Acknowledgements.....	v
Table of Content .....	vii
List of Tables .....	xi
List of Figures .....	xii
List of Schemes.....	xxiv
List of Appendices .....	xxvii
List of Abbreviations and Symbols.....	xxviii
CHAPTER I: INTRODUCTION.....	1
1.1 Preface.....	1
1.2 Peptide Nucleic Acid.....	1
1.3 Synthesis of PNA .....	2
1.3.1 Fmoc-based SPPS.....	3
1.4 Chemical modification of the PNA.....	7
1.4.1 Nucleobase modifications in PNA .....	7
1.4.2 Modification of PNA on the backbone.....	9
1.4.3 Modification of PNA on the nucleobase-backbone linker .....	12
1.4.4 Post-synthetic modification of PNAs and click chemistry.....	13

1.5 Applications of PNA .....	19
1.5.1 PNA beacons and fluoroprobes .....	19
1.5.2 Single nucleotide polymorphisms (SNPs) detection using PNA .....	20
1.5.2 PNA and DNA for Fluorescence In Situ Hybridization .....	23
1.5.3 Antigene and antisense therapy .....	25
1.6 Overview .....	27
1.7 References .....	29
Chapter II: VERSATILE SYNTHESIS OF QUENCHER-FREE PNA MOLECULAR BEACONS VIA POST-SYNTHETIC CLICK CHEMISTRY FUNCTIONALIZATION .....	36
2.1 Introduction to PNA-based molecular beacons.....	36
2.2 Synthesis of QF-PNA beacons.....	39
2.3 Results and discussion.....	41
2.4 Conclusion.....	55
2.5 Experimental .....	56
2.6 Supplementary Information.....	61
2.7 References .....	66
CHAPTER III: SYNTHESIS OF CONVENTIONAL PNA MOLECULAR BEACONS VIA A CONVENIENT “CLICK-COUPLE-CLICK” APPROACH.....	70
3.1 Introduction to conventional PNA beacons .....	70



3.2 Results and discussion.....	78
3.3 Conclusion.....	87
3.4 Experimental .....	89
3.5 Supplementary information.....	94
3.6 References .....	108
CHAPTER IV: SYNTHESIS OF A (Gd(III)-DOTA) <sub>4</sub> -PNA CONJUGATE AS A	
CONTRAST AGENT FOR MR IMAGING .....	
	111
4.1 Introduction .....	111
4.2 Results and discussion.....	120
4.3 Conclusions .....	125
4.4 Experimental .....	126
4.5 Supplementary Information.....	129
4.6 References .....	134
CHAPTER V: BIOCONJUGATION OF OLIGOPEPTIDE TO GOLD	
NANOPARTICLES FOR CT IMAGING VIA STRAIN-PROMOTED AZIDE-	
ALKYNE CYCLOADDITION (SPAAC) .....	
	0
5.1 Introduction to gold nanoparticles and targeted CT imaging.....	0
5.2 Results and discussion.....	5
5.3 Conclusion.....	20
5.4 Experimental .....	21

5.5 Supplementary Information.....	25
5.6 References .....	36
CHAPTER VI CONCLUSION AND OUTLOOK .....	41
Appendices.....	44
Curriculum Vitae .....	57

## List of Tables

Table 2.1 Oligomers investigated in this study.....	43
Table 2.2 Thermal stabilities and switching ratios of duplexes.....	46
Table 2.3 ESI-MS data of PNA sequences in this study. ....	55
Table 3.1 Oligomers investigated in this study.....	80
Table 3.2 Thermal stabilities of duplexes. Conditions:1 $\mu$ M PNA and target in 100 mM NaCl, 10 mM NaH <sub>2</sub> PO <sub>4</sub> , 0.1 mM EDTA, pH 7, 25°C.....	81
Table 3.3 ESI-MS data of PNA sequences in this study. ....	90

## List of Figures

Figure 1.1 Chemical structures of double-stranded DNA and PNA.....	2
Figure 1.2 Standard Fmoc/Bhoc PNA monomers. ....	3
Figure 1.3 Automatic peptide synthesizer [Applied Biosystems ABI-433A]. ....	4
Figure 1.4 The composition of resin for SPPS. ....	6
Figure 1.5 Examples of resins for SPPS. ....	6
Figure 1.6 5-Modified pyrimidines. 5-BrU: 5-bromouracil; 5-IU: 5-iodouracil; 5-MeC: 5-methylcytosine; 5-PAU: 5-(propargyl alcohol)uracil; 1: 5-(p-methoxy-benzylthiopropargyl ether)uracil; 2: 5-(N-(4,5-dimethoxy-2-nitrobenzylpropargylcarbamate)uracil; 3: 5-(ferrocenylpropargylcarboxamide)uracil. ....	8
Figure 1.7 Analogues of thymine and cytosine. ....	9
Figure 1.8 Some examples of backbone modified PNA monomers. ....	10
Figure 1.9 Structures of conformationally rigid PNAs. ....	12
Figure 1.10 Sections of the chemical structures of deoxyribonucleic acids (DNAs), polyamide or peptide nucleic acids (PNAs), and (E)- and (Z)-olefinic polyamide nucleic acids (OPAs) (copyright 2000 John Wiley and Sons). ....	13

Figure 1.11 Clickable PNA monomers.....	15
Figure 1.12 Template-directed click-ligation of PNA-DNA, PNA-PNA (or peptide): (a) schematic structure and (b) chemical structure at ligation point. (copyright 2010 John Wiley and Sons).....	16
Figure 1.13 Illustration of site-specific attachment of fluorophores to the backbone of acpPNA via reductive alkylation and sequential reductive alkylation-click chemistry (copyright 2013 American Chemical Society). .....	18
Figure 1.14 Illustration of click reaction of C <sup>γ</sup> -azido PNA monomer with fluorophore and live cell imaging of the fluorescent oligomers (copyright 2014 American Chemical Society). .....	18
Figure 1.15 Schematic representation of molecular beacon (copyright 2006 Nature Publishing Group). .....	20
Figure 1.16 Design principle of FIT-probes. An intercalator fluorophore (F) serves as a base surrogate and is forced to intercalate adjacent to the expected mutation site. High fluorescence is only obtained upon formation of matched duplexes (copyright 2008 Elsevier). .....	21
Figure 1.17 Typical PNA hybridization results. (top left) Cells of <i>Vibrio fluvialis</i> ATCC 33810 hybridized with the universal probe BacUin (top right). Cells of <i>L. grayi</i> Li07 hybridized with the Listeria-specific probe Lis-16S-1 (bottom left). Cells of <i>L. monocytogenes</i> SLCC2755 hybridized with the <i>L. monocytogenes</i> -specific probe Lm-	

16S-2 (bottom right). Cells of <i>L. ivanovii</i> Li01 hybridized with the <i>L. ivanovii</i> -specific probe Liv-16S-5. (copyright 2012 Elsevier).....	24
Figure 1.18 Representation of antisense and antigene strategies. <sup>65</sup> (copyright 2002 Royal Society of Chemistry) .....	25
Figure 2.1 Schematic representation of pyrene-based QF-MB, which was dually labeled with pyrene at the 3'-and 5'-end of single-stranded oligonucleotides with a stem-loop structure. In the absence of target DNAs, the “closed” stem-loop conformation predominantly emits excimer fluorescence (green) whereas the MB undergoes a dynamic conformational change to emit monomer fluorescence (blue) upon hybridization with target DNAs <sup>21</sup> (copyright 2004 American Chemical Society). .....	39
Figure 2.2 Fluorescence spectra of a) MB1 and b) MB2 in the presence of matched DNA. Conditions: 2 $\mu$ M PNA and target in 100 mM NaCl, 10 mM NaH <sub>2</sub> PO <sub>4</sub> , 0.1 mM EDTA, pH 7, 25 °C. Excitation: $\lambda_{ex}$ = 345 nm. ....	48
Figure 2.3 Fluorescence images at individual strand concentration of 2 $\mu$ M under illumination at $\lambda$ =365 nm. a) Left, MB1; right, MB1 + matched DNA; b) Left, MB2; right, MB2 + matched DNA. ....	48
Figure 2.4 Fluorescence-melting spectra of PNA MB2 in the presence of DNA targets monitored at 475 nm. $\lambda_{ex}$ = 345 nm. ....	50

Figure 2.5 CD spectra of MB2 in the presence of DNA targets. Conditions: 2  $\mu$ M PNA and target strands in 100 mM NaCl, 10 mM NaH<sub>2</sub>PO<sub>4</sub>, 0.1 mM EDTA, pH 7, 25 °C..... 51

Figure 2.6 Time-dependent fluorescence readout of MB2 with addition of target DNA (relative emission intensity = the difference between monomer emission intensity at 397 nm and excimer emission intensity at 475 nm). Conditions: 2  $\mu$ M PNA and target in 100 mM NaCl, 10 mM NaH<sub>2</sub>PO<sub>4</sub>, 0.1 mM EDTA, pH 7, 25 °C.  $\lambda_{\text{ex}}$  = 345 nm. .... 52

Figure 2.7 The target-response curve of MB2 with the increase of target concentration (relative emission intensity = the difference between monomer emission intensity at 397 nm and excimer emission intensity at 475 nm). Conditions: 2  $\mu$ M PNA in 100 mM NaCl, 10 mM NaH<sub>2</sub>PO<sub>4</sub>, 0.1 mM EDTA, pH 7, 25 °C.  $\lambda_{\text{ex}}$  = 345 nm. Limit of detection (LOD) was calculated as 320 nM. .... 53

Figure 2.8 Top: PNA sequences used for the molecular beacons, MB1 and MB2, illustrating the placement of the pyrene monomer (X). N' = N-terminus, C' = C-terminus, K = L-lysine, target sequence underlined. Bottom: Conceptual representation of stemless and stem-loop PNA beacons and their response. .... 56

Figure 2.9 ESI-MS spectra of 1-Az; calculated mass for C<sub>188</sub>H<sub>245</sub>N<sub>82</sub>O<sub>56</sub>: 1137.7289 [M+4H]<sup>4+</sup> (top), 910.3847 [M+5H]<sup>5+</sup> (bottom). .... 61

Figure 2.10 ESI-MS spectra of MB1 calculated mass for C<sub>209</sub>H<sub>254</sub>N<sub>82</sub>O<sub>54</sub>: 1194.9991 [M+4H]<sup>4+</sup> (top), 956.2008 [M+5H]<sup>5+</sup> (bottom). .... 62

Figure 2.11 ESI-MS spectra of PNA 2-Az; calculated mass for C <sub>241</sub> H <sub>309</sub> N <sub>113</sub> O <sub>69</sub> : 1179.5729 [M+5H] <sup>5+</sup> (top), 983.1454 [M+6H] <sup>6+</sup> (bottom).....	63
Figure 2.12 ESI-MS spectra of MB2; calculated mass for C <sub>262</sub> H <sub>319</sub> N <sub>113</sub> O <sub>67</sub> : 1225.6352 [M+5H] <sup>5+</sup> (top), 1021.5307 [M+6H] <sup>6+</sup> (bottom). ....	64
Figure 2.13 ESI-MS spectra of PNA-Ir; calculated mass for C <sub>241</sub> H <sub>282</sub> Ir <sub>2</sub> N <sub>90</sub> O <sub>54</sub> : 1137.4338 [M+5H] <sup>5+</sup> (top), 948.0295 [M+6H] <sup>6+</sup> (bottom); .....	65
Figure 2.14 HPLC-UV absorption spectra of PNA sequences at 265 nm. (a) MB1; (b) MB2. ....	66
Figure 3.1 Structure and sequence of the first PNA-DNA molecular beacon (copyright 1998 Elsevier). ....	71
Figure 3.2 Comparison of A) DNA molecular beacons with B) stemless FIT- PNA beacons in the detection of complementary nucleic acids. In stemless FIT-PNA beacons, an intercalator dye such as thiazole orange (TO) serves as a base surrogate that signals stacking against matched base pairs by FRET to a near infrared dye such as NIR667. PNAs. (copyright 2008 John Wiley and Sons) .....	76
Figure 3.3 Fluorescence spectra of pyrene-1-Q. Conditions: 1 μM PNA and target in 100 mM NaCl, 10 mM NaH <sub>2</sub> PO <sub>4</sub> , 0.1 mM EDTA, pH 7, 25°C. λ <sub>ex</sub> (pyrene-1-Q) = 345 nm. 83	



Figure 3.4 Fluorescence spectra of acridone-1-Q. Conditions:1 $\mu\text{M}$ PNA and target in 100 mM NaCl, 10 mM $\text{NaH}_2\text{PO}_4$ , 0.1 mM EDTA, pH 7, 25°C. $\lambda_{\text{ex}}$ (acridone-1-Q) = 390 nm. ....	84
Figure 3.5 Fluorescence spectra of acridine-1-Q. Conditions:1 $\mu\text{M}$ PNA and target in 100 mM NaCl, 10 mM $\text{NaH}_2\text{PO}_4$ , 0.1 mM EDTA, pH 7, 25°C. $\lambda_{\text{ex}}$ (acridine-1-Q) = 395 nm. ....	84
Figure 3.6 Fluorescence spectra of Fluorescein-1-Q. Conditions:1 $\mu\text{M}$ PNA and target in 100 mM NaCl, 10 mM $\text{NaH}_2\text{PO}_4$ , 0.1 mM EDTA, pH 7, 25°C. $\lambda_{\text{ex}}$ (Fluorescein-1-Q) = 493 nm. ....	85
Figure 3.7 Fluorescence spectra of pyrene-2-Q. Conditions:1 $\mu\text{M}$ PNA and target in 100 mM NaCl, 10 mM $\text{NaH}_2\text{PO}_4$ ,0.1 mM EDTA, pH 7, 25°C. $\lambda_{\text{ex}}$ (pyrene-2-Q) = 345 nm. .	86
Figure 3.8 Fluorescence spectra of Fluorescein-2-Q. Conditions:1 $\mu\text{M}$ PNA and target in 100 mM NaCl, 10 mM $\text{NaH}_2\text{PO}_4$ ,0.1 mM EDTA, pH 7, 25°C. $\lambda_{\text{ex}}$ (Fluorescein-2-Q) = 493 nm. ....	87
Figure 3.9 Synthesis of conventional PNA beacons via “click-couple-click” .....	87
Figure 3.10 Unpublished structures of triazole linked DABCYL monomer, triazole-linked acridone monomer and triazole-linked acridine monomer (from left to right).....	91

Figure 3.11 ESI-MS spectra of Fmoc-1-Az calculated mass for C <sub>176</sub> H <sub>223</sub> N <sub>75</sub> O <sub>53</sub> :	
1413.4014 [M+3H] <sup>3+</sup> , 1060.3030 [M+4H] <sup>4+</sup> .....	94
Figure 3.12 ESI-MS spectra of Fmoc-1-Q calculated mass for C <sub>192</sub> H <sub>238</sub> N <sub>78</sub> O <sub>53</sub> : 898.3070	
[M+5H] <sup>5+</sup> , 748.7572 [M+6H] <sup>6+</sup> .....	95
Figure 3.13 ESI-MS spectra of Fmoc-Az-1-Q calculated mass for C <sub>198</sub> H <sub>247</sub> N <sub>83</sub> O <sub>55</sub> :	
1168.4243 [M+4H] <sup>4+</sup> , 934.9411 [M+5H] <sup>5+</sup> .....	96
Figure 3.14 ESI-MS spectra of pyrene-1-Q calculated mass for C <sub>203</sub> H <sub>249</sub> N <sub>83</sub> O <sub>54</sub> : 944.1554	
[M+5H] <sup>5+</sup> , 786.9641 [M+6H] <sup>6+</sup> .....	97
Figure 3.15 ESI-MS spectra of acridone-1-Q calculated mass for C <sub>201</sub> H <sub>252</sub> N <sub>84</sub> O <sub>55</sub> :	
1182.1942 [M+4H] <sup>4+</sup> , 945.9569 [M+5H] <sup>5+</sup> .....	98
Figure 3.16 ESI-MS spectra of acridine-1-Q calculated mass for C <sub>201</sub> H <sub>251</sub> N <sub>85</sub> O <sub>54</sub> :	
945.3568 [M+5H] <sup>5+</sup> , 787.9653 [M+6H] <sup>6+</sup> .....	99
Figure 3.17 ESI-MS spectra of Fluorescein-1-Q calculated mass for C <sub>209</sub> H <sub>254</sub> N <sub>84</sub> O <sub>60</sub> :	
981.5771 [M+5H] <sup>5+</sup> , 818.1489 [M+6H] <sup>6+</sup> .....	100
Figure 3.18 ESI-MS spectra of Fmoc-2-Az calculated mass for C <sub>230</sub> H <sub>290</sub> N <sub>102</sub> O <sub>69</sub> :	
932.2544 [M+6H] <sup>6+</sup> , 799.2192 [M+7H] <sup>7+</sup> .....	101
Figure 3.19 ESI-MS spectra of Fmoc-2-Q calculated mass for C <sub>246</sub> H <sub>305</sub> N <sub>105</sub> O <sub>69</sub> : 973.8069	
[M+6H] <sup>6+</sup> .....	102

Figure 3.20 ESI-MS spectra of Fmoc-Az-2-Q calculated mass for $C_{252}H_{314}N_{110}O_{71}$ : 1004.3353 [M+6H] <sup>6+</sup> , 861.0028 [M+7H] <sup>7+</sup> .....	103
Figure 3.21 ESI-MS spectra of pyrene-2-Q calculated mass for $C_{257}H_{316}N_{110}O_{70}$ : 1214.2150 [M+5H] <sup>5+</sup> , 1012.0138 [M+6H] <sup>6+</sup> , 867.5844 [M+7H] <sup>7+</sup> .....	104
Figure 3.22 ESI-MS spectra of Fluorescein-2-Q calculated mass for $C_{263}H_{321}N_{111}O_{76}$ : 1043.1987 [M+6H] <sup>6+</sup> , 894.3143 [M+7H] <sup>7+</sup> .....	105
Figure 3.23 HPLC-UV absorption spectrum of pyrene-1-Q at 265 nm. ....	106
Figure 3.24 HPLC-UV absorption spectrum of acridone-1-Q at 265 nm.....	106
Figure 3.25 HPLC-UV absorption spectrum of acridine-1-Q at 265 nm. ....	107
Figure 3.26 HPLC-UV absorption spectrum of Fluorescein-1-Q at 265 nm.....	107
Figure 3.27 HPLC-UV absorption spectrum of pyrene-2-Q at 265 nm. ....	108
Figure 3.28 HPLC-UV absorption spectrum of Fluorescein-2-Q at 265 nm.....	108
Figure 4.1 Some of the Gd(III)-based MRI contrast agents currently used in the clinical practice (copyright 2013 John Wiley and Sons).....	113
Figure 4.2 Examples of macromolecule-based Gd(III) contrast agents (copyright 2013 John Wiley and Sons). ....	115

Figure 4.3 Conceptual scheme of preparation and application of (Gd(III)-DOTA) <sub>4</sub> -PNA. .....	119
Figure 4.4 Job plot of dA <sub>10</sub> (4 μM/strand) and (Gd(III)-DOTA) <sub>4</sub> -PNA (4 μM/strand) mixtures in the molar ratios of 0:100, 10:90, 20:80, 30:70, 40:60, 50:50, 60:40, 70:30, 80:20, 90:10. Solution conditions: 100 mM NaCl, 10 mM NaH <sub>2</sub> PO <sub>4</sub> , 0.1 mM EDTA, pH 7, 25 °C.....	123
Figure 4.5 Longitudinal relaxivity (r <sub>1</sub> ) of [(Gd(III)-DOTA) <sub>4</sub> -PNA] <sub>2</sub> :Poly(rA) triplex and control linear (Gd(III)-DOTA) <sub>4</sub> -PNA with a constant 0.13 mM Gd(III) in 100 mM NaCl, 10 mM NaH <sub>2</sub> PO <sub>4</sub> , 0.1 mM EDTA, 6 M urea, pH 7, 25 °C.....	125
Figure 4.6 ESI-MS spectrum of PNA1 calculated mass for C <sub>79</sub> H <sub>104</sub> GdN <sub>25</sub> O <sub>24</sub> : 973.5574 [M+2H] <sup>2+</sup> . ....	130
Figure 4.7 ESI-MS spectrum of PNA2, calculated mass for C <sub>176</sub> H <sub>240</sub> N <sub>70</sub> O <sub>56</sub> : 1411.7679 [M+3H] <sup>3+</sup> , 1059.0779 [M+4H] <sup>4+</sup> . ....	130
Figure 4.8 ESI-MS spectrum of Fmoc(Gd(III)-DOTA) <sub>4</sub> -PNA, calculated mass for C <sub>252</sub> H <sub>352</sub> Gd <sub>4</sub> N <sub>90</sub> O <sub>84</sub> : 1324.0326 [M+5H] <sup>5+</sup> , 1103.5285 [M+6H] <sup>6+</sup> . ....	131
Figure 4.9 HPLC-UV absorption spectrum of purified (Gd(III)-DOTA) <sub>4</sub> -PNA (top) and ESI-MS spectrum of (Gd(III)-DOTA) <sub>4</sub> -PNA (bottom), calculated mass for C <sub>237</sub> H <sub>342</sub> Gd <sub>4</sub> N <sub>90</sub> O <sub>82</sub> : 914.2765 [[M+7H] <sup>7+</sup> , 711.3279 [M+9H] <sup>9+</sup> .....	132

Figure 4.10 First derivative UV melting plots of [(Gd(III)-DOTA) <sub>4</sub> -PNA] <sub>2</sub> :poly(rA) at 260 nm at a concentration of 2 μM. conditions: 100 mM NaCl, 10 mM NaH <sub>2</sub> PO <sub>4</sub> , 0.1 mM EDTA, 6 M urea, pH 7, 25 °C.....	133
Figure 4.11 NMRD profiles of (Gd(III)-DOTA) <sub>4</sub> -PNA at 25, 38, 60 and 80 °C. conditions: 100 mM NaCl, 10 mM NaH <sub>2</sub> PO <sub>4</sub> , 0.1 mM EDTA, 6 M urea, pH 7, 25 °C. ....	134
Figure 5.1 IR spectrum of azide AuNPs. ....	6
Figure 5.2 TGA of control Me-EG <sub>3</sub> -AuNP (solid line) and of N <sub>3</sub> -EG <sub>4</sub> -AuNP (dashed line). ....	7
Figure 5.3 HPLC-UV absorption analysis at 265 nm of DBCO amine.....	10
Figure 5.4 HPLC-UV absorption analysis at 265 nm of decomposition of DBCO after treatment with concentrated TFA. ....	11
Figure 5.5 IR spectrum of PG-RGD-AuNPs. ....	14
Figure 5.6 IR spectrum of RGD-AuNPs.....	14
Figure 5.7 Bioconjugation of AuNPs with RGD peptide via SPAAC-PAD, 1) acetonitrile, room temperature, 1 h; 2) 90% TFA/DCM, room temperature, overnight; and AuNP size distributions obtained from the corresponding TEM image of RGD-functionalized AuNPs via SPAAC-PAD.....	15

Figure 5.8 Oxidative degradation of RGD-AuNPs by iodine. Disulfide 1 was characterized by ESI-MS. Calculated 1364.5992 and found 1365.6084 [1+] m/z. ....	17
Figure 5.9 IR spectrum of CRGDK-AuNPs. ....	19
Figure 5.10 ESI-MS analysis of “DBCO”-RGD. Calculated mass 849.3657 [M+H] <sup>+</sup> and found mass 849.3472 [M+H] <sup>+</sup> . ....	25
Figure 5.11 ESI-MS analysis of DBCO-(PG)RGD. Calculated mass 1259.5784 [M+H] <sup>+</sup> and found mass 1260.5776 [M+H] <sup>+</sup> . ....	26
Figure 5.12 ESI-MS analysis of DBCO-(PG)CRGDK. Calculated mass 1659.7393 [M+H] <sup>+</sup> and found mass 1660.6294 [M+H] <sup>+</sup> . ....	26
Figure 5.13 ESI-MS analysis of disulfide 1 from re-oxidation of AuNP-RGD by iodine. Calculated mass is 1364.5992 and found mass is 1365.6084 [M+H] <sup>+</sup> for Disulfide 1. ....	27
Figure 5.14 ESI-MS analysis of disulfide 2A (top) and 2B (bottom) from re-oxidation of AuNP-CRGDK by iodine. Calculated mass is 1600.6645 and found mass 800.2318 [M+2H] <sup>2+</sup> for 2A. Calculated mass is 1242.5162 and found mass 621.6824 [M+2H] <sup>2+</sup> for 2B. ....	28
Figure 5.15 HPLC-UV absorption analysis at 265 nm of “DBCO”-RGD. ....	29
Figure 5.16 HPLC-UV absorption analysis at 265 nm of DBCO-(PG)RGD. ....	29
Figure 5.17 HPLC-UV absorption analysis at 265 nm of DBCO-(PG)CRGDK. ....	30

Figure 5.18 $^1\text{H}$ NMR spectra of azide AuNP recorded in acetonitrile- $\text{d}_3$ and referenced against residual acetonitrile (*).	30
Figure 5.19 TGA of control Me-EG $_3$ -AuNP (solid line) and of N $_3$ -EG $_4$ -AuNP (dashed line).	31
Figure 5.20 TEM image of azide AuNPs.	31
Figure 5.21 TEM image of RGD-AuNPs.	32
Figure 5.22 $^1\text{H}$ NMR (top) and ESI-MS (bottom) spectra of DBCO amine (found mass: 278.1120 [1+]). $^1\text{H}$ NMR Spectra were recorded in $\text{CDCl}_3$ .	33
Figure 5.23 $^1\text{H}$ NMR (top) and ESI-MS (bottom) spectra of isolated compound (found mass: 278.3239 [1+]). $^1\text{H}$ NMR Spectra were recorded in $\text{D}_2\text{O}/\text{ACN}-\text{d}_3$ (2:1).	34
Figure 5.24 $^1\text{H}$ NMR (top) and ESI-MS (bottom) spectra of isolated compound (found mass: 302.0555 [1+]) after treatment of DBCO amine with concentrated TFA. $^1\text{H}$ NMR Spectra were recorded in $\text{CDCl}_3$ .	35
Figure 5.25 IR spectrum of DBCO-PG-RGD.	36

## List of Schemes

Scheme 1.1 Fmoc-based PNA synthesis cycle. ....	4
Scheme 2.1 Synthesis of azide PNA monomer (1).....	41
Scheme 2.2 General synthesis of PNA MBs by on-resin CuAAC. a) 1-ethynylpyrene (20 equiv.), CuI (200 equiv.), DIPEA (300 equiv.), THF/pyridine (5:3, v/v); b) 1-ethynylpyrene (15 equiv.), CuSO <sub>4</sub> ·5H <sub>2</sub> O (30 equiv.), sodium ascorbate (120 equiv.), DMEDA (60 equiv.), isopropanol/DMSO/H <sub>2</sub> O (1:1:2, v/v/v); c) 20% piperidine/DMF followed by TFA/TES (95:5, v/v).....	44
Scheme 2.3 Synthesis of PNA-Ir via on-resin CuAAC. (i) Iridium complex (20 equiv.), CuI (200 equiv.), DIPEA (300 equiv.), THF/pyridine 5:3 (v/v) (ii) 20% piperidine/DMF followed by TFA/TES 95:5 (v/v).....	54
Scheme 3.1 Synthetic scheme of first PNA-based MB (copyright 1998 Elsevier). ....	72
Scheme 3.2 Solid-phase synthesis of doubly labeled PNA as probes (copyright 2000 John Wiley and Sons).....	73
Scheme 3.3 Synthesis of FIT probes using Thiazole Orange (TO) as a Fluorescent Base in PNAs. (copyright 2005 John Wiley and Sons).....	75
Scheme 3.4 General synthesis of conventional PNA beacons via “click-couple-click”. a) (E)-4-((4-ethynylphenyl)diazenyl)-N,N-dimethylaniline (7.5 equiv.), CuSO <sub>4</sub> ·5H <sub>2</sub> O (15	



equiv.), sodium ascorbate (60 equiv.), THPTA (30 equiv.), isopropanol/DMSO/H<sub>2</sub>O (1:1:2, v/v/v), microwave 80 °C, 5 min; b) i) Fmoc azide monomer (5 equiv.), DIPEA (10 equiv.), HBTU (5 equiv.), DMF, room temperature, 1.5 hours; ii) 20% piperidine/DMF; iii) Ac<sub>2</sub>O/pyridine/DMF (1:25:25, v/v/v) c) i) same as a except that fluorophore-containing alkynyl molecules were used instead of quencher; ii) TFA/TES (95:5, v/v).. 79

Scheme 4.1 Synthesis of (Gd(III)-DOTA)<sub>4</sub>-PNA by on-resin CuAAC. a) alkynyl-(Gd(III)-DOTA) (30 equiv.), CuSO<sub>4</sub>·5H<sub>2</sub>O (60 equiv.), sodium ascorbate (240 equiv.), DMEDA (120 equiv.), isopropanol/H<sub>2</sub>O(1:2, v/v), RT, overnight; b) TFA/TES (95:5, v/v). ..... 122

Scheme 4.2 Synthesis of Gd(III)-DOTA-PNA1 by on-resin CuAAC. a) alkynyl-(Gd(III)-DOTA) (7.5 equiv.), CuSO<sub>4</sub>·5H<sub>2</sub>O (15 equiv.), sodium ascorbate (30 equiv.), *N,N'*-dimethylethylenediamine (DMEDA) (15 equiv.), isopropanol/H<sub>2</sub>O (1:2, v/v), r.t.; b) TFA/TES (95:5, v/v). ..... 129

Scheme 5.1 Illustration of the attempted routes for the bioconjugation of azide-AuNPs with RGD peptide via SPAAC-PAD. (a) Use of an unprotected peptide (route 1) or use of a protected peptide (route 2), (b) and (c) molecular structures of “DBCO”-RGD and DBCO-(PG)RGD. Protecting groups (PG) are Pbf and tBu..... 8

Scheme 5.2 Synthesis of DBCO-RGD peptide..... 9

Scheme 5.3 Synthesis of DBCO-(PG)RGD peptide..... 13

Scheme 5.4 Synthesis of DBCO-(PG)CRGDK peptide. .... 18

Scheme 5.5 Oxidative decomposition of CRGDK-AuNPs by iodine. Disulfides 2A and 2B was characterized by ESI-MS. 2A calculated 1600.6645 and found 800.2318  $[M+2H]^{2+}$ . 2B calculated 1242.5162 and found 621.6824  $[M+2H]^{2+}$  ..... 20

## **List of Appendices**

Appendix I Copyright Clearance .....	44
--------------------------------------	----

## List of Abbreviations and Symbols

A	adenine
aeg	<i>N</i> -(2-aminoethyl)glycine
aq.	aqueous
AMCA	7-amino-4-methylcoumarion-3-acetic acid
AuNPs	gold nanoparticles
Az	azide
Bhoc	benzhydryloxycarbonyl
Boc	tert-butyloxycarbonyl
Bz	benzoyl
°C	degrees Celsius
C	cytosine
CA	contrast agent
Calc.	calculated
CD	circular dichroism
cDNA	complementary deoxyribonucleic acid
CF	cystic fibrosis
CT	computed tomography

CuAAC	copper(I)-catalyzed azide-alkyne cycloaddition
D	aspartic acid
DABCYL	4-[4-(dimethylamino)phenylazo] benzoic acid
DBCO	dibenzocyclooctyne
DBF	dibenzofulvene
DBU	1,8-diazabicyclo[5.4.0]undec-7ene
DCM	dichloromethane
DIPEA	diisopropylethylamine
DMEDA	<i>N, N'</i> -dimethylethylenediamine
DMF	<i>N,N</i> -dimethylformamide
DMSO	dimethyl sulfoxide
DNA	deoxyribonucleic acid
DOTA	1,4,7,10-tetraazacyclododecane-1,4,7,10-tetraacetic acid
DTPA	diethylenetriaminepentaacetic acid
EDANS	5-(2-aminoethylamino)1-naphthalene sulfonic acid
EDC	<i>N</i> -(3-dimethylaminopropyl)- <i>N</i> -ethylcarbodiimide hydrochloride
EDTA	ethylenediaminetetraacetic acid
ESI	electrospray ionization

equiv	equivalent
EtOH	ethanol
F	fluorophore
FISH	fluorescence <i>in situ</i> hybridization
Fmoc	9-fluorenylmethoxycarbonyl
FRET	Förster resonance energy transfer
FT-IR	Fourier transform infrared spectroscopy
g	grams
G	guanine
h	hours
HATU	2-(7-Aza-1H-benzotriazol-1-yl)- <i>N,N,N,N</i> - tetramethyluronium hexafluorophosphate
HBTU	<i>O</i> -benzotriazol-1-yl- <i>N,N,N,N</i> -tetramethyluronium hexafluorophosphate
HOBt	1-hydroxybenzotriazole
HPLC	high-performance liquid chromatography
HRMS	high-resolution mass spectrometry
HYCRON	hydroxycrotyl-oligoethylene glycol- <i>n</i> -alkanoyl
Hz	hertz

<i>i</i> -Pr	isopropyl
$\lambda$	wavelength
K	lysine
L	litre
LD <sub>50</sub>	lethal dose
LOD	limit of detection
Lys	lysine
$\mu$	micro
MB	molecular beacon
MeCN	acetonitrile
MeOH	methanol
min	minutes
MM	mismatched
mRNA	messenger ribonucleic acid
MRI	Magnetic Resonance Imaging
MS	mass spectrometry
MQ	Milli-Q
MW	molecular weight
MWCO	molecular weight cut-off

NHS	<i>N</i> -hydroxysulfosuccinimide
NMP	<i>N</i> -methyl-2-pyrrolidone
NMR	nuclear magnetic resonance
NMRD	nuclear magnetic relaxation dispersion
PAD	post-assembly deprotection
PCR	polymerase chain reaction
PEG	polyethylene glycol
PET	positron emission tomography
PG	protecting group
Ph	phenyl
PNA	peptide nucleic acid
ppm	parts per million
PS	polystyrene
Q	quencher
QF-MB	quencher-free molecular beacon
QY	quantum yield
R	arginine
RP-HPLC	reversed phase high performance liquid chromatography
RNA	ribonucleic acid
rt	room temperature
SE	succinimide ester
SPAAC	strain-promoted azide-alkyne cycloaddition
SPANC	strain-promoted alkyne-nitrone cycloaddition



SPECT	single photon emission tomography
SPPS	solid phase peptide synthesis
SNP	Single Nucleotide Polymorphism
SR	switching ratio
SS	single stranded
T	thymine
TEM	transmission electron microscopy
TES	triethylsilane
TFA	trifluoroacetic acid
TFMSA	trifluoromethanesulfonic acid
TGA	thermogravimetric analysis
THF	tetrahydrofuran
THPTA	tris(3-hydroxypropyltriazolylmethyl)amine
$T_m$	thermal melt transition temperature (melting temperature for a nucleic acid complex)
TO	thiazole orange
U	uracil
UV	ultraviolet
vis	visible
$\Phi$	quantum yield

# CHAPTER I: INTRODUCTION

## 1.1 Preface

The year 2016 witnessed the 25th anniversary of the disclosure of Peptide Nucleic Acid (PNA). Since the first publication in 1991, PNA has been intensively researched and extensively exploited due to its unique properties especially in regard to the high nucleic acid recognition specificity and affinity in binding to complementary sequences. Great advances in employing PNA for a wide variety of applications in the field of medical diagnostics, drug discovery, molecular biology and nanotechnology have been made.

## 1.2 Peptide Nucleic Acid

PNA, an artificial nucleic acid analogue in which the entire sugar phosphate backbone found in natural nucleic acids, has been replaced with *N*-(2-aminoethyl)glycine (aeg) units and was first described by Nielsen *et al.* in 1991 (Figure 1.1).<sup>1</sup> PNA was originally conceived as a sequence-specific binding reagent targeting the major groove of duplex DNA to form a triplex. The nucleobases (purines and pyrimidines) are joined to the backbone by methylene carbonyl linkages. The intramolecular distances and the identity of the nucleobases are like those in natural nucleic acid molecules. More importantly, specific hybridization occurs between PNA and DNA or RNA sequences obeying Watson-Crick base pairing rules. The neutral polyamide backbone of PNA leads to binding complementary nucleic acid strands with higher affinity whereas electrostatic repulsions occur between the negative phosphate groups on each strand of DNA. Additionally, PNA hybridizes to DNA or RNA sequences under low salt conditions while cations are needed

to counteract the inter-strand repulsion between two negatively charged natural nucleic acid strands which would hamper duplex formation. Although DNA may depurinate under acidic conditions, PNA is more stable across a wide range of temperatures and pH values.<sup>2</sup> It is also resistant to nucleases and proteases unlike natural nucleic acids.<sup>3</sup> All these unique properties have made PNA advantageous hybridization probes in various applications.

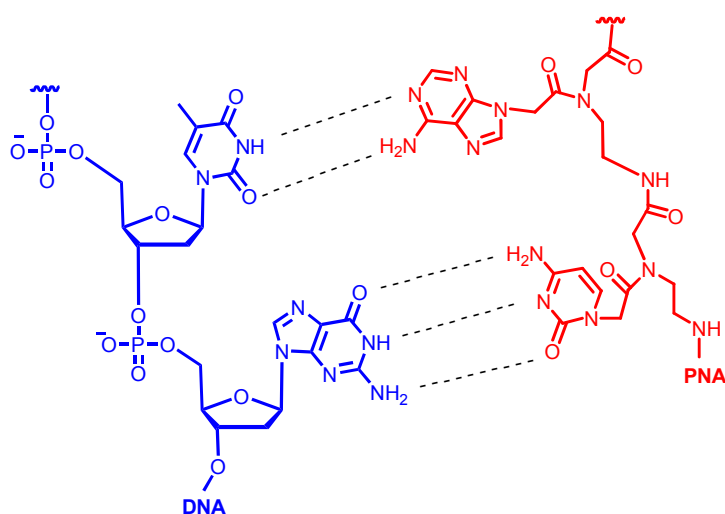


**Figure 1.1** Chemical structures of double-stranded DNA and PNA.

### 1.3 Synthesis of PNA

The preparation of PNA oligomers is based on standard solid phase peptide synthesis (SPPS) protocols developed by Merrifield,<sup>4</sup> after which two different protection schemes: *tert*-butyloxycarbonyl (Boc) and 9-fluorenylmethoxycarbonyl (Fmoc), have been employed. Although Boc chemistry of PNA has been well developed, the detracting qualities cannot be neglected such as the repeated use of extremely hazardous and corrosive TFA that effectively prevents non-chemists from accessing PNA and makes synthesis onerous. Alternatively, Fmoc-based PNA synthesis has milder deprotection/cleavage procedure allows for a wider range of labeled molecules to be prepared and provides for

simplified final cleavage and deprotection in shorter time. Therefore, Fmoc-based SPPS has become the most popular synthetic strategy of PNA synthesis.

### 1.3.1 Fmoc-based SPPS

To apply Fmoc-based SPPS, the protecting group on nucleobases not only needs to be compatible with Fmoc group, but also needs to be removed readily under cleavage conditions and render solubility to the resulting monomers. The benzhydryloxycarbonyl group (Bhoc) has been identified as an appropriate candidate. It allows the PNA monomers to be maintained at 0.2 M in NMP for weeks and it is completely removed in less than 1 minute in neat TFA, which is convenient for cleavage. Fmoc/Bhoc PNA monomers are commercially available (Figure 1.2).

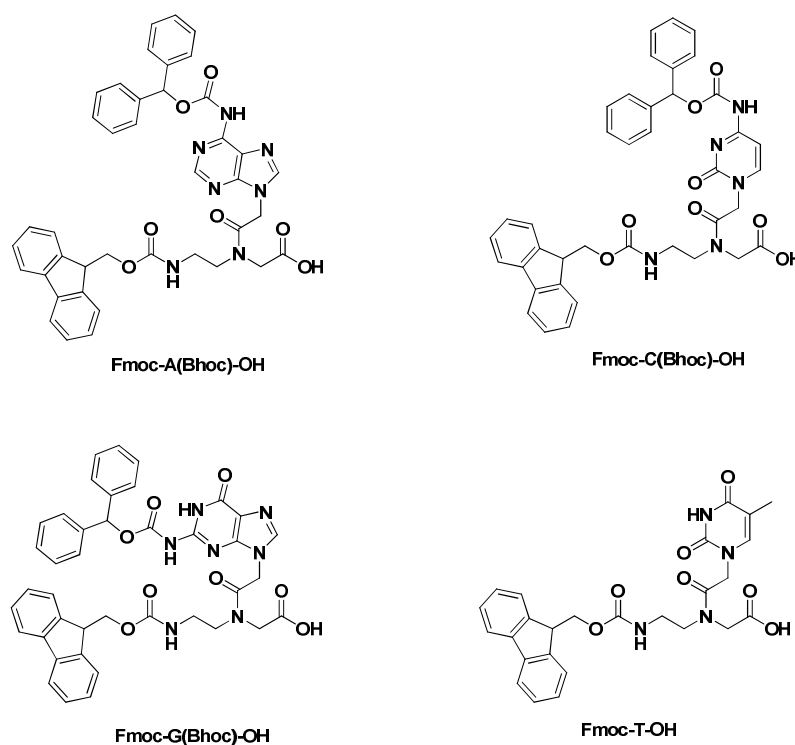
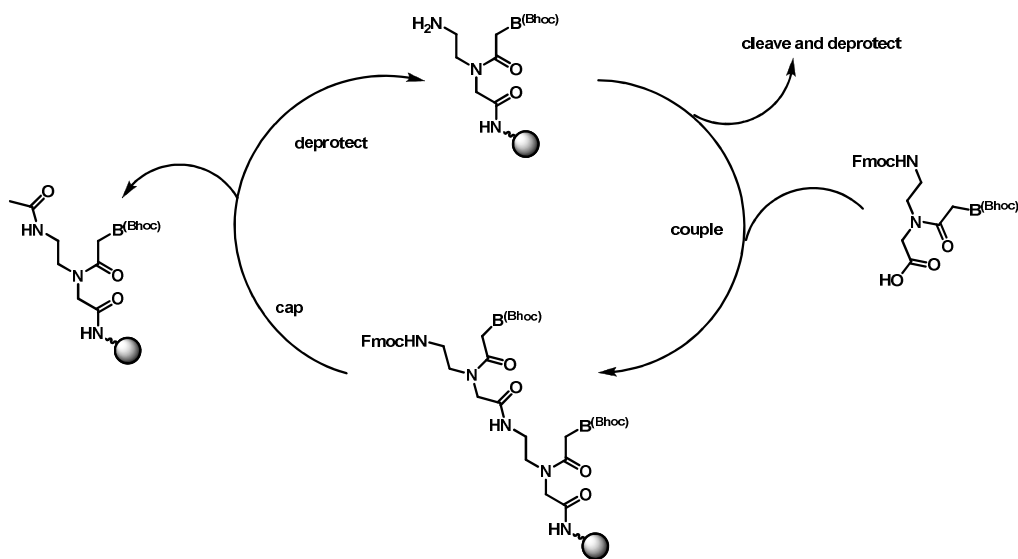


**Figure 1.2** Standard Fmoc/Bhoc PNA constructs for SPPS.

Fmoc-based SPPS consists of repetitive cycles of deprotection, activation-coupling, capping as well as cleavage and deprotection (Scheme 1.1). Fmoc-based SPPS of PNA is usually performed on a peptide synthesizer such as Applied Biosystems ABI-433A (Figure 1.3).



**Scheme 1.1** Fmoc-based PNA synthesis cycle.



**Figure 1.3** Automatic peptide synthesizer [Applied Biosystems ABI-433A].

The deprotection step of PNA synthesis represents the removal of Fmoc group from the primary amine of the PNA backbone. It liberates the amine for subsequent coupling of monomers. Generally, a solution of 20% piperidine in DMF is used for this purpose to decompose Fmoc group to dibenzofulvene (DBF).

In the coupling step, monomer, base and activator are all required. A solution containing 0.2 M DIPEA and 0.3 M lutidine has been used which proved more effective than 0.5 M of either base alone in terms of observed side reactions and coupling yields.<sup>5</sup> *O*-(Benzotriazol-1-yl)-1,1,3,3-tetramethyluronium hexafluorophosphate (HBTU) or 1-[bis(dimethylamino)methylene]-1H-1,2,3-triazolo[4,5-b]pyridinium 3-oxid hexafluorophosphate (HATU) are preferred as the activator for the coupling reaction. The step of combining solutions of monomer, base as well as activator followed by activation before exposure to the solid support is challenging on oligonucleotide synthesis platforms. Therefore, peptide synthesizer which has the same procedure is generally ideal for PNA synthesis.

The acetylation of oligomer that failed to extend is performed post coupling during each cycle of the stepwise synthesis. Capping simplifies the purification of the full length PNA which is highly recommended but not strictly necessary. Capping solution containing 5% acetic anhydride and 6% lutidine in DMF has been demonstrated a longer shelf life (months to years) than acetic anhydride and bases such as DIPEA or pyridine in DMF.

PNA may be deprotected and cleaved from the solid support simultaneously by treatment with TFA/TES (95/5). The use of a scavenger is necessary because the electron rich aromatic rings of the nucleobases will be alkylated by cations generated by the TFA treatment. The removal of Bhoc protection is complete within 1 minute, releasing the

exocyclic amines of the nucleobases and producing benzhydryl cations, which would be effectively scavenged by TES. PNA is also cleaved from the solid support with TFA treatment at the same time and the resulting oligomer is isolated from cleavage mixture by precipitation with diethyl ether.

Resins for SPPS can generally be used for PNA synthesis. The resin consists of three parts: base material, linker and anchoring group (Figure 1.4). Various types of resins have been widely employed depending on base materials: the classic polystyrene (PS) resins, polyamine resins and TentaGel™ resins which contain polyethylene glycol (PEG) attached to PS.

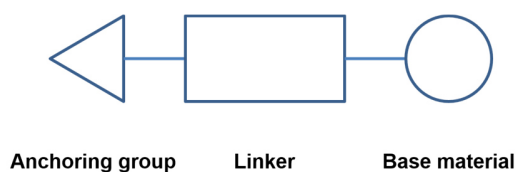


**Figure 1.4** The composition of resin for SPPS.

Most of the resins are commercially available attached with a variety of different linkers. Examples of resins with linkers and anchoring groups for SPPS have been shown in Figure 1.5 including Merrifield resin and Wang resin for synthesis of peptide acids, 2-chlorotrityl chloride resin for synthesis of protected peptide acid, rink amide resin for synthesis of peptide amide.

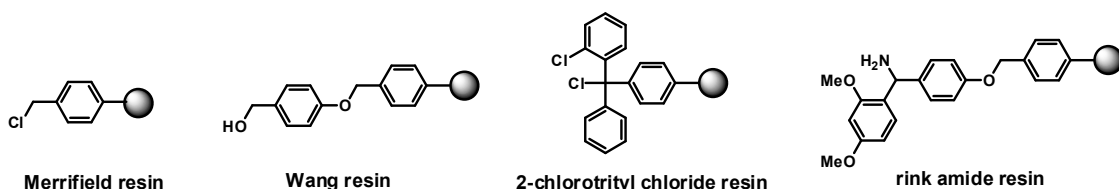


**Figure 1.5** Examples of resins for SPPS.

Different protocols are required to preload the first monomer to the resins depending on the anchoring groups. PNA synthesis is optimally performed on resins loaded below 0.2 mmol/g, because PNA quality would be compromised at higher loading due to aggregation of the extending oligomer during synthesis. Therefore, it is usually necessary to download the resin before PNA synthesis.

## **1.4 Chemical modification of the PNA**

### **1.4.1 Nucleobases modifications in PNA**

The formation of stable duplex and triplex structures is of great significance in most applications of PNA. In this context, the modification of nucleobase of PNA monomer is an effective way to control recognition between nucleic acids strands. Nucleobase modification of PNA has been comprehensively reviewed by Hudson and coworkers.<sup>6</sup> For example, 5-bromouracil (5-<sup>Br</sup>U) and 5-methylcytosine (5-<sup>Me</sup>C) have been found to increase the stability of both double and triple helices in DNA (Figure 1.6). Furthermore, a common method for the derivatization of pyrimidine bases, especially uracil, is to take advantage of transition metal-catalyzed cross-coupling between the halogenated nucleobase and terminal alkynes using the Castro-Stephens/Sonogashira reaction. Various alkynes could be used to introduce tethered functional groups. The synthesis of a variety of 5-alkynyluracil monomers that are compatible with Boc-based oligomerization chemistry has been developed. (Figure 1.6)<sup>7</sup> However, the incorporation of the 5-alkynyl group only produced very modest stabilization, as all PNA-DNA chimeras formed complexes of lower stability than the control DNA:DNA duplex.



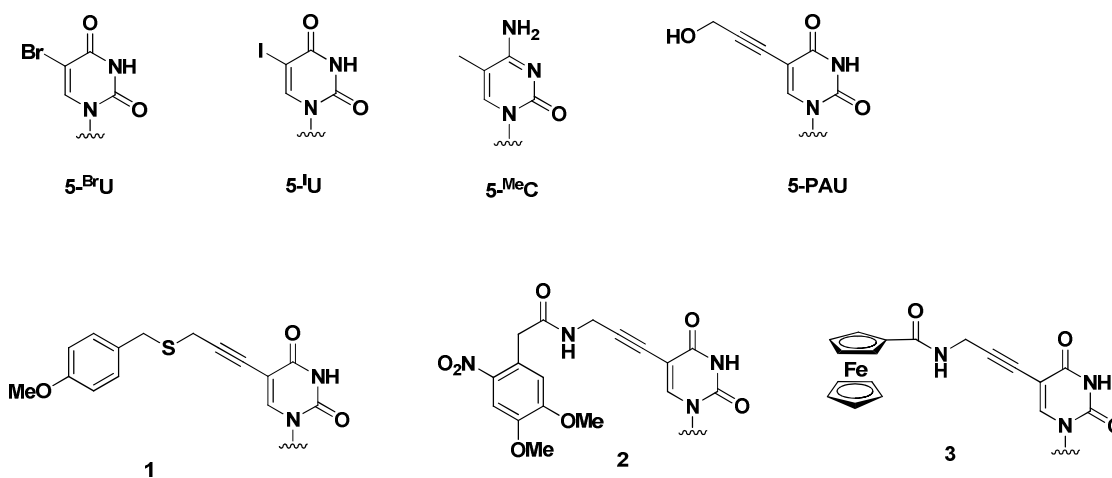


**Figure 1.6** 5-Modified pyrimidines. 5-<sup>Br</sup>U: 5-bromouracil; 5-<sup>I</sup>U: 5-iodouracil; 5-<sup>Me</sup>C: 5-methylcytosine; 5-PAU: 5-(propargyl alcohol)uracil; 1: 5-(p-methoxybenzylthiopropargyl ether)uracil; 2: 5-(N-(4,5-dimethoxy-2-nitrobenzyl)propargylcarbamate)uracil; 3: 5-(ferrocenylpropargylcarboxamide)uracil.

To enhance the stability of complexes formed by PNA and target DNA/RNA, nucleobases with a larger  $\pi$ -surface area for stronger stacking interactions or that are able to make additional H-bonds or that are positively charged have been prepared (Figure 1.7). A series of bicyclic thymine analogs (**bT**) based on the 1,8-naphthyridin-2-(1*H*)-one ring system has been prepared and evaluated by Nielsen and coworkers (Figure 1.7).<sup>8,9</sup> The best performance in terms of stabilization of duplexes and triplexes was 7-chloro-1,8-naphthyridin-2(1*H*)-one (**7-Cl-bT**). Tricyclic analogs of cytosine have shown better performance in oligonucleotide chemistry. A tricyclic cytosine analog (**tC**) has been reported by Nielsen and coworkers which performs well to be stabilizing in duplex-forming sequences, especially in contiguous positions or adjacent to purines. The phenoxazine cytosine analog was used to scaffold a tethered amine that could provide an additional H-bond to its complement. However, it was found to give no or minor stabilization depending

on the target. The G-clamp was prepared in order to build in specific, additional bonding interactions. The G-clamp and propyl-G-clamp led to stabilization while maintaining excellent sequence discrimination.<sup>10</sup> Fmoc/Cbz-protected monomers of the G-clamp and guanidine G-clamp derivatives have been developed.<sup>11</sup> Additionally, Nielson and coworkers have attempted to retain the benzoyl group (Bz) on the exocyclic amine of cytosine. The monomer,  $N^4$ -benzoylcytosine ( $C^{Bz}$ ) is compatible with Boc-oligomerization chemistry. The incorporation of  $C^{Bz}$  into poly-pyrimidine PNA sequences would normally strongly favor triplex formation.

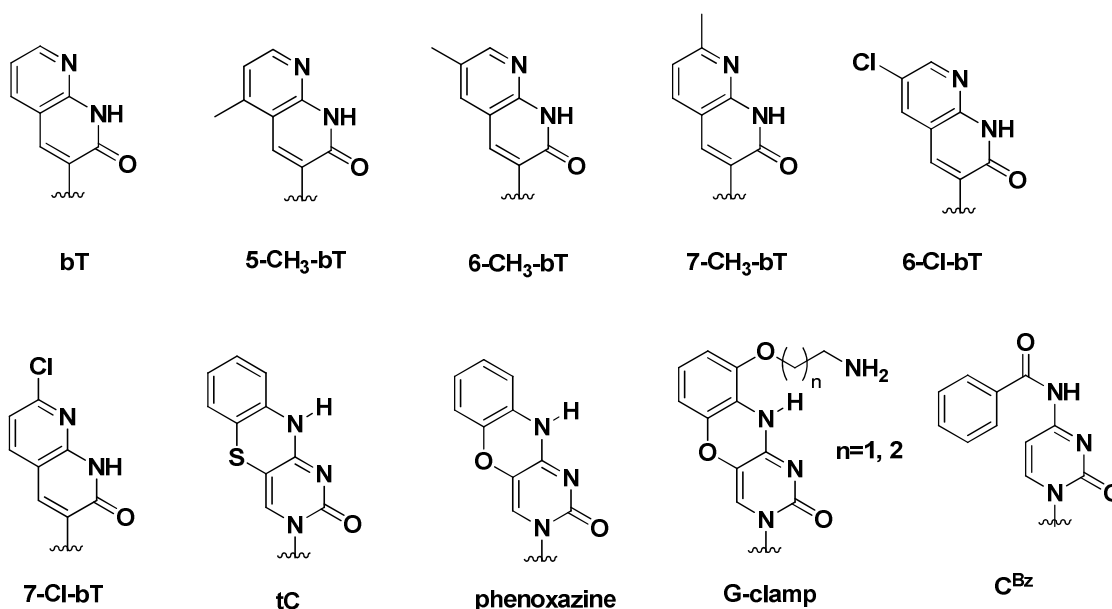


**Figure 1.7** Analogues of thymine and cytosine.

#### 1.4.2 Modification of PNA on the backbone

PNA analogues with a modified backbone have also drawn scientists' attention. The repeating backbone unit has been extended with a methylene group to either *N*-(2-aminoethyl)-alanine or *N*-(3-aminopropyl)glycine or propanoic acid unit with the ethylene carbonyl linker (**4**, **5**, Figure 1.8).<sup>12</sup> However, minor importance for the stability of PNA

has been observed when an extra methylene group is placed in the backbone. Hyrup *et. al.* reported a more flexible backbone containing a secondary amine replacing the secondary amide (PANA) (**6**, Figure 1.8).<sup>13</sup> After coupling of the nucleobase, the double bond of secondary amide is oxidised to aldehyde. The PANA oligomer is then obtained on solid-phase by reductive amination. Surprisingly, the incorporation of one PANA monomer does not destabilize the duplex, either.

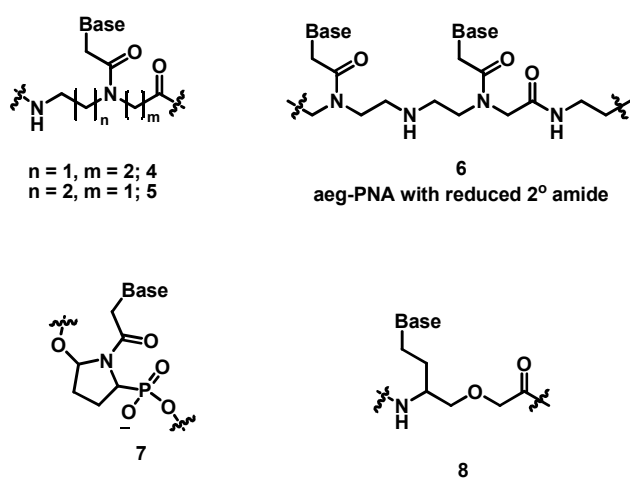


**Figure 1.8** Some examples of backbone modified PNA monomers.

To overcome the poor solubility issue of PNA in aqueous environment, PNAs with a constrained *trans*-4-hydroxy-*N*-acetylpyrrolidine-2-phosphonate backbone (pHypNAs) were introduced. (**7**, Figure 1.8)<sup>14</sup> It has been revealed that they have excellent solubility in water and at the same time preserve biological stability and high hybridization characteristics of classical PNAs.<sup>15,16</sup> These PNA also showed good ability to penetrate cell membranes together with high antisense activity in a cell-free system, in living cells and in model organism.

Oxy-PNA (OPNA) with an ether linkage in the main chain was reported by Kuwahara in 1999. OPNA is chiral with nucleobases attached to the backbone via an ethylene linker.<sup>17</sup> **8**, Figure 1.8) The ether linkage of the backbone improves the solubility of the oligomers in water. Other chiral PNAs (CPNAs) with modification on the backbone have also been obtained by incorporation of substituents at either the  $\alpha$ - or the  $\gamma$ -position. Comparison of the effects of substituents at the  $\alpha$ -position with those of the  $\gamma$ -position revealed that  $\gamma$ -modification is more effective to improve the DNA binding ability.<sup>18</sup> Also, PNA monomers with a methyl group at the  $\beta$ -position have been synthesized.<sup>19</sup>

Additionally, the attempts of rigidifying the backbone of PNAs have been made avoid the problem of rotamers that exist around the tertiary amide bond in regular aeg PNAs, thus obtaining high selectivity in the binding of DNA/RNA (Figure 1.9). For example, aminoprolyl (ap), aminoethylprolyl (aep), aminoethylpyrrolidinone (aepone) and pyrrolidine PNAs have been all synthesized from the same scaffold 4-hydroxyproline. Cyclopropane (cpr) PNA carries a very rigid 3-member ring. Introduction of methylene bridging  $\beta$ -C and  $\gamma$ -C of the aminoethyl moiety as in cyclopentyl (cp) and cyclohexyl (ch) PNAs results in stabilization of DNA and RNA duplexes.

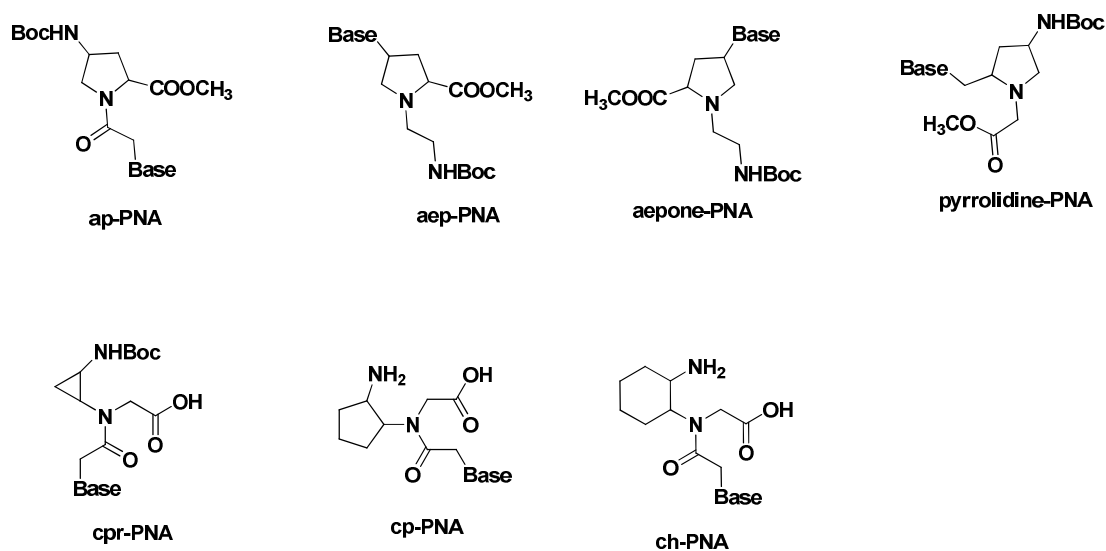


**Figure 1.9** Structures of conformationally rigid PNAs, stereochemistry not shown.

### 1.4.3 Modification of PNA on the nucleobase-backbone linker

Besides nucleobase modified PNAs and backbone modified PNAs, many linkage-modified PNA analogues have also been synthesized. For example, the linker to the nucleobase was extended from methylenecarbonyl to ethylenecarbonyl.<sup>12</sup> The thermal stability of the hybrids between these PNA oligomers and complementary DNA oligonucleotides was significantly lower than that of the corresponding complexes involving unmodified PNA. Therefore, the distance between the backbone and the nucleobases plays a major role in the stability of PNA-DNA hybrids. However, the sequence selectivity was retained.

To understand the role of the nucleobase-backbone linker in the PNA oligomer structure and in the hybridization process, molecules lacking the tertiary amide bond between the base and the backbone were synthesised. It has been investigated that the methylene carbonyl unit was replaced by a flexible ethylene linker (Figure 1.10).<sup>20</sup> The amide functionality in the base-linker unit in PNAs has been found to determine significantly the

affinity and preferred strand orientation in PNA/DNA duplexes. Nevertheless, OPA offers the unique possibility to introduce a fourth substituent on the double bond, which could be of interest for improving binding or solubility properties, or for the attachment of functional units that may act on bound complementary RNA or DNA.

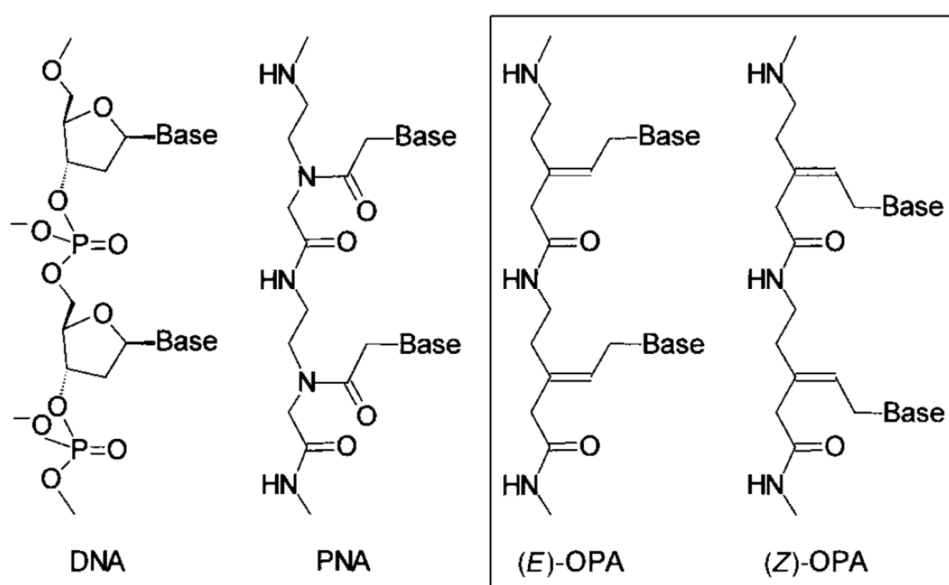


**Figure 1.10** Sections of the chemical structures of deoxyribonucleic acids (DNAs), polyamide or peptide nucleic acids (PNAs), and (E)- and (Z)-olefinic polyamide nucleic acids (OPAs)<sup>20</sup> (copyright 2000 John Wiley and Sons).

#### 1.4.4 Post-synthetic modification of PNAs and click chemistry

A vast number of modified PNA monomers have been reported to be compatible with Boc/Fmoc chemistry. However, individual modification of nucleobases in PNA monomers is always time-consuming and labour intensive. Therefore, post-synthetic functionalization of the PNA oligomer represents a viable alternative to potentially reduce the overall

synthetic effort, as well as introducing a step that is amenable to structural diversification is attractive. In 2001, Ikeda and co-workers synthesized an amino-containing PNA monomer and successfully functionalized a PNA oligomer through a post-synthetic amide bond formation.<sup>21</sup> Later the Hudson group prepared a PNA monomer containing the methyl orotate nucleobase which is compatible with Fmoc-based synthesis. Treatment of the resin-bound oligomers with hydroxide or amines cleanly converted the ester to an orotic acid or orotamide-containing PNA.<sup>22</sup> Additionally, Seitz reported the introduction of Boc-protected N<sup>6</sup>-aminoalkyladenine into PNA oligomer. After the removal of the Boc-group, a fluorescent reporter was post-synthetically attached to the N<sup>6</sup>-position of adenine.<sup>23</sup> More recently, PNA monomers with an alkynyl or azido group have been developed with the aid of click chemistry.<sup>24,25</sup>

Click chemistry was first described by Sharpless and coworkers in 2001.<sup>26</sup> It refers to reactions those are fast and easy to perform, give rise to the intended products in very high yields with little or no byproducts, work well under many conditions, and are unaffected by the nature of the groups being connected to each other. A series of click reactions have been discovered and employed that include copper(I)-catalyzed azide-alkyne cycloaddition (CuAAC), strain-promoted azide-alkyne cycloaddition (SPAAC), strain-promoted alkyne-nitrone cycloaddition (SPANIC), alkene and azide [3+2] cycloaddition, alkene and tetrazine inverse-demand Diels-Alder as well as alkene and tetrazole photoclick reaction. Before long a tremendous number of applications using click reactions emerged among diverse research areas including nucleic acids, drug discovery, material sciences and nanotechnology.

Obviously, click chemistry is also an attractive strategy for modifications of PNA monomers and/or bioconjugation of oligomers. Kumar and co-workers have reported the synthesis of peptide-oligonucleotide conjugates by using CuAAC.<sup>27</sup> An alkyne-containing PNA monomer for the facile insertion of one or two organometallic ferrocenyl moieties into PNA oligomers via CuAAC was reported by Metzler-Nolte and co-workers (**9**, Figure 1.11).<sup>24</sup> Later the same group described the facile N-terminal functionalization of PNA with azide or alkyne functionalities on the solid phase, and their subsequent conversion by click chemistry with different alkynyl and azido ferrocene derivatives to yield a small library of ferrocene-PNA bioconjugates.<sup>28</sup> Additionally, two clickable PNA monomers were reported by Winssinger *et al.* (**10**, **11a**, **11b**, Figure 1.11). PNA fragments may be assembled by using these monomers via CuAAC. N-propargyl analogues (**12a-c**, Figure 1.11) were synthesized and used to synthesize PNAs bearing a triazole in lieu of the amide bond assembled using a “click” cycloaddition.<sup>29</sup> An efficient, versatile PNA ligation method using click chemistry was demonstrated for quantitative conjugation of PNA with DNA, PNA, or peptide under mild conditions (Figure 1.12).<sup>30</sup>

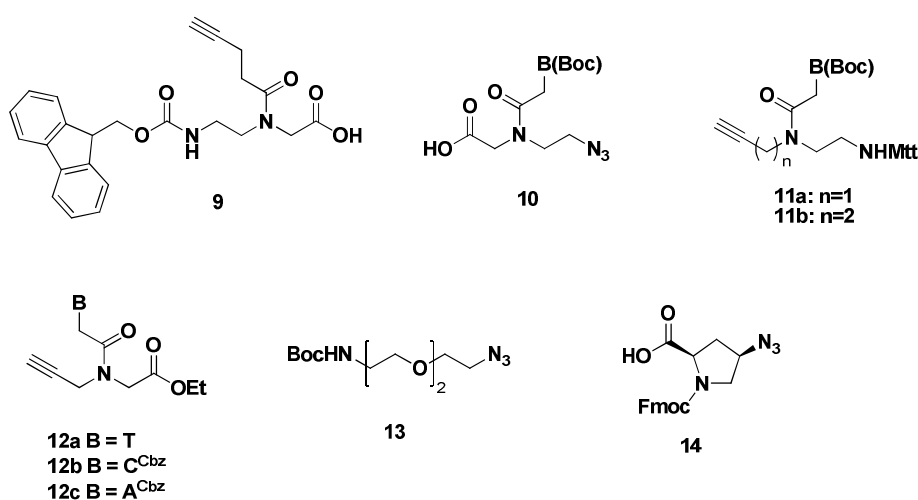


**Figure 1.11** PNA monomers for click chemistry.



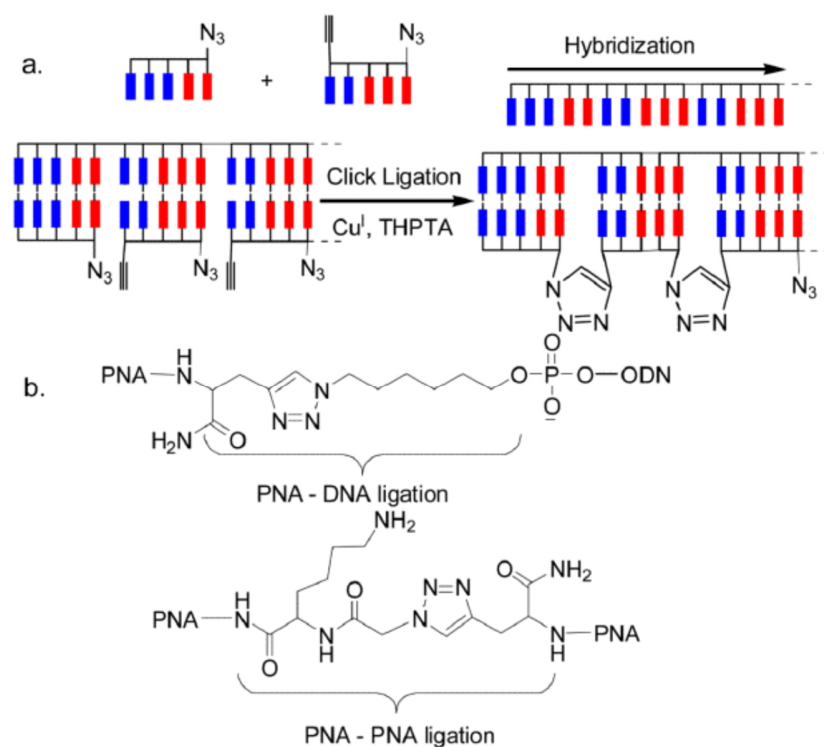


**Figure 1.12** Template-directed click-ligation of PNA-DNA, PNA-PNA (or peptide): (a) schematic structure and (b) chemical structure at ligation point<sup>30</sup> (copyright 2010 John Wiley and Sons).

More recently Manicardi *et al.* reported an Fmoc PNA monomer bearing 5-azidomethyluracil nucleobase.<sup>31</sup> The azide group could be reduced to amine, which was then coupled with naphthalene-2-carboxylic acid. The azide functional group was also exploited as reactive tool for the modification of PNA in solution via CuAAC. Similarly, an azide-containing acpcPNA monomer was synthesized (**14**, Figure 1.11) and modification of *D*-prolyl-2-aminocyclopentane carboxylic acid backbone (acpcPNA) via CuAAC was investigated.<sup>32</sup> Pyrene units could be pre-clicked to the azido acpcPNA monomer or be post-synthetically attached to PNA oligomers via click reaction. The same group also reported an approach for th

e site-specific attachment of fluorophores to the backbone of acpcPNA via reductive alkylation and sequential reductive alkylation-click chemistry (Figure 1.13).<sup>33</sup> Besides, to explore the potential for utilization of clickable PNAs, Hudson group reported the synthesis of an azide containing PNA monomer.<sup>25</sup> The azide group could be used as a tool for on-resin copper catalyzed azide-alkyne Huisgen cycloaddition (CuAAC). At the same time, a simple approach to modify PNA oligomers by post-synthetic on-resin click chemistry was described later by us.<sup>34</sup> In this way, modification of more than one position of a PNA oligomer could be performed in a single step and lends itself to divergent syntheses of modified PNAs. Furthermore, C $\gamma$ -substituted azido PNA monomers were synthesized and inserted into PNA oligomers at specific sites followed by click reaction with propyne carboxyfluorescein (Figure 1.14).<sup>35</sup> The resulting oligomers have been seen by live cell imaging to accumulate around the nuclear membrane in 3T3 cells.

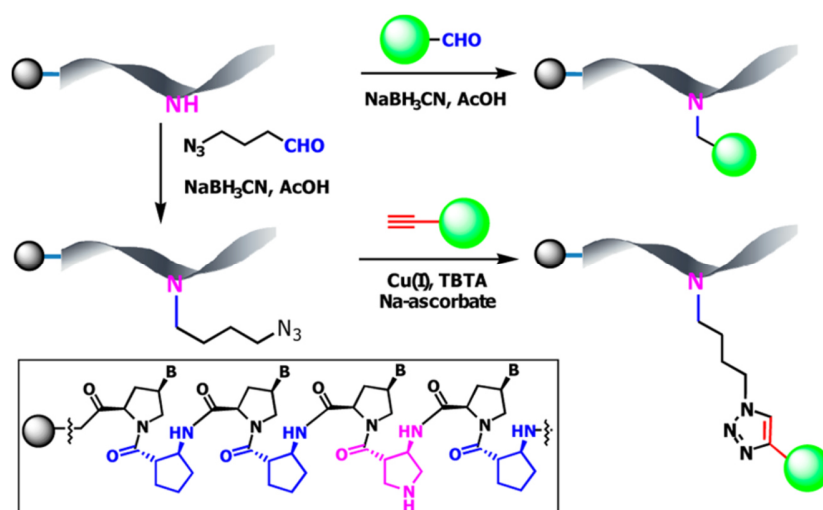


**Figure 1.13** Illustration of site-specific attachment of fluorophores to the backbone of acpPNA via reductive alkylation and sequential reductive alkylation-click chemistry<sup>33</sup> (copyright 2013 American Chemical Society).

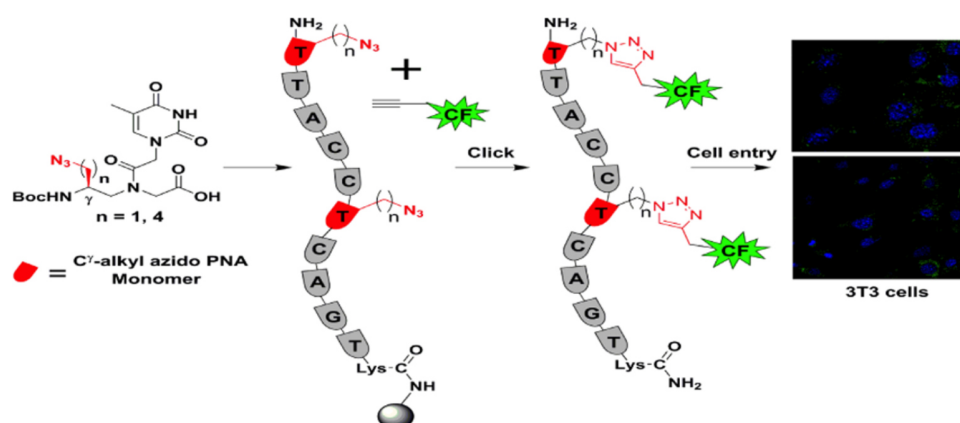


**Figure 1.14** Illustration of click reaction of C $\gamma$ -azido PNA monomer with fluorophore and live cell imaging of the fluorescent oligomers<sup>35</sup> (copyright 2014 American Chemical Society).

Therefore, upon the progress of functionalization of PNAs, success has also been achieved on the application of click chemistry in the modification of nucleobase, backbone as well

as linker of PNA. This facile, convenient method has significantly pushed forward the development of useful targeted PNAs.

### **1.5 Applications of PNA**

As PNA is a powerful molecular tool due to its unique properties and chemistry, extensive applications have been investigated by using PNA.<sup>36-38</sup> Most applications of PNA are focused on the detection of specific nucleic acids by hybridization,<sup>39,40</sup> which has been widely utilized for gene-related research. It has been demonstrated that PNA is of great use for developing diagnostic devices, gene detection and therapeutic agents, and nucleic acid manipulations. *In vitro* studies indicate that PNAs could inhibit both transcription and translation of genes to which they have been targeted, thus holding promise for their use for antigene and antisense therapy.

#### **1.5.1 PNA beacons and fluoroprobes**

Molecular beacon (MB) is a single-stranded oligonucleotide molecule containing a stem-loop structure labeled with a fluorophore (F) and a quencher (Q) on each end (Figure 1.15).<sup>41</sup> It is a powerful probe for selectively detecting DNA and RNA targets. As shown in Figure 1.15, these probes undergo “off-on” switch with a spontaneous fluorogenic conformational change when they hybridize to their targets. In addition to the standard DNA beacon design, a number of PNA beacons have been reported due to the superior properties of PNA. The application of PNA will be further discussed in chapter II.

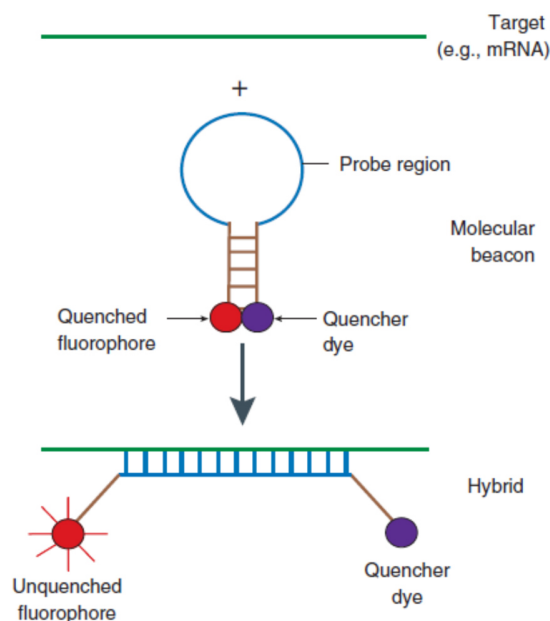


**Figure 1.15** Schematic representation of molecular beacon<sup>42</sup> (copyright 2006 Nature Publishing Group).

### 1.5.2 Single nucleotide polymorphisms (SNPs) detection using PNA

Single Nucleotide Polymorphisms (SNPs) are one of the major sources of genetic variation in human genome. Numerous diseases such as cystic fibrosis, thalassemia and Alzheimer's disease are related to SNPs. The use of PNAs for detections of SNPs has been proved to be one of the most sensitive approach depending on PNA's unique hybridization properties and its great ability to distinguish mismatches of bases.<sup>52</sup> Petersen *et al.* reported a real-time PCR assay for the genotyping of SNPs using short PNA molecular beacons.<sup>43</sup> A method has been described by Ren and coworkers which straightforwardly genotypes SNPs in dsDNA by matrix-assisted laser desorption/ionization time-of-flight mass spectrometry (MALDI-TOF MS) in the presence of PNA.<sup>44</sup> Rockenbauer *et al.* demonstrated a simple, rapid, and robust approach for solid-phase SNP genotyping that combines allele-specific

hybridization, PNA technology, and flow cytometric detection.<sup>45</sup> A strategy employing a combination of PNA probes, an optically amplifying conjugated polymer (CP), and S1 nuclease enzyme has shown the capability of detecting SNPs in a simple, rapid, and sensitive manner.<sup>46</sup> Bethge *et al.* reported forced intercalation probes (FIT-probes) in which an intercalator cyanine dye such as thiazole orange (TO), oxazole yellow (YO), thiazolopyridine (MO), and oxazolopyridine (JO) serves as a replacement of a canonical nucleobase. These FIT-probes have shown potential for detection of SNPs (Figure 1.16).<sup>47</sup> Interestingly, an electrochemical biosensor has also been developed for the detection of SNPs using PNA probes. It takes advantage of the significant structural and physicochemical differences between the full hybrids and SNPs in PNA/DNA and DNA/DNA duplexes. Ferrocene-conjugated chitosan nanoparticles (Chi-Fc) were used as the electroactive indicator of hybridization.<sup>48</sup> Additionally, a new PNA biosensor has been reported for electrochemical detection of point mutation in p53 gene corresponding oligonucleotide based on PNA:double-stranded (ds) DNA triplex formation.<sup>49</sup>

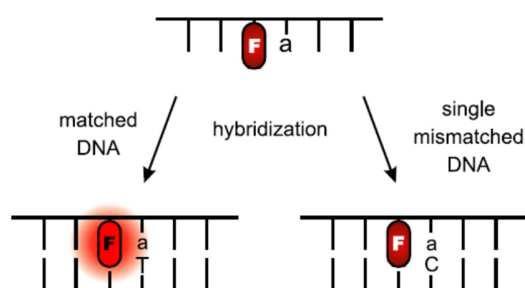


**Figure 1.16** Design principle of FIT-probes. An intercalator fluorophore (F) serves as a base surrogate and is forced to intercalate adjacent to the expected mutation site. High fluorescence is only obtained upon formation of matched duplexes<sup>47</sup> (copyright 2008 Elsevier).

A reliable PNA microarray-based method for accurately detecting SNP in human genes has been described by Mun and coworkers.<sup>50</sup> The technique relies on the mismatched cleavage activity of a single-strand specific (SSS) nuclease. In order to exploit the superior hybridization properties of PNA with target Human papilloma virus (HPV) DNAs, a novel PNA array (PANArray HPV) has been developed.<sup>51</sup> It enables the detection and genotyping of HPVs using 32 type-specific PNA capture probes for medically important HPVs. All tested HPV types showed highly unique hybridization patterns with type-specific PNA probes. Before long studies were carried out to evaluate PANArray™ HPV kit for detection and genotyping of 19 high-risk and 13 low-risk HPV types, and compare it with the commercially available DNA chip kit genotyping of 24 HPVs.<sup>52</sup> The PANArray™ HPV test proved to be highly sensitive and accurate even when multiple HPV infections were present. Then PANArray™ HPV kit became a popular, commercially available product, which takes advantage of PNA's unique properties. In this way, the HPV genotyping can be completed in a shorter time with smaller DNA samples. In addition, multiple infections with several HPV genotypes can be precisely identified for diagnosis. Another advantage is its long shelf life even at room temperature because of chemical stability of PNA. Tedeschi and coworkers designed and synthesized seven modified PNA probes.<sup>53</sup> PNA-microarrays based on these probes were prepared and applied to SNP discrimination in model experiments using oligonucleotide mixtures that simulate the different sequences of the seven tomato varieties. Although the efficiency of binding was somewhat lower than what is shown by standard PNA arrays, the unsurpassed specificity of the PNA probes still makes them very promising for the development of PNA-based genotyping methodologies.

### 1.5.3 PNA and DNA for Fluorescence *In Situ* Hybridization

Fluorescence in situ hybridization (FISH) is a cytogenetic technique that uses fluorescent probes to bind to only those parts of the chromosome with a high degree of sequence complementarity.<sup>54</sup> It is an important molecular assay for determining the number, size and/or location of specific DNA sequences in mammalian cells, which is developed in the combination of the microscopy observation and the specificity hybridization of DNA/rRNA.<sup>55</sup> Perry-O'Keefe reported a standard FISH method using PNA probes for analysis of gram-negative, gram-positive bacteria, as well as yeast. Fluorophore labeled PNA probes were designed targeting specific rRNA sequences of *Escherichia coli*, *Pseudomonas aeruginosa*, *Staphylococcus aureus*, *Salmonella* as well as eubacteria and eucarya.<sup>56</sup> In addition, a PNA probe (CJE195) was designed and found to bind with higher affinity to a previously reported low affinity site on the 16S rRNA than the corresponding DNA probe.<sup>55</sup> Huang *et al.* reported a PNA probe for detection of the toxic dinoflagellate, *Takayama pulchella* TPXM, by employing FISH combined with epifluorescent microscopy and flow cytometry.<sup>57</sup> In 2011, Shiraishi and coworkers developed a pair of biotinylated PNA probes targeting two sequences in 18S rRNA from the parasite *Trypanosoma brucei* at a distance of 191 nt (corresponding to maximum distance of ca. 60 nm) from each other.<sup>58</sup> It has been shown that by simple fluorescence microscopy analysis, PNA probes specifically detect the presence of 18S rRNA in a total RNA extract from less than 300 parasites. Later Zhang *et al.* reported a PNA-FISH method for detection of *Listeria* species (Figure 1.17).<sup>59</sup> *In silico* analysis showed that three PNA probes Lis-16S-1, Lm-16S-2 and Liv-16S-5 were capable to specifically identify *Listeria* genus, *Listeria monocytogenes* and *Listeria ivanovii*, respectively, in comparison with the control probe.



PNA-FISH method has also been applied in identification of probiotic bacteria such as *Lactobacillus* species and *Vibrio* genus, demonstrated by Machado *et al.* and Zhang *et al.*, respectively.<sup>60,61</sup> To date, PNA FISH® tests have been greatly interesting and commercially available for rapid identification of bacteria and yeast directly from positive blood cultures. They not only enhance the efficiency of hospitals for appropriate therapy while avoiding unnecessary use of antibiotic, but also improve patient outcomes as well as lower hospital costs.<sup>62,63</sup>

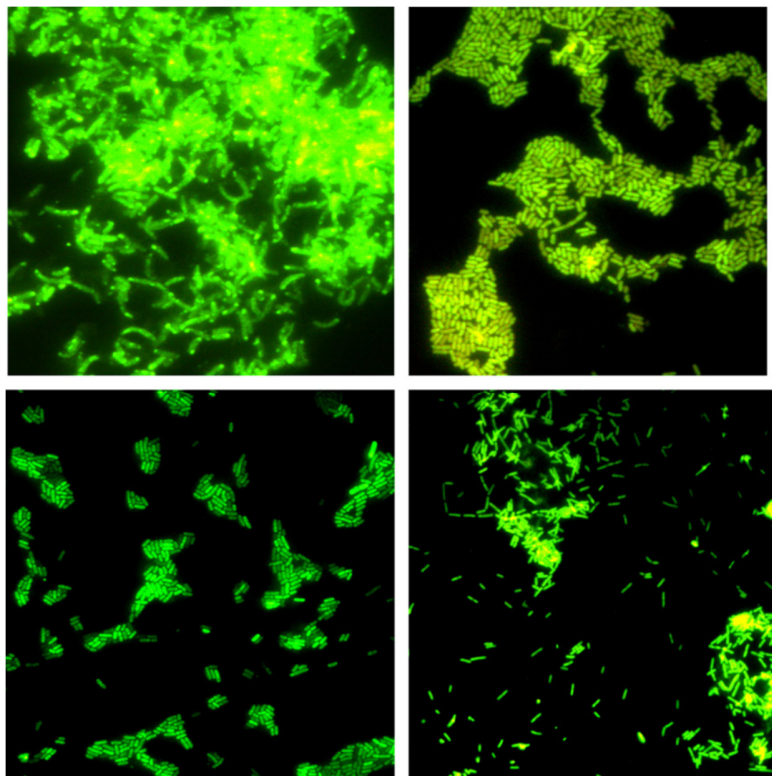


**Figure 1.17** Typical PNA hybridization results. (control, top left) Cells of *Vibrio fluvialis* ATCC 33810 hybridized with the universal probe BacUin. (top right) Cells of *L. grayi* Li07 hybridized with the *Listeria*-specific probe Lis-16S-1. (bottom left) Cells of *L. monocytogenes* SLCC2755 hybridized with the *L. monocytogenes*-specific probe Lm-16S-

2. (bottom right) Cells of *L. ivanovii* Li01 hybridized with the *L. ivanovii*-specific probe Liv-16S-5.<sup>59</sup> (copyright 2012 Elsevier)

#### 1.5.4 Antigene and antisense therapy

Antisense technology is a significant approach to inhibit or down-regulate the production of a target protein by using antisense DNA, RNA and artificial DNA/RNA analogues. An antisense sequence is an oligonucleotide that is perfectly complementary to the target nucleotide sequence present in the cell. There are two possible mechanisms for an antisense effect. The one that relies on targeting of the mRNA is called the antisense strategy. The other one that is designed to bind to the double-stranded DNA or genes situated in the nucleus, is called the antigene strategy (Figure 1.18). Whereas the antisense strategy is well established with several examples of *in vitro* and *in vivo* applications,<sup>64</sup> the antigene approach is still in its infancy and the understanding of the involved mechanism is limited.

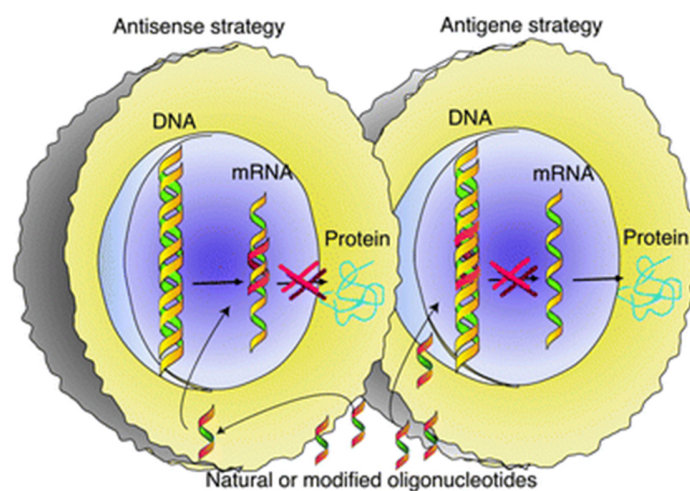


**Figure 1.18** Representation of antisense and antigene strategies.<sup>65</sup> (copyright 2002 Royal Society of Chemistry)

Earlier studies have shown that the binding of PNA to complementary DNA can efficiently block transcriptional elongation and inhibit the binding of transcriptional factors. Boffa and coworkers demonstrated that PNA could invade the CAG triplets of the androgen receptor (AR) and TATA-binding protein (TBP) genes in human prostatic cancer cells. It has been shown that the PNAs readily entered the nuclei of lysolecithin-permeabilized cells and effectively inhibited sense transcription of unique AR and TBP DNA sequences downstream of the site of PNA:DNA hybridization.<sup>66</sup> PNA-mediated inhibition of transcription was also reported for the alpha-chain of the interleukin-2 receptor.<sup>67</sup> Nielsen *et al.* have discussed that even an 8-mer PNA can efficiently block transcription by binding to DNA duplex.<sup>68</sup> Therefore, the antisense potential of duplex-forming and triplex-forming PNAs has been investigated.<sup>69</sup> It has also been found that PNA interacts with mRNA independently of the RNA secondary structure. Studies on the mechanisms of antisense activity have demonstrated that PNA inhibits expression in a different way from regular antisense DNA/RNA which needs RNase-H mediated degradation of the mRNA-oligonucleotide hybrid. Because PNA is not recognized by RNase, its antisense effect acts through steric interference of either RNA processing (transport into cytoplasm) or translation (caused by binding to the mRNA).

Not surprisingly, the antisense and antigene properties of PNA has been described as early as in 1992.<sup>70</sup> It has been shown that PNA or a mixed sequence 15-mer PNA to the transcribed strand of a G-free transcription cassette caused 90 to 100 percent site-specific termination of pol II transcription elongation. Mologni *et al.* reported that three different regions of the PML/RAR $\alpha$  oncogene, including two AUG potential start codons, were studied as targets of translation inhibition by antisense PNA in a cell-free system.<sup>71</sup>

Furthermore, the inhibition of gene expression by peptide nucleic acids (PNAs) inside cells has also been explored.<sup>72</sup> PNA has also been reported to efficiently recognize the RNA component of human telomerase (hTR) and inhibit enzyme activity with IC<sub>50</sub> values in the picomolar to nanomolar range.<sup>73</sup>

An *in vivo* study has been performed by using PNA to inhibit  $\delta$ -opioid receptor gene function.<sup>74</sup> However, the progress using PNA for regulation of gene expression was hampered by the poor cellular uptake of “naked” PNA by live cells. Therefore, modifications of PNA oligomers were necessary to improve the uptake of PNA in eukaryotic living cells. For example, PNA coupled to DNA oligomers, to receptor ligands or to cell penetrating peptides (CPPs), could help deliver PNA into cells.<sup>75</sup> Among these attempts, PNA-CPP conjugates are of great interest since CPPs are rapidly internalized by mammalian cells. Pooga *et al.* reported the use of a PNA-peptide conjugate in the downregulation of the galanin receptor in neuronal cells in culture.<sup>76</sup> Additionally, cationic liposomes have been demonstrated to efficiently complex DNA-PNA hybrid molecules which effectively improves the *in vivo* delivery.<sup>77</sup>

As a hybridization probe, PNA has shown its promise in the above-mentioned applications. However, the poor cellular uptake and water insolubility of PNA limit its utilization in *in vivo* applications.

## **1.6 Overview**

Based on the advantages and development of PNAs, the objective of this research is to develop functionalized PNAs that can be used in various applications via post-synthetic click chemistry. Chapter II describes the design and synthesis of quencher-free PNA

molecular beacons based on solid-phase post-synthetic click chemistry which has been demonstrated to be versatile and convenient. The prepared stem-loop PNA beacon showed rapid binding and response to target cystic fibrosis gene sequence.

Chapter III introduces a “click-couple-click” approach for synthesis of conventional PNA beacons that contain different reporters on each terminus. The current method for the synthesis of PNA MBs is mostly based on amide formation to attach reporters to PNA sequences. However, the complicated protection strategies are required to avoid side reactions as amide formation possibly happens everywhere in PNA oligomers. In this work we develop a new method based on solid-phase microwave-assisted CuAAC, which allows fast, convenient preparation of various conventional PNA beacons. One reporter could be clicked to an azido-containing PNA first followed by coupling of another azide PNA monomer. A different reporter would be clicked to the resulting PNA to yield a PNA MB. This method based on “click-couple-click” is chemically selective, robust and efficient. It is also of great use for screening fluorophore and quencher pairs for PNA MBs.

Chapter IV describes the preparation of a (Gd(III)-DOTA)<sub>4</sub>-PNA conjugate targeting poly(A) tail. On-resin CuAAC has been used to conjugate four units of Gd(III)-DOTA to a PNA oligomer that contains 10 thymine PNA monomers. Hybridization with poly(A) tail would significantly increase the loading of Gd ions in a microenvironment, thus helping enhance the contrast of MRI.

Chapter V shows the bioconjugation of an oligopeptide to gold nanoparticles via strain-promoted azide-alkyne cycloaddition via post-assembly deprotection (SPAAC-PAD). This strategy would be of great use for functionalization of gold nanoparticles with peptides for

targeted CT imaging. The success of this approach also allows for the functionalization of AuNPs with PNAs for various applications.

### 1.7 References

- (1) Nielsen, P. E.; Egholm, M.; Berg, R. H.; Buchardt, O. *Science* **1991**, *254* (5037), 1497.
- (2) Uhlmann, E.; Peyman, A.; Breipohl, G.; Will, D. W. *Angew. Chem. Int. Ed.* **1998**, *37* (20), 2796.
- (3) Demidov, V. V.; Potaman, V. N.; Frank-Kamenetskii, M. D.; Egholm, M.; Buchardt, O.; Sönnichsen, S. H.; Nielsen, P. E. *Biochem. Pharmacol.* **1994**, *48* (6), 1310.
- (4) Merrifield, R. B. *J. Am. Chem. Soc.* **1963**, *85* (14), 2149.
- (5) Carpino, L.; El-Faham, A. *J. Org. Chem.* **1994**, *59*, 695.
- (6) Wojciechowski, F.; Hudson, R. H. E. *Curr. Top. Med. Chem.* **2007**, *7* (7), 667.
- (7) Hudson, R. H. E.; Li, G.; Tse, J. *Tetrahedron Lett.* **2002**, *43* (8), 1381.
- (8) Püschl, A.; Boesen, T.; Zuccarello, G.; Dahl, O.; Pitsch, S.; Nielsen, P. E. *J. Org. Chem.* **2001**, *66* (3), 707.
- (9) Eldrup, A. B.; Christensen, C.; Haaima, G.; Nielsen, P. E. *J. Am. Chem. Soc.* **2002**, *124* (13), 3254.
- (10) Rajeev, K. G.; Maier, M. A.; Lesnik, E. A.; Manoharan, M. *Org. Lett.* **2002**, *4* (25), 4395.

- (11) Ausín, C.; Ortega, J. A.; Robles, J.; Grandas, A.; Pedroso, E. *Org. Lett.* **2002**, *4* (23), 4073.
- (12) Hyrup, B.; Egholm, M.; Nielsen, P. E.; Wittung, P.; Nordc, B.; Buchardt, O. *J. Am. Chem. Soc.* **1994**, *116*, 7964.
- (13) Myers, M. C.; Pokorski, J. K.; Appella, D. H. *Org. Lett.* **2004**, *6* (25), 4699.
- (14) Efimov, V. A.; Birikh, K. R.; Staroverov, D. B.; Lukyanov, S. A.; Tereshina, M. B.; Zarskiy, A. G.; Chakhmakhcheva, O. G. *Nucleic Acids Res.* **2006**, *34* (8), 2247.
- (15) Lefmann, M.; Schweickert, B.; Buchholz, P.; Göbel, U. B.; Ulrichs, T.; Seiler, P.; Theegarten, D.; Moter, A. *J. Clin. Microbiol.* **2006**, *44* (10), 3760.
- (16) Peano, C.; Bordoni, R.; Gulli, M.; Mezzelani, A.; Samson, M. C.; De Bellis, G.; Marmioli, N. *Anal. Biochem.* **2005**, *346* (1), 90.
- (17) Kuwahara, M.; Arimitsu, M.; Sisido, M. *Tetrahedron* **1999**, *55*, 10067.
- (18) Sforza, S.; Tedeschi, T.; Corradini, R.; Marchelli, R. *Eur. J. Org. Chem.* **2007**, 5879.
- (19) Sugiyama, T.; Imamura, Y.; Demizu, Y.; Kurihara, M.; Takano, M.; Kittaka, A. *Bioorg. Med. Chem. Lett.* **2011**, 7317.
- (20) Schutz, R.; Cantin, M.; Roberts, C.; Greiner, B.; Uhlmann, E.; Leumann, C. *Angew. Chem. Int. Ed.* **2000**, *39* (7), 1250.
- (21) Ikeda, H.; Fujimori, F.; Murakami, Y.; Nakamura, Y. *Nucleic Acids Res. Suppl.* **2001**, *1* (1), 177.

- (22) Hudson, R. H. E.; Wojciechowski, F. *Nucleosides Nucleotides Nucleic Acids* **2005**, *24* (5–7), 1123.
- (23) Seitz, O. *Angew. Chem. Int. Ed.* **2000**, *39* (18), 3249.
- (24) Gasser, G.; Hüsken, N.; Köster, S. D.; Metzler-Nolte, N. *Chem. Commun.* **2008**, 3675.
- (25) St Amant, A. H.; Engbers, C.; Hudson, R. H. E. *Artif. DNA PNA XNA* **2013**, *4* (1), 4.
- (26) Kolb, H. C.; Finn, M. G.; Sharpless, K. B. *Angew. Chem Int. Ed.* **2001**, *40*, 2004.
- (27) Gogoi, K.; Mane, M. V.; Kunte, S. S.; Kumar, V. A. *Nucleic Acids Res.* **2007**, *35* (21), e139.
- (28) Hüsken, N.; Gasser, G.; Köster, S. D.; Metzler-Nolte, N. *Bioconjug. Chem.* **2009**, *20* (8), 1578.
- (29) Chouikhi, D.; Barluenga, S.; Winssinger, N. *Chem. Commun.* **2010**, *46*, 5476.
- (30) Peng, X.; Li, H.; Seidman, M. *Eur. J. Org. Chem.* **2010**, *22*, 4194.
- (31) Manicardi, A.; Accetta, A.; Tedeschi, T.; Sforza, S.; Marchelli, R.; Corradini, R. *Artif. DNA PNA XNA* **2012**, *3* (2), 53.
- (32) Mansawat, W.; Boonlua, C.; Siriwong, K.; Vilaivan, T. *Tetrahedron* **2012**, *68* (21), 3988.
- (33) Ditmangklo, B.; Boonlua, C.; Suparpprom, C.; Vilaivan, T. *Bioconjug. Chem.* **2013**, *24* (4), 614.



- (34) Wang, X.; Hudson, R. H. E. *ChemBioChem* **2015**, *16* (15), 2156.
- (35) Jain, D. R.; Ganesh, K. N. *J. Org. Chem.* **2014**, *79*, 6708.
- (36) Tech, A.; Med, B.; Siddiquee, S.; Rovina, K.; Azriah, A. *Adv. Tech. Biol. Med.* **2015**, *3* (2), 1000131.
- (37) Demeunynck, M.; Charmantray, F.; Martelli, A. *Curr. Pharm. Des.* **2001**, *7*, 1703.
- (38) Marin, V. L.; Roy, S.; Armitage, B. A. *Expert Opin. Biol. Ther.* **2004**, *4* (3), 337.
- (39) Panyutin, I. G.; Onyshchenko, M. I.; Englund, E. A.; Appella, D. H.; Neumann, R. D. *Curr. Pharm. Des.* **2012**, *18* (14), 1984.
- (40) Gambari, R.; Borgatti, M.; Bezzetti, V.; Nicolis, E.; Lampronti, I.; Dechecchi, M. C.; Mancini, I.; Tamanini, A.; Cabrini, G. *Biochem. Pharmacol.* **2010**, *80*, 1887.
- (41) Tyagi, S.; Kramer, F. R. *Nat. Biotechnol.* **1996**, *14*, 303.
- (42) Mhlanga, M. M.; Tyagi, S. *Nat. Protoc.* **2006**, *1*, 1392.
- (43) Petersen, K.; Vogel, U.; Rockenbauer, E.; Nielsen, K. V.; Kølvrå, S.; Bolund, L.; Nexø, B. *Mol. Cell. Probes* **2004**, *18*, 117.
- (44) Ren, B.; Zhou, J.-M.; Komiyama, M. *Nucleic Acids Res.* **2004**, *32* (4), e42.
- (45) Rockenbauer, E.; Petersen, K.; Vogel, U.; Bolund, L.; Kølvrå, S.; Nielsen, K. V.; Nexø, B. A. *Cytom. Part A* **2005**, *64* (2), 80.
- (46) Gaylord, B. S.; Massie, M. R.; Feinstein, S. C.; Bazan, G. C. *Proc. Natl. Acad. Sci. U. S. A.* **2005**, *102* (1), 34.
- (47) Bethge, L.; Jarikote, D. V.; Seitz, O. *Bioorg. Med. Chem.* **2008**, *16*, 114.

- (48) Kerman, K.; Saito, M.; Tamiya, E. *Anal. Bioanal. Chem.* **2008**, *391* (8), 2759.
- (49) Hamidi-Asl, E.; Raoof, J. B.; Ojani, R.; Golabi, S. M.; Hejazi, M. S. *J. Iran. Chem. Soc.* **2013**, *10* (6), 1075.
- (50) Mun, H. Y.; Girigoswami, A.; Jung, C.; Cho, D. Y.; Park, H. G. *Biosens. Bioelectron.* **2009**, *24* (6), 1706.
- (51) Choi, J. J.; Kim, C.; Park, H. *J. Clin. Microbiol.* **2009**, *47* (6), 1785.
- (52) Song, H. J.; Lee, J. W.; Kim, B. G.; Song, S. Y.; Bae, D. S.; Kim, D. S. *Biochip J.* **2010**, *4* (3), 167.
- (53) Tedeschi, T.; Calabretta, A.; Bencivenni, M.; Manicardi, A.; Corrado, G.; Caramante, M.; Corradini, R.; Rao, R.; Sforza, S.; Marchelli, R. *Mol. Biosyst.* **2011**, *7* (6), 1902.
- (54) Langer-Safer, P. R.; Levine, M.; Ward, D. C. *Proc. Natl. Acad. Sci. U. S. A.* **1982**, *79* (14), 4381.
- (55) Lehtola, M. J.; Loades, C. J.; Keevil, C. W. *J. Microbiol. Methods* **2005**, *62* (2), 211.
- (56) Perry-O'Keefe, H.; Rigby, S.; Oliveira, K.; Sørensen, D.; Stender, H.; Coull, J.; Hyldig-Nielsen, J. J. *J. Microbiol. Methods* **2001**, *47* (3), 281.
- (57) Huang, B.; Hou, J.; Lin, S.; Chen, J.; Hong, H. *Harmful Algae* **2008**, *7* (4), 495.
- (58) Shiraishi, T.; Deborggraeve, S.; Buscher, P.; Nielsen, P. E. *Artif. DNA PNA XNA* **2011**, *2* (2), 60.

- (59) Zhang, X.; Wu, S.; Li, K.; Shuai, J.; Dong, Q.; Fang, W. *Int. J. Food Microbiol.* **2012**, *157* (2), 309.
- (60) Machado, A.; Almeida, C.; Carvalho, A.; Boyen, F.; Haesebrouck, F.; Rodrigues, L.; Cerca, N.; Azevedo, N. F. *Int. J. Food Microbiol.* **2013**, *162* (1), 64.
- (61) Zhang, X.; Li, K.; Wu, S.; Shuai, J.; Fang, W. *Int. J. Food Microbiol.* **2015**, *206*, 39.
- (62) Forrest, G. N.; Mankes, K.; Jabra-Rizk, M. A.; Weekes, E.; Johnson, J. K.; Lincalis, D. P.; Venezia, R. A. *J. Clin. Microbiol.* **2006**, *44* (9), 3381.
- (63) Forrest, G. N.; Mehta, S.; Weekes, E.; Lincalis, D. P.; Johnson, J. K.; Venezia, R. A. *J. Antimicrob. Chemother.* **2006**, *58* (1), 154.
- (64) Wagner, R. W. *Nature* **1994**, *372*, 333.
- (65) Imanishi, T.; Obika, S. *Chem. Commun.* **2002**, 1653.
- (66) Boffai, L. C.; Morris, P. L.; Carpaneto, E. M.; Louissaint, M.; Allfrey, V. G. *J. Biol. Chem.* **1996**, *271* (22), 13228.
- (67) Vickers, T. A.; Griffith, M. C.; Ramasamy, K.; Risen, L. M.; Freier, S. M. *Nucleic Acids Res.* **1995**, *23* (15), 3003.
- (68) Nielsen, P. E.; Egholm, M.; Buchardt, O. *Gene* **1994**, *149* (1), 139.
- (69) Knudsen, H.; Nielsen, P. E. *Nucleic Acids Res.* **1996**, *24* (3), 494.
- (70) Hanvey, J. C.; Peffer, N. J.; Bisi, J. E.; Thomson, S. A.; Cadilla, R.; Josey, J. A.; Ricca, D. J.; Hassman, C. F.; Bonham, M. A.; Au, K. G.; Carter, S. G.;

- Bruckenstein, D. A.; Boyd, A. L.; Noble, S. A.; Babiss, L. E. *Science* **1992**, *258*, 1481.
- (71) Mologni, L.; LeCoutre, P.; Nielsen, P. E.; Gambacorti-Passerini, C. *Nucleic Acids Res.* **1998**, *26* (8), 1934.
- (72) Doyle, D. F.; Braasch, D. A.; Simmons, C. G.; Janowski, B. A.; Corey, D. R. *Biochemistry* **2001**, *40* (1), 53.
- (73) Norton, J. J. C.; Piatyszek, M. A. M.; Wright, W. E. W.; Shay, J. W.; Corey, D. R. *Nat. Biotechnol.* **1996**, *14* (5), 615.
- (74) Fraser, G. L.; Holmgren, J.; Clarke, P. B.; Wahlestedt, C. *Mol. Pharmacol.* **2000**, *57*, 725.
- (75) Cutrona, G.; Carpaneto, E. M.; Ulivi, M.; Roncella, S.; Landt, O.; Ferrarini, M.; Boffa, L. C. *Nat. Biotechnol.* **2000**, *18* (3), 300.
- (76) Pooga, M.; Soomets, U.; Hällbrink, M.; Valkna, a; Saar, K.; Rezaei, K.; Kahl, U.; Hao, J. X.; Xu, X. J.; Wiesenfeld-Hallin, Z.; Hökfelt, T.; Bartfai, T.; Langel, U. *Nat. Biotechnol.* **1998**, *16* (9), 857.
- (77) Nastruzzi, C.; Cortesi, R.; Esposito, E.; Gambari, R.; Borgatti, M.; Bianchi, N.; Feriotto, G.; Mischianti, C. *J. Control. Release* **2000**, *68* (2), 237.

## **Chapter II: VERSATILE SYNTHESIS OF QUENCHER-FREE PNA MOLECULAR BEACONS VIA POST-SYNTHETIC CLICK CHEMISTRY FUNCTIONALIZATION**

Chapter 2 has been published as a research paper, and it is reprinted (adapted) with permission from Xiaoxiao Wang, Robert H. E. Hudson\*, ChemBioChem, 2015, 16, 2156–2161. Copyright 2015 John Wiley and Sons.

### **2.1 Introduction to PNA-based molecular beacons**

First reported by Tyagi and Kramer in 1996, a molecular beacon (MB) is a single-stranded oligonucleotide molecule containing a stem-loop structure labeled with a fluorophore (F) and a quencher (Q) on each end.<sup>1</sup> MBs are powerful hybridization probes for simple and rapid detection of specific DNA/RNA sequences. These probes undergo “off-on” switch with a spontaneous fluorogenic conformational change when they hybridize to their targets.

A typical MB structure consists of a loop, a stem and reporters. The loop is a 18-30 single-strand region of the MB which is complementary to the target sequence. The stem contains two short (4-6 nucleotide residues) oligonucleotides that are complementary to each other to maintain the closed hairpin structure. Reporters represent a fluorophore and a quencher.

Two forms of energy transfer mechanism in MBs have been proposed: dynamic and static fluorescence quenching.<sup>2</sup> Dynamic quenching includes Förster transfer energy transfer (FRET) and Dexter transfer (collisional quenching or electron-transfer quenching). For dynamic quenching, the distance between donor and the acceptor needs to be within 20-100 Å, as the two moieties move closer, reduced fluorescence intensity will result. The spectral overlap should be between the donor's emission and the acceptor's absorption spectra. The relative orientation of the donor and acceptor needs to be approximately

parallel. Static quenching requires formation of an intramolecular dimer with unique properties, such as unique absorption spectrum or being nonfluorescent.<sup>2-5</sup> Therefore, appropriate contact between the two moieties is necessary for both mechanisms. It is known that planar aromatic dyes such as phenanthrene and pyrene<sup>6</sup> may participate in  $\pi$ - $\pi$  stacking, thus preferring a static quenching.

To improve signal-to-background ratio, the choice of fluorophore and quencher pair is critical. A systematic study of quenching efficiencies for different fluorophore and quencher pairs has been reported.<sup>5</sup> Matching the fluorophore with an effective quencher can lead to improvements in detection by reducing the background from the MB in the absence of targets.

DNA-based MBs have become well-known in gene detection, biosensing, bioimaging and therapy. However, they are very susceptible to nucleolytic degradation during *in vitro* and *in vivo* studies. Thus artificial nucleic acids analogues, such as locked nucleic acid (LNA) and unlocked nucleic acid (UNA), have been introduced and employed in the applications of MBs and light-up probes in recent years.<sup>7-9</sup> PNA beacons have also been investigated due to their superior hybridization features, resistance to nucleases and proteases, chemical robustness, and sequence discrimination.<sup>10-12</sup>

To date, various PNA MBs have been developed. A summary of conventional PNA beacons will be presented in chapter III. In the development of MBs, background signal has always been a critical aspect to consider. On one hand, it could come from the probe itself, for example, it is very difficult to achieve complete quenching in a conventional MB and this may result in a significant background signal. On the other hand, it also occurs from the native fluorescence of many molecular species in the biological environment.

These issues deteriorate assay sensitivity and compromise probe selectivity, thus complicating the analysis of small molecules, nucleic acids, and proteins in a complex sample. Therefore, the challenge to minimize background signal and to tolerate complex biological sample interference becomes critical. Researchers around the world have successfully modified and synthesized various MBs to suit their needs. Recently, variation on the MB theme has been made to improve their function by eliminating false signals, increasing specificity, and providing enhanced detection limits. Quencher-free molecular beacons (QF-MBs) are one of the significant modifications of the conventional MB, in which the quencher moiety has been eliminated. Based on the design, the reported QF-MBs can be broadly classified into two different types: mono-labelled QF-MBs and dual-labelled QF-MBs. Mono-labelled QF-MBs contain a fluorophore at the middle or end of the oligonucleotide while dual-labelled MBs contain two fluorophores at the stem or at the ends. Singly-labeled PNA probes carrying one environmentally sensitive dye, such as fluorene,<sup>13</sup> pyrene<sup>14-17</sup> or thiazole orange have been reported.<sup>18-20</sup> MBs containing two pyrene fluorophores are archetype of dual-labelled QF-MBs. (Figure 2.1)<sup>21</sup> Compared to conventional MBs with on/off output patterns, pyrene-based QF-MBs are attractive due to unambiguous detection of the target by changes in excimer/monomer ratios.<sup>21-23</sup> The excimer complex also results in a long fluorescence lifetime (30-60 ns) of the excited state of pyrene compared to the auto fluorescence of cellular extracts (~7 ns). In spite of this, pyrene has been reported to have low quantum yields when attached to biomolecules and relatively short absorption and emission wavelengths which can suffer from interference from cellular auto fluorescence.<sup>7,24</sup> However, pyrene-modified quencher-free PNA-based

QF-MBs are not widely described, with only one based on the modified acpPNA scaffold reported recently.<sup>25</sup>

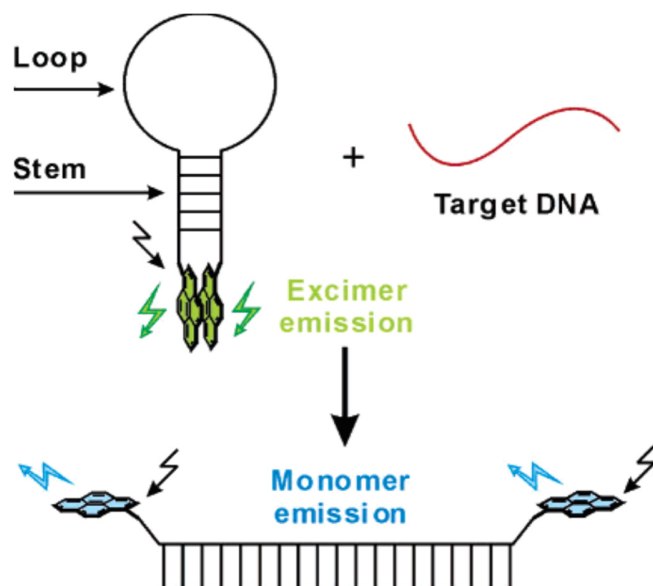


**Figure 2.1** Schematic representation of pyrene-based QF-MB, which was dually labeled with pyrene at the 3'-and 5'-end of single-stranded oligonucleotides with a stem-loop structure. In the absence of target DNAs, the “closed” stem-loop conformation predominantly emits excimer fluorescence (green) whereas the MB undergoes a dynamic conformational change to emit monomer fluorescence (blue) upon hybridization with target DNAs<sup>21</sup> (copyright 2004 American Chemical Society).

## 2.2 Synthesis of QF-PNA beacons

PNA beacons are usually synthesized by SPPS using standard and modified monomers that contain a fluorophore or quencher. However, the synthesis of modified monomers is rather laborious and time-consuming. Often, luminophore-functionalized monomers cannot be directly introduced into PNA oligomers efficiently due to incompatibility with the chemical conditions (acidic or basic) of SPPS. Hence, post-synthetic functionalization of the PNA



oligomer represents a viable alternative to potentially reduce the overall synthetic effort, as well as introducing a step that is amenable to structural diversification.

Some post-synthetic methodologies for the preparation of modified PNAs have been reported. For example, in 2001, Ikeda and co-workers synthesized an amino-containing PNA monomer and successfully functionalized a PNA oligomer through a post-synthetic amide bond formation.<sup>26</sup> Nevertheless, more convenient and selective methods are needed, because some luminophores are unstable under the coupling conditions, or the conditions to reveal the amino group concomitantly remove other protecting groups on the oligomer. In the same year, click chemistry was described by Sharpless and co-workers,<sup>27</sup> after which a tremendous number of applications of click reactions appeared. These reactions are touted to proceed under mild, simple conditions, being fast, chemoselective, and high yielding; thus, these are attractive candidates for the post-synthetic functionalization step. The archetypal click reaction, copper(I)-catalyzed Huisgen azide-alkyne cycloaddition (CuAAC) yielding the chemically robust 1,4-disubstituted 1,2,3-triazole derivatives,<sup>28</sup> was an obvious starting point for post-synthetic functionalization of PNA.

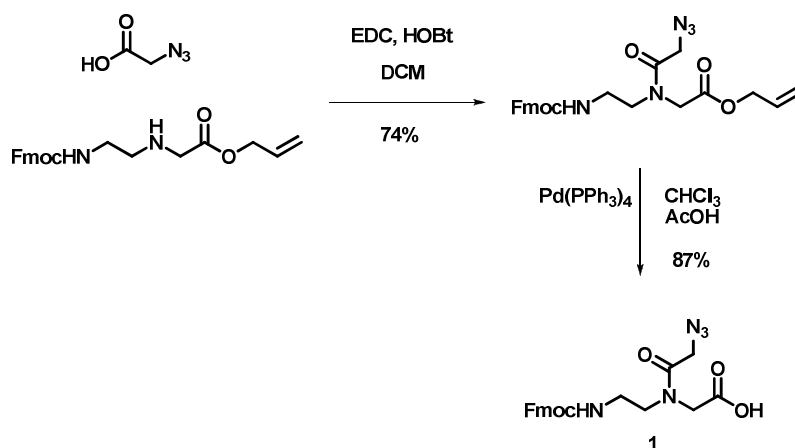
A number of groups have reported modifications of PNA monomers and/or bioconjugation of oligomers by using CuAAC.<sup>29-31</sup> However, most of those PNA-CuAAC approaches were performed in solution. Our attention turned to on-resin CuAAC, because it combines advantages of click chemistry and SPPS in which an excess of reactants can be used and are easily washed away from the solid support without tedious work up; it is operationally easy to perform, and often gives quantitative yields.

Herein, a post-synthetic method based on on-resin CuAAC was developed and utilized in simultaneous functionalization of PNA, which allows the preparation of pyrene-based

PNA beacons more efficient. Two pyrene-based PNA beacons, **MB1** and **MB2**, were successfully synthesized and evaluated.

### 2.3 Results and discussion

To apply post-synthetic click chemistry to developing PNA MBs, we designed and synthesized an azide PNA monomer in which a nucleobase was replaced with an azide group<sup>31</sup> (Scheme 2.1). One or more azide monomers can be inserted into a PNA sequence by automated SPPS in any position without concern for incompatibility.



**Scheme 2.1** Synthesis of azide PNA monomer (1).

In the work of this chapter, two azide-containing PNA sequences (**PNA1-Az** and **PNA2-Az**) have been synthesized via Fmoc SPPS protocol targeting cystic fibrosis (CF), is a genetic disease caused by loss or mutation of the cystic fibrosis transmembrane conductance regulator (CFTR) gene (Table 2.1). Then the simultaneous modification of **PNA1-Az** for preparation of pyrene-based QF-MBs by post-synthetic on-resin click chemistry was performed (Scheme 2.2). Directly after oligomer synthesis, the resin-bound PNA was subjected to CuAAC in the presence of excess 1-ethynylpyrene. The excess reagents, solvents, and catalyst were easily washed from the resin, whereas the workup to

remove these materials can be laborious in solution-based methods. After cleavage of the oligomer from the resin, only the usual HPLC purification was required. By using this method, a stemless PNA beacon, **MB1**, was successfully prepared and characterized. Seitz and co-workers first demonstrated that PNA molecular beacon constructs do not require the stem-loop structure that is obligate for DNA MBs.<sup>13</sup> However, it is conceivable that the sequence and identity of the fluorophores might impact the degree of interaction, especially in this example, where both proximity and orientation are important in order for the pyrene units to effectively  $\pi$ - $\pi$  stack (excimer formation). Therefore, stem-loop **MB2** was designed and synthesized by using the same method.

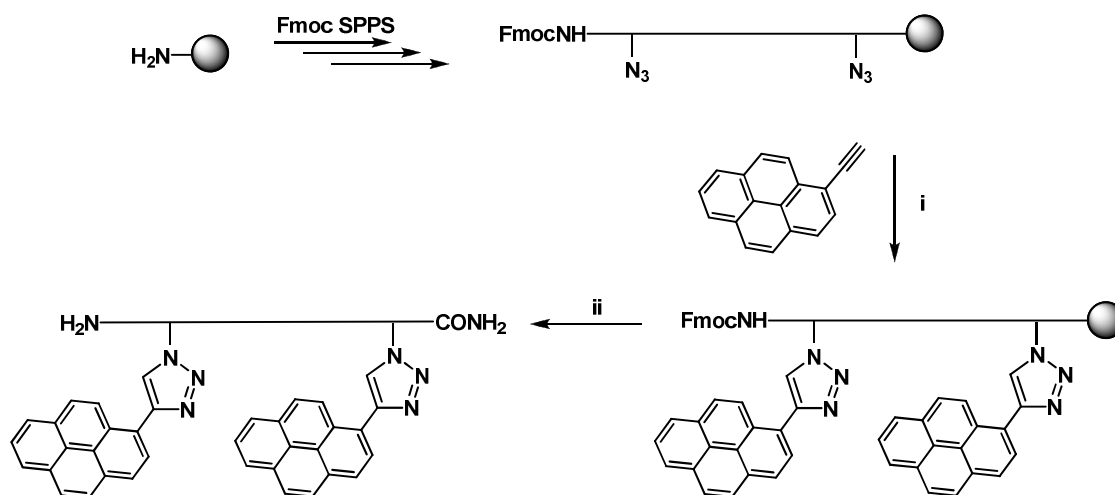
Shown in Scheme 2.2, azide-containing PNA oligomers (**PNA1-Az**, **PNA2-Az**) were synthesized by using an azide monomer with automated Fmoc SPPS protocols. Two conditions for solid-phase CuAAC have been developed. For condition **a**, CuI was used as the catalyst, and DIPEA was employed to help dissolve copper in the solvent. The resin was shaken in the mixture at room temperature under N<sub>2</sub>. Reaction progress was monitored by ESI-MS. The click reaction was observed to be complete after two days. As CuI is not stable in the presence of air or moisture, the more robust catalyst system of CuSO<sub>4</sub>·5H<sub>2</sub>O, along with a reducing agent, sodium ascorbate, was employed for condition **b** and stabilized by *N,N'*-dimethylethylenediamine (DMEDA). A mixture of isopropanol/DMSO/H<sub>2</sub>O (1:1:2, v/v/v) was used as the solvent. The resin was shaken in the aqueous solution at room temperature under N<sub>2</sub>, and the reaction was deemed complete via mass spectrometry after 16 h. The excess reactants and copper complexes were then removed by sequentially washing the resin with DMF, CH<sub>2</sub>Cl<sub>2</sub>, H<sub>2</sub>O, MeOH, and DCM. After Fmoc deprotection and resin cleavage, the pyrene-based PNA beacons were purified

by standard HPLC methods. Characterization of the oligomers was carried out by ESI-MS, which showed that two units of pyrene were simultaneously clicked to the PNA oligomer quantitatively on the solid support. The resulting oligomers, **MB1** and **MB2**, have been characterized by ESI-MS. The peaks corresponding to full-length, fully modified oligomers were observed while the mass of “unclicked” sequences were not detected.

**Table 2.1** Oligomers investigated in this study.

Name	Sequence (5'-3' or N-C)*
<b>PNA1-Az</b>	K- <b>Az</b> -CTTTCCT <u>I</u> CACTGT- <b>Az</b> -K
<b>MB1</b>	K- <b>Py</b> -CTTTCCT <u>I</u> CACTGT- <b>Py</b> -K
<b>PNA2-Az</b>	K-CAT- <b>Az</b> -CTTTCCT <u>C</u> CACTG- <b>Az</b> -ATG-K
<b>MB2</b>	K-CAT- <b>Py</b> -CTTTCCT <u>C</u> CACTG- <b>Py</b> -ATG-K
<b>PNA-Ir</b>	K- <b>Ir</b> -CTTTCCT <u>I</u> CACTGT- <b>Ir</b> -K
<b>CF-A</b>	ACAGTG <u>A</u> AGGAAAG
<b>CF-T</b>	ACAGTG <u>I</u> AGGAAAG
<b>CF-G</b>	ACAGTG <u>G</u> AGGAAAG
<b>CF-C</b>	ACAGTG <u>C</u> AGGAAAG

\*The complementary of mismatched are underlined.



**Scheme 2.2** General synthesis of PNA MBs by on-resin CuAAC. a) 1-ethynylpyrene (20 equiv.), CuI (200 equiv.), DIPEA (300 equiv.), THF/pyridine (5:3, v/v); b) 1-ethynylpyrene (15 equiv.), CuSO<sub>4</sub>·5H<sub>2</sub>O (30 equiv.), sodium ascorbate (120 equiv.), DMEDA (60 equiv.), isopropanol/DMSO/H<sub>2</sub>O (1:1:2, v/v/v); c) 20% piperidine/DMF followed by TFA/TES (95:5, v/v).

The easily accessible azide PNA monomer has the potential to facilitate screening of various PNA constructs. For example, in this work, the resin-bound azide containing PNA oligomers (5  $\mu$ mol synthesis scale) was split into several portions used for various click reactions. Thus, without the need to repeat PNA synthesis, different conditions to optimize the chemistry for the click reaction were tested. Moreover, different fluorophore alkynes could be employed to produce varied PNA probes with similar ease while the traditional method requires onerous labour and a relatively large amount of each fluorophore-containing PNA monomer.

The stability of the PNA:DNA duplexes was determined by thermal denaturation studies after annealing of PNA beacons **MB1** and **MB2** to the perfectly matched or one-base

mismatched (MM) DNA target strands. The  $T_m$  values (Table 2.2) show that the matched duplex of **MB1** demonstrated somewhat typical discrimination over single-MM targets ( $\Delta T_m=6-9$  °C), whereas the single-stranded **MB1** did not display a melt transition. On the other hand, **MB2**, designed with a stem-loop structure of four PNA base pairs and two intercalated pyrene units showed an intramolecular  $T_m$  that was comparable to its fully matched duplex with DNA. This demonstrates that PNA:PNA hybridization is extremely stable, and an even shorter stem for PNA MBs should be considered to ensure that the stem-loop structure would be disrupted upon hybridization with complementary DNA. Interestingly, thermal denaturation studies of **MB2** and MM-DNAs showed biphasic melting profiles. This might be due to a mixture of single-stranded (SS) PNA and PNA:MM-DNA duplex existing together under the experimental conditions.

Thermal denaturation studies were also carried out to determine the stability of PNA **MB2**:CF RNA duplexes (Table 2.2). The PNA:RNA duplexes showed greater thermal stability than the same DNA sequences, yet the discrimination for mismatches remained the same ( $\Delta T_m=8-10$  °C). Interestingly, the UV melt curves with RNA were monophasic.

**Table 2.2** Thermal stabilities and switching ratios of duplexes.

Oligomers <sup>[a]</sup>	$\Phi$ <sup>[b]</sup>	B <sup>[c]</sup>	SR <sup>[d]</sup>	$T_m$ (°C)
<b>MB1</b>	0.05	2750	--	n.d.
<b>MB1</b> + matched DNA	0.06	4540	1.3	59
<b>MB1</b> + MM-T DNA	0.09	5090	2.2	51
<b>MB1</b> + MM-G DNA	0.1	5690	1.6	53
<b>MB1</b> + MM-C DNA	0.1	5110	1.7	50
<b>MB2</b>	0.12	5630	--	60
<b>MB2</b> + matched DNA	0.07	3030	4.5	59
<b>MB2</b> + MM-A DNA	0.04	2240	3.2	46 & 63 <sup>[e]</sup>
<b>MB2</b> + MM-T DNA	0.04	2600	3.6	48 & 61 <sup>[e]</sup>
<b>MB2</b> + MM-C DNA	0.04	2640	3.5	48 & 64 <sup>[e]</sup>
<b>MB2</b> + matched RNA	0.1	2930	6.4	71
<b>MB2</b> + MM-A RNA	0.09	2970	5.7	63
<b>MB2</b> + MM-T RNA	0.1	3000	5.6	61
<b>MB2</b> + MM-C RNA	0.09	4400	5.4	62

[a] Annealed samples; [b] Quantum yield (0.546 for quinine sulphate in 0.5 M H<sub>2</sub>SO<sub>4</sub> as standard [c] Brightness (QY×ε356). [d] Switching ratio (F397/F475)<sub>ds</sub>/(F397/F475)<sub>ss</sub>; [e] Biphasic melting curves.

It is noteworthy that all mismatched duplexes were stable at room temperature ( $T_m$  values >25 °C), indicating that optimum discrimination of mismatched targets could only be achieved at a higher temperature. For DNA-based systems, the melting temperatures

were much more sensitive to ionic conditions, which can be manipulated to provide assay stringency, whereas PNA hybridization is much less affected by ionic conditions.

To evaluate the ability of pyrene-labeled PNAs to act as molecular beacons, their fluorescence emission spectra were recorded in the absence or presence of DNA target strands. As shown in Figure 2.2a, broad emission centred at about 475 nm (black squares) indicated excimer emission from SS-**MB1**. The two shorter wavelength emission bands at 385 and 401 nm represent monomer fluorescence. As expected, only monomer emission was observed when **MB1** was hybridized to a DNA target. The colour change could be readily detected (Figure 2.3). However, the change in excimer/monomer ratios was modest. The fluorescence spectra of one-base mismatched duplexes with **MB1** were also recorded, and the switching ratio (SR), a parameter for judging discrimination, was calculated for all duplexes (Table 2.2). The perfectly matched duplex (Table 2.2) had an SR of only 1.3; the SRs of MM duplexes are higher, thus indicating that **MB1** cannot satisfactorily discriminate fully matched targets from mismatched targets at room temperature. We hypothesized that the stemless **MB1** conformation does not sufficiently favour excimer formation; thus, in this construct, a stem-loop structure might be necessary to bias pyrene excimer formation.



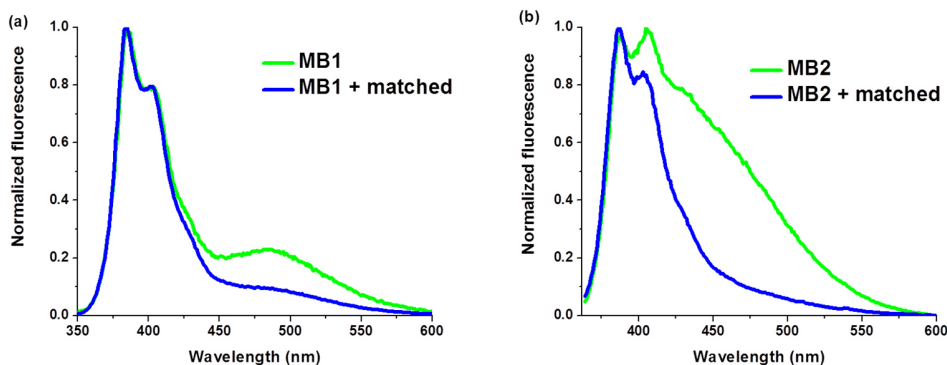


**Figure 2.2** Fluorescence spectra of a) **MB1** and b) **MB2** in the presence of matched DNA. Conditions: 2  $\mu\text{M}$  PNA and target in 100 mM NaCl, 10 mM  $\text{NaH}_2\text{PO}_4$ , 0.1 mM EDTA, pH 7, 25  $^\circ\text{C}$ . Excitation:  $\lambda_{\text{ex}} = 345$  nm.

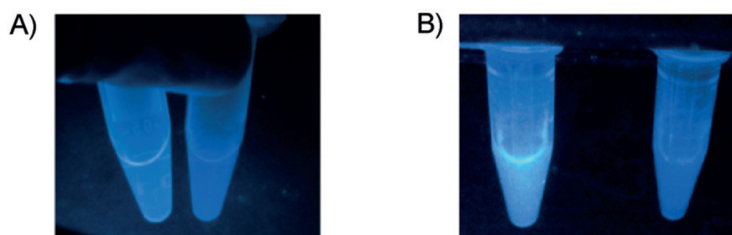


**Figure 2.3** Fluorescence images at individual strand concentration of 2  $\mu\text{M}$  under illumination at  $\lambda=365$  nm. a) Left, **MB1**; right, **MB1** + matched DNA; b) Left, **MB2**; right, **MB2** + matched DNA.

**MB2** exhibited higher fluorescence efficiency than **MB1** in terms of its better quantum yield (0.12 vs. 0.05) and brightness (5630 vs. 2750). More importantly, the fluorescence emission of stem-loop **MB2** is shown in Figure 2.2b. Prominent emission at 475 nm indicated excimer emission, along with the shorter wavelength emission peaks due to the fraction of the population of molecular beacons that possess pyrenes as discrete monomers. Likely, the stacking of pyrene chromophores in the stem region of **MB2** is partly

responsible for the excimer emission of **MB2** being recorded as a shoulder instead of as a discrete band. The addition of target DNA caused a significant decrease in the fluorescence intensity at 475 nm, indicating the disappearance of excimer. It was observed that the monomer emission of the duplex decreased as well in terms of lower quantum yields and brightness, implying a quenching phenomenon.<sup>32</sup> The origin of the quenching is likely due to the adjacent GC base pairs in the sequence of the **MB2**:DNA duplex. Nevertheless, the change in fluorescence of **MB2** before and after hybridization with target DNA is obvious at room temperature (Figure 2.3b). In contrast to the stemless MB construct, when **MB2** was challenged with the perfectly matched complement, an SR of 4.5 was observed (Table 2.2), as well as better fluorimetric discrimination of one-base mismatched targets ( $\Delta$ SR=0.9-1.3). Moreover, **MB2**:matched RNA showed the best switch (SR 6.4) and better discrimination of mismatched targets ( $\Delta$ SR=0.7-1). However, the change in excimer/monomer ratios of **MB2** was not as pronounced as that reported for stemless MB based on pyrene-modified acpcPNA (SR from 1.1 to 30.8).<sup>33</sup> Therefore, fluorescence/melting studies were performed to help us understand the relatively poor discrimination of PNA:matched duplexes over one-base mismatched duplexes (Figure 2.4). It was observed that all matched and one-base mismatched duplexes showed similar excimer emission at 25 °C and ideal differences among SS, matched duplex, and MM duplexes at around 50 °C. This indicates the best discrimination would be achieved when fluorescence studies of **MB2** are performed at 50 °C instead of at room temperature.

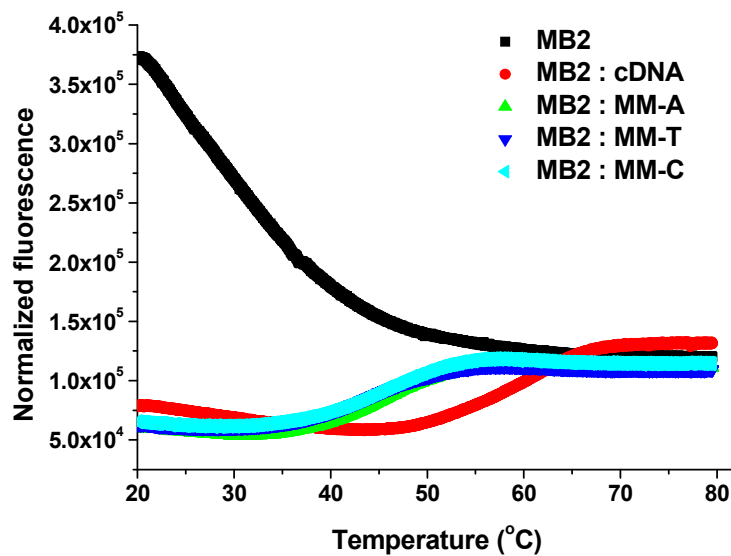


**Figure 2.4** Fluorescence-melting spectra of PNA **MB2** in the presence of DNA targets monitored at 475 nm.  $\lambda_{\text{ex}} = 345$  nm.

The formation of PNA:DNA helical structure was investigated by circular dichroism measurements. Without the target, **MB2** characteristically showed no CD signal (Figure 2.5). In the presence of a fully matched DNA target, the duplex of **MB2** displayed a positive Cotton effect at 264 nm, a shoulder at 275 nm, and a positive peak at 220 nm. Similar spectral features of one-base MM duplexes were observed and produced weaker CD signals than the fully matched duplex. This confirmed that **MB2** could form helical structures with complementary DNAs.

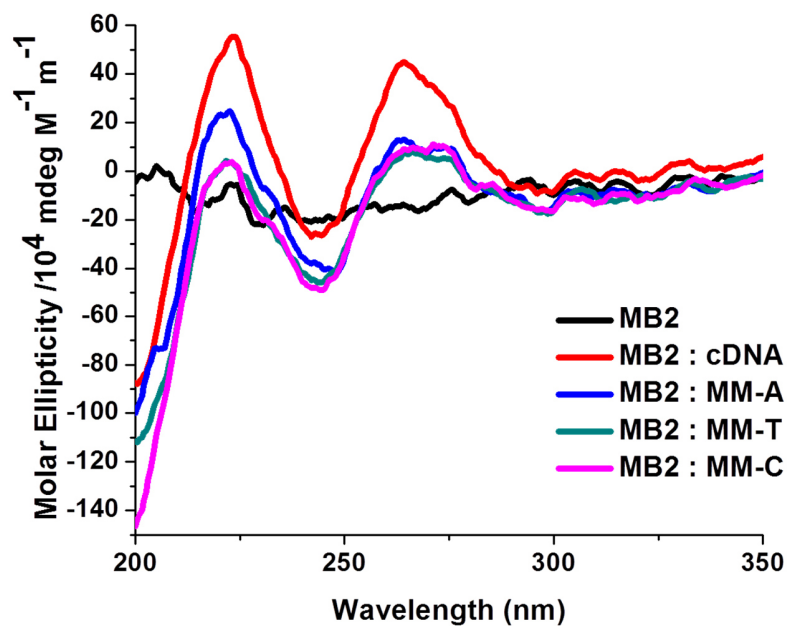


**Figure 2.5** CD spectra of **MB2** in the presence of DNA targets. Conditions: 2  $\mu$ M PNA and target strands in 100 mM NaCl, 10 mM NaH<sub>2</sub>PO<sub>4</sub>, 0.1 mM EDTA, pH 7, 25 °C.

To judge the hybridization kinetics of **MB2**, time-dependent fluorescence studies were carried out. As shown in Figure 2.6, the fluorescence intensity that represented the change in excimer/monomer ratios reached  $\sim$ 87% of the maximum readout within 1 min after the addition of fully matched target DNA. This showed the ability of **MB2** to rapidly bind DNA without an annealing step.

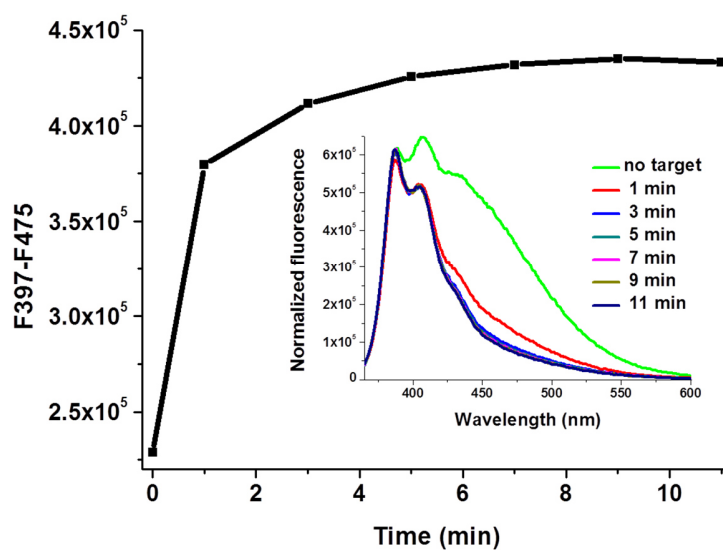


**Figure 2.6** Time-dependent fluorescence readout of **MB2** with addition of target DNA (relative emission intensity = the difference between monomer emission intensity at 397 nm and excimer emission intensity at 475 nm). Conditions: 2  $\mu$ M PNA and target in 100 mM NaCl, 10 mM NaH<sub>2</sub>PO<sub>4</sub>, 0.1 mM EDTA, pH 7, 25 °C.  $\lambda_{\text{ex}}$  = 345 nm.

The target-response curve shown in Figure 2.7 was measured by fluorescence titration under in vivo-like conditions. With the addition of 0-1.2 equiv. of target into a solution of 2  $\mu$ M **MB2**, the change in excimer/monomer ratios (F397-F475) was increased and reached a maximum at around 1 equiv. The excess target led to no further spectral changes. Furthermore, target titration studies suggested that the matched CF gene could be detected at 320 nM at the maximum change in excimer/monomer ratios when **MB2** was used as the probe.

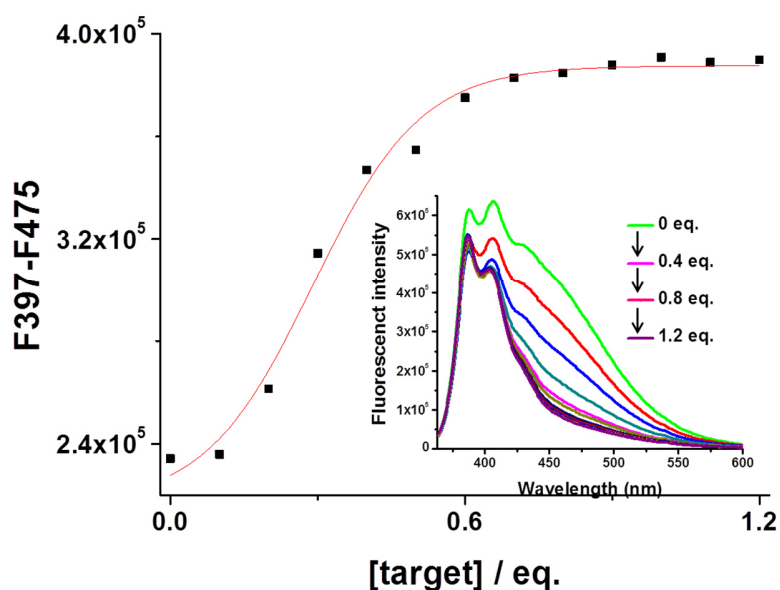
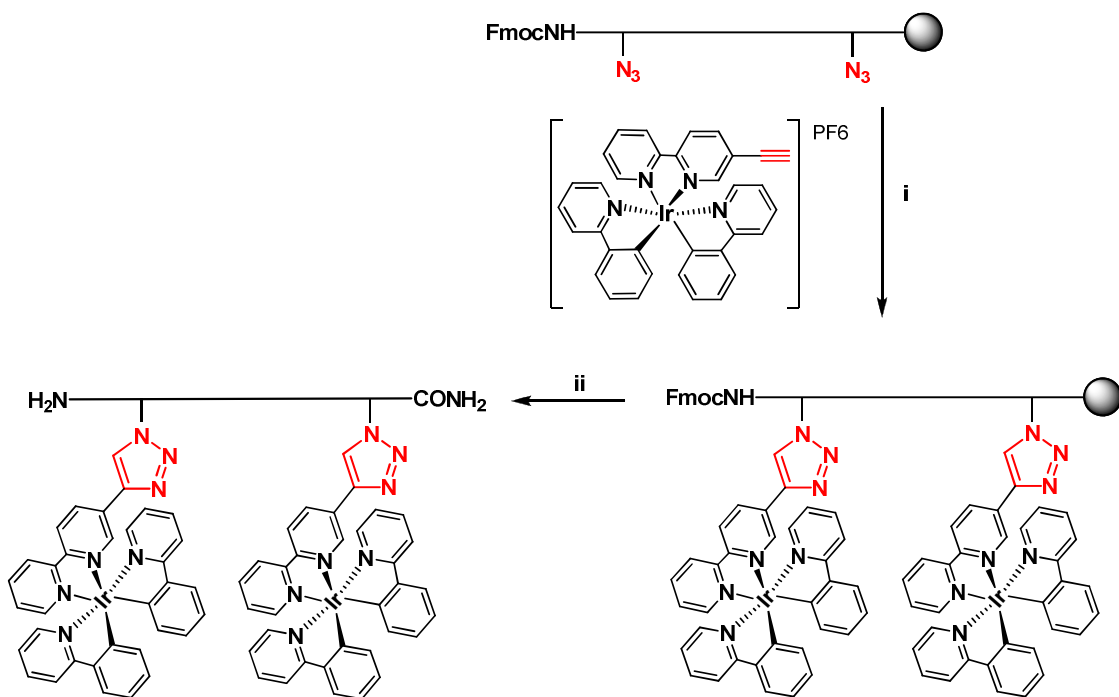


**Figure 2.7** The target-response curve of **MB2** with the increase of target concentration (relative emission intensity = the difference between monomer emission intensity at 397 nm and excimer emission intensity at 475 nm). Conditions: 2  $\mu$ M PNA in 100 mM NaCl, 10 mM NaH<sub>2</sub>PO<sub>4</sub>, 0.1 mM EDTA, pH 7, 25 °C.  $\lambda_{\text{ex}}$  = 345 nm. Limit of detection (LOD) was calculated as 320 nM.

To test the versatility of this method, the insertion of two iridium complex moieties into a PNA sequence by on-resin CuAAC was demonstrated in this work (Scheme 2.3). Characterization of the oligomer PNA-Ir by ESI-MS showed that two units of iridium complexes were successfully incorporated into the PNA oligomer quantitatively on the solid support (Table 2.3). This is in addition to our demonstration of successful insertion of single fluorenyl and pyrenyl moieties, as well as a dual pyridyl-modified PNA.<sup>31</sup>



**Scheme 2.3** Synthesis of **PNA-Ir** via on-resin CuAAC. (i) Iridium complex (20 equiv.), CuI (200 equiv.), DIPEA (300 equiv.), THF/pyridine 5:3 (v/v) (ii) 20% piperidine/DMF followed by TFA/TES 95:5 (v/v).

**Table 2.3** ESI-MS data of PNA sequences in this study.<sup>[a]</sup>

PNA	Sequence	Found m/z [M+H] <sup>+</sup>	Calc. m/z [M+H] <sup>+</sup>
<b>1-Az</b>	K- <b>Az</b> -CTTTCCTTCACTGT- <b>Az</b> -K	4547.87	4547.89
<b>MB1</b>	K- <b>Py</b> -CTTTCCTTCACTGT- <b>Py</b> -K	4776.90	4776.97
<b>2-Az</b>	K-CAT- <b>Az</b> -CTTTCCTTCACTGT- <b>Az</b> -ATG-K	5891.08	5890.42
<b>MB2</b>	K-CAT- <b>Py</b> -CTTTCCTTCACTGT- <b>Py</b> -ATG-K	6121.45	6120.51
<b>PNA- Ir</b>	K- <b>Ir</b> -CTTTCCTTCACTGT- <b>Ir</b> -K	5683.79	5683.14

[a] Az = Azide monomer, Py = triazole-linked pyrene monomer.

## 2.4 Conclusion

In summary, we have proposed a versatile and convenient method to develop new PNA molecular beacons by using on-resin click chemistry. The modification of more than one position of a PNA oligomer could be performed in a single step and lends itself to divergent syntheses of modified PNAs. Two quencher-free PNA beacons were designed and synthesized by using this method, and their properties were investigated. (Figure 2.8) Compared with stemless beacon **MB1**, stem-loop beacon **MB2** showed better discrimination upon hybridization with target sequences based on changes in



excimer/monomer ratios, indicating that the stem region is necessary in the design of PNA MBs due to the variable interactions between pyrene and neighboring base sequences. Under in vivo-like conditions, **MB2** showed rapid binding and response to target DNA. However, to achieve an excimer-monomer switching ratio as high as the previously reported pyrene-based MBs, further modification of **MB2** is still need.

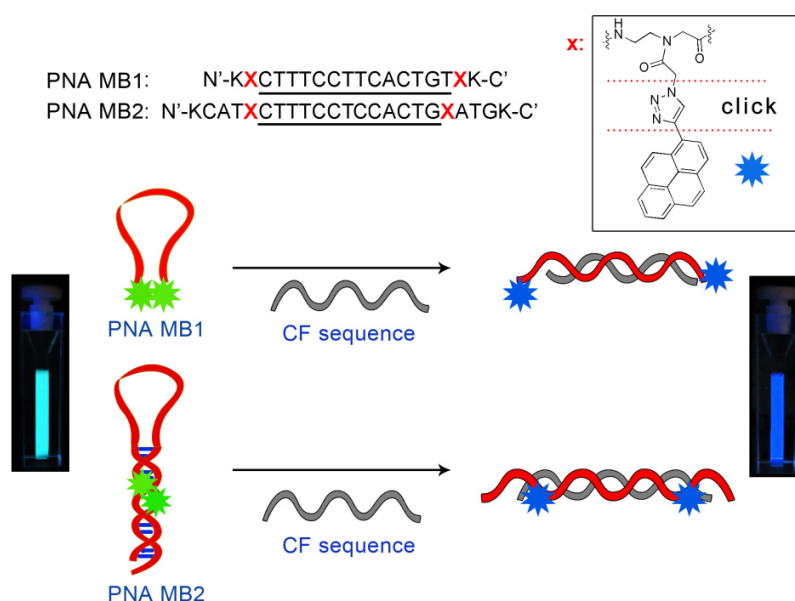


**Figure 2.8** Top: PNA sequences used for the molecular beacons, **MB1** and **MB2**, illustrating the placement of the pyrene monomer (X). N' = N-terminus, C' = C-terminus, K = *L*-lysine, target sequence underlined. Bottom: Conceptual representation of stemless and stem-loop PNA beacons and their response.

## 2.5 Experimental

### Synthesis of PNA sequences (PNA1-Az, PNA2-Az)

PNA synthesis was performed on a 5  $\mu$ mol scale using an automated ABI 433a peptide synthesizer. TGR Tentagel R-Lys(Boc)-Fmoc resin (loading 0.045 mmol/g) and PEGA-

Lys(Boc)-Fmoc resin (loading 0.113 mmol/g) were used for condition **a** and condition **b**, respectively. The synthesis was terminated without the final Fmoc deprotection. A small portion of the resin was taken for characterization and the oligomer was cleaved/deprotected under standard conditions for the characterization of **PNA1-Az** and **PNA2-Az** by ESI-MS. Other portions of the resin were taken and manipulated in manual peptide synthesis vessels.

### **General procedure for on-resin click chemistry**

Condition **a**: The resin with PNA-Az was placed in THF:pyridine (5:3) (0.8 mL) in a peptide synthesis vessel. 1-Ethynyl pyrene (20 equiv.), CuI (200 equiv.), DIPEA (300 equiv.) were added to the resin successively. The resin was shaken in the mixture at room temperature under N<sub>2</sub> for 2 days. After the reaction was deemed complete by Waters LCT Premier ESI-MS, the solvent was drained and the resin was washed sequentially with DMF, DCM, H<sub>2</sub>O, MeOH and finally DCM.

Condition **b**: 1-Ethynylpyrene (15 equiv.) in isopropanol: DMSO (1:1) (0.5 mL), CuSO<sub>4</sub>·5H<sub>2</sub>O (30 equiv.) in H<sub>2</sub>O (0.5 mL), NaAscorbate (120 equiv.) in H<sub>2</sub>O (0.5 mL) and DMEDA (60 equiv.) were added to the resin in a peptide vessel. The resin was shaken at room temperature under N<sub>2</sub> overnight. After the reaction was deemed completed by ESI-MS, the solvent was drained and the resin was washed sequentially with DMF, DCM, H<sub>2</sub>O, MeOH and finally DCM.

After condition **a** or **b**, the resin was shaken in 2 mL 20% piperidine/DMF for 15 min to remove the fmoc protecting group. Then PNA was cleaved, purified and characterized following by our previously reported procedure.<sup>34</sup>

### **Quantification of PNA oligomers**

UV-visible spectrophotometer was used to determine the concentrations of PNA solutions. 10  $\mu$ L of stock PNA sample was diluted to 1 mL for quantification and the absorbance at 260 nm of the sample was measured. 13700, 8800, 6600, 11700 and 28400<sup>16</sup> M<sup>-1</sup>cm<sup>-1</sup> were used as  $\epsilon_{260}$  values of A, T, G, C and the pyrene-modified monomer, respectively. The equation below was used for calculation.

$$c (\mu\text{M}) = \frac{1000 \times A_{260}}{13.7N_A + 8.8N_T + 11.7N_G + 6.6N_C + 28.4N_{py}}$$

### **Thermal denaturation experiments of oligomers**

UV melting experiments were carried out to measure the  $T_m$  values of oligomers in this study using the following ionic conditions: 100 mM NaCl, 10 mM Na<sub>2</sub>HPO<sub>4</sub>, 0.1 mM EDTA, pH 7.0. Samples at 2  $\mu$ M concentration were heated to 95  $^{\circ}$ C, cooled to room temperature over 1-2 hours, and placed at 4  $^{\circ}$ C overnight. Denaturation was performed from 15 to 90  $^{\circ}$ C at a temperature ramp rate of 0.5  $^{\circ}$ C/min. The  $T_m$  values are an average of three measurements and are rounded to the nearest 1  $^{\circ}$ C. The error in  $T_m$  values was  $\pm$  0.9  $^{\circ}$ C.  $T_m$  values were estimated for cooperative transitions by the first derivative method. Temperature dependent UV spectra that lacked upper and lower baselines, lacked sigmoidal shape or were indistinguishable from SS PNA intramolecular melting were deemed not to be cooperative transitions.

### **Fluorescence studies of oligomers**

Samples for all fluorescence studies were prepared in a quartz cell (path length: 1 cm) in the same ionic conditions as for the denaturation experiments. Parameters for fluorescence spectra are: excitation wavelength, 345 nm; scanning range, 350-600 nm; data interval, 0.1 nm; scan rate: 1 nm/s; temperature, 25 °C. Fluorescence denaturation was performed from 20 to 80 °C at a temperature ramp rate of 0.5 °C/min.

In the target titration fluorescence studies, a series of solutions containing the corresponding DNA target (0.2, 0.4, 0.6, 0.8, 1.0, 1.2, 1.4, 1.6, 1.8, 2.0, 2.2, 2.4  $\mu\text{M}$ ) were mixed with **MB2** (2  $\mu\text{M}$ ). The LOD value was defined as the lowest concentration of the target in a series detected at the corresponding maximum change in excimer-monomer ratios such that the fluorescence signal to noise ratio (S/N) relative to the blank solution of a medium salt buffer was  $\geq 3$ .<sup>8,32</sup>

### **Calculation of photophysical properties**

For calculation of quantum yield (QY), quinine sulfate in 0.5 M  $\text{H}_2\text{SO}_4$  ( $\Phi = 0.546$ , excitation at 355 nm) was used as standard material.<sup>7</sup> The QYs of **MB1**, **MB2** and their duplexes were calculated according to a previous report.<sup>8</sup> Absorbance at 356 nm was measured and used for excitation of the oligomers. Refractive indices were 1.333. For calculation of extinction coefficients of oligonucleotides, Beer–Lambert law ( $A = \epsilon l c$ ,  $l$ : 1 cm,  $c$ : 2  $\mu\text{M}$ ) was used. The brightness was expressed by  $\text{QY} \times \epsilon_{356}$ .

### **CD studies of oligomers**

CD spectra were measured under the same conditions of concentration and ionic strength as for denaturation experiments. Cuvette path length was 1 mm and scans were made from 400-200 nm at a rate of 100 nm/min with a data pitch of 0.5 nm and response time of 0.5 sec. Scans were averaged over 10 accumulations and are presented as molar ellipticity ( $\text{deg}\cdot\text{cm}^2\cdot\text{dmol}^{-1}$ ). Savitzky-Golay smoothing method was used.

## 2.6 Supplementary Information

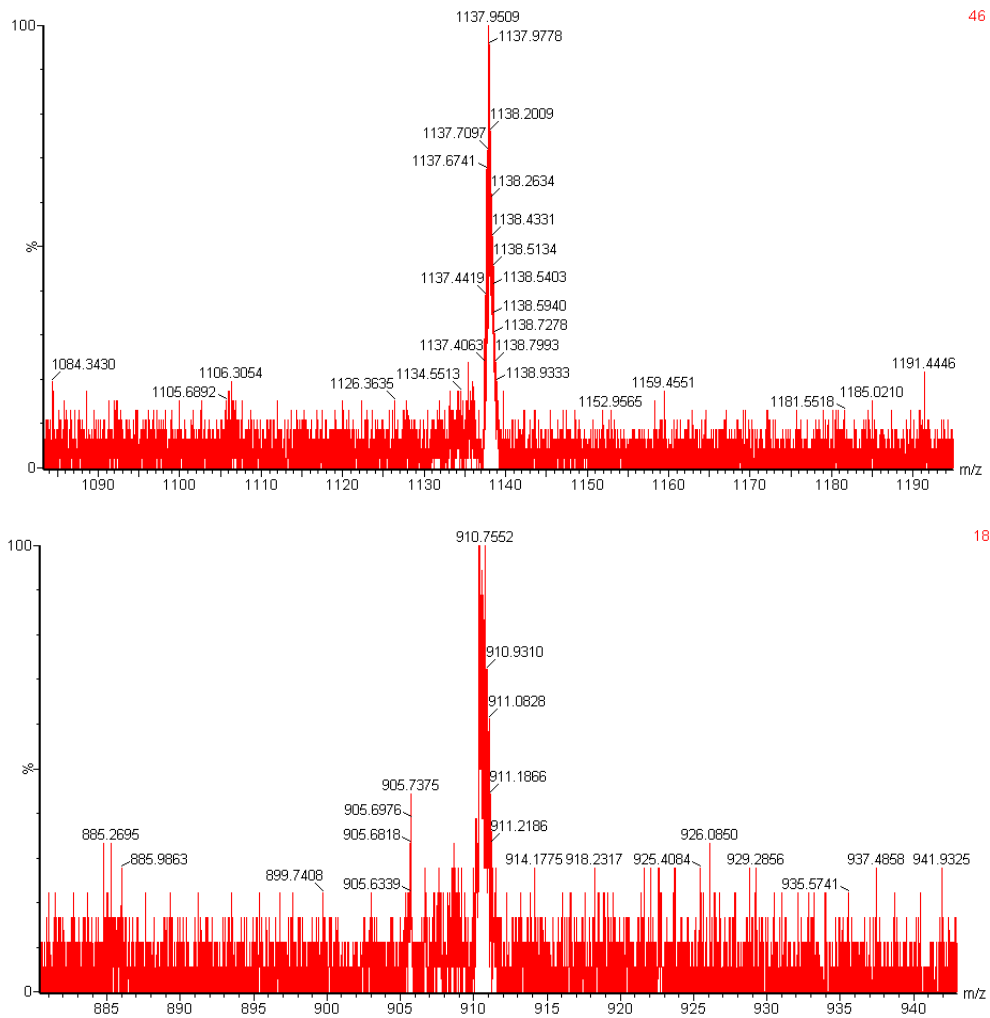
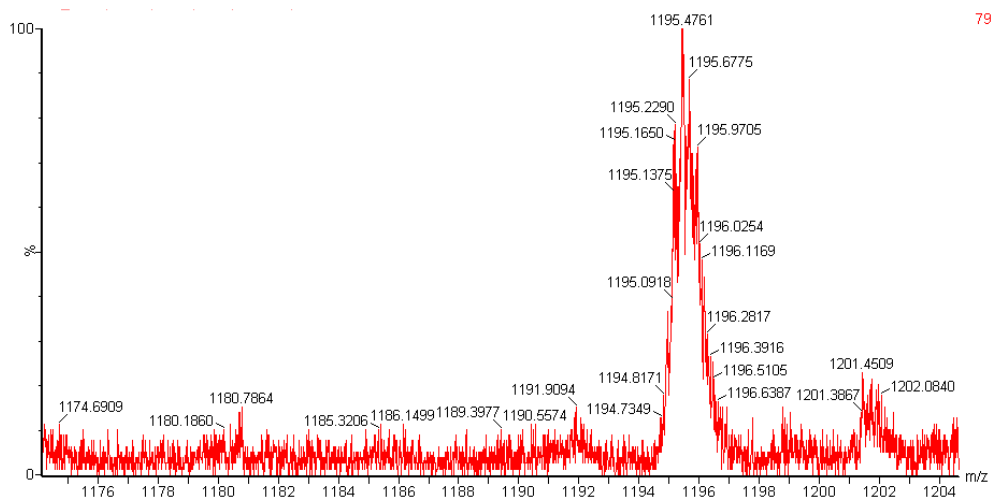
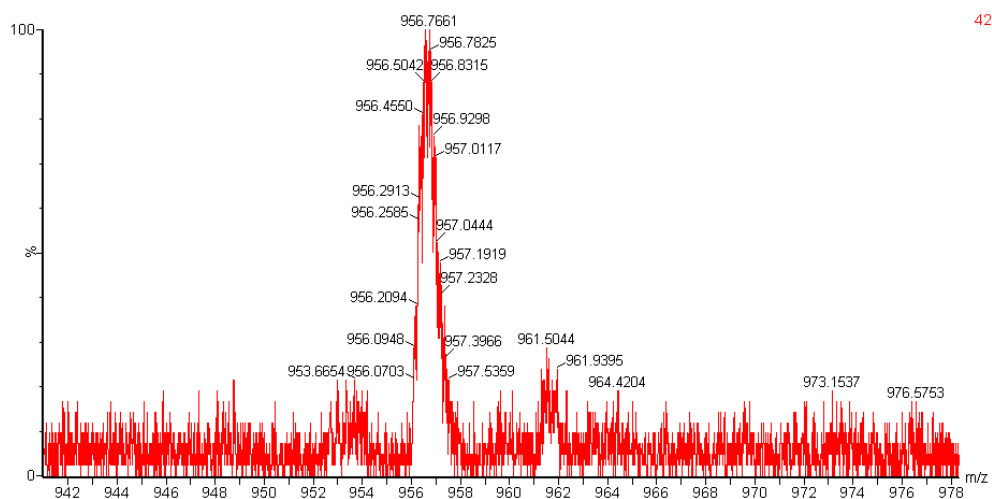


**Figure 2.9** ESI-MS spectra of 1-Az; calculated mass for  $C_{188}H_{245}N_{82}O_{56}$ : 1137.7289

$[M+4H]^{4+}$  (top),  $[M+5H]^{5+}$  (bottom).

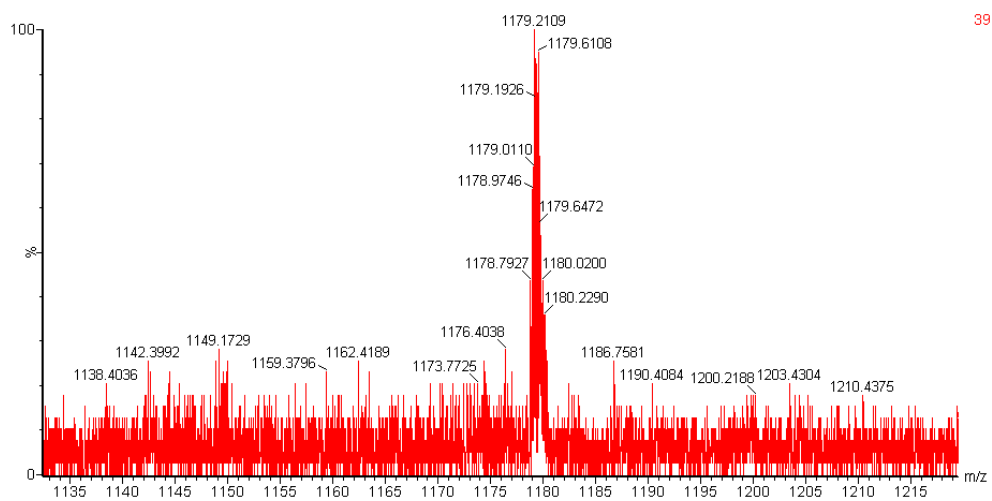


79

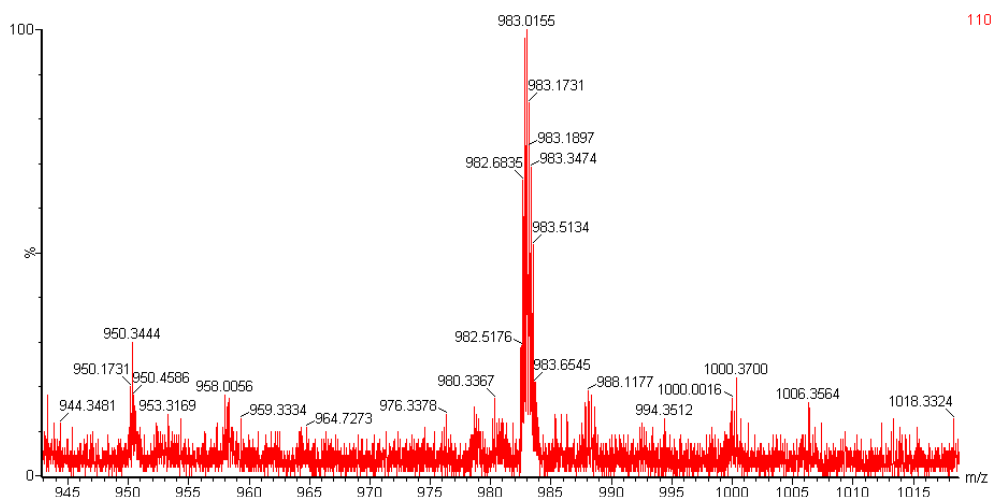


42

**Figure 2.10** ESI-MS spectra of MB1 calculated mass for  $C_{209}H_{254}N_{82}O_{54}$ : 1194.9991 [M+4H]<sup>4+</sup> (top), 956.2008 [M+5H]<sup>5+</sup> (bottom).



39

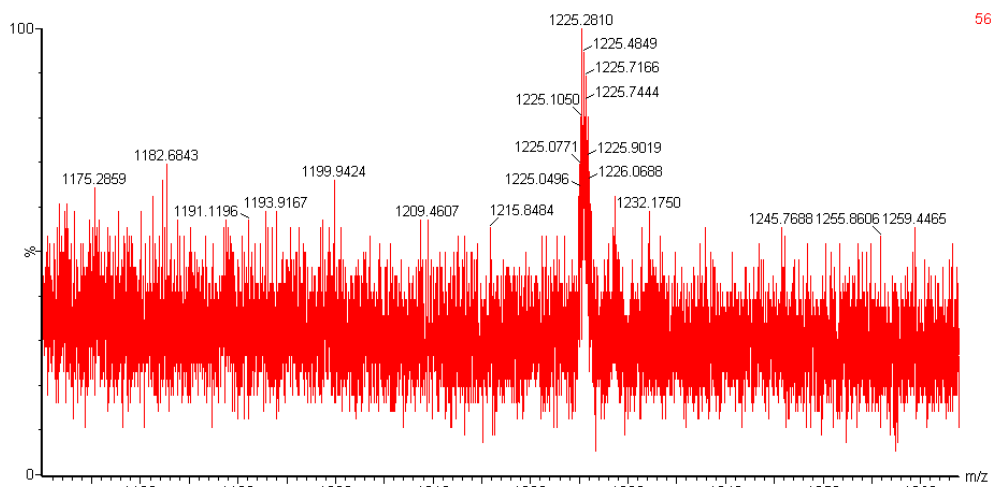


110

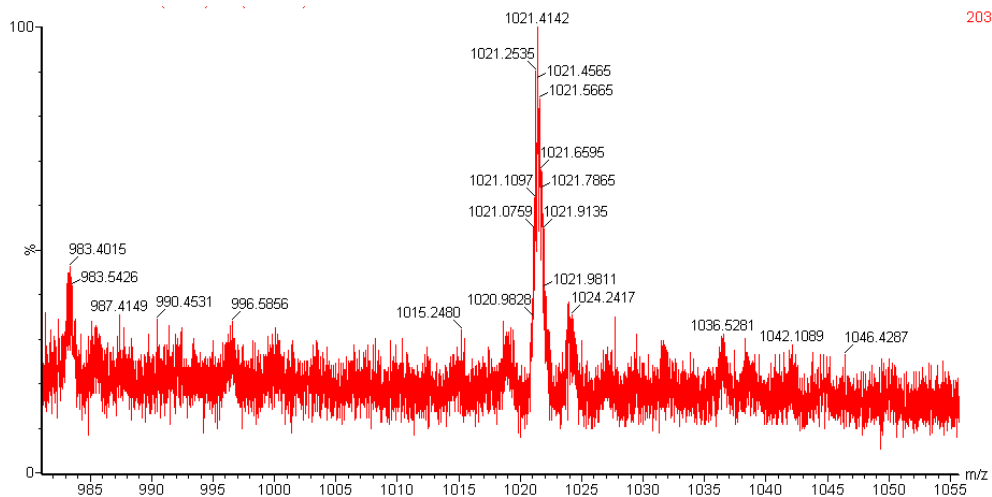
**Figure 2.11** ESI-MS spectra of PNA 2-Az; calculated mass for  $C_{241}H_{309}N_{113}O_{69}$ :

1179.5729  $[M+5H]^{5+}$  (top), 983.1454  $[M+6H]^{6+}$  (bottom).



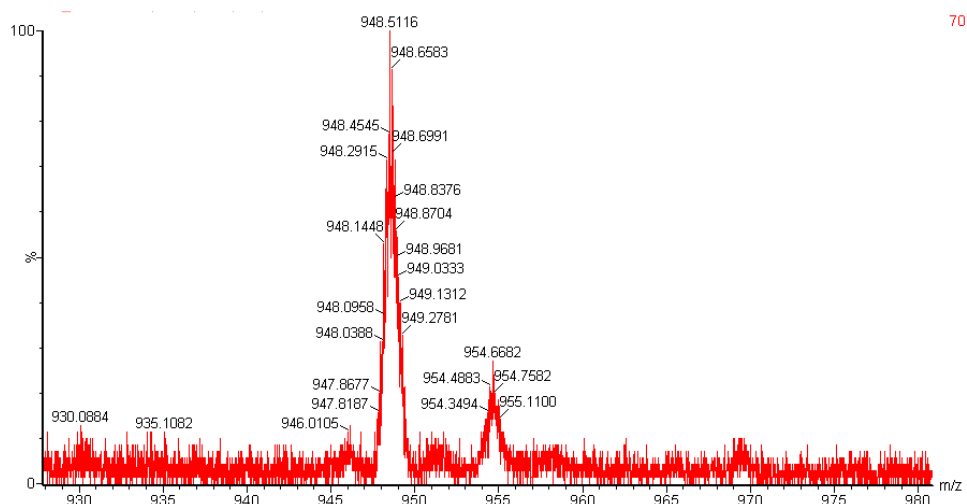


56

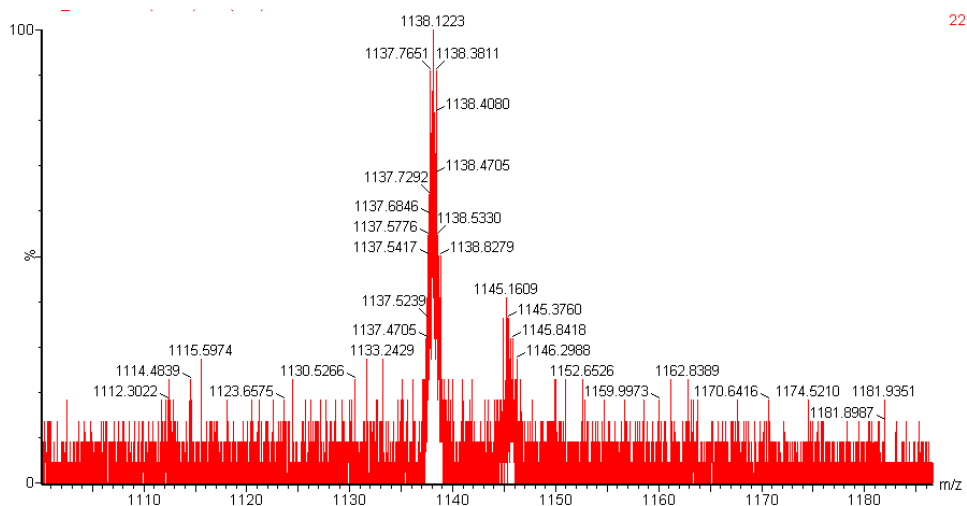


203

**Figure 2.12** ESI-MS spectra of MB2; calculated mass for  $C_{262}H_{319}N_{113}O_{67}$ : 1225.6352  $[M+5H]^{5+}$  (top), 1021.5307  $[M+6H]^{6+}$  (bottom).



70



22

**Figure 2.13** ESI-MS spectra of **PNA-Ir**; calculated mass for  $C_{241}H_{282}Ir_2N_{90}O_{54}$ : 1137.4338

[M+5H]<sup>5+</sup> (top), 948.0295 [M+6H]<sup>6+</sup> (bottom);

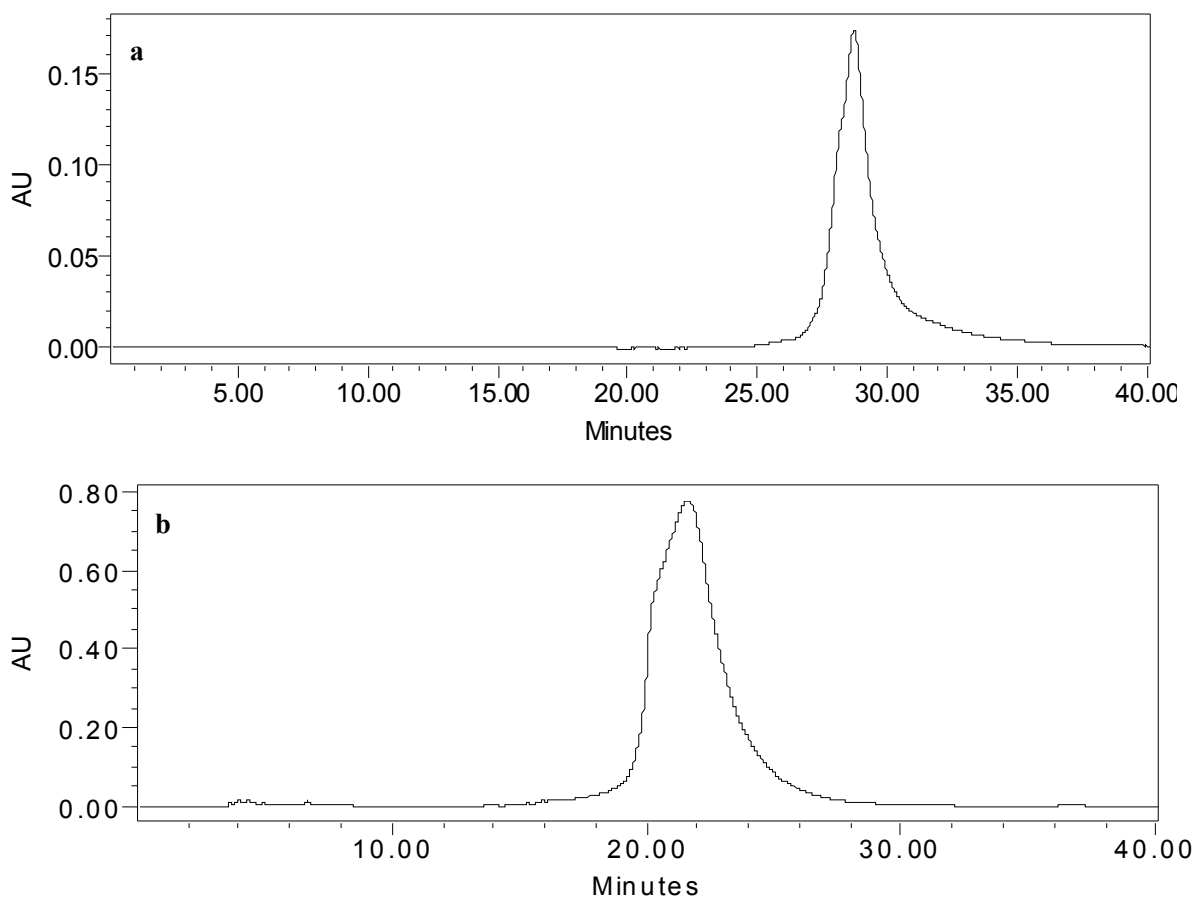


**Figure 2.14** HPLC-UV absorption spectra of PNA at 265 nm. (a) **MB1**; (b) **MB2**.

## 2.7 References

- (1) Tyagi, S.; Kramer, F. R. *Nat. Biotechnol.* **1996**, *14*, 303.
- (2) Lakowicz, J. R. *Principles of Fluorescence Spectroscopy Principles of Fluorescence Spectroscopy*; 2006.
- (3) Tyagi, S.; Bratu, D. P. D.; Kramer, F. R. *Nat. Biotechnol.* **1998**, *16*, 49.
- (4) Bernacchi, S.; Mély, Y. *Nucleic Acids Res.* **2001**, *29* (13), e62.

- (5) Marras, S. a E.; Kramer, F. R.; Tyagi, S. *Nucleic Acids Res.* **2002**, *30* (21), e122.
- (6) Garo, F.; Haner, R. *Bioconjug. Chem.* **2012**, *23*, 2105.
- (7) Karlsen, K. K.; Okholm, A.; Kjems, J.; Wengel, J. *Bioorganic Med. Chem.* **2013**, *21* (20), 6186.
- (8) Astakhova, I. K.; Samokhina, E.; Babu, B. R.; Wengel, J. *ChemBioChem* **2012**, *13* (10), 1509.
- (9) Karlsen, K. K.; Pasternak, A.; Jensen, T. B.; Wengel, J. *ChemBioChem* **2012**, *13* (4), 590.
- (10) Ortiz, E.; Estrada, G.; Lizardi, P. M. *Mol. Cell. Probes* **1998**, *12* (4), 219.
- (11) Kitagawa, F.; Ohori, Y.; Ikeda, H.; Fujimori, H.; Murakami, Y.; Nakamura, Y. *Nucleic Acids Res. Suppl.* **2002**, *2*, 143.
- (12) Xi, C.; Balberg, M.; Boppart, S. A.; Raskin, L. *Appl. Environ. Microbiol.* **2003**, *69* (9), 5673.
- (13) Englund, E. A.; Appella, D. H. *Org. Lett.* **2005**, *7* (16), 3465.
- (14) Tedeschi, T.; Tonelli, A.; Sforza, S.; Corradini, R.; Marchelli, R. *Artif. DNA PNA XNA* **2010**, *1* (2), 83.
- (15) Boonlua, C.; Vilaivan, C.; Wagenknecht, H. A.; Vilaivan, T. *Chem. - An Asian J.* **2011**, *6* (12), 3251.
- (16) Mansawat, W.; Boonlua, C.; Siriwong, K.; Vilaivan, T. *Tetrahedron* **2012**, *68* (21), 3988.

- (17) Reenabthue, N.; Boonlua, C.; Vilaivan, C.; Vilaivan, T.; Suparpprom, C.  
*Bioorganic Med. Chem. Lett.* **2011**, *21* (21), 6465.
- (18) Svanvik, N.; Westman, G.; Wang, D.; Kubista, M. *Anal. Biochem.* **2000**, *281* (1), 26.
- (19) Bethge, L.; Jarikote, D. V.; Seitz, O. *Bioorg. Med. Chem.* **2008**, *16*, 114.
- (20) Köhler, O.; Jarikote, D. V.; Seitz, O. *ChemBioChem* **2005**, *6* (1), 69.
- (21) Fujimoto, K.; Shimizu, H.; Inouye, M. *J. Org. Chem* **2004**, *69*, 3271.
- (22) Conlon, P.; Yang, C. J.; Wu, Y.; Chen, Y.; Martinez, K.; Kim, Y.; Stevens, N.; Marti, A. A.; Jockusch, S.; Turro, N. J.; Tan, W. *J Am Chem Soc.* **2008**, *130* (9), 336.
- (23) Seo, Y. J.; Hwang, G. T.; Kim, B. H. *Tetrahedron Lett.* **2006**, *47* (24), 4037.
- (24) Astakhova, I. V.; Ustinov, A. V.; Korshun, V. A.; Wengel, J. *Bioconjug. Chem.* **2011**, *22* (4), 533.
- (25) Ikeda, H.; Fujimori, F.; Murakami, Y.; Nakamura, Y. *Nucleic Acids Res. Suppl.* **2001**, *1*, 177.
- (26) Kolb, H. C.; Finn, M. G.; Sharpless, K. B. *Angew. Chem. Int. Ed.* **2001**, *40*, 2004.
- (27) Huisgen, R. *Proc. Chem. Soc.* **1961**, 357.
- (28) Gasser, G.; Hüsken, N.; Köster, S. D.; Metzler-Nolte, N. *Chem. Commun.* **2008**, 3675.
- (29) Peng, X.; Li, H.; Seidman, M. *European J. Org. Chem.* **2010**, *2010* (22), 4194.

- (30) Manicardi, A.; Accetta, A.; Tedeschi, T.; Sforza, S.; Marchelli, R.; Corradini, R. *Artif. DNA PNA XNA* **2012**, *3* (2), 53.
- (31) St Amant, A. H.; Engbers, C.; Hudson, R. H. E. *Artif. DNA PNA XNA* **2013**, *4* (1), 4.
- (32) Manoharan, M.; Tivel, K. L.; Zhao, M.; Nafisi, K.; Netzel, T. L. *J. Phys. Chem.* **1995**, *99* (48), 17461.
- (33) Maneelun, N.; Vilaivan, T. *Tetrahedron* **2013**, *69* (51), 10805.
- (34) Hudson, R. H.; Liu, Y.; Wojciechowski, F. *Can. J. Chem.* **2007**, *85* (4), 302.

## **CHAPTER III: SYNTHESIS OF CONVENTIONAL PNA MOLECULAR BEACONS VIA A CONVENIENT “CLICK- COUPLE-CLICK” APPROACH**

### **3.1 Introduction to conventional PNA beacons**

The significance of molecular beacon (MB) technology was discussed in Chapter II. The focus of this chapter is on the development of synthetic strategies for conventional PNA beacons. The first PNA-based MB that contained a PNA probe domain and a hybrid PNA-DNA stem was developed by Lizardi and co-workers in 1998 (Figure 3.1).<sup>1</sup> The reporter groups used in this study were 7-amino-4-methylcoumarin-3-acetic acid (AMCA) as the fluorophore and *p*-(dimethylaminophenylazo)benzoic acid (DABCYL) as the quencher. The synthetic scheme shows that DABCYL-succinimidyl ester was coupled to the DNA sequence which possessed an aminated thymidine by formation of a stable carboxamide. The AMCA was coupled to the amino group of glycine on PNA strand via the same reaction (Scheme 3.1). Then the modified DNA and PNA were conjugated by formation of disulfide. It has been found that this probe undergoes a fluorescent change in the presence of a complementary DNA target.

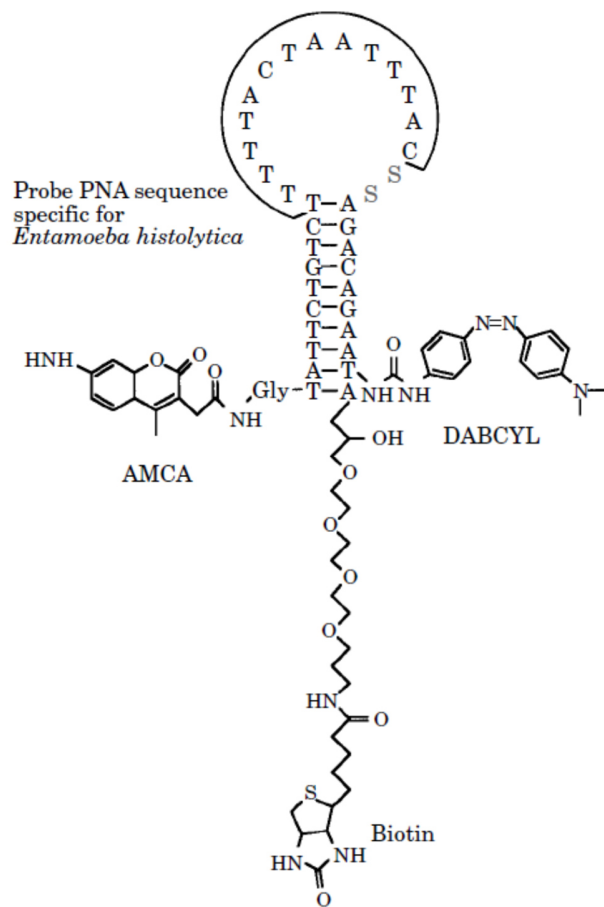
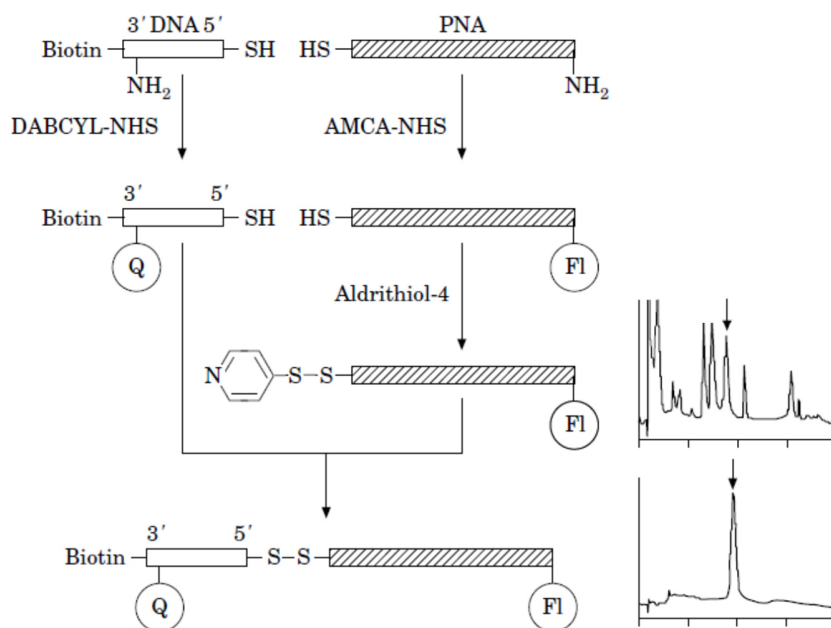


**Figure 3.1** Structure and sequence of the first PNA-DNA molecular beacon<sup>1</sup> (copyright 1998 Elsevier).

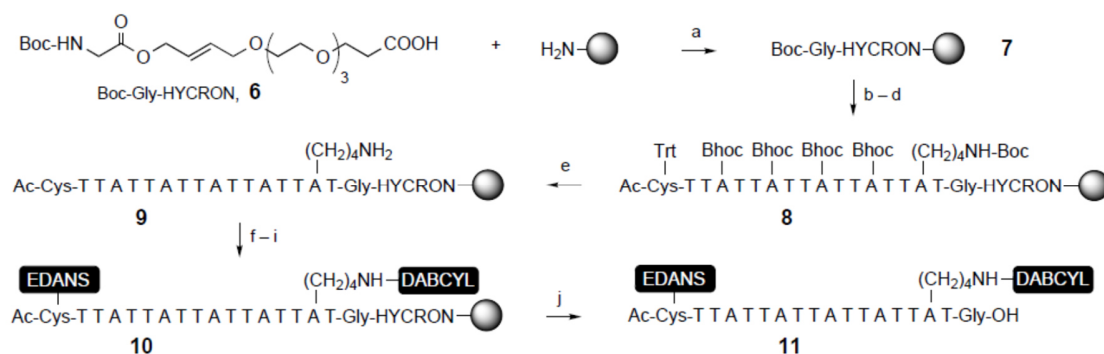




**Scheme 3.1** Synthetic scheme of first PNA-based MB<sup>1</sup> (copyright 1998 Elsevier).

Before long the synthesis of PNA MBs based on solid-phase peptide synthesis was investigated and disclosed. Different from conventional DNA MB constructs which contain a stem-loop structure, PNA MBs are usually stemless, due to the tendency of PNA to form secondary structures that results in the appended FRET pair (usually at opposite termini) being in close proximity. For example, Seitz reported a stemless PNA molecular beacon in 2000.<sup>2</sup> SPPS of PNA was performed by using a hydroxycrotyl-oligoethylene glycol-*n*-alkanoyl (HYCRON) anchor on the solid support,<sup>3</sup> which is stable under acid- or base-deprotection protocols (Scheme 3.2). The protection groups of the nucleobases on the resin-bound PNA were then removed, followed by treatment with DABCYL-hydroxysuccinimide ester (SE) in order to attach the quencher to PNA via amide formation. However, the unprotected thiol groups were found to readily form disulfide. Thus, a dithiothreitol reduction was used in order to liberate the thiol groups, to which the 5-(2-aminoethylamino)1-naphthalene sulfonic acid (EDANS) group was attached by a selective

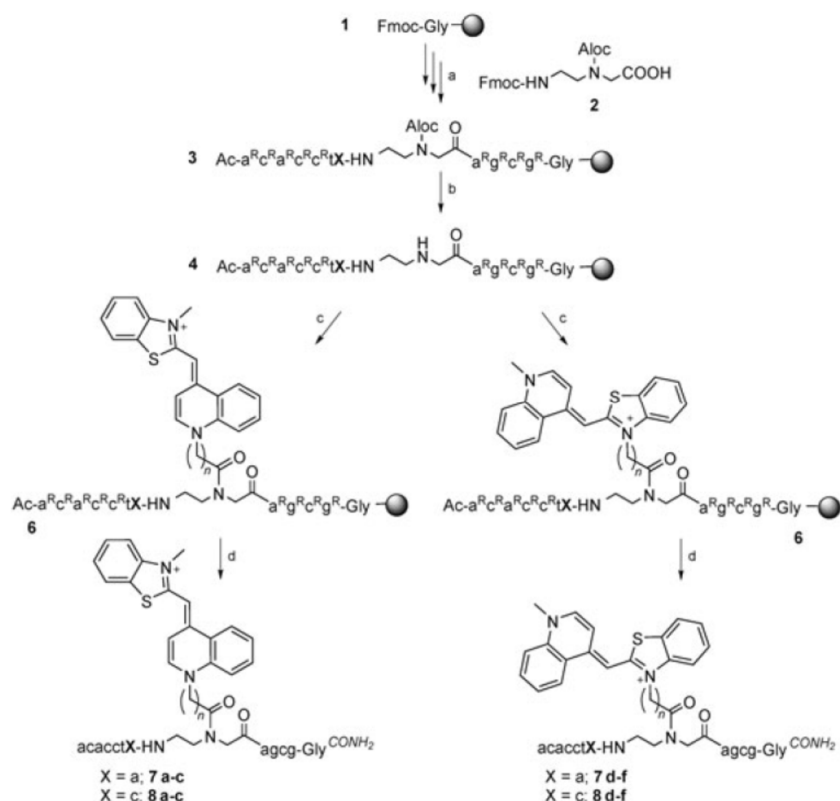
alkylation with 5-(2'-iodoacetamidoethyl)aminonaphthalene sulfonic acid (IAEDANS). Finally, the resin was cleaved by using a Pd<sup>0</sup>-catalyzing allyl transfer with morpholine scavenger. The resulting PNA beacon was demonstrated to fluoresce weakly in the single-strand state, but showed a vivid fluorescence enhancement after hybridization with a complementary oligonucleotide.



**Scheme 3.2** Solid-phase synthesis of doubly labeled PNA as probes<sup>2</sup> (copyright 2000 John Wiley and Sons).

Kitagawa *et al.* also described the synthesis of a PNA MB in 2002.<sup>4</sup> They first prepared a DABCYL-containing PNA monomer and incorporate it into PNA oligomers via Boc-based SPPS. However, the DABCYL moiety decomposed during the step of cleaving MBHA resin using a TFMSA/TFA solvent system. Therefore, they started to consider a post-synthetic method to introduce DABCYL into the PNA oligomer. Fmoc/Cbz-protected resin-bound PNA was prepared and treated with piperidine to remove Fmoc group but retain Cbz groups on all nucleotides as well as the C-lysine. The fluorescein moiety could then be coupled to PNA. Subsequently, the removal of Cbz group was accomplished followed by attachment of DABCYL to PNA. The conjugation of both fluorescein and DABCYL is achieved via amide formation.

Due to the desirable and useful properties of PNA, PNA MBs have become commercially available and the applications of PNA MBs have been extensively investigated.<sup>5-12</sup> In some studies, the fluorophore and quencher were conjugated to PNA oligomers either via the  $\epsilon$ -amino group of Lys or the N<sup>7</sup>-amino group of Glu (e.g., fluorescein-E-GCTGCCTCCCGTAGGA-K-K-DABCYL). Success was achieved by using PNA to detect and quantify rRNA in solution.<sup>8</sup> Additionally, PNA MB was able to quantify 16S rRNA of specific populations in RNA extracts of environmental samples for the genera *Dechloromonas* and *Dechlorosoma*.<sup>9</sup> Petersen *et al.* reported that short PNA beacons are effective for real-time PCR allelic discrimination of SNP.<sup>10</sup> PNA MB was also demonstrated useful for the detection of PCR amplicons in droplet-based microfluidic devices.<sup>11</sup> Two stemless PNA beacons were synthesized later by Totsingan *et al.* for the detection of full-matched or single mismatched DNA and showed high mismatch recognition via ion exchange HPLC.<sup>12</sup>



**Scheme 3.3** Synthesis of FIT probes using Thiazole Orange (TO) as a Fluorescent Base in PNAs<sup>13</sup> (copyright 2005 John Wiley and Sons).

In 2005, Seitz *et al.* developed FIT (forced intercalation) PNA fluorescent probes to distinguish single-base mutation under non-stringent hybridization condition.<sup>5,13–15</sup> These PNA probes were demonstrated sensitive hybridization probes with outstanding fluorescence enhancements upon hybridization. In the original FIT probes, the intercalator dye thiazole orange (TO) serves as a base surrogate. The TO fluorophore was first equipped with carboxyalkyl spacers of varying length in order to enable coupling with the PNA backbone (Scheme 3.3). As the central building block, an orthogonally protected backbone, Fmoc/Aloc-protected aminoethylglycine was incorporated during the Fmoc-based PNA SPPS. However, the coupling of TO moiety with the backbone that contains one free amino

group was unsuccessful due to the poor solubility of TO derivatives and low reactivity of the *N*-alkyl amino acid structure in oligomer **4**. Ultimately, pyridinium *p*-toluenesulfonate was found to help increase the solubility of TO and enable the coupling with resin-bound PNA oligomer **4**. FIT probes were further modified by adding an additional Lys conjugated with a fluorophore on the N-terminus as stemless PNA beacons (Figure 3.2).<sup>14,16</sup> The shift of the emission wavelength from the intercalator dye to the near infrared dye with high sensitivity and specificity at nonstringent conditions has been observed, which may be useful for reducing background

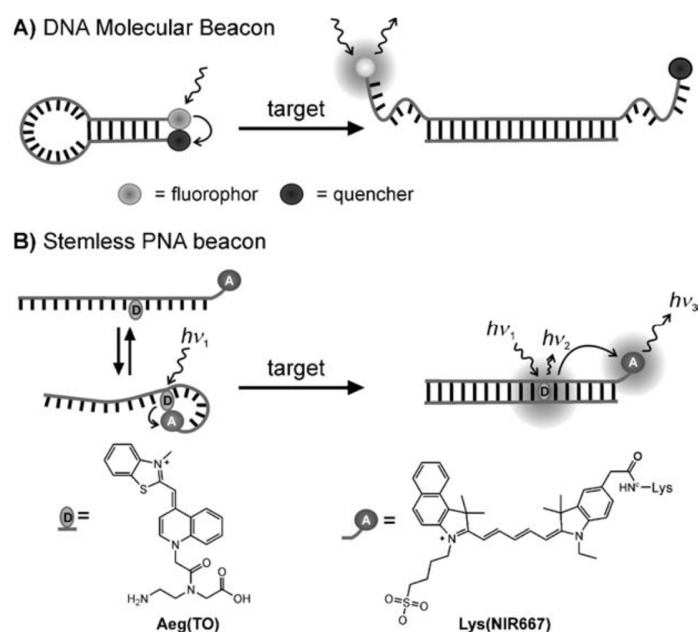


**Figure 3.2** Comparison of A) DNA molecular beacons with B) stemless FIT- PNA beacons in the detection of complementary nucleic acids. In stemless FIT-PNA beacons, an intercalator dye such as thiazole orange (TO) serves as a base surrogate that signals stacking against matched base pairs by FRET to a near infrared dye such as NIR667. PNAs.<sup>14</sup> (copyright 2008 John Wiley and Sons)

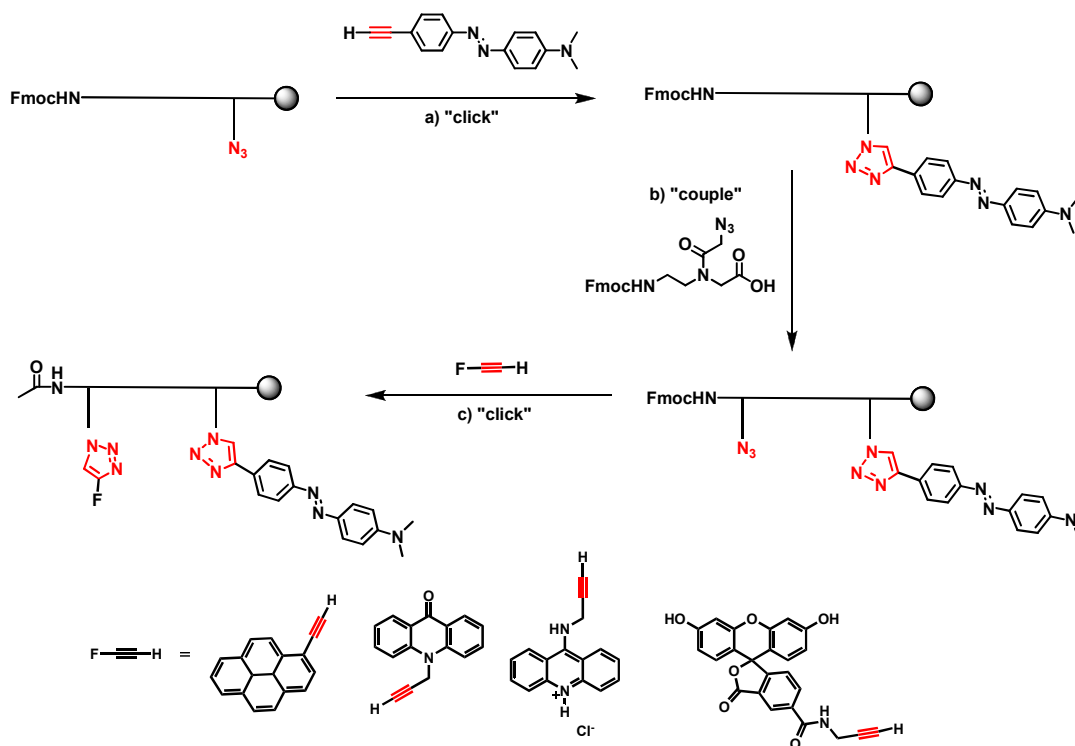
in single-base-mutation analyses and in live-cell RNA imaging. Similarly, a thiazole orange modified PNA MB (TO-PNA-MB) was reported by Yavin *et al.* and demonstrated effective to detect endogenous *K-ras* mRNA in living cells at a single base resolution.<sup>17</sup>

Although useful PNA MBs have been synthesized and have shown promise in various applications, the limitations of the conventional methods for functionalization of PNA cannot be neglected. Synthesis of a luminophore-containing PNA monomer is always tedious and labour-intensive. Insertion into a PNA sequence requires a large amount of precious modified monomer. Moreover, some modified PNA monomers are not compatible with SPPS or coupling yield is poor. Thus post-synthetic functionalization has been attempted. However, the current approach is still based on the “deprotection-coupling-deprotection-coupling” scheme, which is obviously not optimum. In order to achieve orthogonal functionalization, different protecting strategies are necessary, in which the conditions to remove the various protecting groups and the conditions to cleave the resin are usually complicated or harsh, making the procedure difficult to operate. Moreover, some fluorophores or quenchers are insoluble or unstable under coupling conditions. Additionally, it is still tedious and not very chemo-selective. Minor change of the substrates, solvents or reaction conditions would lead to failure of the whole process or low yields. Therefore, more robust and higher chemically selective post-synthetic methods are needed for developing PNA MBs. Copper-catalyzed click chemistry is obviously one of the most promising choices. My attention turned to on-resin CuAAC resulting in successful results of preparation of pyrene-based quencher-free PNA MBs (Chapter 2). However, to the best of our knowledge, click chemistry has not been applied in the development of conventional PNA beacons which contain different reporters. Hence, in this chapter a “click-couple-

click” post-synthetic approach, which is based on microwave-assisted on-resin CuAAC for divergent synthesis of conventional PNA beacons is described. This approach has the potential to significantly simplify the procedure of sequentially attaching fluorophore and quencher to PNA oligomers. It may also facilitate the screening of fluorophores or quenchers in the development of most effective PNA MBs.

### **3.2 Results and discussion**

An azide monomer has been designed and synthesized in which a nucleobase was replaced with an azide group.<sup>18</sup> It was incorporated into a PNA sequence by automated SPPS in the position close to C-terminus. DABCYL, the quencher used in this study, could be attached to PNA oligomer via microwave-assisted on-resin CuAAC followed by coupling reaction of an additional azide monomer to PNA. To improve the efficiency of on-resin CuAAC, another chelator ligand, tris(3-hydroxypropyltriazolylmethyl)amine (THPTA), was used in this study.<sup>19,20</sup> The use of THPTA reduces the tendency for copper(I) species to aggregate, while the kinetically labile triazolyl-copper binding allows rapid ligand exchange providing the alkyne and azide substrates with access to the copper center. In addition, the 3-hydroxypropyl group of THPTA enhances the aqueous solubility of the ligand which is desired in our click conditions. Moreover, the use of THPTA facilitate the removal of copper from the resin, which is crucial for the next step of coupling reaction. The functionalized PNA was subjected to Fmoc deprotection and capping on the N-terminus. A fluorophore-containing alkyne would be then clicked to the oligomer via the same click reaction. After cleavage of resin, the resulting crude PNA was purified by HPLC and characterized by ESI-MS. By using “click-couple-click”, four PNA MBs, **Py-1-Q**, **Acridone-1-Q**, **Acridine-1-Q** and **Fluorescein-1-Q**, were first synthesized (Table 3.1).



**Scheme 3.4** General synthesis of conventional PNA beacons via “click-couple-click”. **a)** (*E*)-4-((4-ethynylphenyl)diazenyl)-*N,N*-dimethylaniline (7.5 equiv.),  $\text{CuSO}_4 \cdot 5\text{H}_2\text{O}$  (15 equiv.), sodium ascorbate (60 equiv.), THPTA (30 equiv.), isopropanol/DMSO/ $\text{H}_2\text{O}$  (1:1:2, *v/v/v*), microwave 80 °C, 5 min; **b)** i) Fmoc azide monomer (5 equiv.), DIPEA (10 equiv.), HBTU (5 equiv.), DMF, room temperature, 1.5 hours; ii) 20% piperidine/DMF; iii)  $\text{Ac}_2\text{O}$ /pyridine/DMF (1:25:25, *v/v/v*) **c)** i) same as **a** except that fluorophore-containing alkyne molecules were used instead of quencher; ii) TFA/TES (95:5, *v/v*).



**Table 3.1** Oligomers investigated in this study.

Name	Sequence (5'-3' or N-C)
<b>Fmoc-1-Az</b>	CTTTCCTTCACTGT- <b>Az</b> -K
<b>Fmoc-2-Az</b>	CATCTTTCCTTCACTGTTG- <b>Az</b> -K
<b>Fmoc-1-Q</b>	CTTTCCTTCACTGT- <b>Q</b> -K
<b>Fmoc-2-Q</b>	CATCTTTCCTTCACTGTTG- <b>Q</b> -K
<b>pyrene-1-Q</b>	<b>pyrene</b> -CTTTCCTTCACTGT- <b>Q</b> -K
<b>acridone-1-Q</b>	<b>acridone</b> -CTTTCCTTCACTGT- <b>Q</b> -K
<b>acridine-1-Q</b>	<b>acridine</b> -CTTTCCTTCACTGT- <b>Q</b> -K
<b>Fluorescein-1-Q</b>	Fluorescein-CTTTCCTTCACTGT- <b>Q</b> -K
<b>pyrene-2-Q</b>	<b>pyrene</b> -CATCTTTCCTTCACTGTTG- <b>Q</b> -K
<b>Fluorescein-2-Q</b>	Fluorescein-CATCTTTCCTTCACTGTTG- <b>Q</b> -K
<b>CF-A*</b>	ACAGTG <u>A</u> AGGAAAG
<b>CF-MM-T*</b>	ACAGTG <u>T</u> AGGAAAG
<b>CF-MM-G*</b>	ACAGTG <u>G</u> AGGAAAG
<b>CF-MM-C*</b>	ACAGTG <u>C</u> AGGAAAG

\* CF = cystic fibrosis gene; CF-A is fully matched; MM-T, MM-G, MM-C are sequences with mismatched T, G, C respectively.

The stability of the PNA:DNA duplexes was determined by thermal denaturation studies after annealing of three PNA beacons to the perfectly matched or one-base mismatched (MM) DNA target strands. The  $T_m$  values (Table 3.2) show that the matched duplex of all PNA beacons demonstrated good discrimination over one base-MM targets ( $\Delta T_m=10-20$  °C), whereas the single-stranded PNAs did not display a melt transition. However, one

base-MM duplexes all have melting temperatures above 42 °C, indicating that no discrimination between matched and one-base MM duplexes could be detected at room temperature.

**Table 3.2** Thermal stabilities of duplexes. Conditions: 1  $\mu$ M PNA and target in 100 mM NaCl, 10 mM NaH<sub>2</sub>PO<sub>4</sub>, 0.1 mM EDTA, pH 7, 25°C.

Oligomers <sup>[a]</sup>	$T_m$ (°C)	$\Delta T_m$ (°C)
<b>pyrene-1-Q</b>	nd	--
<b>pyrene-1-Q + matched DNA</b>	60	--
<b>pyrene-1-Q + MM-T</b>	49	-11
<b>pyrene-1-Q + MM-G</b>	50	-10
<b>pyrene-1-Q + MM-C</b>	44	-16
<b>acridone-1-Q</b>	nd	--
<b>acridone-1-Q + matched DNA</b>	62	--
<b>acridone-1-Q + MM-T</b>	44	-18
<b>acridone-1-Q + MM-G</b>	50	-12
<b>acridone-1-Q + MM-C</b>	42	-20
<b>acridine-1-Q</b>	nd	--
<b>acridine-1-Q + matched DNA</b>	61	--
<b>acridine-1-Q + MM-T</b>	46	-15
<b>acridine-1-Q + MM-G</b>	49	-12
<b>acridine-1-Q + MM-C</b>	42	-19
<b>Fluorescein-1-Q</b>	--	--

<b>Fluorescein-1-Q</b> + matched DNA	63	--
<b>Fluorescein-1-Q</b> + MM-T	46	-17
<b>Fluorescein-1-Q</b> + MM-G	51	-12
<b>Fluorescein-1-Q</b> + MM-C	48	-15
<b>pyrene-2-Q</b>	nd	--
<b>pyrene-2-Q</b> + matched DNA	62	--
<b>pyrene-2-Q</b> + MM-T	47	-15
<b>pyrene-2-Q</b> + MM-G	49	-13
<b>pyrene-2-Q</b> + MM-C	52	-10
<b>Fluorescein-2-Q</b>	48	--
<b>Fluorescein-2-Q</b> + matched DNA	63	--
<b>Fluorescein-2-Q</b> + MM-T	48	-15
<b>Fluorescein-2-Q</b> + MM-G	49	-14
<b>Fluorescein-2-Q</b> + MM-C	47	-16

<sup>[a]</sup> Annealed samples;

To evaluate the ability of the PNAs to act as molecular beacons, their fluorescence emission spectra were recorded in the absence or presence of DNA target strands at room temperature. As shown in Figure 3.3a, the emission of matched duplex showed slightly higher fluorescence intensity than that of single stranded **pyrene-1-Q**. Expectedly, the discrimination of one-base MM duplexes from the matched duplex was not observed, although MM-G and MM-C duplexed yielded same fluorescence intensity as that from the SS PNA. However, emission of matched **acridone-1-Q** did not exhibit higher fluorescence intensity than SS PNA, indicating no “turn-on” effect of **acridone-1-Q** as a MB.

Interestingly, **acridine-1-Q** and its duplexes did not show fluorescence whereas high fluorescence intensity was found after the samples were heated for hours, suggesting decomposition of 9-aminoacridine.<sup>21</sup> In the state of single strand, **Fluorescein-1-Q** still showed comparable fluorescence to that from matched duplex, indicating low quenching efficiency.

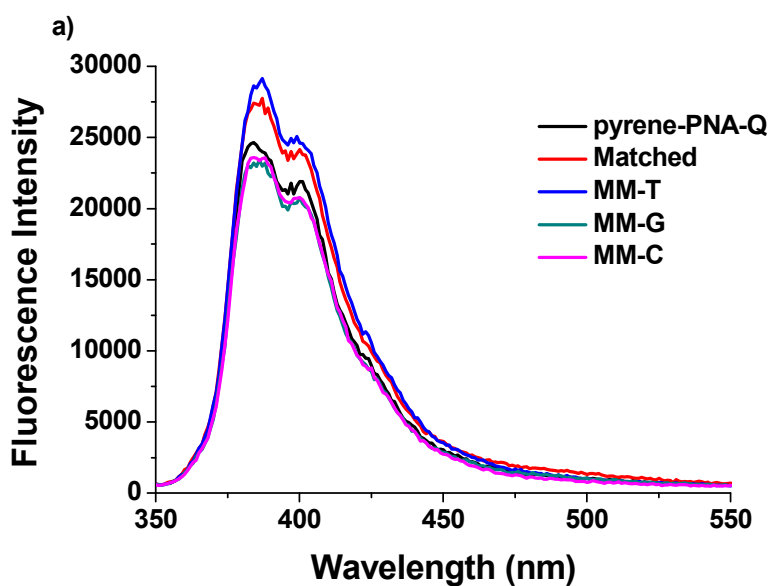


**Figure 3.3** Fluorescence spectra of **pyrene-1-Q**. Conditions: 1  $\mu$ M PNA and target in 100 mM NaCl, 10 mM  $\text{NaH}_2\text{PO}_4$ , 0.1 mM EDTA, pH 7, 25°C.  $\lambda_{\text{ex}}$  (**pyrene-1-Q**) = 345 nm.

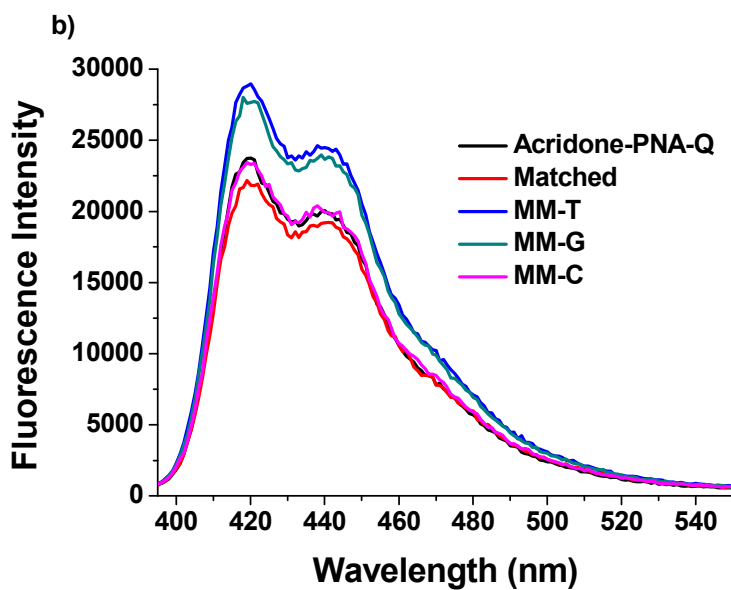


**Figure 3.4** Fluorescence spectra of **acridone-1-Q**. Conditions: 1  $\mu\text{M}$  PNA and target in 100 mM NaCl, 10 mM  $\text{NaH}_2\text{PO}_4$ , 0.1 mM EDTA, pH 7, 25°C.  $\lambda_{\text{ex}}$  (**acridone-1-Q**) = 390 nm.

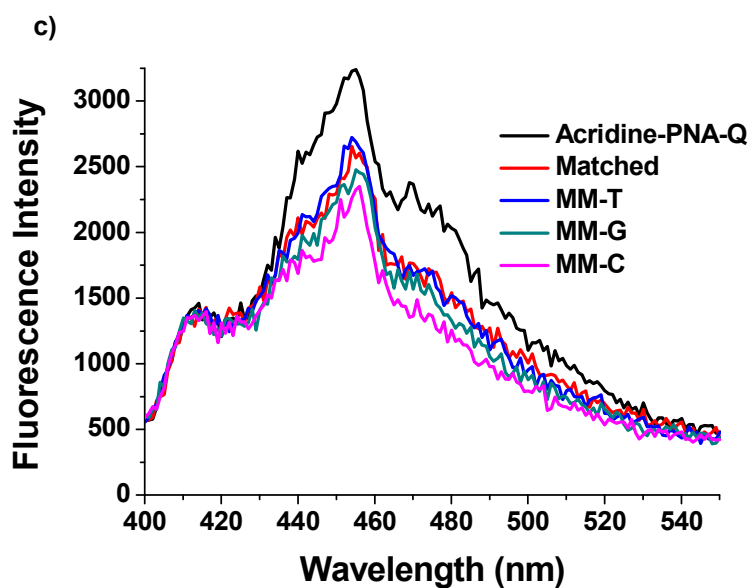


**Figure 3.5** Fluorescence spectra of **acridine-1-Q**. Conditions: 1  $\mu\text{M}$  PNA and target in 100 mM NaCl, 10 mM  $\text{NaH}_2\text{PO}_4$ , 0.1 mM EDTA, pH 7, 25°C.  $\lambda_{\text{ex}}$  (**acridine-1-Q**) = 395 nm.

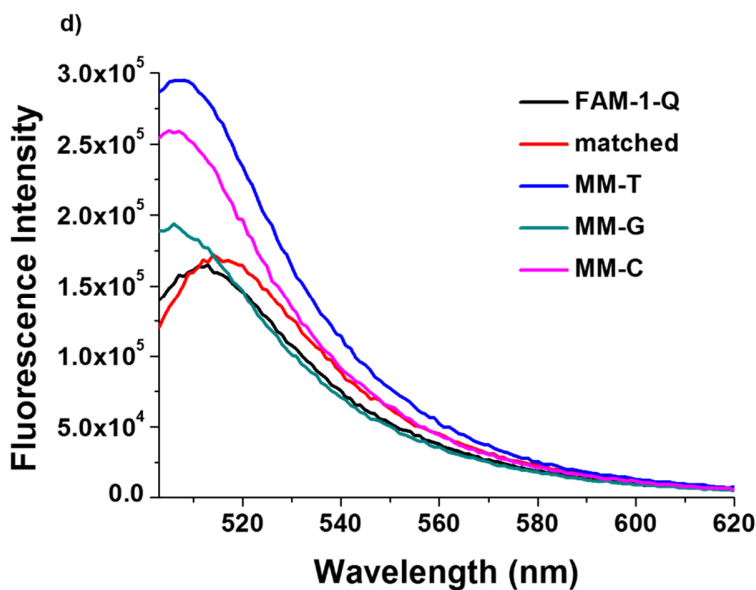


**Figure 3.6** Fluorescence spectra of **Fluorescein-1-Q**. Conditions:  $1 \mu\text{M}$  PNA and target in  $100 \text{ mM NaCl}$ ,  $10 \text{ mM NaH}_2\text{PO}_4$ ,  $0.1 \text{ mM EDTA}$ ,  $\text{pH } 7$ ,  $25^\circ\text{C}$ .  $\lambda_{\text{ex}}$  (**Fluorescein-1-Q**) =  $493 \text{ nm}$ .

To circumvent the weak “light-on” effect and poor discrimination of stemless PNA beacons, a stem-loop PNA beacon which contains one fluorophore and one quencher was designed and prepared. Considering that hairpin structure PNA was too stable to measure in water<sup>18</sup>, a PNA sequence **2** with a one-base mismatched stem was synthesized via Fmoc SPPS followed by “click-couple-click” of **2** to yield **pyrene-2-Q** and **Fluorescein-2-Q** by using pyrene and fluorescein as the fluorophores (Table 3.1). The successful preparation of **pyrene-2-Q** and **Fluorescein-2-Q** demonstrated that our “click-couple-click” method is not sequence-sensitive, which would be of great benefit in developing various PNA MBs.

Thermal studies were performed to investigate the stability of these two stem-loop PNA MBs. Surprisingly, the melting curves of **pyrene-2-Q** did not show binding, indicating no stem was formed. Matched duplex of **pyrene-2-Q** has been found to have good

discrimination over the one-base mismatched targets (10-15 °C) (Table 3.2). However, the melting profiles of **Fluorescein-2-Q** displayed a  $T_m$  value of 48 °C and decent discrimination between matched and one-base mismatched duplexes (14-16 °C), demonstrating weak binding of the stem region of PNA oligomer **2**.

In order to assess the ability as PNA MBs of **Py-2-Q** and **Fluorescein-2-Q**, fluorescence studies were carried out. Disappointedly, their SS, matched duplex and MM's all showed similar fluorescence intensity, suggesting ineffective quenching.

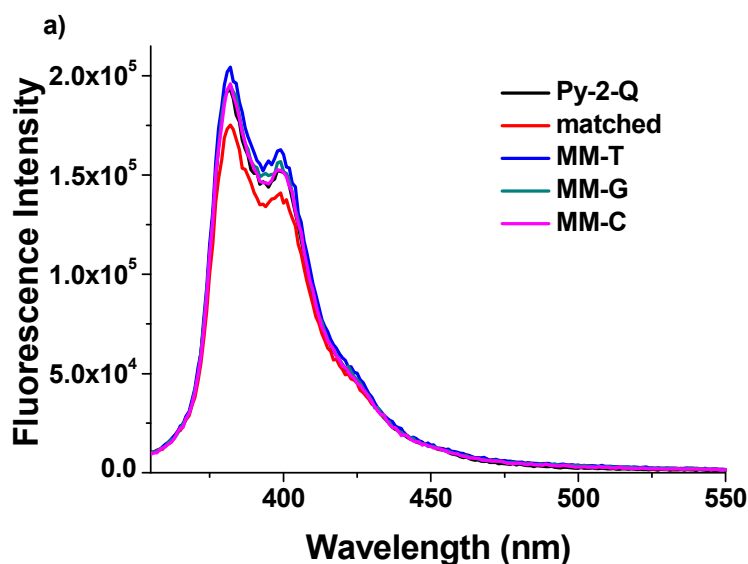


**Figure 3.7** Fluorescence spectra of **pyrene-2-Q**. Conditions: 1  $\mu$ M PNA and target in 100 mM NaCl, 10 mM  $\text{NaH}_2\text{PO}_4$ , 0.1 mM EDTA, pH 7, 25°C.  $\lambda_{\text{ex}}$  (**pyrene-2-Q**) = 345 nm.

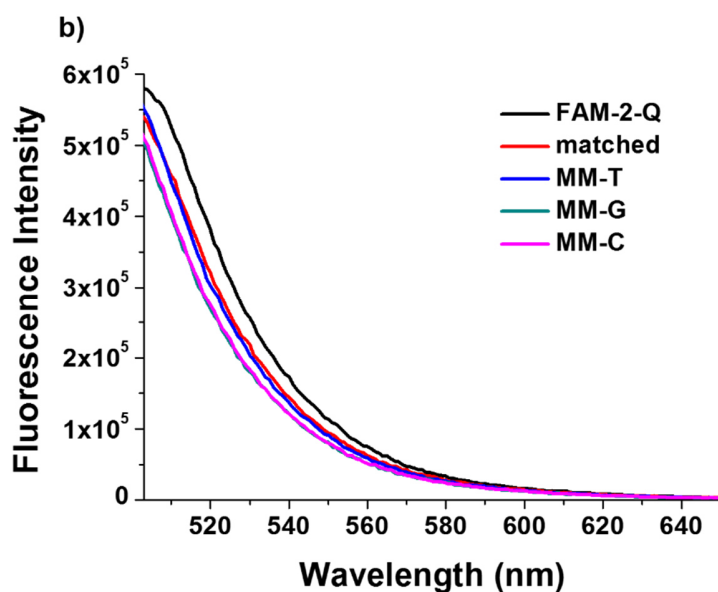


**Figure 3.8** Fluorescence spectra of **Fluorescein-2-Q**. Conditions: 1  $\mu$ M PNA and target in 100 mM NaCl, 10 mM NaH<sub>2</sub>PO<sub>4</sub>, 0.1 mM EDTA, pH 7, 25°C.  $\lambda_{\text{ex}}$  (**Fluorescein-2-Q**) = 493 nm.

### 3.3 Conclusion

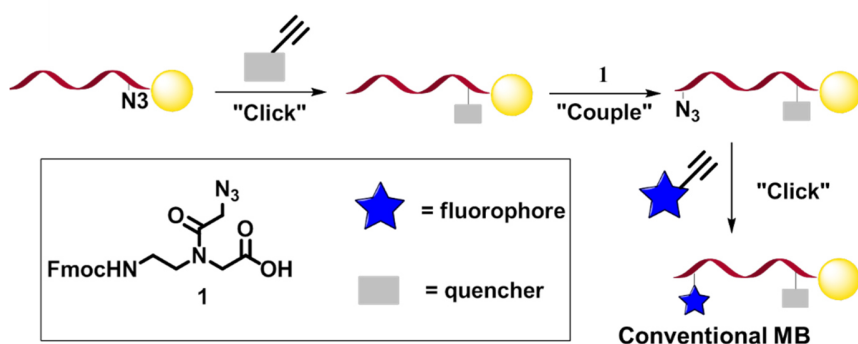


**Figure 3.9** Synthesis of conventional PNA beacons via “click-couple-click”.

In this chapter, an approach based on on-resin “click-couple-click” method has been developed (Figure 3.9). It has several advantages: 1) fast; the microwave-assisted CuAAC only takes 5 minutes and the coupling of second azide monomer 1.5 hours. the whole



synthetic procedure of “click-couple-click” could be completed within 3 hours giving quantitative yields without the need of preparing modified PNA monomers or extremely different reaction conditions; 2) robust; the click reaction is mild and highly chemically selective without any incompatibility issue with other functional moieties on reactants; the reaction condition is operated easily because it is not sensitive to water, oxygen or light; 3) facile; like other post-synthetic methodologies, multi-functionalization of PNA oligomers could be achieved in one step; the resin-bound PNA-Q may be split into portions and each portion would be used for the click of various fluorophores; in this way, a series of PNA beacons could be synthesized and evaluated; this is also helpful in screening useful fluorophores for the application of PNA MBs; 4) convenient; only washing the resin with solvents is required for the work up that is operationally simple and fast; only final HPLC purification after resin cleavage is needed.

In spite of convenience and versatility of “click-couple-click” method for the development of PNA MBs have been demonstrated, the PNA MBs did not yield “turn-on” results or discrimination of single-base mismatch at room temperature. The observed poor quenching effect could be influenced by the sequence, as other studies have shown promising results by using Fluorescein and DABCYL in stemless PNA MBs.<sup>4,5,8,18</sup> Further studies are aimed to improve the ability of PNA MBs such as attachment of two or more DABCYL molecules on one end of the sequence or use of a different type of quencher to improve the quenching effects.

### 3.4 Experimental

#### Synthesis of Fmoc-1-Az and Fmoc-2-Az

PNA synthesis was performed on a 5  $\mu$ mol scale using an automated ABI 433a peptide synthesizer. SpheriTide-Lys(Boc)-Fmoc resin (loading 0.057 mmol/g) was used. The synthesis was terminated without the final Fmoc deprotection. A small portion of the resin was taken for characterization and the oligomer was cleaved/deprotected under standard conditions for the characterization of **Fmoc-1-Az** and **Fmoc-2-Az** by Waters LCT Premier ESI-MS. Other portions of the resin were taken and manipulated in manual peptide vessels.

#### General procedure for microwave on-resin click chemistry

The resin with PNA-Az was placed in isopropanol (0.25 mL) in a peptide vessel. Alkyne (7.5 equiv.) in DMSO (0.25 mL), sodium ascorbate (60 equiv.) in water (0.2 mL), THPTA (30 equiv.) in water (0.2 mL) and  $\text{CuSO}_4 \cdot 5\text{H}_2\text{O}$  (15 equiv.) in water (0.1 mL) were added to the resin successively. The resin was heated to 80 °C for 5 min by using CEM Discover microwave reactor. After this, the solvent was drained and the resin was washed sequentially with DMF, DCM,  $\text{H}_2\text{O}$ , DMF and finally DCM.

#### General procedure for on-resin coupling reaction

The resin with PNA-Q was shaken in 2 mL 20% piperidine/DMF for 15 min to remove the Fmoc protecting group and washed with DMF as well as DCM. Fmoc azide monomer (5 equiv.) was stirred in DMF (3 mL) in a round bottom flask on ice. HBTU (5 equiv.) and DIPEA (10 equiv.) were added into the flask. The mixture was stirred on ice for 15 min and added to the resin. The resin was then shaken at room temperature for 1.5 hr. After the

reaction, the solvent was drained and the resin was washed with DMF as well as DCM. The resin was then shaken in 2 mL 20% piperidine/DMF for 15 min to remove the terminal Fmoc group and shaken in 3 mL Ac<sub>2</sub>O/pyridine/DMF (×2) for 15 min to cap the terminal amine group. After “click-couple-click”, PNA was cleaved, purified and characterized following by our previously reported procedure.<sup>22</sup>

**Table 3.3** ESI-MS data of PNA sequences in this study.<sup>[a]</sup>

Name	Sequence (5'-3' or N-C)	Calc.	
		Found m/z	m/z
		[M+H] <sup>+</sup>	[M+H] <sup>+</sup>
<b>Fmoc-1-Az</b>	CTTTCCTTCACTGT- <b>Az</b> -K	4238.3296	4238.1883
<b>Fmoc-2-Az</b>	CATCTTTCCTTCACTGTTG- <b>Az</b> -K	5588.1495	5588.4866
<b>Fmoc-1-Q</b>	CTTTCCTTCACTGT- <b>Q</b> -K	4487.6560	4487.5036
<b>Fmoc-2-Q</b>	CATCTTTCCTTCACTGTTG- <b>Q</b> -K	5837.9668	5837.8019
<b>Fmoc-Az-1-Q</b>	Fmoc- <b>Az</b> -CTTTCCTTCACTGT- <b>Q</b> -K	4670.9842	4670.6735
<b>Fmoc-Az-2-Q</b>	Fmoc- <b>Az</b> -CATCTTTCCTTCACTGTTG- <b>Q</b> -K	6021.0658	6020.9719
<b>Pyrene-1-Q</b>	<b>Pyrene</b> -CTTTCCTTCACTGT- <b>Q</b> -K	4716.31	4716.745
<b>Acridone-1-Q</b>	<b>Acridone</b> -CTTTCCTTCACTGT- <b>Q</b> -K	4725.1156	4725.753
<b>Acridine-1-Q</b>	<b>Acridine</b> -CTTTCCTTCACTGT- <b>Q</b> -K	4722.7174	4722.7524
<b>Fluorescein-1-Q</b>	<b>Fluorescein</b> -CTTTCCTTCACTGT- <b>Q</b> -K	4903.8030	4903.8539
<b>Pyrene-2-Q</b>	<b>Pyrene</b> -CATCTTTCCTTCACTGTTG- <b>Q</b> -K	6067.0258	6067.0434
<b>Fluorescein-2-Q</b>	<b>Fluorescein</b> -CATCTTTCCTTCACTGTTG- <b>Q</b> -K	6253.9048	6254.1522

<sup>a</sup> Az = Azide monomer, Q = triazole linked DABCYL monomer, Pyrene = triazole-linked pyrene monomer, Acridone = triazole-linked acridone monomer, Acridine = triazole-linked acridine monomer, Fluorescein = triazole-linked acridine monomer.

**Calculation of the extinction coefficient for triazole linked DABCYL monomer, triazole-linked acridone monomer and triazole-linked acridine monomer**

The triazole monomers were prepared by Ms. Christie Ettles. A stock solution of luminophore-triazole compounds was prepared in 10% DMSO/H<sub>2</sub>O (1 mg in 1.0 mL). From this solution an intermediate diluted solution was prepared, which was used to prepare the final solutions with a 10  $\mu$ L, 20  $\mu$ L, 30  $\mu$ L, 40  $\mu$ L, 50  $\mu$ L, 60  $\mu$ L, and 70  $\mu$ L of the diluted solution in 1 mL H<sub>2</sub>O. Each solution was prepared in triplicate and the absorbance of the solutions were evaluated within the range of 200-500 nm at a scan speed of 600 nm/min.

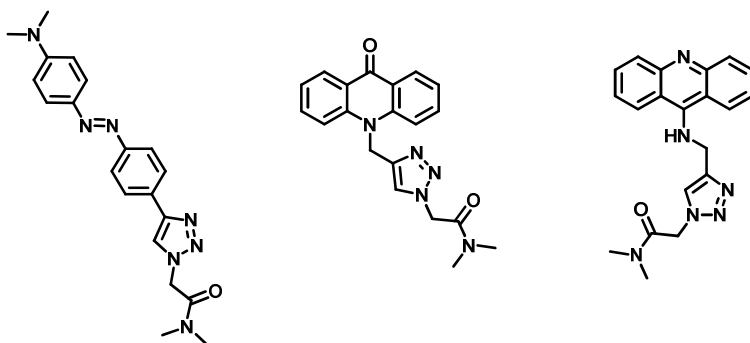


**Figure 3.10** Unpublished structures of triazole linked DABCYL monomer, triazole-linked acridone monomer and triazole-linked acridine monomer (from left to right).

### **Quantification of PNA oligomers**

UV-visible spectrophotometer was used to determine the concentrations of PNA solutions. 10  $\mu\text{L}$  of stock PNA sample was diluted to 1 mL for quantification and the absorbance at 260 nm of the sample was measured. 13700, 8800, 6600, 11700, 2490, 28400,<sup>23</sup> 42870, 43740 and 21000<sup>24</sup>  $\text{M}^{-1}\text{cm}^{-1}$  were used as  $\epsilon_{260}$  values of A, T, G, C, pyrene-modified, acridone-modified and acridine-modified monomer, respectively. The equation  $A=\epsilon cl$  was used for calculation.  $\epsilon_{260}$  of each PNA MB was the sum of the extinction coefficients of the individual bases that comprises the oligomer.

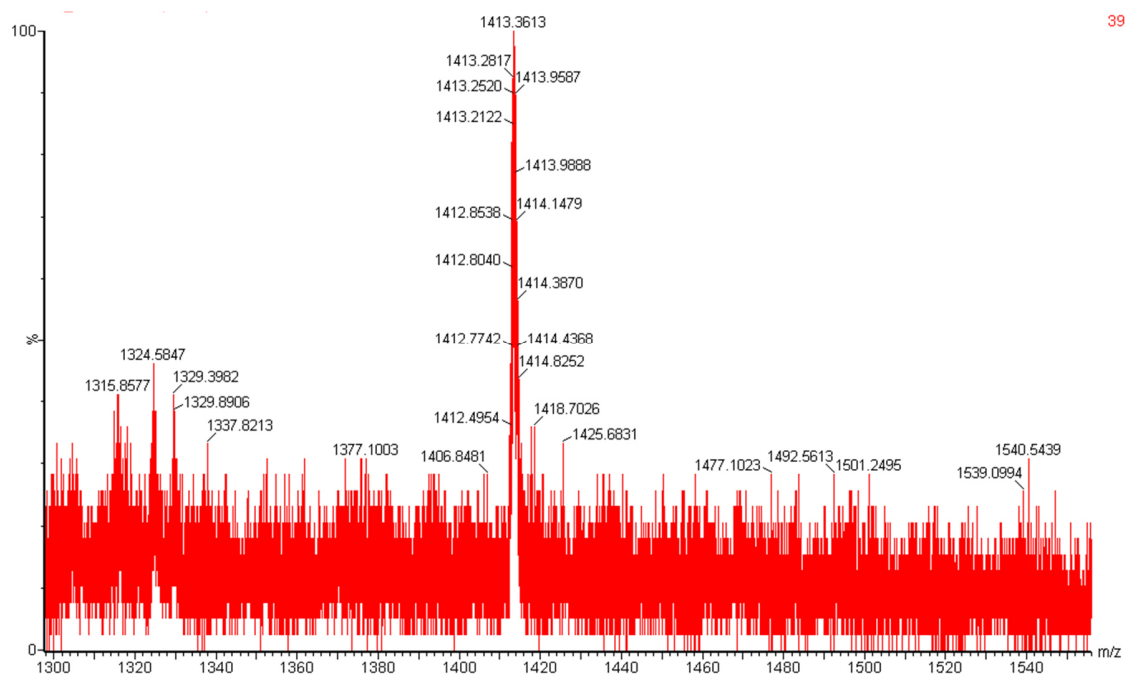
### **Thermal denaturation experiments of oligomers**

UV melting experiments were carried out to measure the  $T_m$  values of oligomers in this study using the following ionic conditions: 100 mM NaCl, 10 mM  $\text{Na}_2\text{HPO}_4$ , 0.1 mM EDTA, pH 7.0. Samples at 1  $\mu\text{M}$  concentration were heated to 95  $^\circ\text{C}$ , cooled to room temperature over 1-2 hours, and placed at 4  $^\circ\text{C}$  overnight. Denaturation was performed from 15 to 90  $^\circ\text{C}$  at a temperature ramp rate of 0.5  $^\circ\text{C}/\text{min}$ . The  $T_m$  values are an average of three measurements and are rounded to the nearest 1  $^\circ\text{C}$ . The error in  $T_m$  values was  $\pm 0.9$   $^\circ\text{C}$ .  $T_m$  values were estimated for cooperative transitions by the first derivative method. Temperature dependent UV spectra that lacked upper and lower baselines, lacked sigmoidal shape or were indistinguishable from SS PNA intramolecular melting were deemed not to be cooperative transitions.

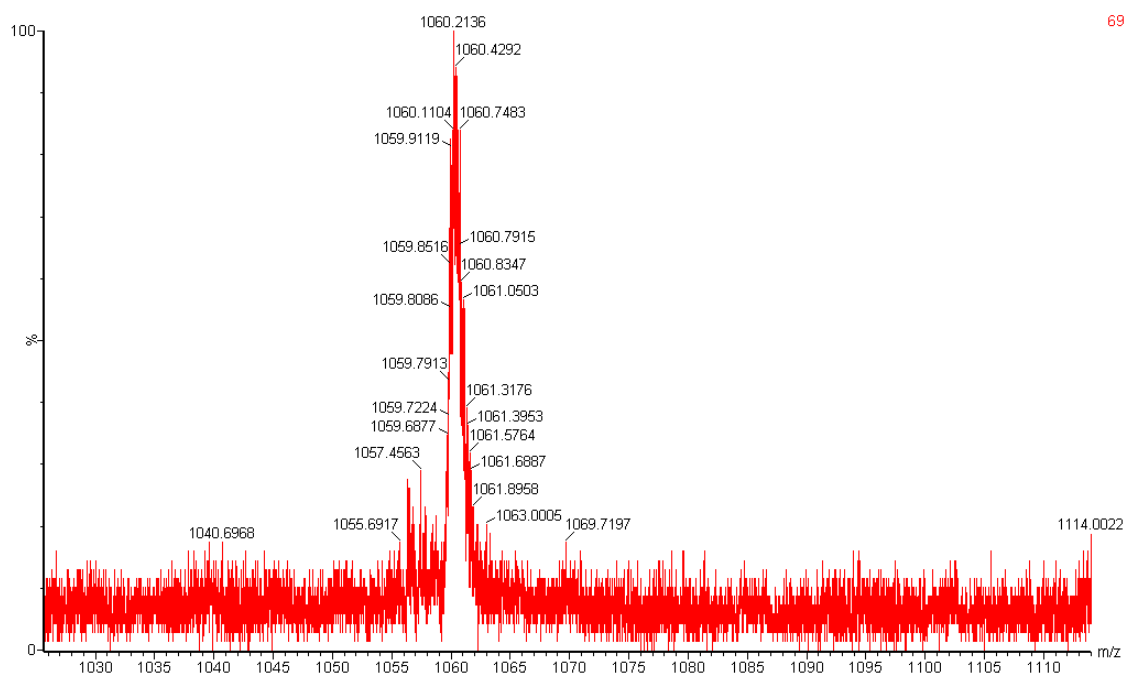
### **Fluorescence studies of oligomers**

Samples for all fluorescence studies were prepared in a quartz cell (path length: 1 cm) in the same ionic conditions as for the denaturation experiments. Parameters for fluorescence spectra are: excitation wavelength, 345 nm; scanning range, 350-600 nm; data interval, 0.1 nm; scan rate: 1 nm/s; temperature, 25 °C.

### 3.5 Supplementary information

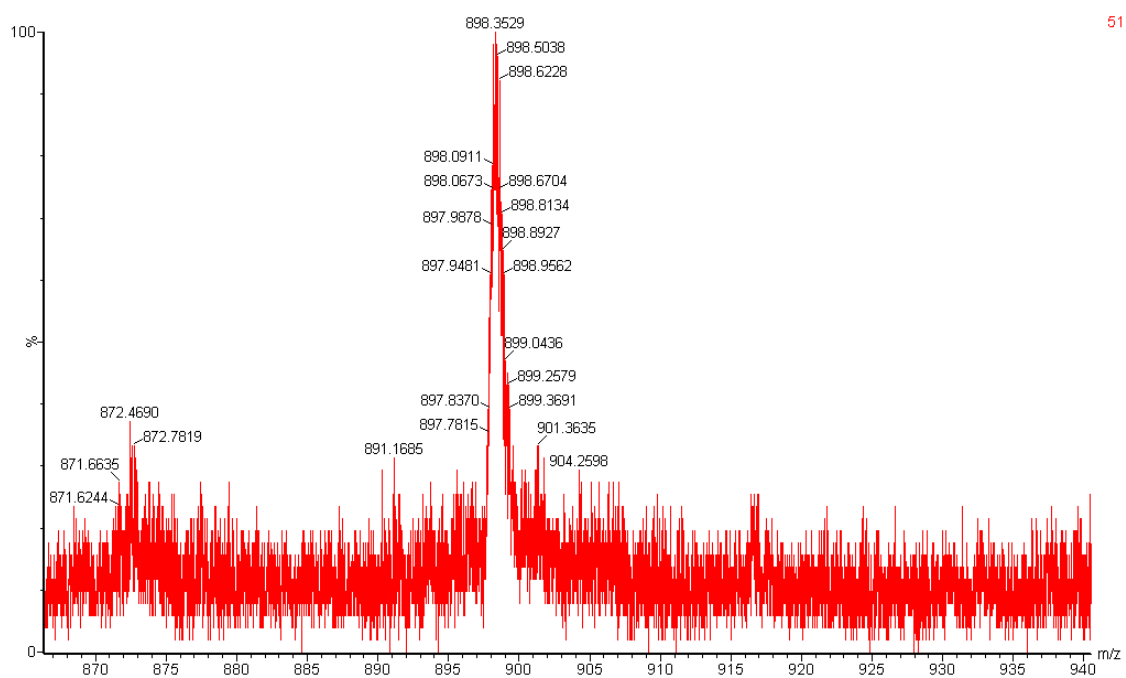


39

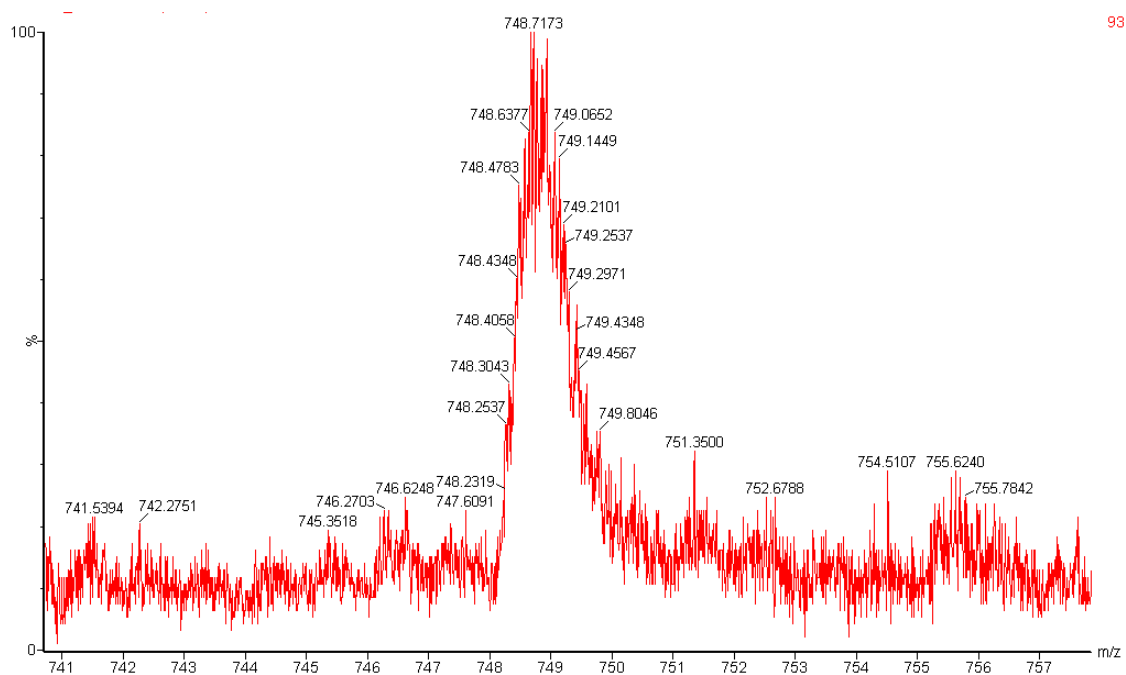


69

**Figure 3.11** ESI-MS spectra of **Fmoc-1-Az** calculated mass for  $C_{176}H_{223}N_{75}O_{53}$ :  
1413.4014  $[M+3H]^{3+}$ , 1060.3030  $[M+4H]^{4+}$ .



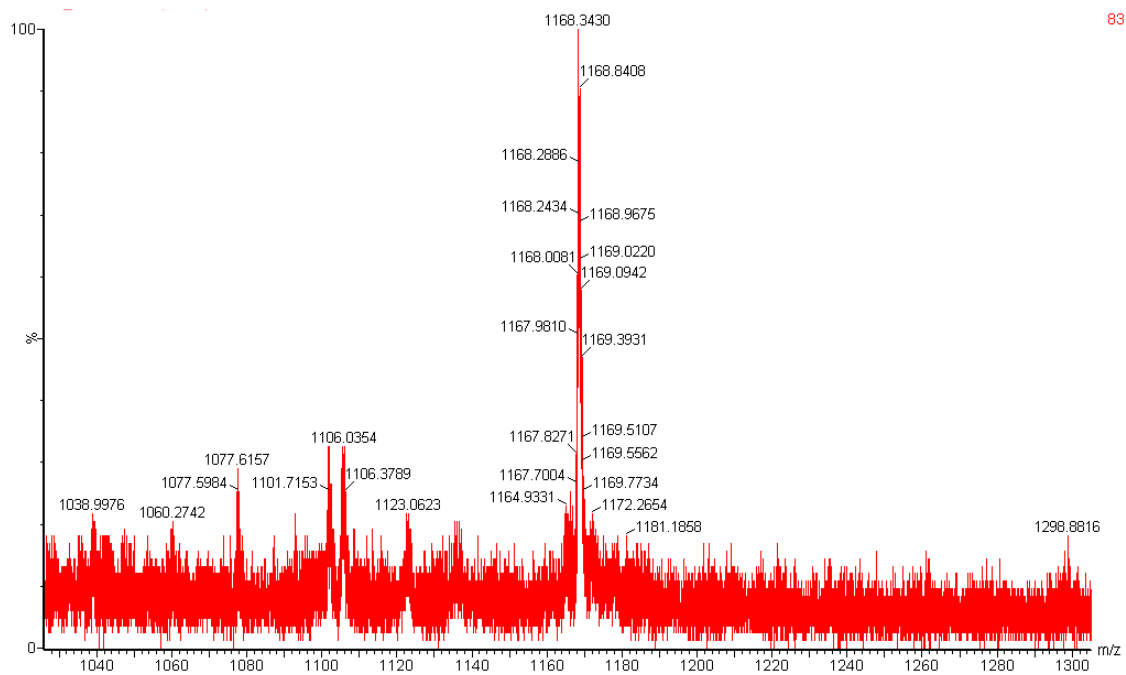
51



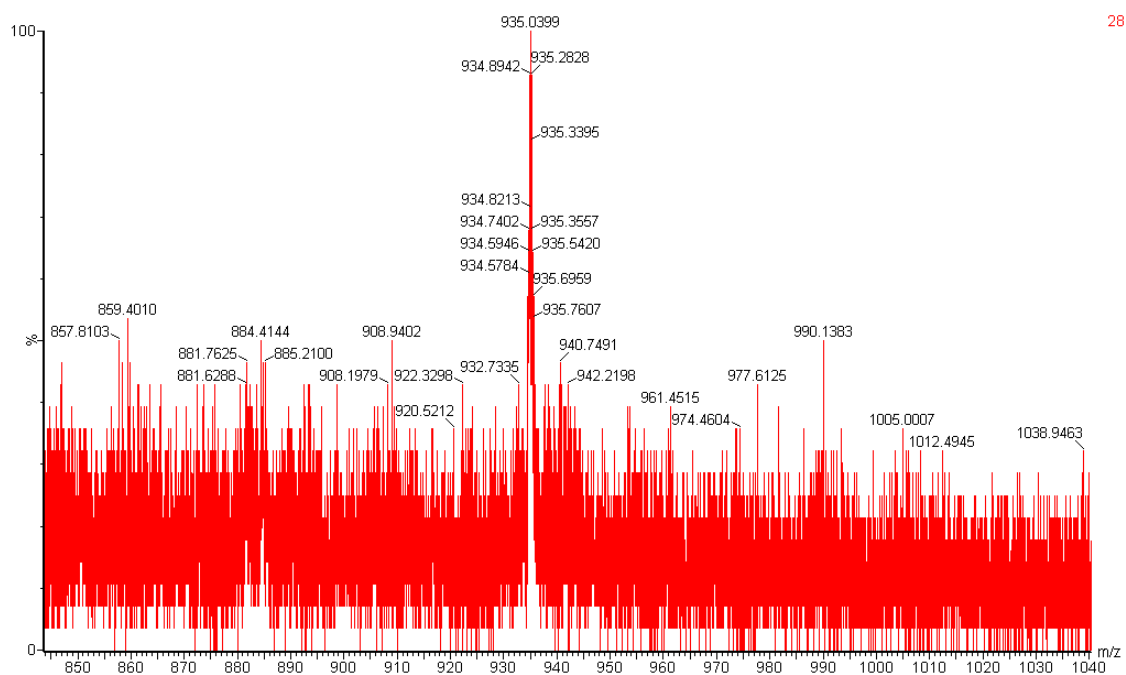
93

**Figure 3.12** ESI-MS spectra of **Fmoc-1-Q** calculated mass for  $C_{192}H_{238}N_{78}O_{53}$ : 898.3070  $[M+5H]^+$ , 748.7572  $[M+6H]^+$ .





83



28

**Figure 3.13** ESI-MS spectra of **Fmoc-Az-1-Q** calculated mass for  $C_{198}H_{247}N_{83}O_{55}$ :

1168.4243  $[M+4H]^{4+}$ , 934.9411  $[M+5H]^{5+}$ .

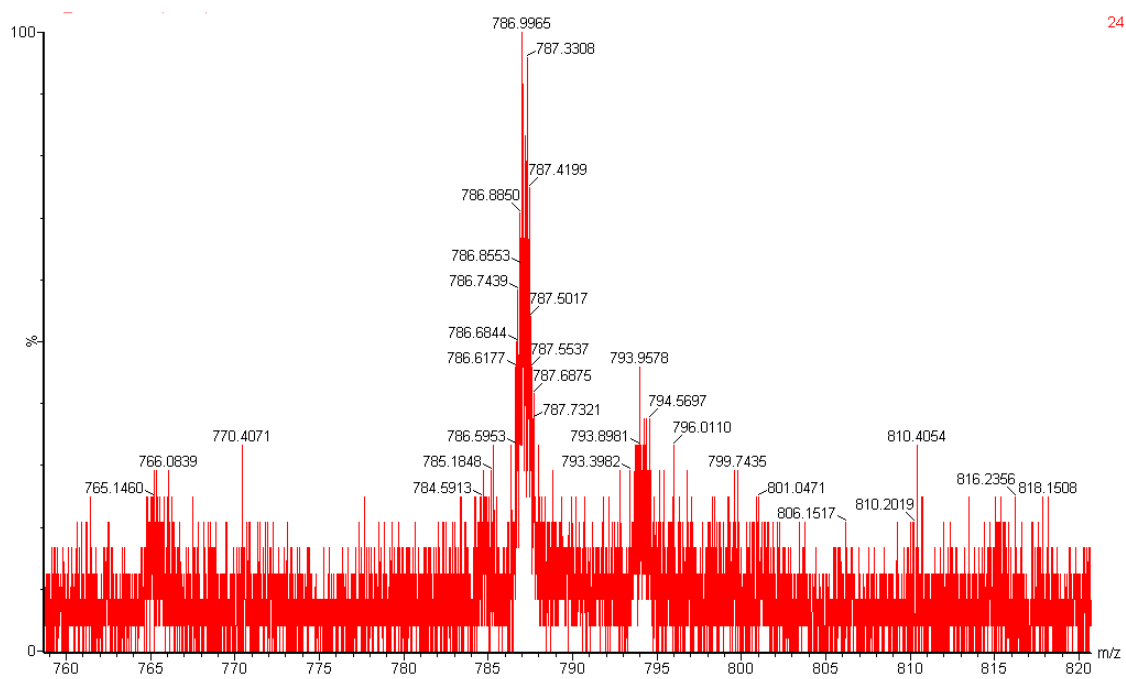
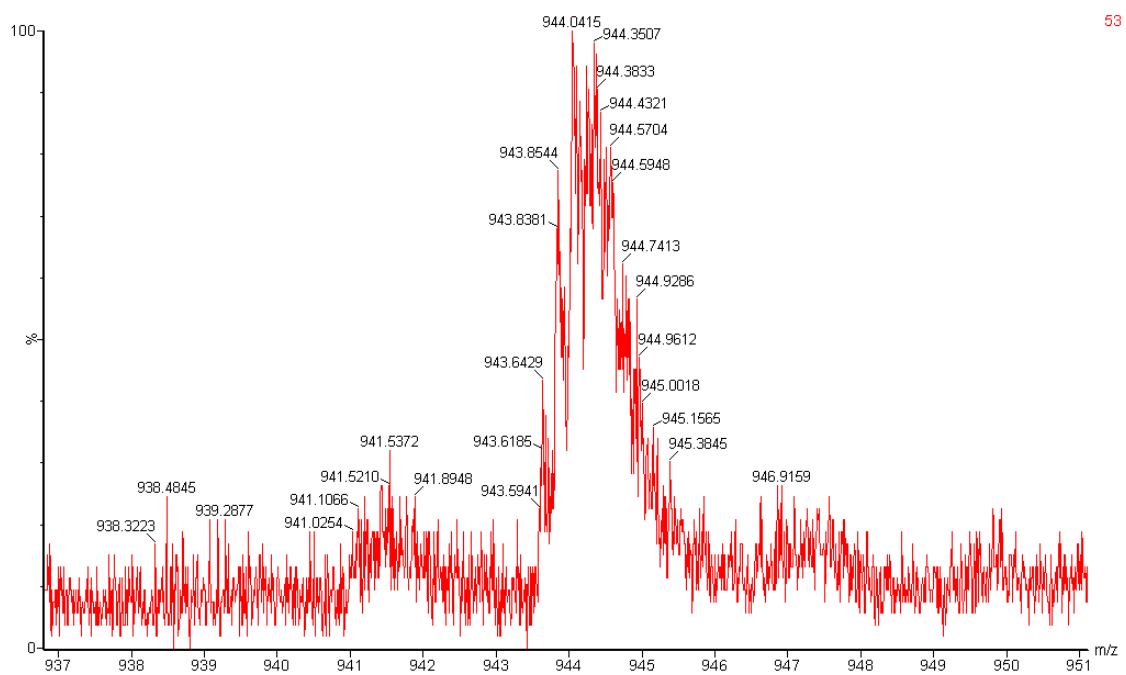
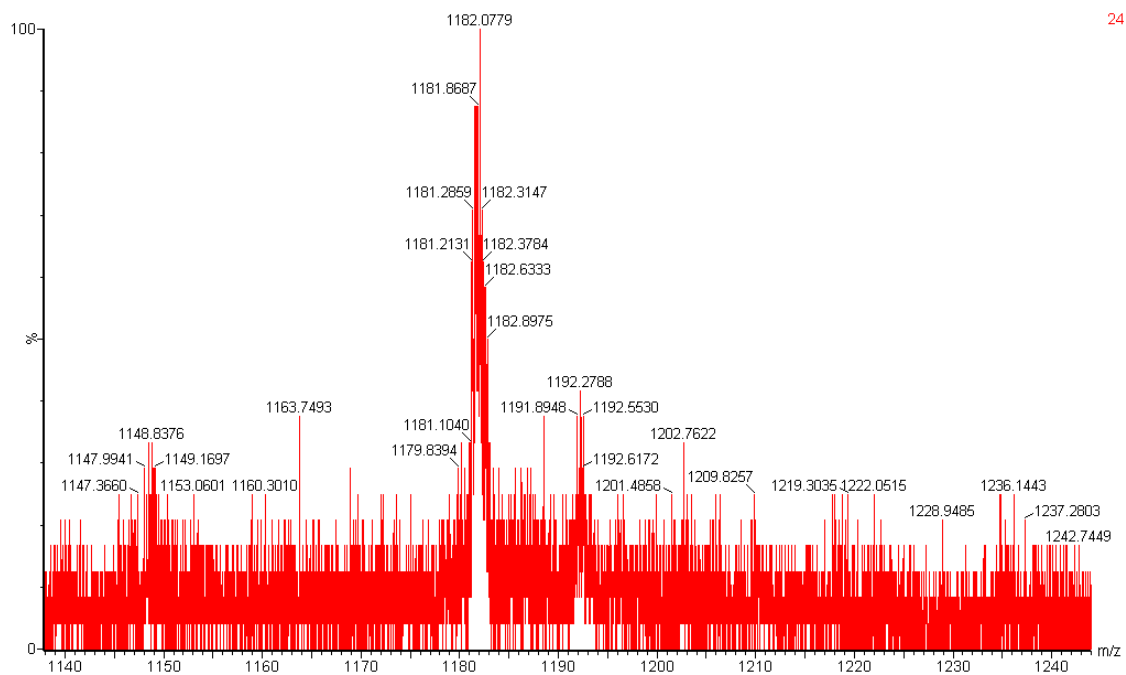
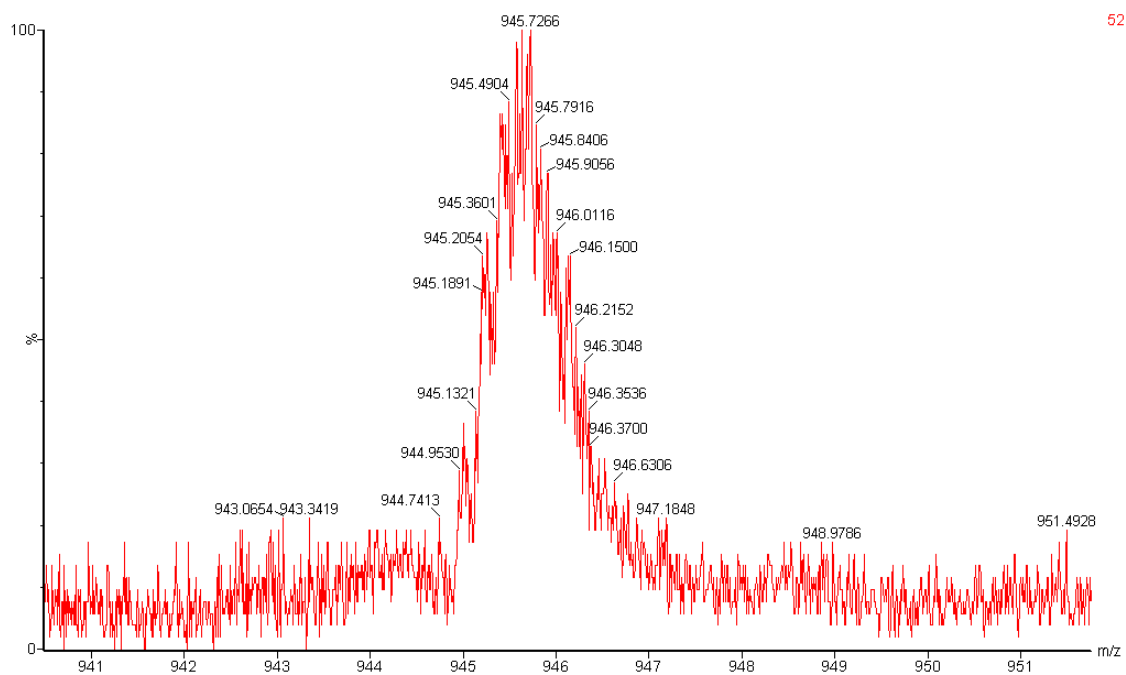


**Figure 3.14** ESI-MS spectra of **pyrene-1-Q** calculated mass for  $C_{203}H_{249}N_{83}O_{54}$ : 944.1554  $[M+5H]^{5+}$ , 786.9641  $[M+6H]^{6+}$ .



24



52

**Figure 3.15** ESI-MS spectra of **acridone-1-Q** calculated mass for  $C_{201}H_{252}N_{84}O_{55}$ :

1182.1942  $[M+4H]^{4+}$ , 945.9569  $[M+5H]^{5+}$ .

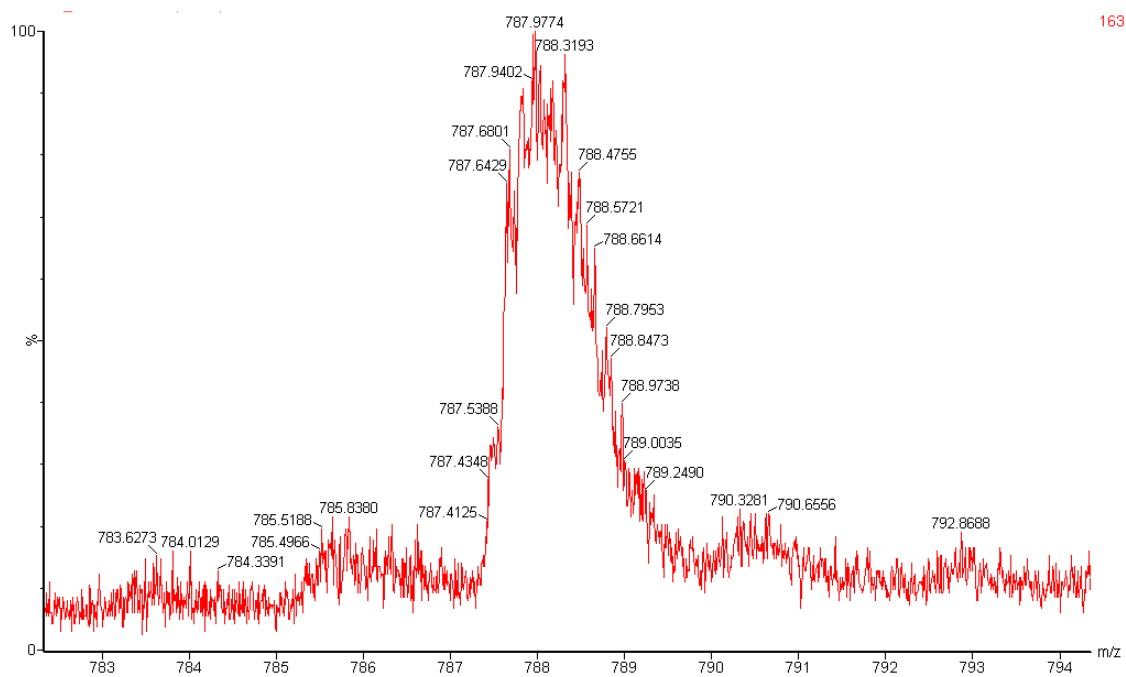
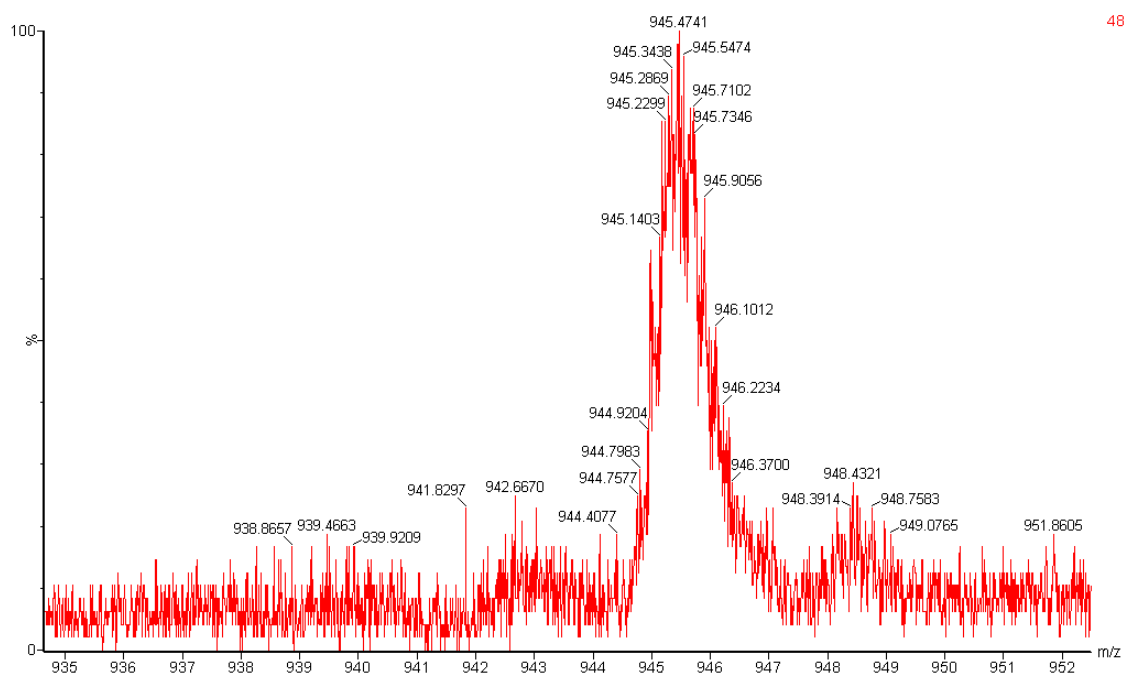
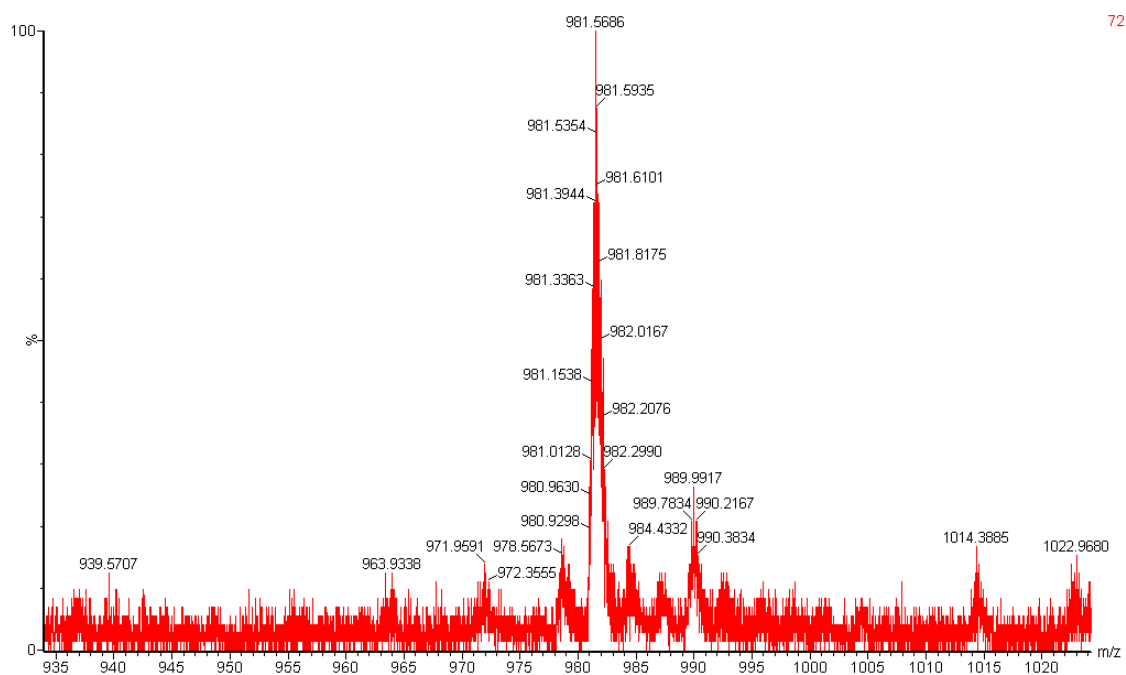
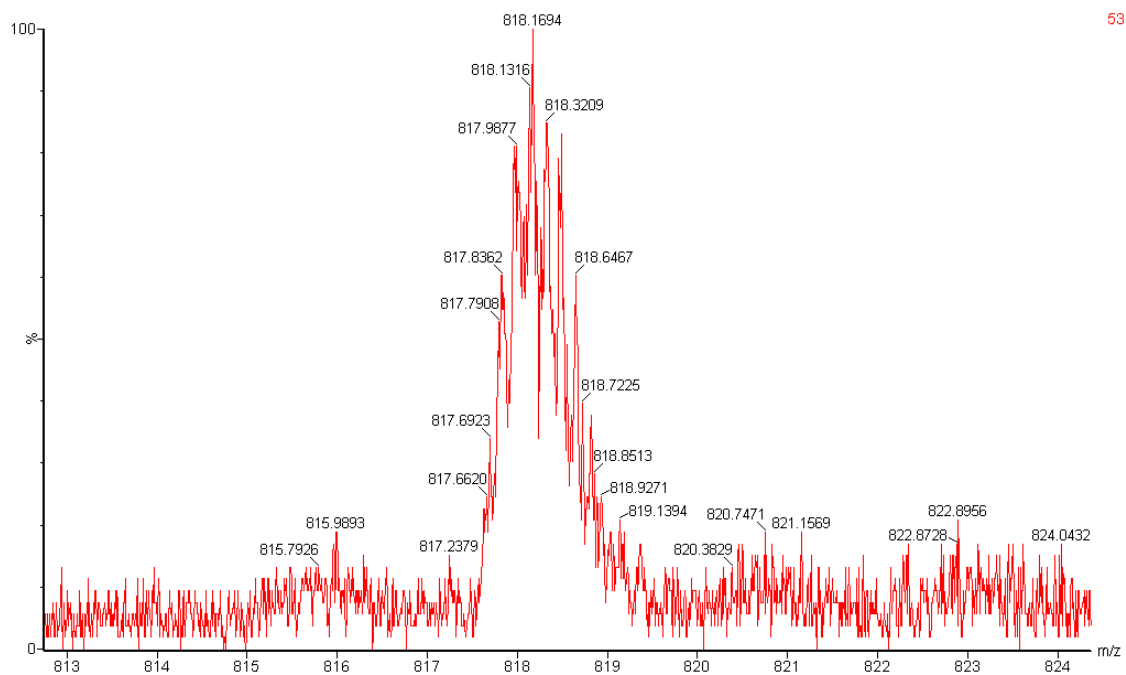


**Figure 3.16** ESI-MS spectra of **acridine-1-Q** calculated mass for  $C_{201}H_{251}N_{85}O_{54}$ :  
 945.3568 [M+5H]<sup>5+</sup>, 787.9653 [M+6H]<sup>6+</sup>.

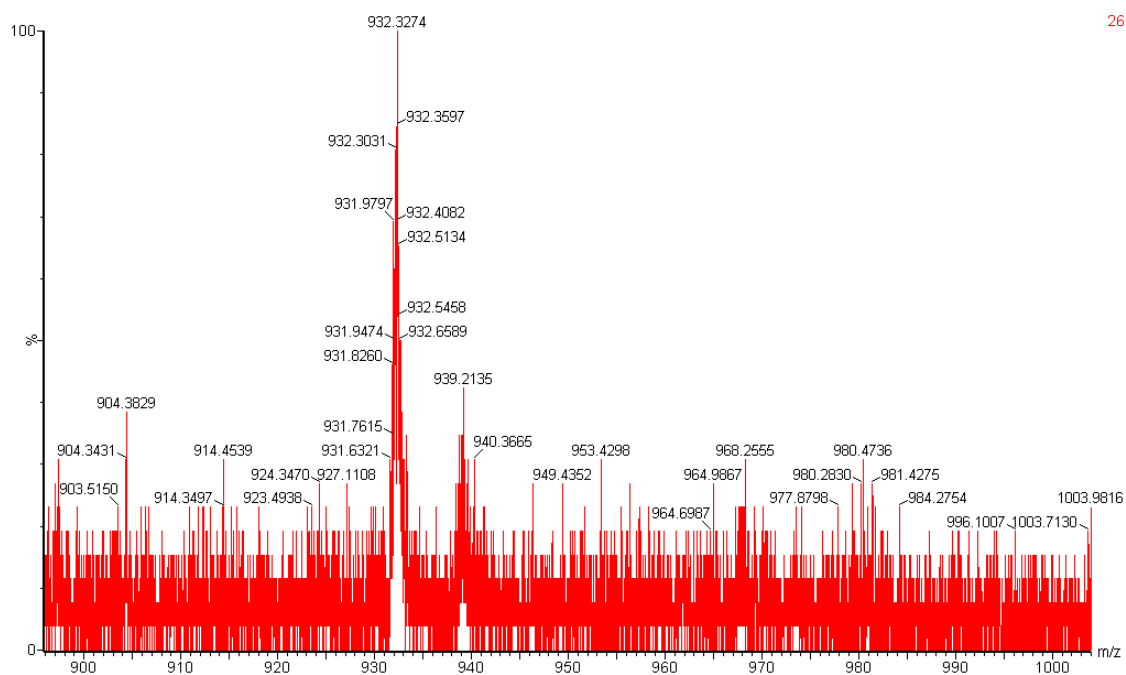


72

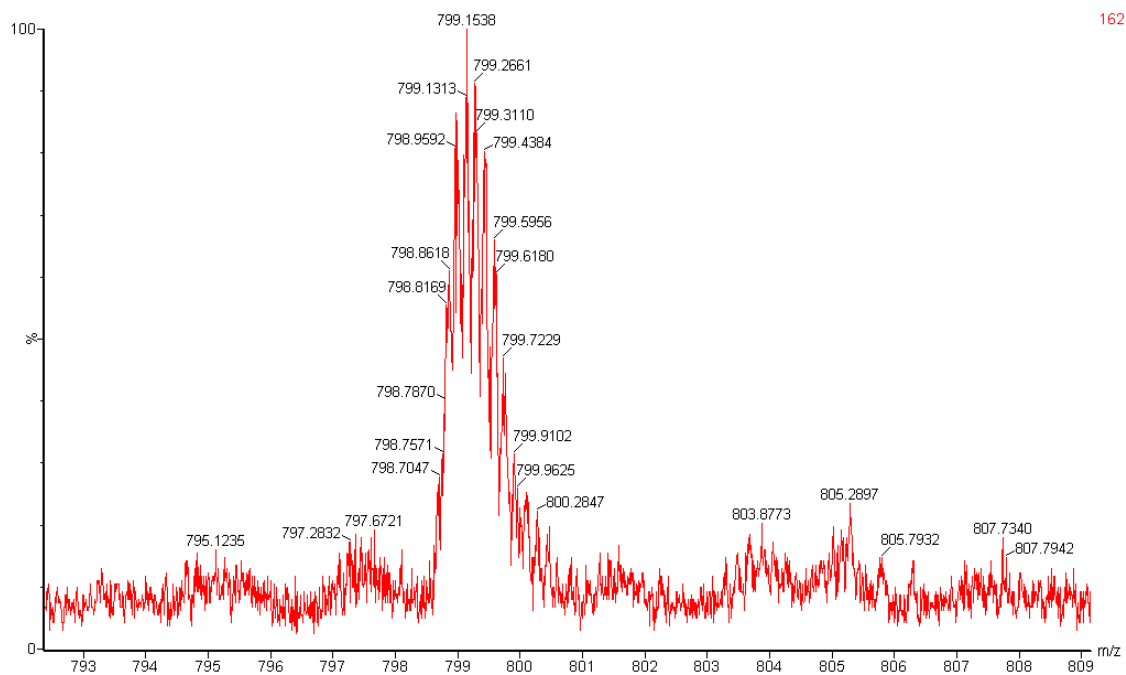


53

**Figure 3.17** ESI-MS spectra of **Fluorescein-1-Q** calculated mass for  $C_{209}H_{254}N_{84}O_{60}$ :  
 981.5771  $[M+5H]^{5+}$ , 818.1489  $[M+6H]^{6+}$ .



26



162

**Figure 3.18** ESI-MS spectra of **Fmoc-2-Az** calculated mass for  $C_{230}H_{290}N_{102}O_{69}$ : 932.2544  $[M+6H]^{6+}$ , 799.2192  $[M+7H]^{7+}$ .

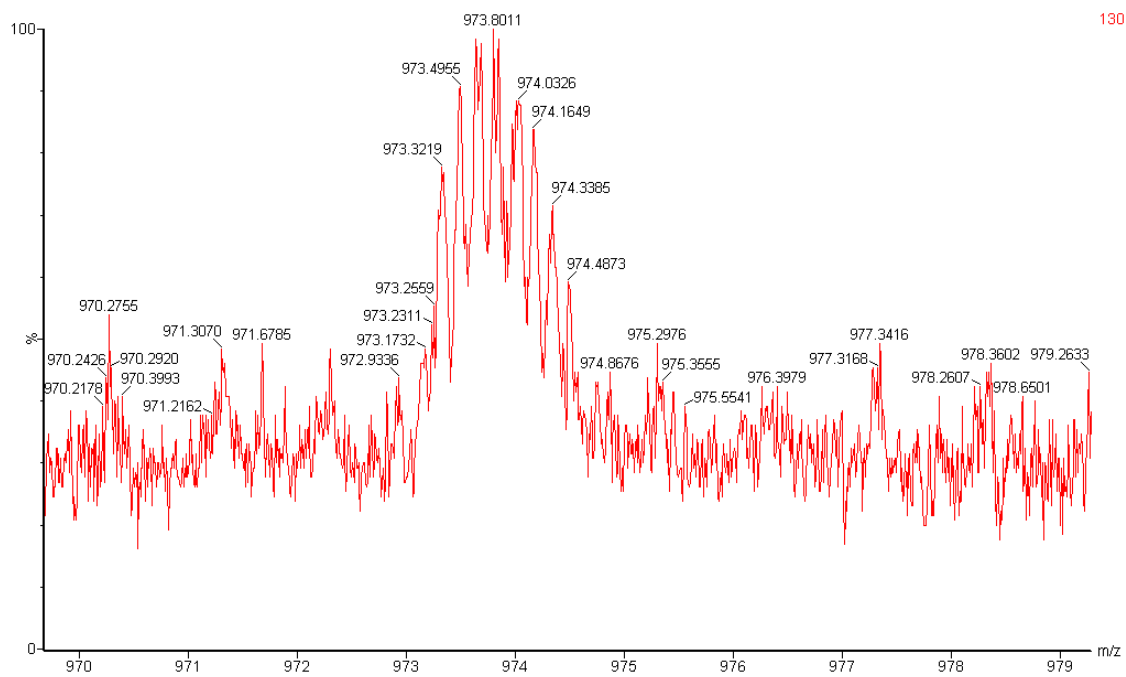
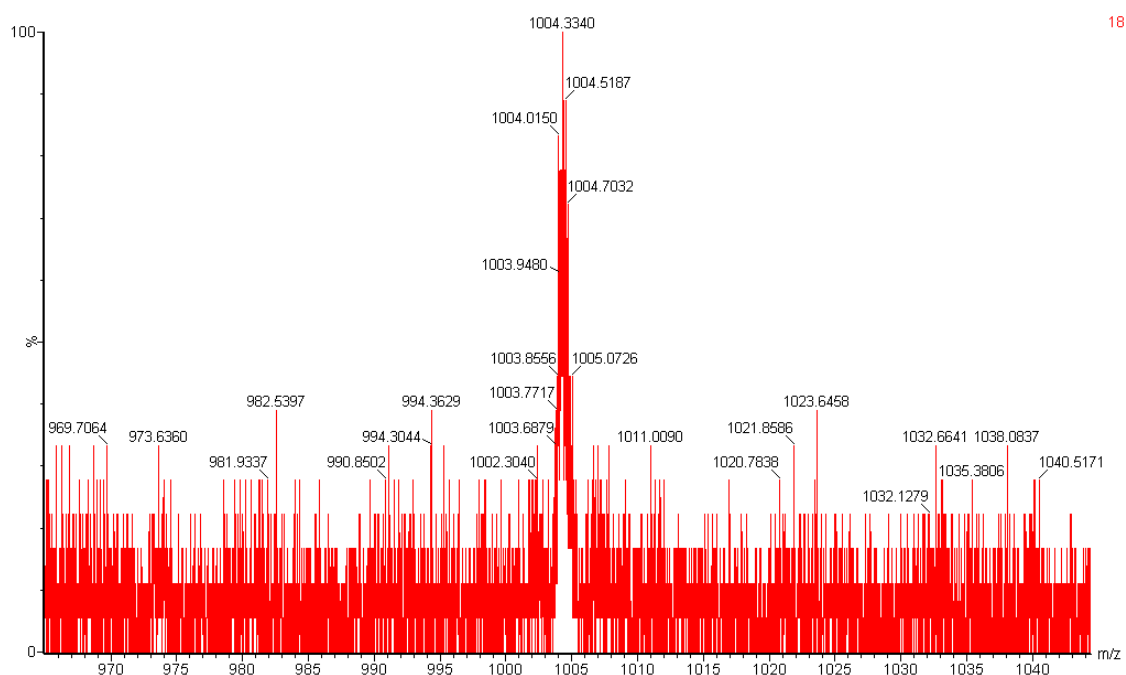
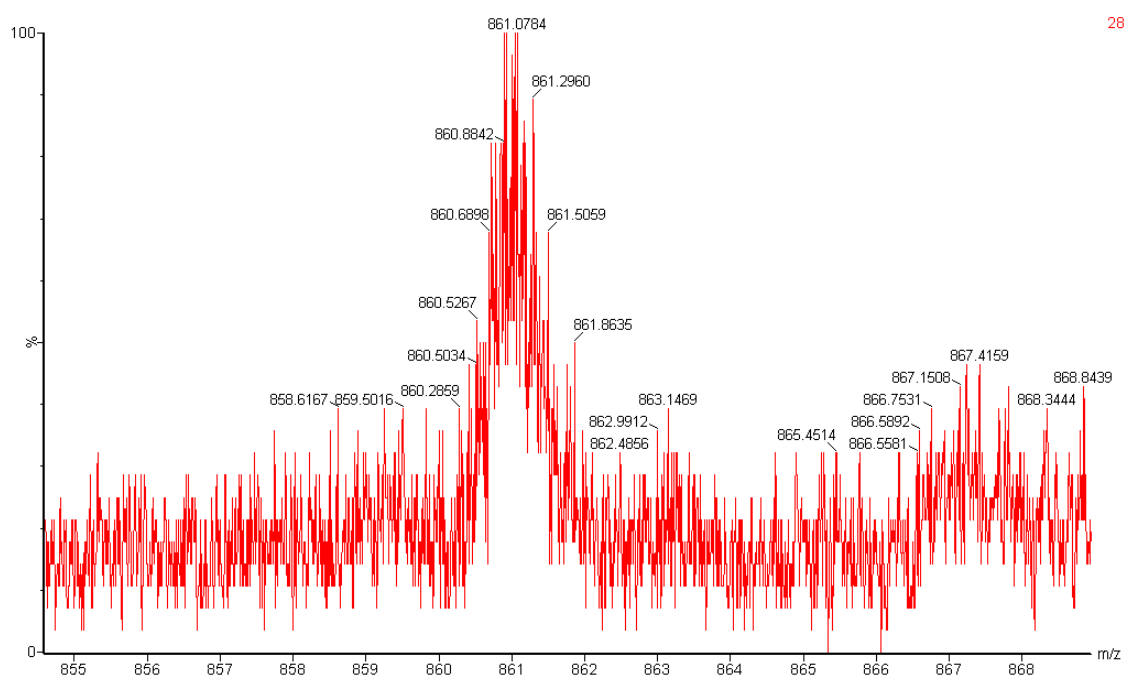


**Figure 3.19** ESI-MS spectra of Fmoc-2-Q calculated mass for  $C_{246}H_{305}N_{105}O_{69}$ : 973.8069  
[M+6H]<sup>6+</sup>.



18



28

**Figure 3.20** ESI-MS spectra of **Fmoc-Az-2-Q** calculated mass for  $C_{252}H_{314}N_{110}O_{71}$ :  
 1004.3353  $[M+6H]^{6+}$ , 861.0028  $[M+7H]^{7+}$ .



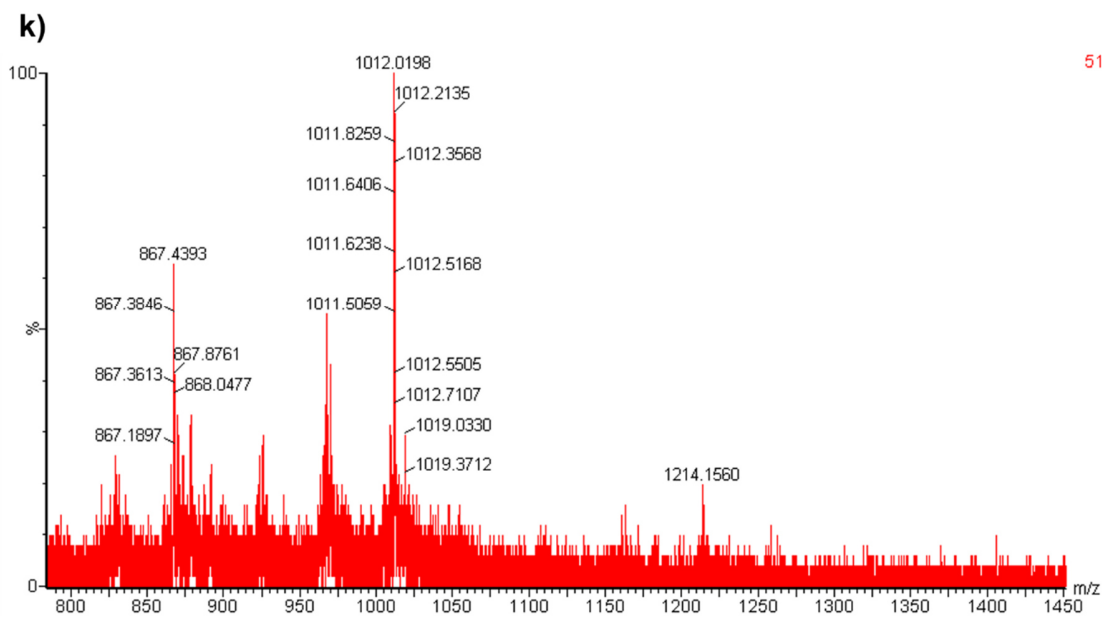
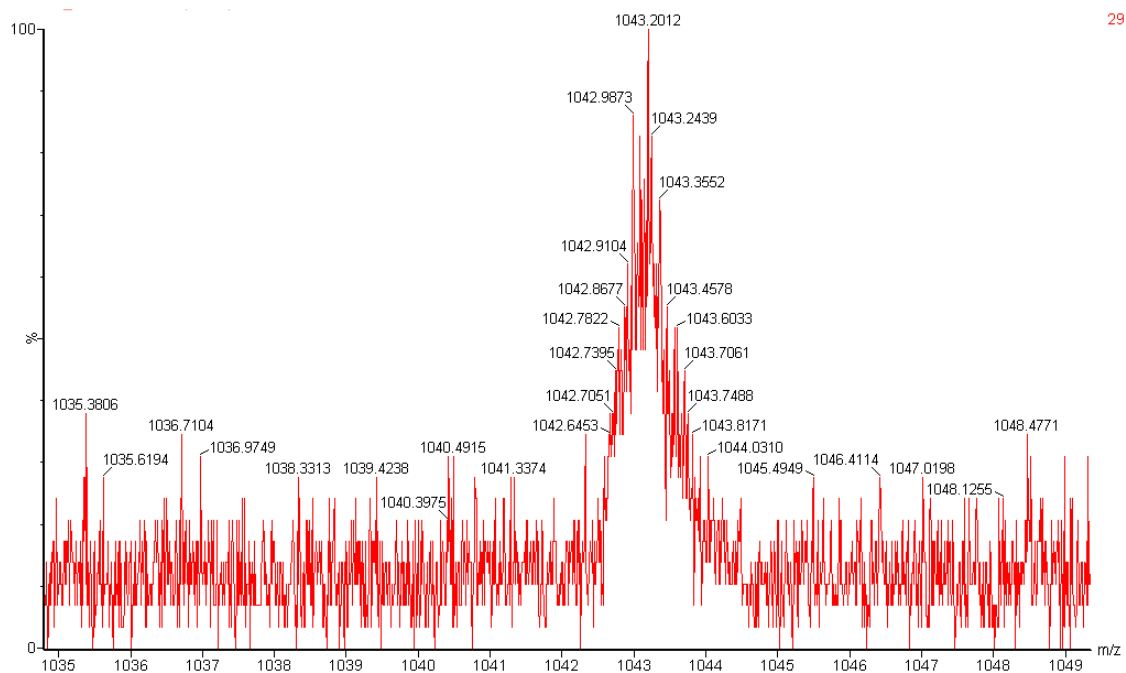
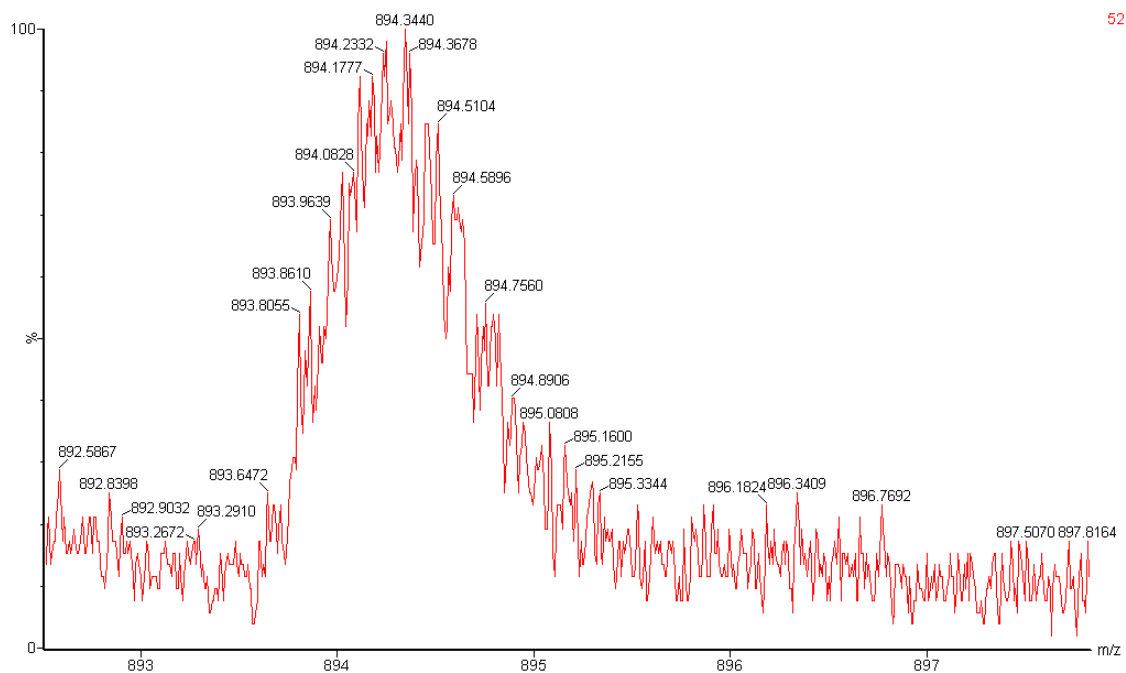


**Figure 3.21** ESI-MS spectra of **pyrene-2-Q** calculated mass for  $C_{257}H_{316}N_{110}O_{70}$ :  
 1214.2150  $[M+5H]^{5+}$ , 1012.0138  $[M+6H]^{6+}$ , 867.5844  $[M+7H]^{7+}$ .



29



52

**Figure 3.22** ESI-MS spectra of **Fluorescein-2-Q** calculated mass for  $C_{263}H_{321}N_{111}O_{76}$ :  
 1043.1987 [M+6H]<sup>6+</sup>, 894.3143 [M+7H]<sup>7+</sup>.

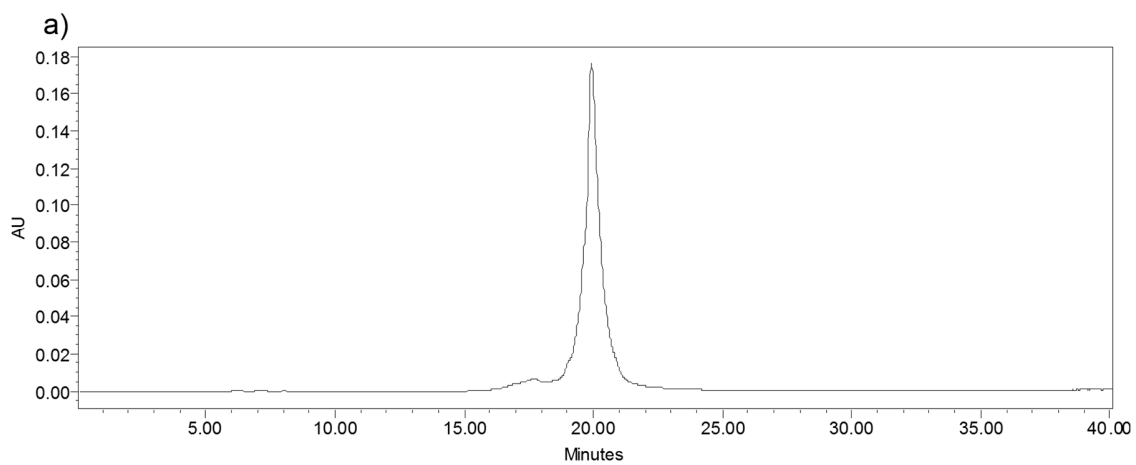


**Figure 3.23** HPLC-UV absorption spectrum of **pyrene-1-Q** at 265 nm.

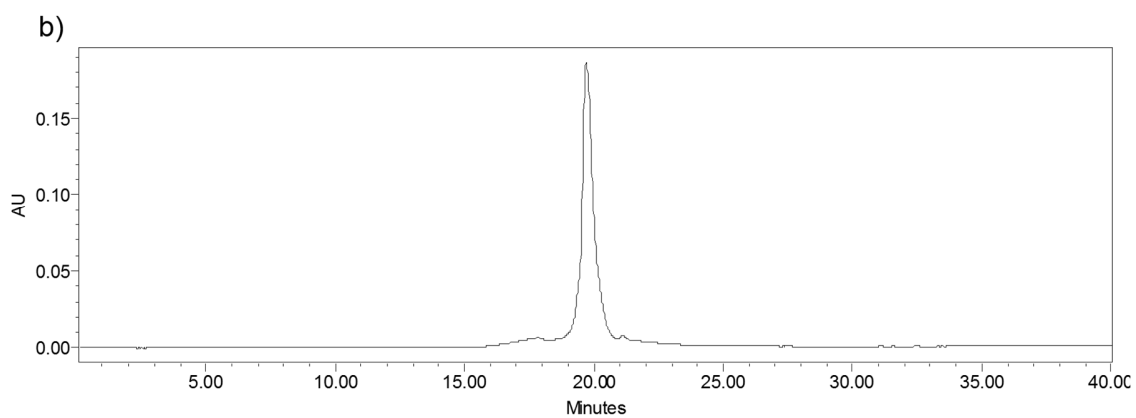


**Figure 3.24** HPLC-UV absorption spectrum of **acridone-1-Q** at 265 nm.

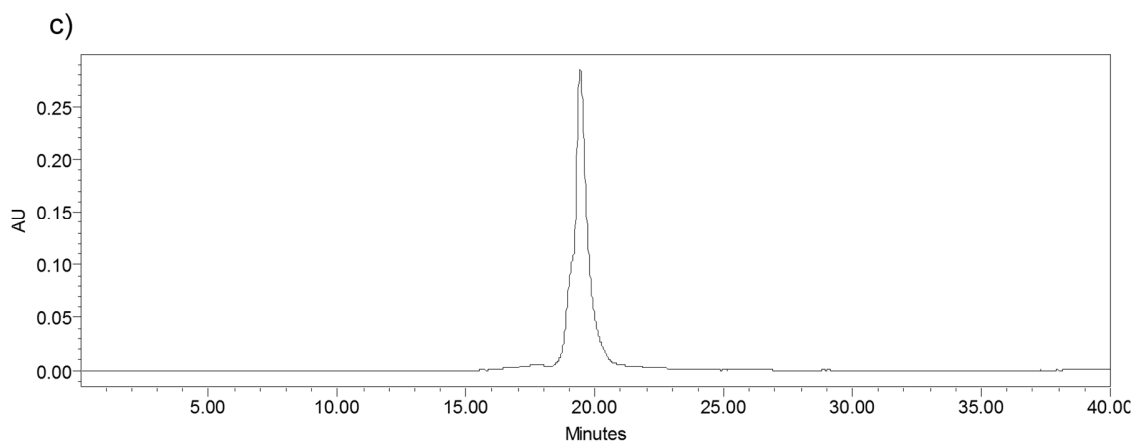


**Figure 3.25** HPLC-UV absorption spectrum of **acridine-1-Q** at 265 nm.

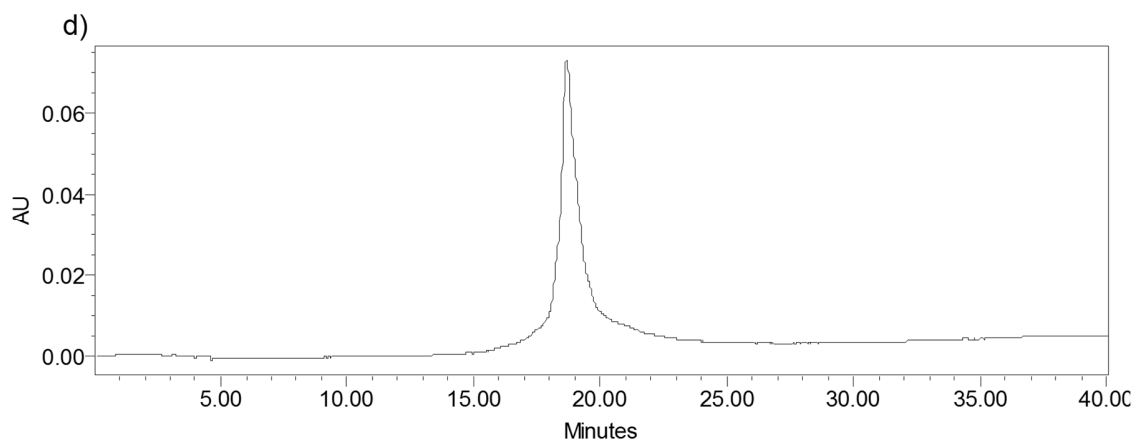


**Figure 3.26** HPLC-UV absorption spectrum of **Fluorescein-1-Q** at 265 nm.

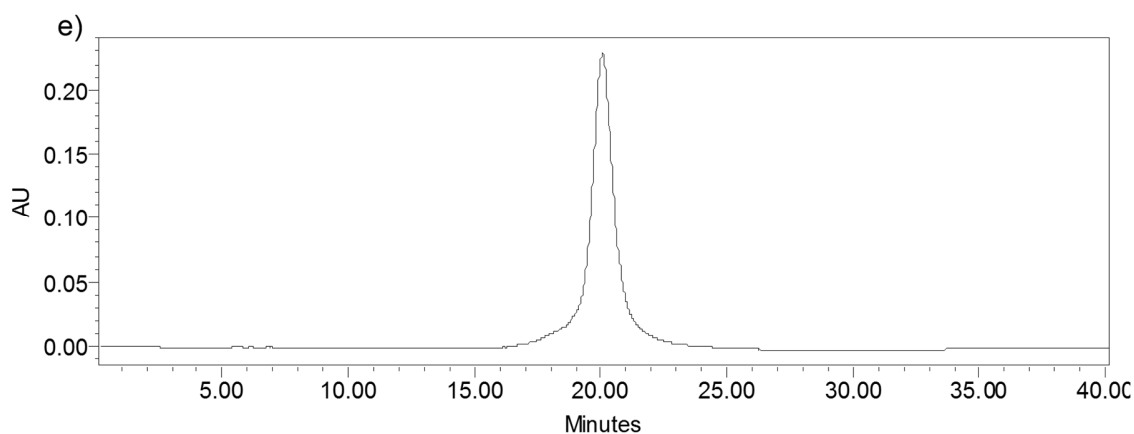


**Figure 3.27** HPLC-UV absorption spectrum of **pyrene-2-Q** at 265 nm.

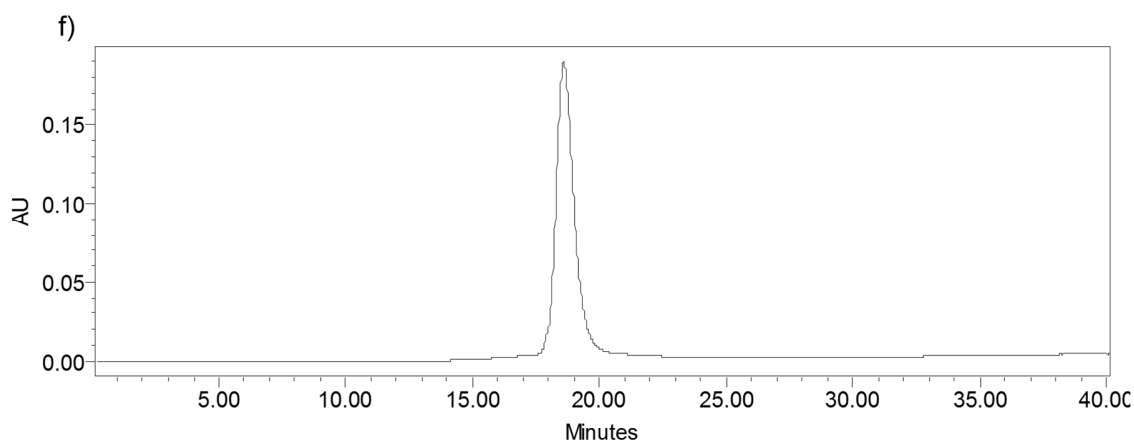


**Figure 3.28** HPLC-UV absorption spectrum of **Fluorescein-2-Q** at 265 nm.

### 3.6 References

- (1) Ortiz, E.; Estrada, G.; Lizardi, P. M. *Mol. Cell. Probes* **1998**, *12* (4), 219.
- (2) Seitz, O. *Angew. Chem. Int. Ed.* **2000**, *39* (18), 3249.
- (3) Seitz, O. *Angew. Chem. Int. Ed.* **1995**, *34* (7), 803.
- (4) Kitagawa, F.; Ohori, Y.; Ikeda, H.; Fujimori, H.; Murakami, Y.; Nakamura, Y. *Nucleic Acids Res. Suppl.* **2002**, *2*, 143.

- (5) Kuhn, H.; Demidov, V. V.; Coull, J. M.; Fiandaca, M. J.; Gildea, B. D.; Frank-Kamenetskii, M. D. *J. Am. Chem. Soc.* **2002**, *124* (6), 1097.
- (6) Coull, J. M.; Gildea, B. D.; Hyldig-Nielsen, J. Methods, kits and compositions pertaining to PNA molecular beacons. WO-A 9922018 A2 19990506, 1999.
- (7) Kuhn, H.; Demidov, V. V.; Gildea, B. D.; Fiandaca, M. J.; Coull, J. C.; Frank-kamenetskii, M. D. *Antisense Nucleic Acid Drug Dev.* **2001**, *11*, 265.
- (8) Xi, C.; Balberg, M.; Boppart, S. A.; Raskin, L. *Appl. Environ. Microbiol.* **2003**, *69* (9), 5673.
- (9) Li, X.; Morgenroth, E.; Raskin, L. *Appl. Environ. Microbiol.* **2008**, *74* (23), 7297.
- (10) Petersen, K.; Vogel, U.; Rockenbauer, E.; Nielsen, K. V.; Kølvråa, S.; Bolund, L.; Nexø, B. *Mol. Cell. Probes* **2004**, *18*, 117.
- (11) Zanolì, L. M.; Licciardello, M.; D'Agata, R.; Lantano, C.; Calabretta, A.; Corradini, R.; Marchelli, R.; Spoto, G. *Anal. Bioanal. Chem.* **2013**, *405* (2–3), 615.
- (12) Totsingan, F.; Rossi, S.; Corradini, R.; Tedeschi, T.; Sforza, S.; Juris, A.; Scaravelli, E.; Marchelli, R. *Org. Biomol. Chem.* **2008**, *6* (7), 1232.
- (13) Köhler, O.; Jarikote, D. V.; Seitz, O. *ChemBioChem* **2005**, *6* (1), 69.
- (14) Socher, E.; Bethge, L.; Knoll, A.; Jungnick, N.; Herrmann, A.; Seitz, O. *Angew. Chem. Int. Ed.* **2008**, *47*, 9555.
- (15) Jarikote, D. V.; Köhler, O.; Socher, E.; Seitz, O. *European J. Org. Chem.* **2005**, No. 15, 3187.
- (16) Socher, E.; Knoll, A.; Seitz, O. *Org. Biomol. Chem.* **2012**, *10*, 7363.
- (17) Kam, Y.; Rubinstein, A.; Nissan, A.; Halle, D.; Yavin, E. *Mol. Pharm.* **2012**, *9*, 685.

- (18) St Amant, A. H.; Engbers, C.; Hudson, R. H. E. *Artif. DNA PNA XNA* **2013**, *4* (1), 4.
- (19) Michaels, H.; Zhu, L. *Encycl. Reagents Org. Synth.* **2011**, 3.
- (20) Presolski, S. L.; Hong, V. P.; Finn, M. G. *Curr. Protoc. Chem. Biol.* **2011**, *3* (4), 153.
- (21) Matarazzo, A.; Moustafa, M. E.; Hudson, R. H. E. *Can. J. Chem.* **2013**, *91*, 1202.
- (22) Hudson, R. H.; Liu, Y.; Wojciechowski, F. *Can. J. Chem.* **2007**, *85* (4), 302.
- (23) Mansawat, W.; Boonlua, C.; Siritwong, K.; Vilaivan, T. *Tetrahedron* **2012**, *68* (21), 3988.
- (24) Davies, B. P. A Homogenous Fluorescence Assay of micro RNA Maturation ( Doctoral dissertation), Humboldt-Universität zu Berlin, 2008.

## **CHAPTER IV: SYNTHESIS OF A (Gd(III)-DOTA)<sub>4</sub>-PNA CONJUGATE AS A CONTRAST AGENT FOR MR IMAGING**

A manuscript of this chapter is in preparation for submission. Xiaoxiao Wang, Mark Milne, Francisco Martínez, Timothy J. Scholl and Robert H. E. Hudson\*, Synthesis of a Poly(Gd(III)-DOTA)-PNA Conjugate as a Potential MRI Contrast Agent via Post-Synthetic Click Chemistry Functionalization.

### **4.1 Introduction**

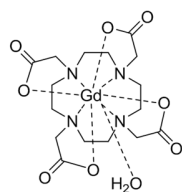
Molecular imaging has been employed in clinical medicine for the past decades by using modalities such as magnetic resonance imaging (MRI), single photon emission tomography (SPECT)/positron emission tomography (PET) and optical imaging. Although SPECT/PET is very sensitive, the requirement of radioactive agents limits its application. SPECT/PET is only used when suspect masses are evident or highly likely due to the potential risks of radioisotope exposure. Optical imaging has been widely employed, but disadvantages such as low efficiency of light transmission through tissues and difficult quantification, cannot be neglected.<sup>1</sup> Therefore, by comparison, MRI is an attractive alternative for molecular imaging because it is non-invasive, does not require exposure to radiation and provides three-dimensional images with high spatial resolution and high contrast. After the introduction of MRI in the clinic in 1980s, it has shown unparalleled power in diagnostic medicine, especially for the detection and characterization of diseased soft tissues such as solid tumors.

The quality of MR images, including spatial resolution, signal-to-noise and contrast-to-noise ratios (SNR and CNR), has been substantially improved in the past years owing to the use of higher magnetic fields and the development of safe and effective MRI contrast

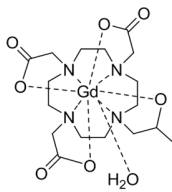


agents (CAs). MRI CAs are biocompatible magnetic materials that alter the longitudinal ( $T_1$ ) and transverse ( $T_2$ ) relaxation rates of the surrounding water protons, therefore enhancing image contrast in tissues of interest. They are generally categorized as  $T_1$  and  $T_2$  CAs based on their magnetic properties and relaxation mechanisms. CAs have become essential for improving the image quality by increasing the image contrast between normal and diseased tissues.<sup>2-5</sup> Gadolinium [Gd(III)] chelates could increase  $T_1$  relaxation rate ( $1/T_1$ ) and have been commonly used as  $T_1$  CAs by generating a positive image contrast. Superparamagnetic iron oxide nanoparticles have been found more effective for increasing  $T_2$  relaxation rate ( $1/T_2$ ), thus commonly used as  $T_2$  CA, which produces negative image contrast. To date, the majority of MRI CAs used in clinical practice are Gd(III) chelates (Figure 4.1), with over 10 million contrast enhanced MRI scans on an annual basis, because of their high paramagnetism, favorable properties in term of relaxation enhancement, relatively high stability, and tolerance in the body.

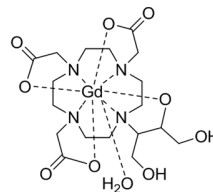
**Macrocyclic Gd(III) chelates:**



**Gd-DOTA (DOTAREM®)**

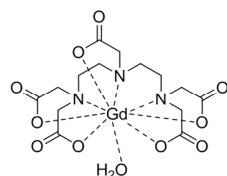


**Gd-(HP-DO3A) (Prohance®)**

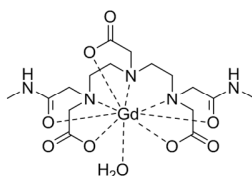


**Gd-(DO3A-butrol) (Gadovist®)**

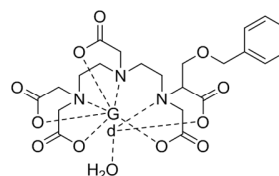
**Linear Gd(III) chelates:**



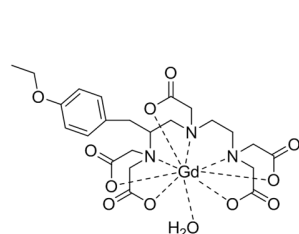
**Gd-DTPA (MAGNEVIST®)**



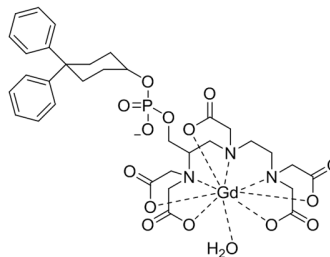
**Gd-(DTPA-BMA) (OMNISCAN®)**



**Gd-(EOB-DTPA) (EOVIST®)**



**Gd-BOPTA (Multihance®)**



**MS-325 (Vasovist®)**

**Figure 4.1** Some of the Gd(III)-based MRI contrast agents currently used in the clinical practice<sup>55</sup> (copyright 2013 John Wiley and Sons).

Biocompatibility of the MRI CA is an important consideration for clinical applications. Gd(III) ions are highly toxic in ionic form, acutely interfering with calcium channels and protein-binding sites.<sup>6,7</sup> Free Gd ions accumulate in the liver, spleen, kidney and bones and have an  $LD_{50} = 0.2 \text{ mmol}^{-1}\text{kg}^{-1}$  in mice. To overcome this issue, Gd(III) ions are generally complexed with chelating ligands to prevent tissue interaction and minimize toxic side effects. Nevertheless, toxic Gd(III) ions may still be released from some of the chelates by exchange with ions such as  $\text{Zn}^{2+}$ ,  $\text{Ca}^{2+}$ , and  $\text{Cu}^{2+}$  in the body and by protonation of the ligands at low pH that may cause chelate dissociation *in vivo*.<sup>8,9</sup> A serious adverse reaction

called nephrogenic systemic fibrosis may be associated to the use of Gd(III)-based CA in a very small percentage of patients with renal malfunctions due to incomplete excretion and possibly chelate disassociation of the agents.<sup>10</sup> The US Food and Drug Administration (FDA) has issued a black box warning to prohibit the use of Gd(III)-based CA in the patients with renal malfunctions. Therefore, safer Gd(III) chelate-based MRI CAs are required. The CAs need to be excreted after the contrast-enhanced MRI within hours. Moreover, small Gd(III) chelates have a relatively low relaxivity and extravasate non-selectively from blood into the interstitium of both normal tissue and tumor, which has been a major limitation for their clinical applications. Therefore, macromolecular Gd(III) complexes have been proposed with higher relaxivity and prolonged retention in blood circulation. It has been demonstrated that attaching Gd(III) chelates to macromolecules slows down the rotational motion of the complexes, thus increasing relaxivities.<sup>11</sup> Macromolecular Gd(III) chelates have relatively higher relaxivity ( $r_1$ ) per Gd(III) ion than that of small molecular Gd(III) chelates. For example, Gd-DTPA conjugated to polylysine (PLL) with the molecular weights ranging from 3.3 up to 102 kDa has a  $r_1$  per Gd(III) ion 2.5 times higher than that of Gd-DTPA (measure at 2.4 T).<sup>12</sup> P792 (Vistarem<sup>®</sup>), a macromolecular Gd-DOTA derivative (Figure 4.2), has a  $r_1$  relaxivity as high as 39 mM<sup>-1</sup>second<sup>-1</sup> per Gd(III) ion (0.47 T, 37 °C, in water) whereas  $r_1$  is 3.4 mM<sup>-1</sup>second<sup>-1</sup> for Gd-DOTA (0.47 T, 37 °C, in water).<sup>12,13</sup> Higher relaxivity of macromolecular Gd(III) complexes can help generate more efficient contrast enhancement. Thus they can be used at significantly reduced doses. On the other hand, macromolecular CAs could effectively target clinically important targets like DNA, mRNA or proteins/enzymes. For example, targeted delivery of CAs into tumor tissues is crucial in cancer diagnostic MRI, because

tumors are physiologically different from normal tissues and have leaky blood vasculature. Tumor tissues usually abundantly express cancer-related biomarkers on cell surface, extracellular matrix and angiogenic microvessels, which would be ideal targets for molecular imaging. Therefore, ligands with high-binding affinity are essential for the design of targeting CA in order to generate sufficient contrast enhancement of visualizing these biomarkers with the aid of MRI.

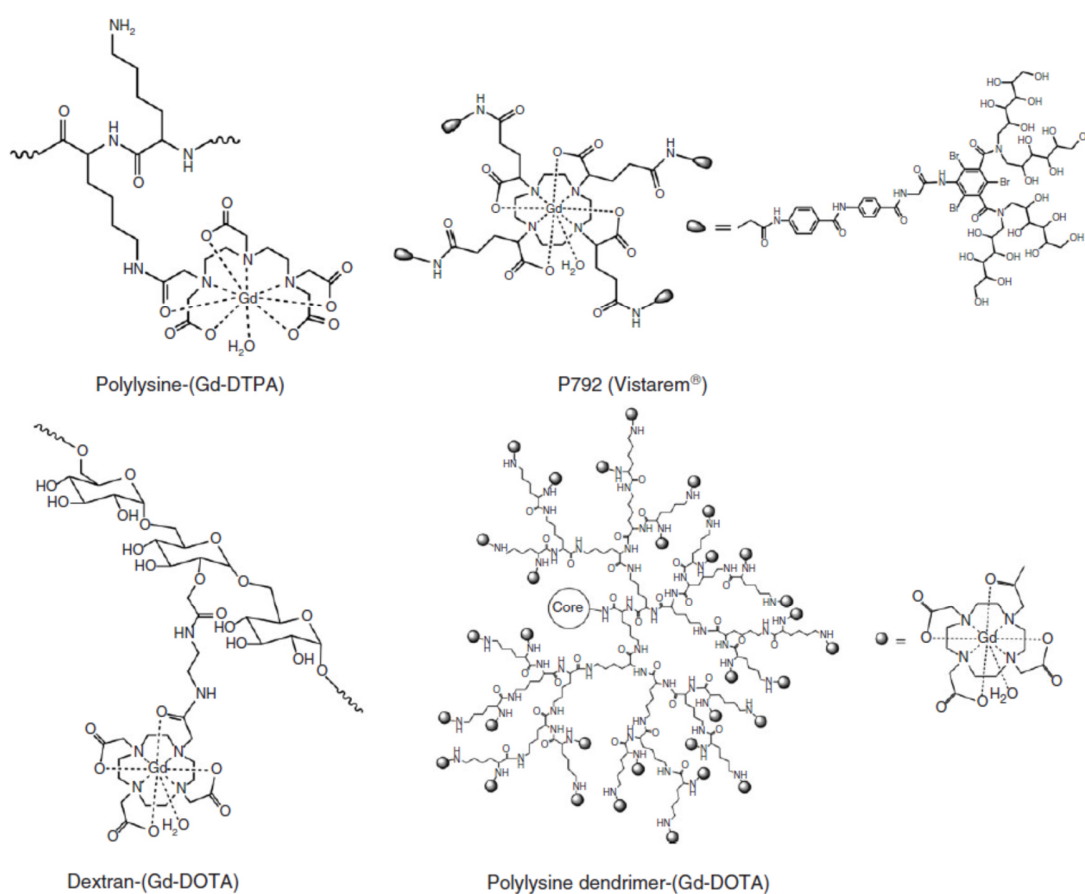


**Figure 4.2** Examples of macromolecule-based Gd(III) contrast agents<sup>55</sup> (copyright 2013 John Wiley and Sons).

The 3'-ends of all fully processed eukaryotic mRNAs except most histone genes have a polyadenylic acid [poly(rA)] tail. It consists of 200-250 adenine bases and occupies a

significant role for mRNA stability, translation and transport.<sup>14-16</sup> Poly(rA) tail has also been recognized as a contributor in increasing length and as a platform to recruit mRNA export factors.<sup>17</sup> Polyadenylation of mRNA is a critical cellular event in the transcription process for the maturation of all eukaryotic mRNAs. It is catalyzed by the enzyme poly(rA) polymerase (PAP). Neo-PAP, a recently identified human poly(rA) polymerase, is significantly over-expressed in human cancer cells in comparison to its expression in normal or virally transformed cells, and may represent a tumor-specific target.<sup>18,19</sup> This suggests the poly(rA) tail acts as a potential malignancy specific target for the development of hybridization probes.<sup>20</sup> Probes that can recognize and bind to the poly(rA) tail of mRNA might interfere with the full processing of mRNA by PAP and switch off protein synthesis. Some small molecules like protoberberine alkaloids have been found to bind to poly(rA) with high affinity leading to self-structure formation. Self-structure formation is very significant with respect to its biological importance.<sup>20-22</sup> On the other hand, it would be interesting to apply antisense agents to binding poly(rA), blocking transcriptional elongation and inhibiting the binding of transcriptional factors. Unlike regular antisense DNA/RNAs, PNA with high affinity, specificity and stability, would have great potential as a binder of poly(rA). It is also resistant to degradation in biological fluids as it is not recognized by nucleases or proteases. It has been proven that a PNA probe could efficiently recognize and bind to the poly(rA) tail.<sup>23</sup> However, the studies using PNA as a hybridization probe targeting poly(rA) via MRI has not been disclosed yet. Therefore, it would be interesting to know if Gd(III)-chelated PNA would be a useful poly(rA)-targeted CA.

Macromolecular MRI CA are mainly prepared by conjugating Gd-DOTA and Gd-DTPA to biocompatible macromolecules. Various bifunctional chelates of DTPA and DOTA have been developed with attachments such as anhydride, N-hydroxysuccinimide activated carboxylic acid, maleimide, alkynyl, and azide for conjugation. Bifunctional ligands and small molecular Gd(III) chelates can be readily attached to high-molecular-weight macromolecules including proteins,<sup>24</sup> polymers,<sup>25</sup> self-assembled peptide amphiphile nanofibers<sup>26</sup> and oligonucleotides<sup>27</sup>. The structures of some macromolecular Gd(III)-based CAs are shown in Figure 4.2. Generally, there are two main strategies for labelling of PNA with Gd(III) chelates. One of them is adding a Gd(III)-DOTA-containing monomer to the sequence during solid-phase synthesis. For example, a Fmoc-Lys(DOTA)-OH has been synthesized and inserted into PNA via solid-phase peptide synthesis.<sup>28</sup> The imaging radio-metal was chelated to the resulting PNA-DOTA. This type of labelling method has obvious drawbacks, such as laborious and time-consuming synthesis of modified PNA monomers and low yield of the coupling of the modified monomer due to potential incompatibility with the chemical conditions (acidic or basic) of SPPS. Hence, the other strategy via post-synthetic labelling either in solution or on the solid-phase resin has been attempted. For example, as Wickstrom reported, DOTA-(t-OBu)<sub>3</sub>COOH was coupled to the amino groups of PNA oligomer on solid-phase followed by cleavage and Gd chelation.<sup>29</sup> However, this procedure is still tedious and includes deprotection, activation, coupling, capping, deprotection again and Gd chelation. Also, protection of DOTA-COOH by t-OBu is required in this study to avoid side reactions as carboxylic group would participate in the coupling step. Therefore, an approach that is chemically selective, robust to functionalities on PNA and operationally easy is still needed. With the inspiration by our previous work

on post-synthetic click chemistry for functionalization of PNA,<sup>30</sup> a labelling strategy utilizing copper-catalysed click chemistry on polymer supported targets has been pursued. Although most of PNA-CuAAC approaches were performed in solution, our attention stayed on on-resin CuAAC, because it combines advantages of click chemistry and SPPS in which an excess of reactants can be used and easily washed away from the solid support without tedious workup; it is operationally easy to perform, and often to give quantitative yields. On the other hand, post-synthetic functionalization of the PNA oligomer represents a viable alternative to potentially reduce the overall synthetic effort, as well as introducing a step that is amenable to structural diversification. To apply on-resin CuAAC to post-synthetically functionalize PNA, an Fmoc-azide PNA monomer in which a nucleobase was replaced with an azide group has been synthesized.<sup>21</sup> Up to four azide monomers have been coupled into a PNA sequence by automated SPPS in different positions without any concern for incompatibility.

Accumulation of Gd-containing probes at the target site is usually a main concern owing to the limited concentration of the specific mRNAs in cancer cells. This has been addressed in Wickstrom's study in which multiple Gd chelators have been conjugated to PNA-peptide dendrimer.<sup>29,31</sup> In this way, the number of chelated Gd(III) ions per hybridization probe has been increased. In this way, the number of chelated Gd(III) ions per hybridization probe was increased by conjugation of PNA to a dendrimer labelled with Gd(III) chelators. They demonstrated that the relaxivity per probe rose as the number of Gd(III) per probe rose.

To develop an effective PNA probe as a potential MRI contrast agent that can recognize and bind to poly(rA), a hybridization probe, (Gd(III)-DOTA)<sub>4</sub>-PNA was designed and synthesized in this work. Unlike a dendrimer-shape PNA-Gd probe, this probe is a comb-

shape PNA with four Gd chelators. It could bind to long Poly(rA) tail and form a triplex structure, which could also concentrate Gd ions by taking advantage of the target sequence (Figure 4.3), thus enhancing the contrast of MR images. The limitations such as tedious work up and low yield of traditional approach that requires complicated protection strategy for conjugation of PNA with Gd chelators, cannot be neglected. Therefore, a method based on on-resin click chemistry is described in this chapter. A PNA sequence including four azide monomers and ten thymine residues targeting poly(rA) tail was first synthesised.<sup>32-34</sup> Alkynyl-(Gd(III)-DOTA) molecules could be “clicked” to the PNA oligomer via on-resin CuAAC to yield the hybridization probe, (Gd(III)-DOTA)<sub>4</sub>-PNA, which was successfully characterized and evaluated.

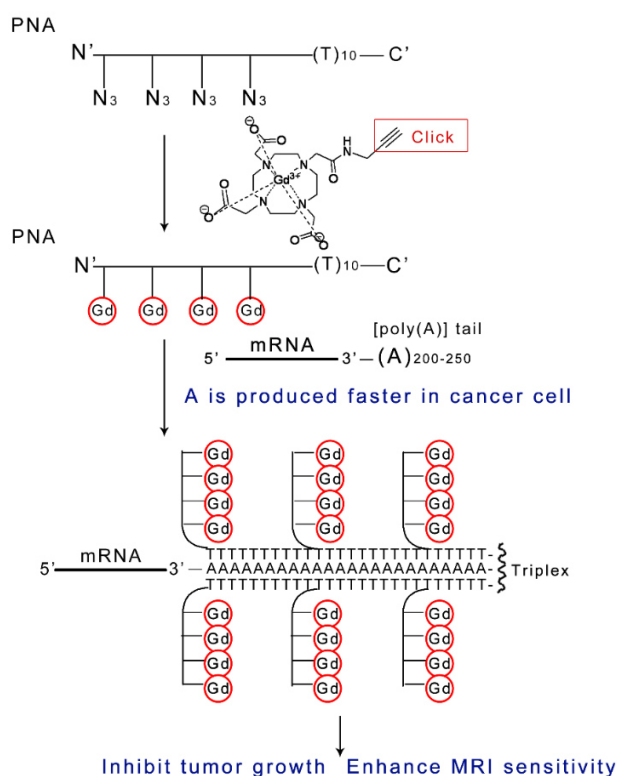


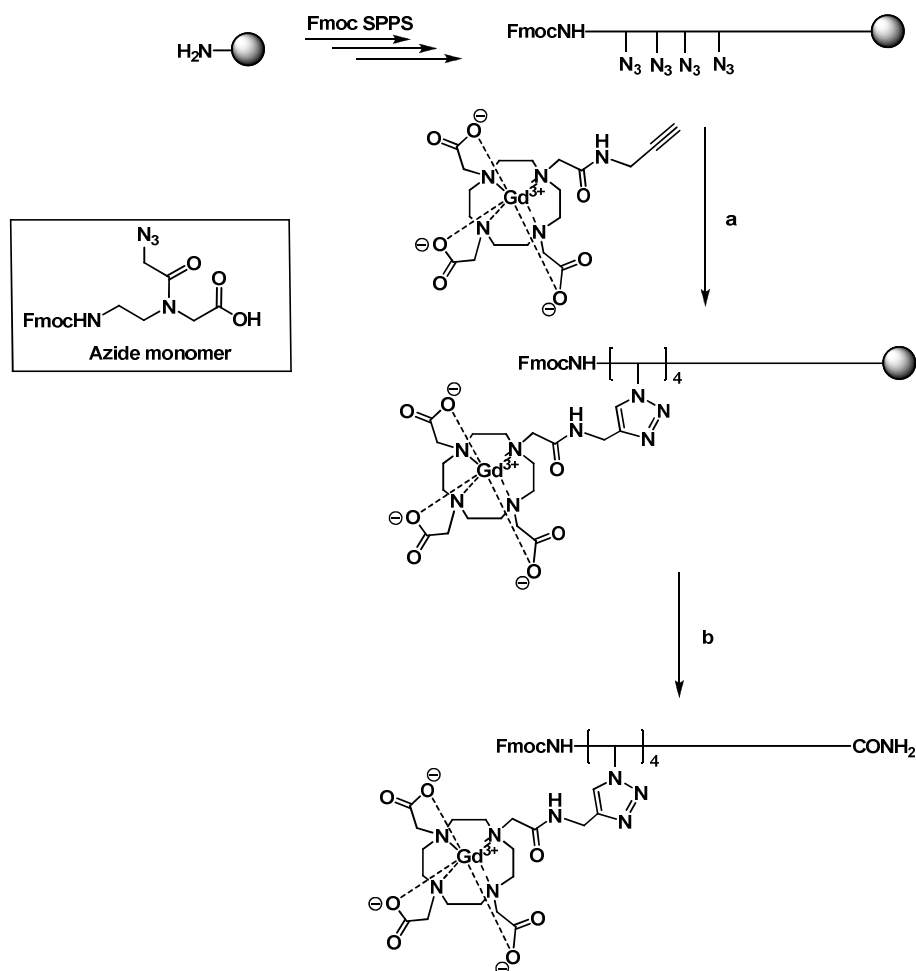
**Figure 4.3** Conceptual scheme of preparation and application of (Gd(III)-DOTA)<sub>4</sub>-PNA.



## 4.2 Results and discussion

In order to optimize the derivatization chemistry, a test sequence, Fmoc-TTT-Az-K (**PNA1**), containing one azide unit (Az, Scheme 4.1) was first synthesized. Without purification, the crude resin-bound **PNA1** was placed in a peptide vessel. Alkynyl-(Gd(III)-DOTA)<sup>35-37</sup> (30 equiv.), CuSO<sub>4</sub>·5H<sub>2</sub>O (60 equiv.), sodium ascorbate (240 equiv.), and the ligand *N,N'*-dimethylethylenediamine (DMEDA) (60 equiv.) were added and isopropanol/H<sub>2</sub>O(1:2, v/v) was used as the solvent. After the resin was shaken at room temperature (12 h), Gd(III)-DOTA was found to be successfully attached to **PNA1** with no underivatized **PNA1** being detected by LC/MS methods. The ESI-MS analysis showed a mass of 973.4175 [M+2H]<sup>2+</sup> and 648.9204 [M+3H]<sup>3+</sup> which were consistent with the calculated mass of 973.5574 [M+2H]<sup>2+</sup> and 649.3742 [M+3H]<sup>3+</sup>. We then proceeded to prepare a PNA containing four azide monomers, **PNA2** (Fmoc-K-Az-β-Az-β-Az-β-Az-K-TTTTTTTTTT-K) by using regular PNA T monomers, Fmoc-Lys(Boc)-OH, Fmoc-β-Ala-OH and Fmoc azide monomer (Scheme 4.1). A small portion of PNA was cleaved off the resin and characterization was performed by reversed phase HPLC and ESI-HRMS. The m/z of 1411.6052 [M+3H]<sup>3+</sup> and 1058.9668 [M+4H]<sup>4+</sup> agree well with the calculated m/z of 1411.7679 [M+3H]<sup>3+</sup> and 1059.0779 [M+4H]<sup>4+</sup>. Without purification, the resin-bound **PNA2** was subjected to CuAAC in the presence of excess alkynyl-(Gd(III)-DOTA) (Scheme 4.1). By using this approach, Fmoc(Gd(III)-DOTA)<sub>4</sub>-PNA conjugate (Fmoc-K-Gd-β-Gd-β-Gd-β-Gd-K-TTTTTTTTTT-K) has been successfully synthesised with quantitative conjugation yields via on-resin CuAAC. The excess reagents, solvents, and catalyst were easily washed from the resin, whereas the workup to remove these materials using solution phase methods can be laborious in our experience. ESI-HRMS of

Fmoc(Gd(III)-DOTA)<sub>4</sub>-PNA conjugate showed 1324.0796 [M+5H]<sup>5+</sup> and 1103.4063 [M+6H]<sup>6+</sup> which are in accordance with the calculated mass of 1324.0326 [M+5H]<sup>5+</sup> and 1103.5285 [M+6H]<sup>6+</sup>. After Fmoc deprotection and cleavage of the oligomer from the resin, only the usual reversed phase HPLC purification was required. MS results of (Gd(III)-DOTA)<sub>4</sub>-PNA (K-Gd-β-Gd-β-Gd-β-Gd-K-TTTTTTTTTT-K) showed 914.5258 [M+7H]<sup>7+</sup> and 710.6509 [M+9H]<sup>9+</sup> corresponding to the calculated mass of 914.2765 [M+7H]<sup>7+</sup> and 711.3279 [M+9H]<sup>9+</sup>.



**Scheme 4.1** Synthesis of  $(\text{Gd(III)-DOTA})_4\text{-PNA}$  by on-resin CuAAC. a) alkynyl- $(\text{Gd(III)-DOTA})$  (30 equiv.),  $\text{CuSO}_4 \cdot 5\text{H}_2\text{O}$  (60 equiv.), sodium ascorbate (240 equiv.), DMEDA (120 equiv.), isopropanol/ $\text{H}_2\text{O}$ (1:2, v/v), RT, overnight; b) TFA/TES (95:5, v/v).

To determine the stoichiometry of the binding of  $(\text{Gd(III)-DOTA})_4\text{-PNA}$  conjugate with poly(rA), Job plots from UV-vis data were constructed and DNA-A<sub>10</sub> was used as the counterpart of  $(\text{Gd(III)-DOTA})_4\text{-PNA}$ . The results were obtained at two wavelengths (260 and 283 nm)<sup>24</sup> (Figure 4.4). They indicated a binding stoichiometry of about 2 : 1 for  $(\text{Gd(III)-DOTA})_4\text{-PNA}:\text{DNA-dA}_{10}$  complexes, which demonstrated the formation of  $[(\text{Gd(III)-DOTA})_4\text{-PNA}]_2 : \text{DNA}$  triplexes.<sup>33</sup> Moreover, as the triplex formation of  $(\text{PNA}-$

$T_8)_2$ : poly(rA<sub>40</sub>) has been reported,<sup>32</sup> we believe that (Gd(III)-DOTA)<sub>4</sub>-PNA would form a triplex with poly(rA) with stoichiometry of 2:1.

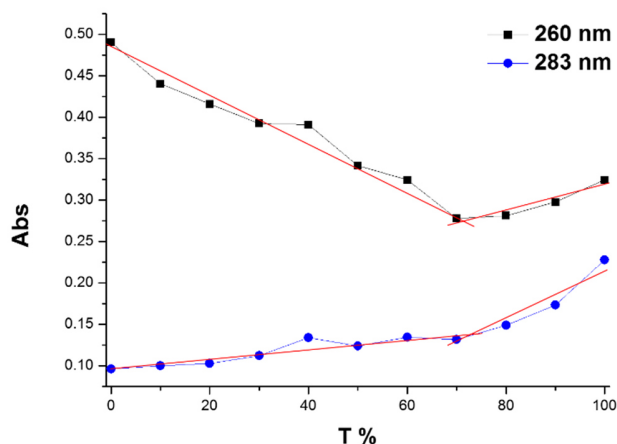


**Figure 4.4** Job plot of dA<sub>10</sub> (4  $\mu$ M/strand) and (Gd(III)-DOTA)<sub>4</sub>-PNA (4  $\mu$ M/strand) mixtures in the molar ratios of 0:100, 10:90, 20:80, 30:70, 40:60, 50:50, 60:40, 70:30, 80:20, 90:10. Solution conditions: 100 mM NaCl, 10 mM NaH<sub>2</sub>PO<sub>4</sub>, 0.1 mM EDTA, pH 7, 25  $^{\circ}$ C.

Thermal studies were performed by UV-melting in the presence of 2  $\mu$ M [(Gd(III)-DOTA)<sub>4</sub>-PNA]<sub>2</sub> : poly(rA). Urea was used as chaotropic agent because the triplex was found to be too stable to measure.<sup>38</sup> The melting curves illustrates a biphasic profile with  $T_m$  values of 56  $^{\circ}$ C and 85  $^{\circ}$ C in the presence of 6 M urea (Supplementary Information, Figure 4.8), indicating the existence of triplex, which is also demonstrated by the Job plot studies. Experiments were repeated thrice and the  $T_m$  values were measured from the first derivative plots.

To evaluate our (Gd(III)-DOTA)<sub>4</sub>-PNA probe, we acquired its NMRD profiles at a series of temperatures. A value of 5.6 mM<sup>-1</sup>s<sup>-1</sup> is observed at 20 MHz and 25  $^{\circ}$ C per Gd ion (Figure

4.6). NMRD profile of the triplex, [(Gd(III)-DOTA)<sub>4</sub>-PNA]<sub>2</sub> : Poly(rA), has also been achieved at 25 °C with r<sub>1</sub> of 6.6 mM<sup>-1</sup>s<sup>-1</sup> at 20 MHz. These findings are in good agreement with other DO3A monoamide compounds (4-5 mM<sup>-1</sup>s<sup>-1</sup>) under similar conditions.<sup>39</sup> Evaluation over the entire profile gives some indication of the solution structure of our probe. An increase in relaxivity is seen at ~20 MHz for both (Gd(III)-DOTA)<sub>4</sub>-PNA and the triplex, [(Gd(III)-DOTA)<sub>4</sub>-PNA]<sub>2</sub> : Poly(rA) at 298K. This increase has been attributed to the slowing of rotation,<sup>40</sup> possibly due to the aggregation of the (Gd(III)-DOTA)<sub>4</sub>-PNA and to a lesser extent the triplex formation in the presence of poly(rA). This is further seen in the temperature studies where the increase in relaxivity at 20 MHz is not present for higher temperatures, most likely due to the unfolding of the aggregate or destabilization of the triplex formation (supplemental information). It is also noteworthy that triplex formation of this probe with a poly(rA) tail would deliver 160–200 Gd<sup>3+</sup> ions to a localized microenvironment compared with dendrimeric developed contrast agents that have achieved a loading of 150-200 chelators using a generation 6 PAMAM dendrimers.<sup>41</sup> While there are 256 potential sites available in a G6 PAMAM dendrimer, a typical loading would be ~170 Gd<sup>3+</sup> ions per dendrimer. Other dendrimers up to G10 have been synthesised with a loading of 1860 Gd<sup>3+</sup> ions.<sup>42</sup> However, all these structures lack the specificity that is necessary for molecular MRI and incorporation of molecules such as polysaccharides,<sup>43–46</sup> oligopeptides,<sup>47–50</sup> proteins,<sup>47,51</sup> antibodies<sup>52</sup> and oligonucleotides<sup>53</sup> is needed. In comparison, our (Gd(III)-DOTA)<sub>4</sub>-PNA probe not only consists of targeting oligomer, but also concentrate and deliver a high load of Gd ions.

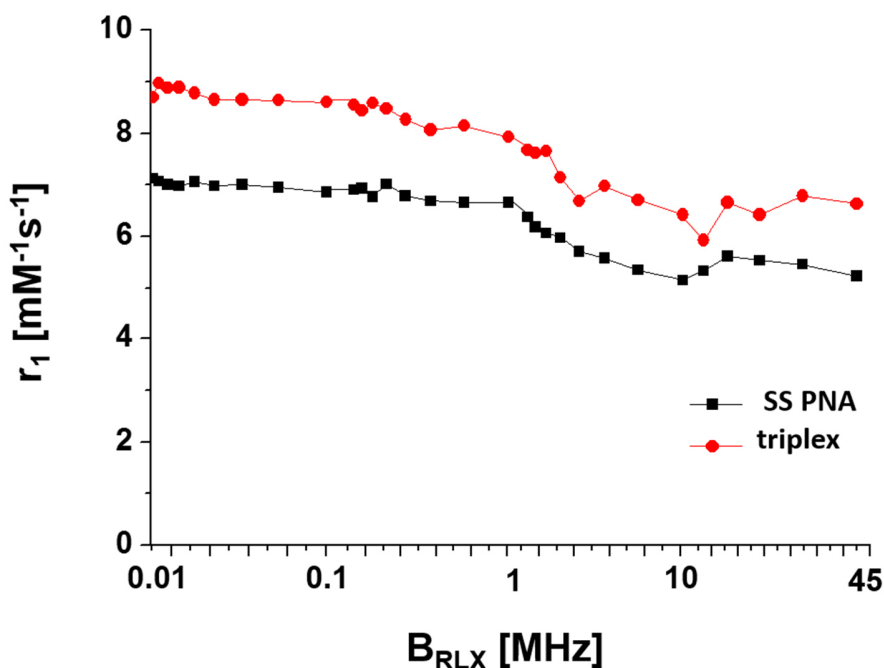


**Figure 4.5** Longitudinal relaxivity ( $r_1$ ) of  $[(\text{Gd(III)-DOTA})_4\text{-PNA}]_2\text{:Poly(rA)}$  triplex and control linear  $(\text{Gd(III)-DOTA})_4\text{-PNA}$  with a constant 0.13 mM Gd(III) in 100 mM NaCl, 10 mM  $\text{NaH}_2\text{PO}_4$ , 0.1 mM EDTA, 6 M urea, pH 7, 25 °C.

### 4.3 Conclusions

In summary, a poly(Gd(III)-DOTA)-PNA probe has been prepared via on-resin click chemistry, which is robust, operationally convenient and efficient for conjugation of PNA with Gd chelators. The resulting PNA oligomer could recognize poly(rA) tail of mRNA and form a stable triplex. The probe and its triplex with poly(rA) have been evaluated by NMRD studies. An increase in relaxivity is seen at 20MHz for the triplex,  $[(\text{Gd(III)-DOTA})_4\text{-PNA}]_2\text{: Poly(rA)}$  at 25 °C compared with  $(\text{Gd(III)-DOTA})_4\text{-PNA}$ . The relaxivity of  $(\text{Gd(III)-DOTA})_4\text{-PNA}$  at 38 °C ( $\sim 4.2 \text{ mM}^{-1}\text{s}^{-1}$ ) is comparable to the clinical agents Magnevist<sup>®</sup> (gadopentetate dimeglumine, Gd-DTPA), Dotarem<sup>®</sup> (gadoterate, Gd-

DOTA), Prohance<sup>®</sup> (gadoteridol, Gd(HP-DO3A)) and Omniscan<sup>®</sup> (gadodiamide, Gd(DTPA-BMA)) (3.5-3.8 mM<sup>-1</sup>s<sup>-1</sup> at 20 MHz and 37 °C). By binding to poly(rA), Gd ions would be significantly loaded to a localized microenvironment, which may improve the enhancement of contrast in MR images.

#### 4.4 Experimental

All chemicals and solvents were used as received unless specified. All solvents were peptide synthesis grade, except water (18.2 MΩ·cm<sup>-1</sup>). The “Fmoc-azide monomer” was prepared according to previously reported protocols.<sup>38</sup> All reagents for synthesis of PNAs were commercially available.

##### Synthesis of PNA1

PNA synthesis was performed on a 5 μmol scale using an automated ABI 433a peptide synthesizer. PEGA-Lys(Boc)-Fmoc resin (loading 0.113 mmol/g) were used as the solid support. The synthesis was terminated retaining the terminal Fmoc protecting group. A small portion of the resin was taken for characterization and the oligomer was cleaved/deprotected under standard conditions for the characterization of PNAs by ESI-MS. Other portions of the resin were taken and manipulated in manual peptide vessels.

##### General procedure for on-resin click chemistry

Alkynyl-(Gd(III)-DOTA) (30 equiv.) in isopropanol (0.5 mL), CuSO<sub>4</sub>·5H<sub>2</sub>O (60 equiv.) in H<sub>2</sub>O (0.33 mL), sodium ascorbate (120 equiv.) in H<sub>2</sub>O (0.33 mL), and *N,N'*-dimethylethylenediamine (DMEDA) (60 equiv.) in H<sub>2</sub>O (0.33 mL) were added to the resin in a peptide vessel. The resin was shaken at room temperature under N<sub>2</sub> overnight. After

the reaction was deemed completed by ESI-MS, the solvent was drained and the resin was washed sequentially with DMF, DCM, H<sub>2</sub>O, MeOH and finally DCM. Then PNA was cleaved from the resin, purified and characterized following by our previously reported procedure.<sup>54</sup>

The crude poly(Gd(III)-DOTA)-PNA probe purified by reversed phase HPLC at 50 °C on a 250 × 4.6 mm VARIAN C18 column eluted with a gradient of 0-5 min, 1% MeCN, 5-20 min, linear from 1% to 60% MeCN, 20-35 min, linear from 60% to 100% MeCN and 35-40 min, linear from 100% MeCN to 100% H<sub>2</sub>O. Both H<sub>2</sub>O and MeCN solvents contain 0.05% TFA.

#### **UPLC/Mass Spectroscopy of PNA oligomers**

Ultra-performance liquid chromatography (UPLC) was performed using a BEH C18 column (particle size 1.7 μm; 1.0 i.d.×100 mm), Waters LCT Premier high-resolution electrospray ionization mass spectroscopy (HR-ESI-MS) and diode array UV detectors. The mobile phase was 100% H<sub>2</sub>O to 100% MeCN over 5 min by linear gradient, and 100% MeCN over 2 min, at flow rate 0.1 mL/min. Both solvents contain 0.1% HCOOH.

#### **Quantification of oligomers**

UV-visible spectrophotometer was used to determine the concentrations of oligomer solutions. The absorbance at 258 nm and 260 nm of the samples were measured for poly(rA) and PNA, respectively. 9800 M<sup>-1</sup>cm<sup>-1</sup> was used as ε<sub>258</sub> of each nucleobase on poly(rA). The equation below was used for calculating the concentration of nucleobases of poly(rA).

$$c (\mu\text{M}) = \frac{1000 \times A_{258}}{9.8}$$



8800 M<sup>-1</sup>cm<sup>-1</sup> were used as  $\epsilon_{260}$  values of T. The equation below was used for calculating the concentration of nucleobases of poly(Gd(III)-DOTA)-PNA.

$$c (\mu\text{M}) = \frac{1000 \times A_{260}}{8.8}$$

### **Thermal denaturation experiments of oligomers**

UV melting experiments were carried out to measure the  $T_m$  values of oligomers in this study using the following ionic conditions: 100 mM NaCl, 10 mM Na<sub>2</sub>HPO<sub>4</sub>, 0.1 mM EDTA, pH 7.0. Samples at 2  $\mu\text{M}$  concentration were heated to 95 °C, cooled to room temperature over 1-2 hours, and placed at 4 °C overnight. Denaturation was performed from 15 to 90 °C at a temperature ramp rate of 0.5 °C/min. The  $T_m$  values are an average of three measurements and are rounded to the nearest 1 °C. The error in  $T_m$  values was  $\pm$  0.5 °C.  $T_m$  values were estimated for cooperative transitions by the first derivative method. Temperature dependent UV spectra that lacked upper and lower baselines, lacked sigmoidal shape or were indistinguishable from SS PNA intramolecular melting were deemed not to be cooperative transitions.

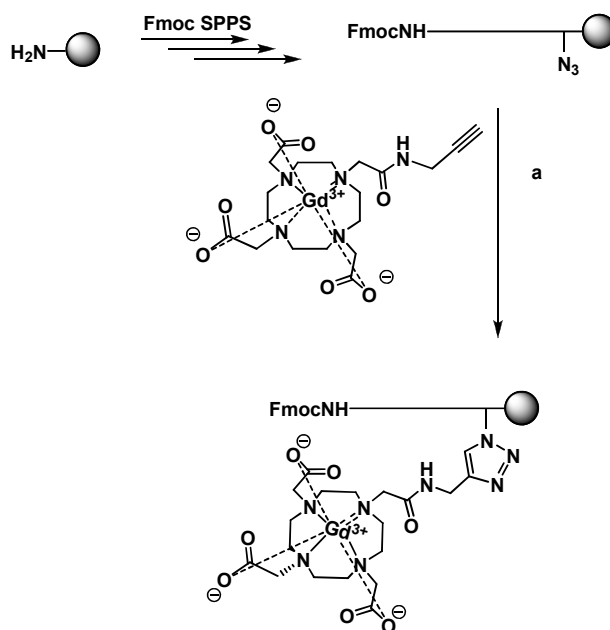
### **General procedure for drawing Job plot by UV-vis method**

A series solutions containing (Gd(III)-DOTA)<sub>4</sub>-PNA and dA<sub>10</sub> in the ratios of 0:100, 10:90, 20:80, 30:70, 40:60, 50:50, 60:40, 70:30, 80:20, 90:10 and 100:0, respectively, were prepared with the concentration of 4  $\mu\text{M}$  at pH 7.0 in the condition of 100 mM NaCl, 10 mM Na<sub>2</sub>HPO<sub>4</sub>, 0.1 mM EDTA, pH 7.0. The absorbances at 260 nm and 283 nm were plotted against the percentage of (Gd(III)-DOTA)<sub>4</sub>-PNA.

## Nuclear Magnetic Relaxation Dispersion (NMRD) studies of single strand, (Gd(III)-DOTA)<sub>4</sub>-PNA and the triplex, [(Gd(III)-DOTA)<sub>4</sub>-PNA]<sub>2</sub>:Poly(rA)

The T<sub>1</sub> NMRD profiles of 1 mL samples were acquired with a fast field-cycling NMR relaxometer (SpinMaster FFC2000 1T C/DC, Stelar, s.r.l. Mede, Pavia (PV) - Italy). All experiments were acquired with controlled temperatures (25, 38, 60 and 80 °C) and changing the relaxation field in 30 steps, logarithmically distributed from 0.01 to 42.485 MHz (0.23 mT up to 1 T) and using an acquisition field of 16.2 MHz. The quantitative relaxivity (r<sub>1</sub>) values were normalized to the reported gadolinium concentration for each sample.

### 4.5 Supplementary Information



**Scheme 4.2** Synthesis of Gd(III)-DOTA-PNA1 by on-resin CuAAC. a) alkyne-(Gd(III)-DOTA) (7.5 equiv.), CuSO<sub>4</sub>·5H<sub>2</sub>O (15 equiv.), sodium ascorbate (30 equiv.), *N,N'*-dimethylethylenediamine (DMEDA) (15 equiv.), isopropanol/H<sub>2</sub>O (1:2, v/v), r.t.; b) TFA/TES (95:5, v/v).

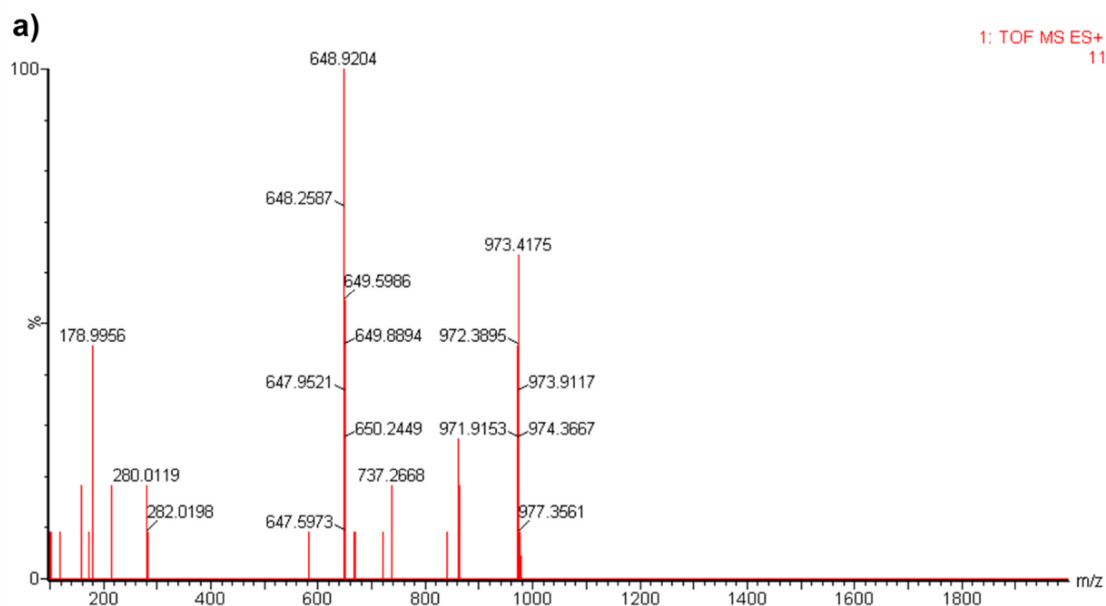


**Figure 4.6** ESI-MS spectrum of **PNA1** calculated mass for  $C_{79}H_{104}GdN_{25}O_{24}$ : 973.5574  $[M+2H]^{2+}$ .

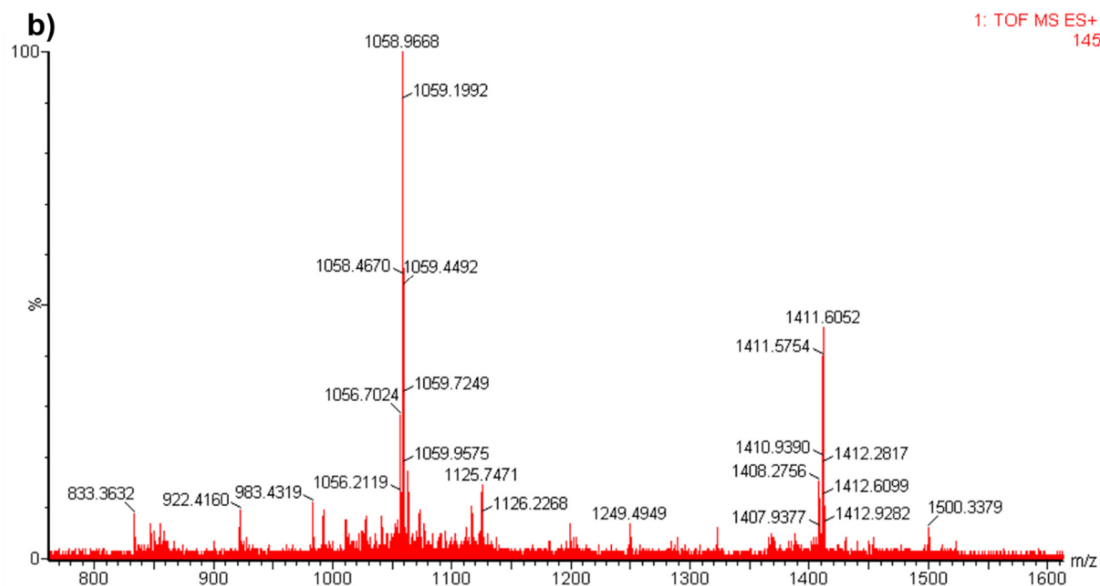


**Figure 4.7** ESI-MS spectrum of **PNA2**, calculated mass for  $C_{176}H_{240}N_{70}O_{56}$ : 1411.7679  $[M+3H]^{3+}$ , 1059.0779  $[M+4H]^{4+}$ .

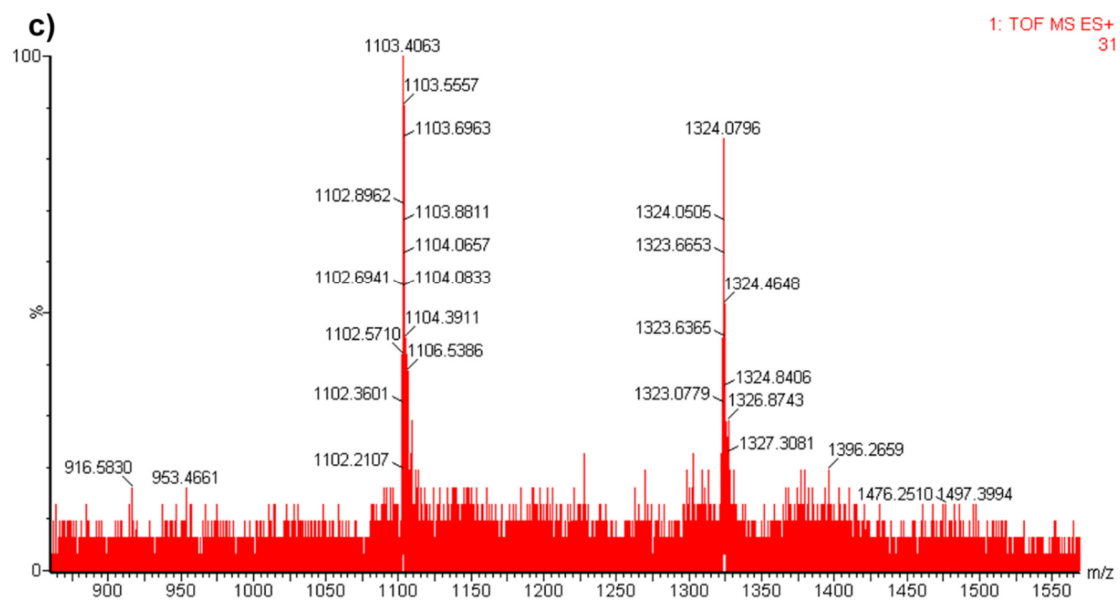


**Figure 4.8** ESI-MS spectrum of **Fmoc(Gd(III)-DOTA)<sub>4</sub>-PNA**, calculated mass for  $C_{252}H_{352}Gd_4N_{90}O_{84}$ : 1324.0326  $[M+5H]^{5+}$ , 1103.5285  $[M+6H]^{6+}$ .

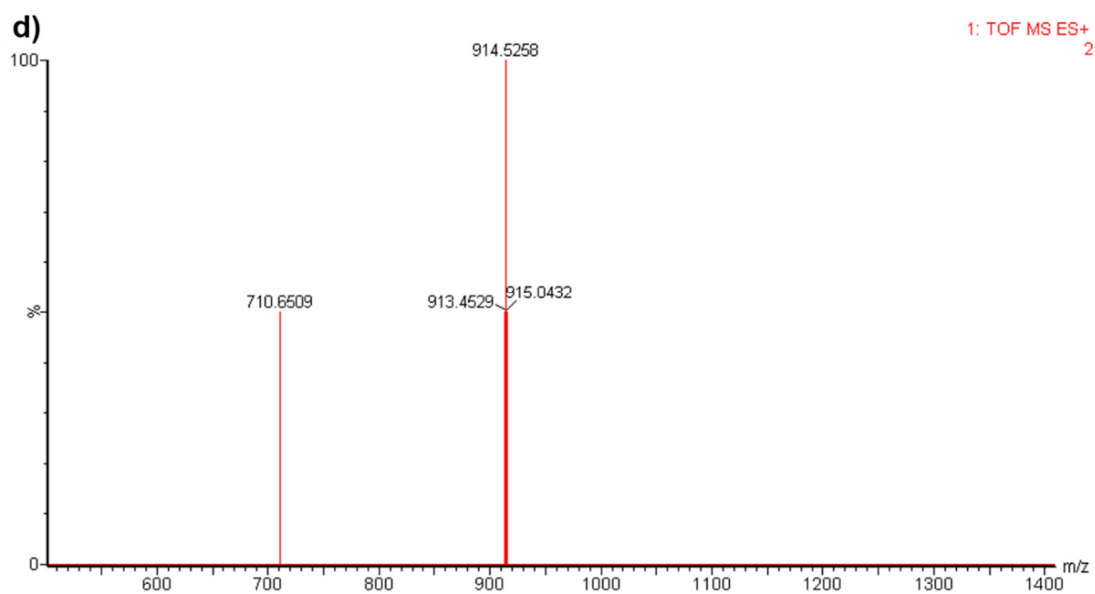
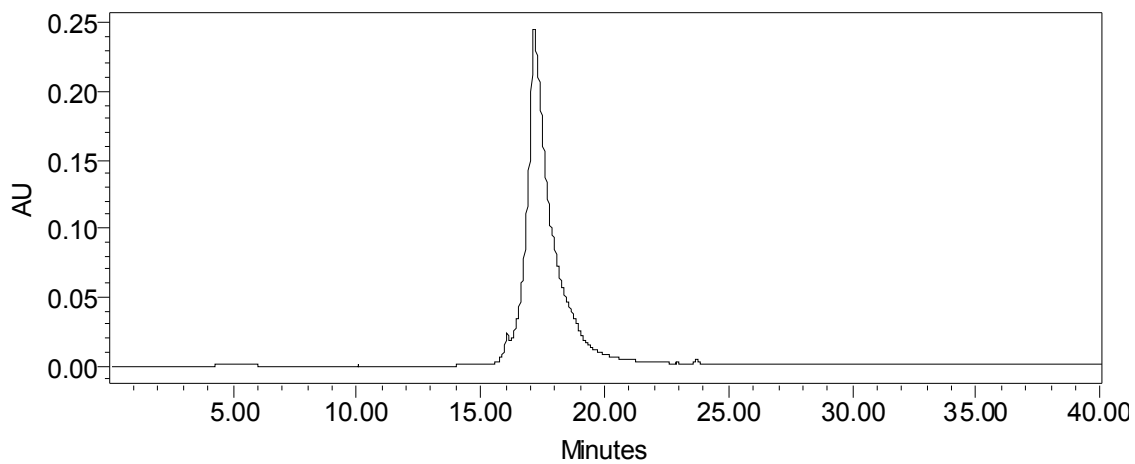


**Figure 4.9** HPLC-UV absorption spectrum of purified **(Gd(III)-DOTA)<sub>4</sub>-PNA** (top) and ESI-MS spectrum of **(Gd(III)-DOTA)<sub>4</sub>-PNA** (bottom), calculated mass for  $C_{237}H_{342}Gd_4N_{90}O_{82}$ : 914.2765  $[[M+7H]^7+$ , 711.3279  $[M+9H]^9+$ .

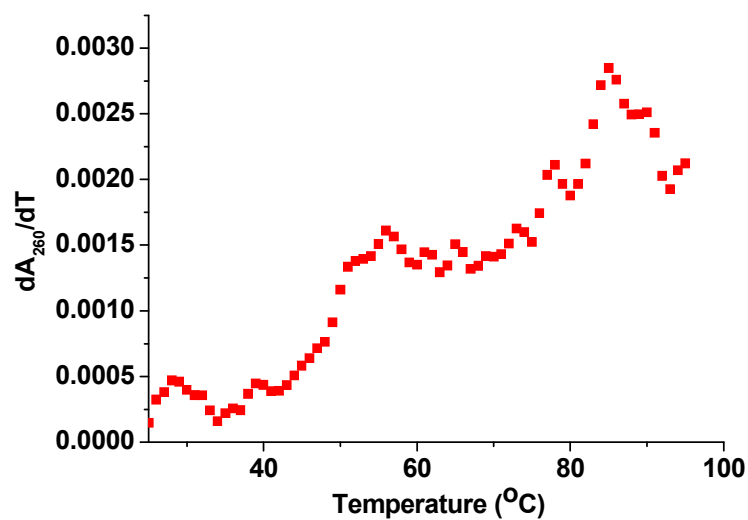


**Figure 4.10** First derivative UV melting plots of  $[(\text{Gd}(\text{III})\text{-DOTA})_4\text{-PNA}]_2\text{:poly}(\text{rA})$  at 260 nm at a concentration of 2  $\mu\text{M}$ . conditions: 100 mM NaCl, 10 mM  $\text{NaH}_2\text{PO}_4$ , 0.1 mM EDTA, 6 M urea, pH 7, 25 °C.

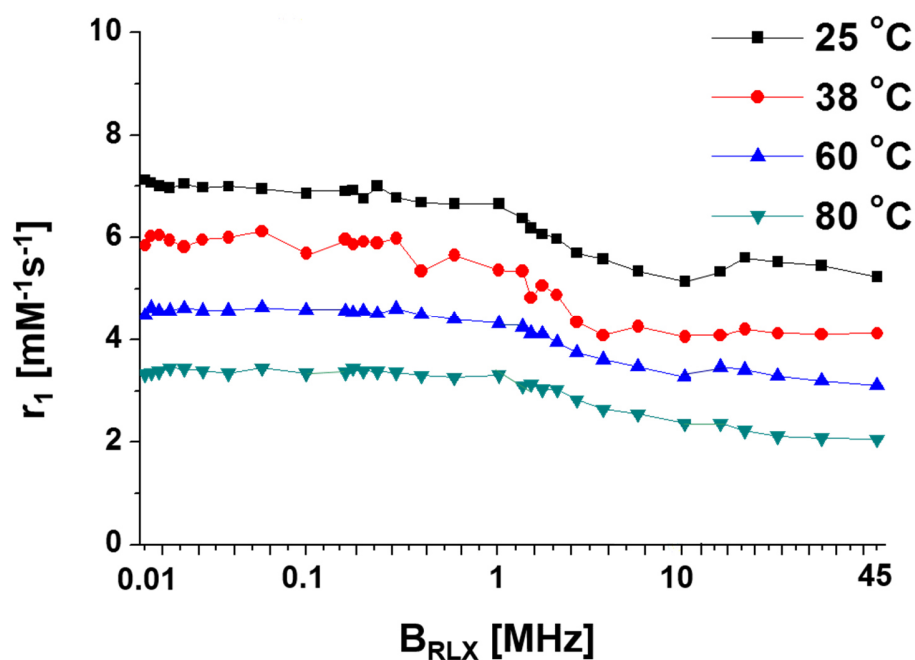


**Figure 4.11** NMRD profiles of (Gd(III)-DOTA)<sub>4</sub>-PNA at 25, 38, 60 and 80 °C. conditions: 100 mM NaCl, 10 mM NaH<sub>2</sub>PO<sub>4</sub>, 0.1 mM EDTA, 6 M urea, pH 7, 25 °C.

#### 4.6 References

- (1) Massoud, T. F.; Gambhir, S. S.; Gambhir, S. S. *Genes Dev.* **2003**, 545.
- (2) Tóth, É.; Helm, L.; Merbach, A. E. *Top. Curr. Chem.* **2002**, 221, 123.
- (3) Sung, M. H.; Salvatore, L.; De Lorenzi, R.; Indrawan, A.; Pasparakis, M.; Hager, G. L.; Bianchi, M. E.; Agresti, A. *PLoS One* **2009**, 4 (9).
- (4) Lauffer, R. B. *Chem. Rev.* **1987**, 87 (5), 901.
- (5) Caravan, P.; Ellison, J. J.; McMurry, T. J.; Lauffer, R. B. *Chem. Rev.* **1999**, 99 (9), 2293.

- (6) Biagi, B. A.; Enyeart, J. J. *Am. J. Physiol.* **1990**, *259*, 515.
- (7) Lansman, J. B. *J. Gen. Physiol.* **1990**, *95* (April 1990), 679.
- (8) Greenberg, S. a. *Radiology* **2010**, *257* (3), 670.
- (9) Laurent, S.; Elst, L. V; Copoix, F.; Muller, R. N. *Invest. Radiol.* **2001**, *36* (2), 115.
- (10) Thomsen, H. S. *Eur. Radiol.* **2006**, *16* (12), 2619.
- (11) Botta, M.; Tei, L. *Eur. J. Inorg. Chem.* **2012**, No. 12, 1945.
- (12) Spanoghe, M.; Lanens, D.; Dommissie, R.; Van der Linden, A.; Alderweireldt, F. *Magn. Reson. Imaging* **1992**, *10* (6), 913.
- (13) Fries, P.; Runge, V. M.; Bucker, A.; Schürholz, H.; Reith, W.; Robert, P.; Jackson, C. B.; Lanz, T.; Schneider, G. *Invest. Radiol.* **2009**, *44* (4), 200.
- (14) Jacobson, A. *Annu. Rev. Biochem.* **1996**, *65*, 693.
- (15) Lewis, J. D.; Gunderson, S. I.; Mattaj, I. W. *J Cell Sci Suppl* **1995**, *19*, 13.
- (16) Wickens, M.; Anderson, P.; Jackson, R. J. *Curr. Opin. Genet. Dev.* **1997**, *7* (2), 220.
- (17) Fuke, H.; Ohno, M. *Nucleic Acids Res.* **2008**, *36* (3), 1037.
- (18) Topalian, S. L.; Kaneko, S.; Gonzales, M. I.; Bond, G. L.; Ward, Y.; Manley, J. L. *Mol. Cell. Biol.* **2001**, *21* (16), 5614.
- (19) Topalian, S. L.; Gonzales, M. I.; Ward, Y.; Wang, X.; Wang, R. F. *Cancer Res.* **2002**, *62*, 5505.



- (20) Xing, F.; Song, G.; Ren, J.; Chaires, J. B.; Qu, X. *FEBS Lett.* **2005**, *579* (22), 5035.
- (21) Giri, P.; Kumar, G. S. *Arch. Biochem. Biophys.* **2008**, *474* (1), 183.
- (22) Giri, P.; Suresh Kumar, G. *Mol. Biosyst.* **2010**, *6*, 81.
- (23) Kawakami, J.; Wang, Z.-M.; Fujiki, H.; Izumi, S.; Sugimoto, N. *Chem. Lett.* **2004**, *33* (12), 1554.
- (24) Karfeld, L. S.; Bull, S. R.; Davis, N. E.; Meade, T. J.; Barron, A. E. *Bioconjug. Chem.* **2007**, *18* (6), 1697.
- (25) Langereis, S.; de Lussanet, Q. G.; van Genderen, M. H. P.; Meijer, E. W.; Beets-Tan, R. G. H.; Griffioen, A. W.; van Engelshoven, J. M. A.; Backes, W. H. *NMR Biomed.* **2006**, *19* (1), 133.
- (26) Yang, X.; Loos, J.; Veenstra, S. C.; Verhees, W. J. H.; Wienk, M. M.; Kroon, J. M.; Michels, M. A. J.; Janssen, R. A. J. *Nano Lett.* **2005**, *5* (4), 579.
- (27) Mishra, R.; Su, W.; Pohmann, R.; Pfeuffer, J.; Sauer, M. G.; Ugurbil, K. *Bioconjug. Chem.* **2009**, *20*, 1860.
- (28) Lewis, M. R.; Jia, F.; Gallazzi, F.; Wang, Y.; Zhang, J.; Shenoy, N.; Lever, S. Z.; Hannink, M. *Bioconjug. Chem.* **2002**, *13* (6), 1176.
- (29) Amirkhanov, N. V.; Dimitrov, I.; Opitz, A. W.; Zhang, K.; Lackey, J. P.; Cardi, C. a.; Lai, S.; Wagner, N. J.; Thakur, M. L.; Wickstrom, E. *Biopolymers* **2008**, *89* (12), 1061.
- (30) Wang, X.; Hudson, R. H. E. *ChemBioChem* **2015**, *16* (15), 2156.

- (31) Amirkhanov, N. V.; Wickstrom, E. *Nucleosides Nucleotides Nucleic Acids* **2005**, 24 (5–7), 423.
- (32) Gourishankar, A.; Ganesh, K. N. *Artif. DNA. PNA XNA* **2012**, 3 (1), 5.
- (33) Kim, S. K.; Nielsen, P. E.; Egholm, M.; Buchardt, O.; Berg, R. H.; Vef, B. N. *J. Am. Chem. Soc.* **1993**, 115 (15), 6477.
- (34) Almarsson, O.; Bruice, T. C. *Proc. Natl. Acad. Sci. U. S. A.* **1993**, 90 (20), 9542.
- (35) Prasuhn, D. E.; Yeh, R. M.; Obenaus, A.; Manchester, M.; Finn, M. G. *Chem. Commun. (Camb)*. **2007**, No. 12, 1269.
- (36) Viguier, R. F. H.; Hulme, A. N. *J. Am. Chem. Soc.* **2006**, 128 (35), 11370.
- (37) Wojciechowski, F.; Groß, A.; Holder, I. T.; Knörr, L.; Drescher, M.; Hartig, J. S. *Chem. Commun.* **2015**, 13850.
- (38) St Amant, A. H.; Engbers, C.; Hudson, R. H. E. *Artif. DNA PNA XNA* **2013**, 4 (1), 4.
- (39) Aime, S.; Anelli, P. L.; Botta, M.; Fedeli, F.; Grandi, M.; Paoli, P.; Uggeri, F. *Inorg. Chem.* **1992**, 31 (1), 2421.
- (40) Aime, S.; Botta, M.; Terreno, E. *Advances in Inorganic Chemistry*; 2005; 57, 173–232.
- (41) Wiener, E. C.; Brechbiel, M. W.; Brothers, H.; Magin, R. L.; Gansow, O. A.; Tomalia, D. A.; Lauterbur, P. C. *Magn. Reson. Med.* **1994**, 31 (1), 1.
- (42) Bryant, L. H.; Brechbiel, M. W.; Wu, C.; Bulte, J. W. M.; Herynek, V.; Frank, J.

- A. J. Magn. Reson. Imaging* **1999**, *9* (2), 348.
- (43) Zanini, D.; Roy, R. *J. Am. Chem. Soc.* **1997**, *119* (9), 2088.
- (44) Wolfenden, M. L.; Cloninger, M. J. *Bioconjug. Chem.* **2006**, *17* (4), 958.
- (45) Zanini, D.; Pamam, S. *J. Org. Chem.* **1998**, *63*, 3486.
- (46) Woller, E. K.; Walter, E. D.; Morgan, J. R.; Singel, D. J.; Cloninger, M. J. *J. Am. Chem. Soc.* **2003**, *125* (29), 8820.
- (47) van Baal, I.; Malda, H.; Synowsky, S. A.; van Dongen, J. L. J.; Hackeng, T. M.; Merkx, M.; Meijer, E. W. *Angew. Chem. Int. Ed. Engl.* **2005**, *44* (32), 5052.
- (48) Rijkers, D. T. S.; van Esse, G. W.; Merkx, R.; Brouwer, A. J.; Jacobs, H. J. F.; Pieters, R. J.; Liskamp, R. M. J. *Chem. Commun.* **2005**, *0* (36), 4581.
- (49) Crespo, L.; Sanclimens, G.; Pons, M.; Giralt, E.; Royo, M.; Albericio, F. *Chem. Rev.* **2005**, *105* (5), 1663.
- (50) Sadler, K.; Tam, J. P. *Rev. Mol. Biotechnol.* **2002**, *90* (3–4), 195.
- (51) Kluger, R.; Zhang, J. *J. Am. Chem. Soc.* **2003**, *125* (20), 6070.
- (52) Wu, C.; Brechbiel, M. W.; Kozak, R. W.; Gansow, O. A. *Bioorganic Med. Chem. Lett.* **1994**, *4* (3), 449.
- (53) Choi, Y.; Mecke, A.; Orr, B. G.; Banaszak Holl, M. M.; Baker, J. R. *Nano Lett.* **2004**, *4* (3), 391.
- (54) Hudson, R. H.; Liu, Y.; Wojciechowski, F. *Can. J. Chem.* **2007**, *85* (4), 302.
- (55) Zhou, Z. and Lu, Z.-R. *Wiley Interdiscip. Rev. Nanomed. Nanobiotechnol.*, **2013**,

5, 1-18.

## **CHAPTER V: BIOCONJUGATION OF OLIGOPEPTIDE TO GOLD NANOPARTICLES FOR CT IMAGING VIA STRAIN-PROMOTED AZIDE-ALKYNE CYCLOADDITION (SPAAC)**

Chapter 5 has been published as a research paper, and it is reprinted (adapted) with permission from Xiaoxiao Wang, Pierangelo Gobbo, Mojmir Suchy, Mark S. Workentin\* and Robert H. E. Hudson\*, RSC Advances, 2014, 4, 43087-43091. Copyright 2014 Royal Society of Chemistry.

### **5.1 Introduction to gold nanoparticles and targeted CT imaging**

Gold in its bulk scale is a popular material and has been widely used in jewelry, coinage, and electronics. Gold has been found of great help in applications ranging from catalysts<sup>1-3</sup> to anti-arthritis medications.<sup>4</sup> Unlike bulk- or molecular-scale gold, gold nanoparticles (AuNPs) exhibit unique properties due to their size.<sup>5</sup> The word *nano* describes any material or property with dimensions on the nanometre scale (1-100 nm). In 2012, Dreaden and coworkers have summarized AuNPs of various sizes and shapes with potential applications in biomedicine.<sup>6</sup> They could preferentially accumulate at tumor or inflammation sites and enter cells through different but faster pathways than small molecules. Due to their facile surface chemistry, AuNPs loaded with binding ligands can be used as artificial antibodies. Their binding affinity can be precisely tuned by varying the density of binding ligands on the surfaces. AuNPs can also efficiently convert light into heat, so they would lead to highly specific thermal ablation of diseased or infected tissues. Multivalency of gold enables AuNPs to shield unstable drugs or poorly soluble imaging contrast agents (CAs) and to facilitate effective delivery to otherwise inaccessible regions of the body. Because of the greater number of electrons of gold, AuNPs attenuate X-rays more effectively than iodine-

based CAs and therefore produces superior contrast for diagnostic computed tomography (CT) scans. More importantly, it is possible that all of the above-mentioned advantages of gold nanoparticles can be chemically combined into one construct allowing for simultaneous targeting, diagnostic, and therapeutic functionalities which are helpful for a particular patient or a disease.<sup>5</sup>

CT has become one of the most widespread molecular imaging technologies due to its high sensitivity and spatial resolution, cost effectiveness, deep penetration capability, and facile three-dimensional imaging reconstruction technique.<sup>7,8</sup> To obtain high-quality CT imaging of soft tissues, CAs are usually required such as iodine-based small molecules. However, their disadvantages like short imaging time due to their fast clearance by kidney, renal toxicity at a relatively high concentration,<sup>9</sup> and especially non-specificity cannot be neglected. Therefore, it is essential to develop novel targeted CT contrast agents to overcome these shortcomings.

Nanoscale CAs for CT imaging have become extremely attractive thanks to the development of nanotechnology. Various nanoparticles-based CAs, such as bismuth sulfide nanoparticles,<sup>10-13</sup> lanthanide-doped BaYbF<sub>5</sub> upconversion nanoprobe,<sup>14</sup> lutetium-based nanoparticulate CAs,<sup>15</sup> ytterbium-based NPs,<sup>16,17</sup> tantalum oxide NPs,<sup>18</sup> and AuNPs,<sup>19</sup> have been employed for targeted CT imaging of different biological systems. Among the diverse types of nanoscale CT CAs, AuNPs have been given considerable attention owing to their better X-ray attenuation than iodinated CT contrast agents, chemical stability, and good biocompatibility after surface functionalization.<sup>8,20-23</sup>

In 1971, Faulk and Taylor reported a technique to conjugate antibodies with colloidal gold for direct electron microscopic visualization of Salmonella surface antigens.<sup>24</sup> From then

on, functionalized AuNPs have been extensively investigated in the fields of diagnostics, bioimaging, drug and gene delivery, immunology and plasmonic biosensors.<sup>6,25–28</sup> The success of AuNPs in these fields has led to the Food and Drug Administration (FDA) approval for AuNP-based *in vitro* diagnostic systems in clinical trials for cancer treatments.<sup>29</sup> To develop effective systems for targeted cancer diagnosis and therapies, it is necessary to functionalize AuNPs with biomolecules such as DNA, proteins and peptides. Peptide-AuNP conjugates have been exploited recently as CAs and nanocarriers in targeted imaging for early stage cancer diagnosis and in the pharmaceutical field for targeted intracellular drug/gene delivery, respectively.<sup>27,30</sup>

Thus our attention has been turned to the development of targeted CT CAs via functionalization of AuNP with PNA or oligopeptides which would be a good start. The main challenge of conjugation of peptides to AuNPs lies in understanding and controlling the interfacial chemistry between the peptide and the nanomaterial surface on the molecular scale. The reported strategies for bioconjugation of AuNPs with peptides include sulphur-gold bond formation by the direct reaction of cysteine-terminated peptides with the gold surface and electrostatic interactions between a particle and peptides that have been coupled to bovine serum albumin (BSA).<sup>31</sup> Although the first method is operationally easy to perform, it is difficult to achieve a high degree of substitution. AuNP bioconjugation via electrostatic interactions has good stability in aqueous solution, but the layer-by-layer assembly results in large hydrodynamic radii of nanoparticles, which limits their application under certain conditions, and offers poor control over the degree of functionalization. Alternatively, a strategy via amide bonds formation involving a water-soluble carbodiimide, *N*-(3-dimethylaminopropyl)-*N*-ethylcarbodiimide hydrochloride

(EDC), was developed for bioconjugation of AuNPs. Carboxylic groups can be activated by EDC and reacted with primary amines through a condensation reaction to yield amide bonds. Moreover, sulfo-NHS (*N*-hydroxy sulfosuccinimide) is used to increase the stability of active intermediates in coupling reactions via the formation of active ester functional groups with carboxylates. EDC/NHS coupling has been widely used in preparation of AuNP-peptide conjugates.<sup>32</sup> However, this method is still a challenge as quite often, the peptides do not couple efficiently to AuNPs.<sup>33,34</sup> Additionally, EDC/NHS coupling method is not very selective as it involves the reaction between an amine and carboxylic acid groups, which widely exist in peptides.<sup>35</sup>

In order to overcome the aforementioned difficulties, recent effort has focused on the use of “click chemistry” for conjugation of AuNPs with biomolecules.<sup>33</sup> For example, the copper-catalyzed azide-alkyne cycloaddition (CuAAC) has been utilized to conjugate large azido-containing AuNPs with alkyne functionalized horseradish peroxidase (HRP).<sup>34</sup> However, the requirement of using copper ion as catalyst complicates the reaction and could increase *in vivo* biological toxicity. The strain-promoted azide-alkyne cycloaddition (SPAAC), also known as Cu-free alkyne-azide cycloaddition, can be used to overcome these problems. The SPAAC reaction has been developed as a powerful bioconjugation tool that displays outstanding chemoselectivity, excellent biocompatibility and takes place under very mild reaction conditions. Since its first development,<sup>36</sup> much effort has been directed toward the synthesis of cycloalkynes with increased ring strain (to accelerate the reaction) and higher hydrophilic character (for *in vivo* applications). The challenge behind the syntheses of these interesting molecules relies on finding the right balance between reactivity and chemoselectivity. Indeed, the greater the ring strain, the more susceptible the



triple bond is to nucleophilic attack (i.e., addition reactions or rearrangement of cyclooctynes) thus lowering the chemoselectivity towards the cycloaddition with an azide. For example, it has been reported that highly strained biarylazacyclooctynone and analogous bioconjugation reagents undergo rearrangement and addition reactions leading to tetracyclic products.<sup>37</sup> The rate of rearrangement was found to be accelerated as the concentration of acid increased. This is problematic because concentrated TFA, such as 95% TFA with scavengers, is the typical reagent for cleavage of peptides from solid supports like Wang resin, Rink Amide resin, etc. together with the removal of the side chain protecting groups. This limits the applications of strained alkynes for preparation of clickable peptides. Additionally, strained alkynes have been shown to undergo side reactions with cellular cysteines and other nucleophilic residues.<sup>38,39</sup> However, nucleophilic side chain functionalities, such as hydroxyl (Tyr, Ser, Thr), amino (Lys), guanidine (Arg) or sulfhydryl (Cys), widely exist in bioactive peptides and may react with highly reactive cyclooctynes through a nucleophilic attack.<sup>40</sup> This also limits the application of SPAAC. Interestingly, the application of interfacial SPAAC for bioconjugation of AuNPs with peptides had not yet been disclosed prior to the work described herein.

In this chapter, the development of a novel general method for the synthesis of AuNP-peptide bioconjugates is described that takes into account the side reactivity of the strained alkynes and therefore combines an interfacial SPAAC with a post assembly deprotection (PAD) for the conjugation of dibenzocyclooctyne (DBCO)-oligopeptides to small, water-soluble azide-AuNPs. It is shown that how this approach overcomes the aforementioned drawbacks and extends the application of SPAAC to the bioconjugation of metallic

nanoparticles in a quick, reliable and facile way. Importantly, the undesired side reactions of the strained alkyne in the presence of concentrated TFA and with nucleophilic sites on peptides are avoided through mild cleavage condition and retention of side-chain protecting groups on the peptides during the SPAAC reaction. The protecting groups can then be easily removed, i.e. post assembly deprotection (PAD), under reaction conditions that preserve the integrity of the gold core, and the AuNP bioconjugate can be easily purified by dialysis. Finally, the amount of conjugated peptide can be easily calculated.

## 5.2 Results and discussion

To showcase this SPAAC-PAD strategy an azide-AuNPs based on tri- and tetra-ethylene glycol ligands that impart both water- and organic solvent-solubility to final AuNPs was used. This is useful for manipulating the AuNP in organic solvents to facilitate both the SPAAC reaction and the deprotection reaction, as well as maintaining solubility in water for further *in vivo* applications.

The azide-AuNPs were prepared and characterized following our previously reported procedure.<sup>41</sup> Briefly, triethylene glycolmonomethyl ether AuNP (Me-EG<sub>3</sub>-AuNP) with a gold core diameter of  $3 \pm 0.5$  nm were synthesized via a modified Brust-Schiffrin method. The azide ligand N<sub>3</sub>-EG<sub>4</sub>-SH was synthesized and introduced onto the surface of Me-EG<sub>3</sub>-AuNP using a place-exchange reaction. In a typical synthesis 42.5 mmol of N<sub>3</sub>-EG<sub>4</sub>-SH were stirred for 20 minutes in acetone and in presence of 50 mg of Me-EG<sub>3</sub>-AuNP.

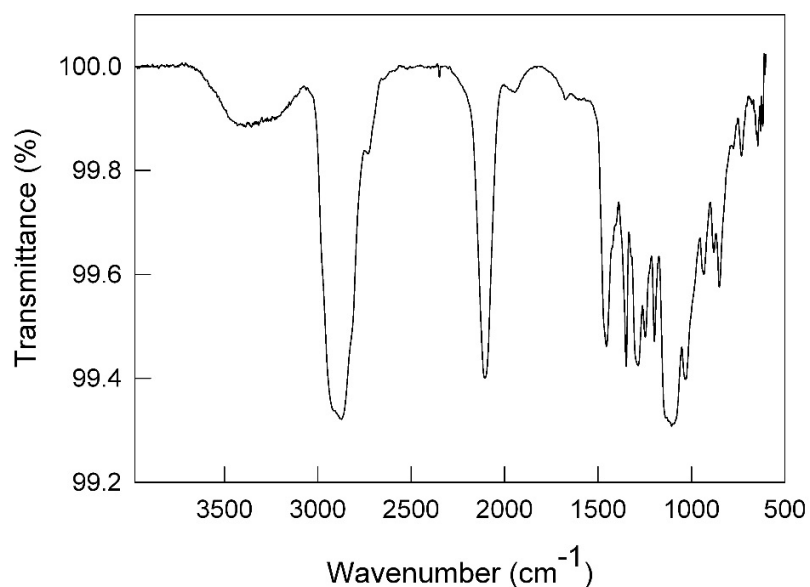


**Figure 5.1** IR spectrum of azide AuNPs.

The free thiols were subsequently removed by trituration of the dried AuNP film first with hexanes and followed by isopropanol. Azide-AuNPs were characterized by thermogravimetric analysis (TGA), transmission electron microscopy (TEM) and FT-IR spectroscopy. The IR spectrum of resulting AuNPs showed the appearance of asymmetrical stretching of the azide group at  $2110\text{ cm}^{-1}$  (Figure 5.1). TGA data indicated that the corona of the AuNP is composed of 35% of azide ligands (Figure 5.2) and thus these nanoparticles contain azide functionalities at a concentration of  $0.745\text{ }\mu\text{mol mg}^{-1}$ . Based on  $^1\text{H}$  NMR spectrum and TGA data, and assuming that the nanoparticles have a spherical shape and that their size is monodispersed, we can estimate a nanoparticle formula of  $\text{Au}_{1000}(\text{Me-EG}_3\text{-S})_{455}(\text{N}_3\text{-EG}_4\text{-S})_{245}$  (calculation reported in Experimental).

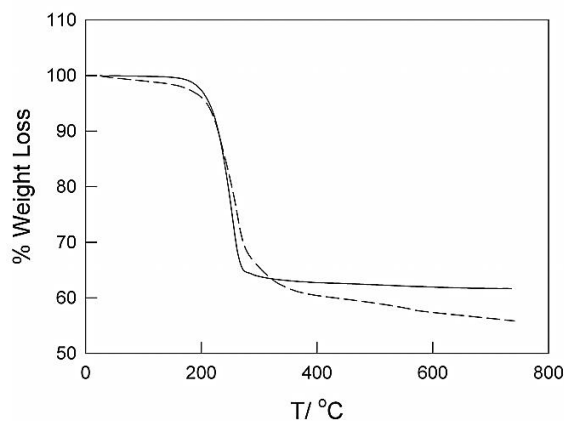
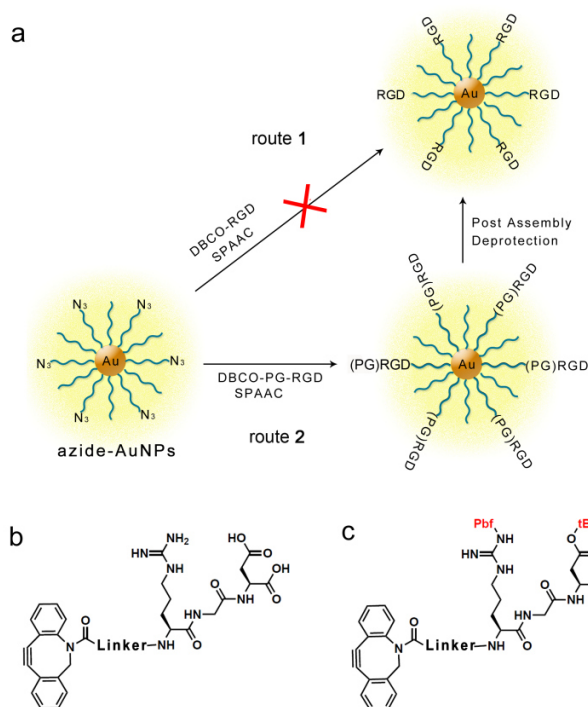


**Figure 5.2** TGA of control Me-EG<sub>3</sub>-AuNP (solid line) and of N<sub>3</sub>-EG<sub>4</sub>-AuNP (dashed line).

The effectiveness of our SPAAC-PAD approach is shown through the example of bioconjugation of the arginyglycylaspartic acid (RGD) peptide. This peptide was chosen because it has targeting relevance. It is well-known to be specifically recognized by the integrin  $\alpha_v\beta_3$  receptor and can act as tumour and angiogenesis marker.<sup>42,43</sup>

In Scheme 5.1 two potential routes are illustrated for bioconjugation of the azide-AuNP with the RGD peptide. The first approach (Route 1, Scheme 5.1), involves preparing a “naked” peptide consisting of a dibenzocyclooctyl (DBCO) moiety connected via a polyethylglycol (PEG) linker to the RGD tripeptide (hereafter named “DBCO”-RGD). After preparation PEG-containing RGD, DBCO was constructed to the peptide via standard peptide coupling reaction. The resulting peptide, “DBCO”-RGD, was cleaved from the resin and deprotected by using 95/5 TFA/TES. After purification, it was then directly reacted with the azide-AuNP. The second approach (Route 2, Scheme 5.1) applies a construct possessing a side-chain protected peptide fragment (DBCO-(PG)RGD). It is noteworthy that dilute TFA (5/5/90 TFA/TES/DCM) was used as the reagent for cleavage of the peptide from the resin and for retention of protecting groups on peptide side chains.

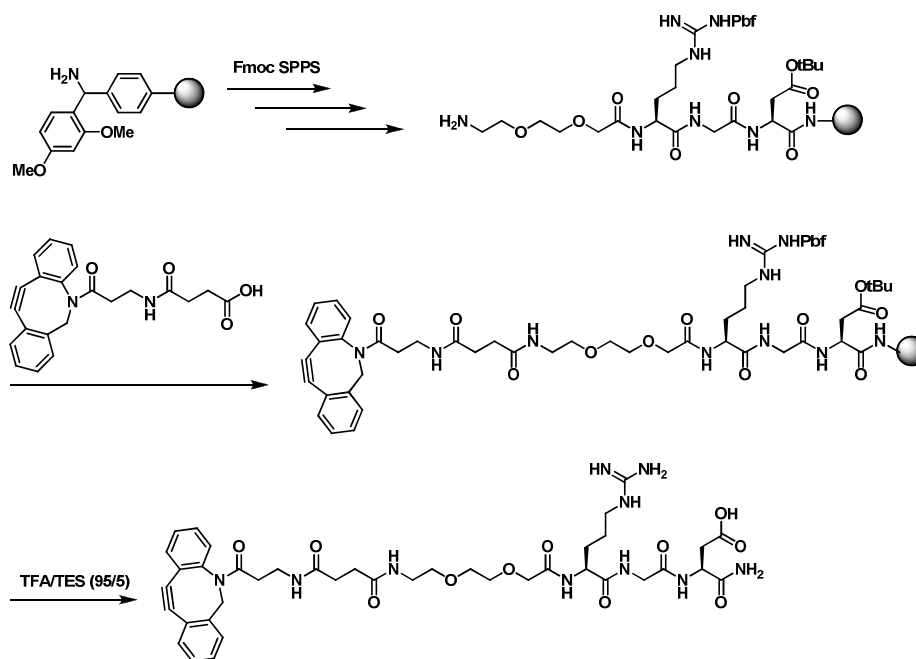
The peptide reacted with the azide-AuNPs via an I-SPAAC and all protecting groups were removed in a post-assembly deprotection step.



**Scheme 5.1** Illustration of the attempted routes for the bioconjugation of azide-AuNPs with RGD peptide via SPAAC-PAD. (a) Use of an unprotected peptide (route 1) or use of a protected peptide (route 2), (b) and (c) molecular structures of “DBCO”-RGD and DBCO-(PG)RGD. Protecting groups (PG) are Pbf and *t*Bu.

To undertake the approach described by Route 1, RGD peptide was synthesized via standard SPPS procedure using rink amide resin as the solid support (Scheme 5.2) and DBCO acid was coupled to N-terminus of the peptide. Cleavage from the resin and protecting group removal was done in one step by treatment with 95/5 TFA/TES. The resulting native peptide was purified by HPLC and characterized by ESI-MS. The observed molecular mass of 849.3472 was in agreement with the calculated mass (849.3657). In

spite of this, close examination of the UV-spectrum of the peptide indicated that the chromophore was changed from DBCO thus implying decomposition of DBCO had occurred (supplementary information).



**Scheme 5.2** Synthesis of DBCO-RGD peptide.

A control experiment was carried out to determine if the standard Fmoc-based oligomerization chemistry cleavage condition of concentrated TFA induced decomposition of DBCO. Starting with DBCO amine, we measured its purity by HPLC before and after treatment with 95% TFA/DCM (rt, 1 hr). HPLC-UV absorption spectroscopy of the reaction mixture, along with subsequent  $^1\text{H}$  NMR and high resolution mass spectral analysis, clearly showed the complete consumption of starting material and the production of several products (Figure 5.3 and Figure 5.4). The two major components of the mixture, i.e. the peaks with retention time of 20-20.5 min and of 26-26.5 min do not correspond to DBCO. On-line monitoring showed significant changes the UV spectrum indicating

structural changes in the chromophore. The  $^1\text{H}$  NMR spectra of the two isolated compounds confirmed neither was DBCO (supplementary information). Mass spectral analysis showed that the earlier eluting peak retained the same mass as DBCO implying a molecular rearrangement had occurred,<sup>31</sup> while the later eluting peak possessed a greater mass. It's also noteworthy that the UV absorption spectrum of the first peak in Figure 5.4 showed strong absorbance at 344 nm, which has also been detected in UV spectrum of “DBCO”-RGD, indicating that DBCO on peptide RGD had decomposed under the standard cleavage condition of 95% TFA. To study the stability of the DBCO moiety toward TFA, DBCO was exposed to a series of solutions of 0-50% TFA/DCM for 1 h at room temperature. Under these conditions, DBCO was found to be stable when the TFA concentration was less than 30%.

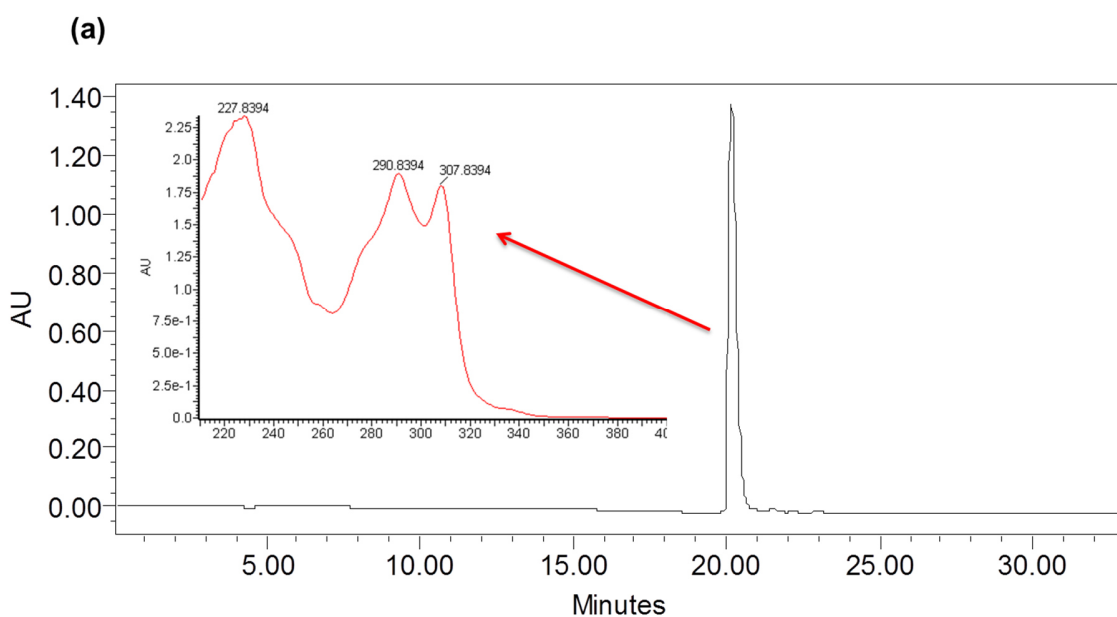


**Figure 5.3** HPLC-UV absorption analysis at 265 nm of DBCO amine.

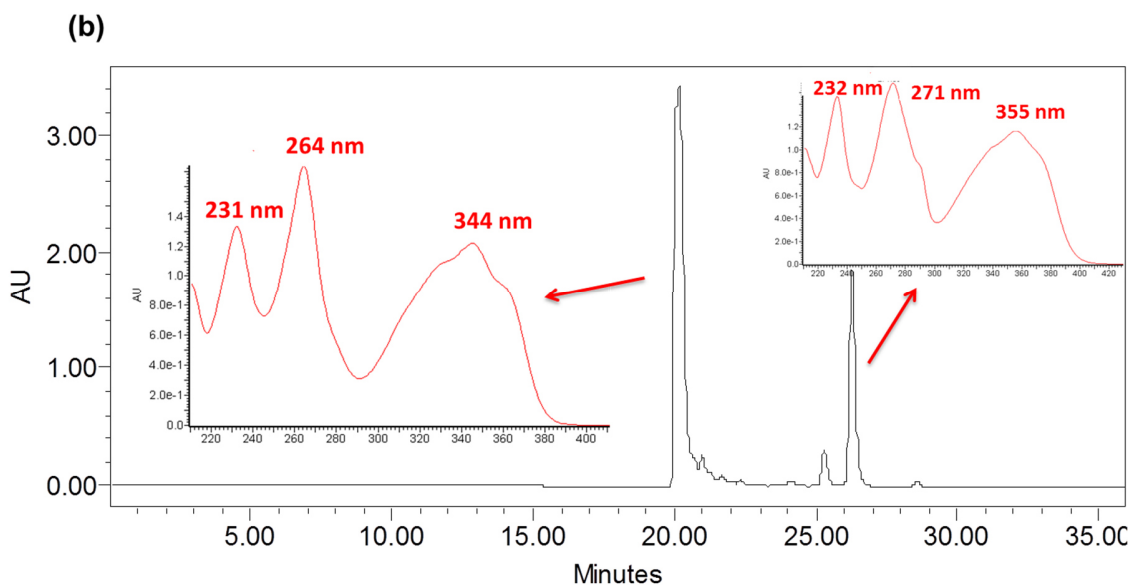


**Figure 5.4** HPLC-UV absorption analysis at 265 nm of decomposition of DBCO after treatment with concentrated TFA.

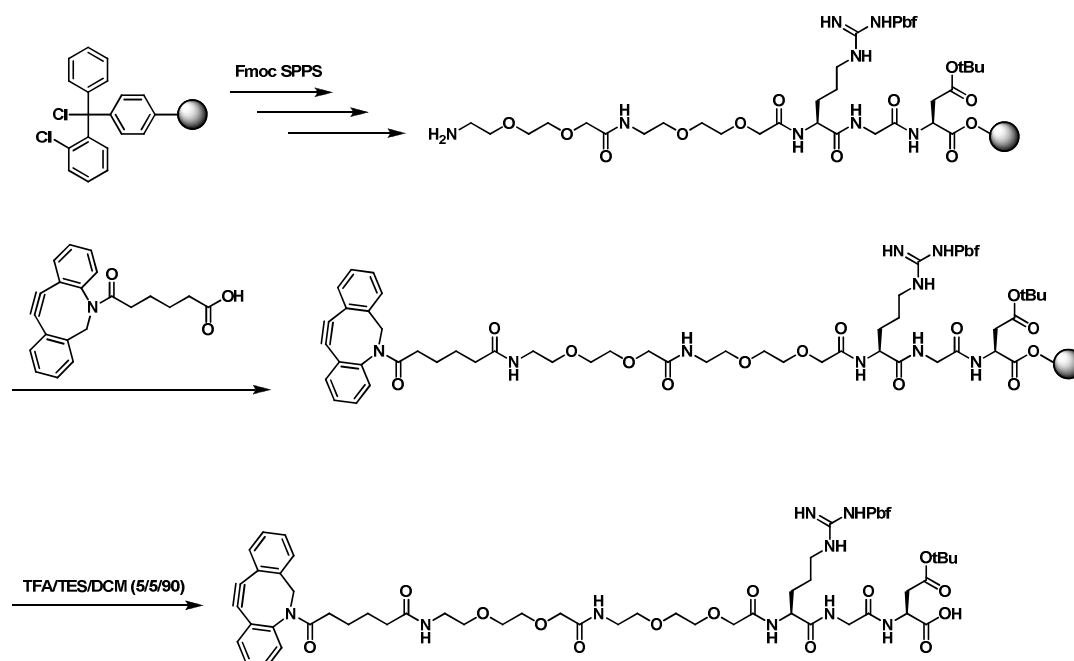
Another control experiment was performed to model the interfacial SPAAC reaction by using “DBCO”-RGD peptide with an azide, namely  $\omega$ -azido-triethylene glycol-monomethyl ether (Me-EG<sub>3</sub>-N<sub>3</sub>) as the reactive partner. The reactions were carried out in either water or acetonitrile solutions and the course of the reaction was monitored by UPLC/ESI-MS. Only the two starting materials were detected over 4 hours, indicating that the “DBCO”-RGD peptide and Me-EG<sub>3</sub>-N<sub>3</sub> were not undergoing the SPAAC. Independently it was determined that the Me-EG<sub>3</sub>-N<sub>3</sub> was capable of participating in SPAAC with DBCO. Therefore, “DBCO”-RGD lost the ability of click and cannot be used as clickable peptide for bioconjugation of AuNPs. As a control for further study, the peptide “DBCO”-RGD was still added into azide-AuNPs (azide group:peptide, 1 : 1.2 ratio). The mixture was stirred in water at room temperature for 1 h. After removal of solvent, AuNPs were purified by centrifugal filtration (Millipore centrifugal filter units



MWCO 10 kDa). As expected, characterization of these AuNPs by IR spectroscopy showed the absorption of the azide group at  $2110\text{ cm}^{-1}$  was still present with similar intensity to the starting material, which indicated lack of SPAAC reactivity, and showed no stretching at  $1685\text{ cm}^{-1}$  corresponding to the amide functional groups.

To circumvent the problem of decomposition of DBCO, Route **2** was devised. First we prepared DBCO-(PG)RGD by using a mild cleavage condition and it was then clicked to the azide-AuNP and subsequently the peptide was deprotected (Scheme 5.1). To synthesize the DBCO-(PG)RGD, the acid sensitive 2-chlorotriylchloride resin was used as solid support. The synthesis of DBCO-containing peptide followed the above procedure, except that the cleavage was performed with TFA/TES/DCM (5/5/90). This treatment effected the cleavage of the peptide from the resin but left the protecting groups intact and did not destroy DBCO (Scheme 5.3). The resulting protected peptide was purified by HPLC and characterized by ESI-MS. The UV spectrum of DBCO-(PG)RGD showed the agreement with DBCO with absorbance at 290 nm and 308 nm. A model click was carried out with DBCO-(PG)RGD and Me-EG<sub>3</sub>-N<sub>3</sub> in acetonitrile. Characterization of the reaction by UPLC/ESI-MS showed successful click, indicating that DBCO was not destroyed in the cleavage step. Then SPAAC between azide-AuNPs and DBCO-(PG)RGD was simply performed by adding them (azide:peptide, 1 : 1.2) in acetonitrile and stirring the resultant mixture at room temperature for 1 h (Figure 5.5). After reaction, the AuNPs were purified by using centrifugal filtration (Millipore centrifugal filter units MWCO 10 kDa) and washed with 60% MeOH/H<sub>2</sub>O until no unreacted peptide was observed in the UPLC/ESI-MS analysis of the filtrate. The unreacted peptide was recovered from the filtrate and washings and the amount indicates that approximately 31% of the azide groups on AuNPs

had reacted. Therefore, the approximate nanoparticle formula can be calculated as  $\text{Au}_{1000}((\text{PG})\text{RGD-linker-S})_{75}(\text{N}_3\text{-EG}_4\text{-S})_{170}(\text{MeEG}_3\text{S})_{450}$ . The IR spectrum of the purified (PG) RGD-AuNPs showed that the azide stretching mode at  $2110\text{ cm}^{-1}$  had markedly decreased while it had not changed in Route 1 (Figure 5.6). Additionally, concomitant with the azide disappearance the appearance of stretching at  $1685\text{ cm}^{-1}$  corresponding to the amide functional groups was observed, indicating that the protected peptide was covalently bonded to the AuNP via SPAAC.



**Scheme 5.3** Synthesis of DBCO-(PG)RGD peptide.

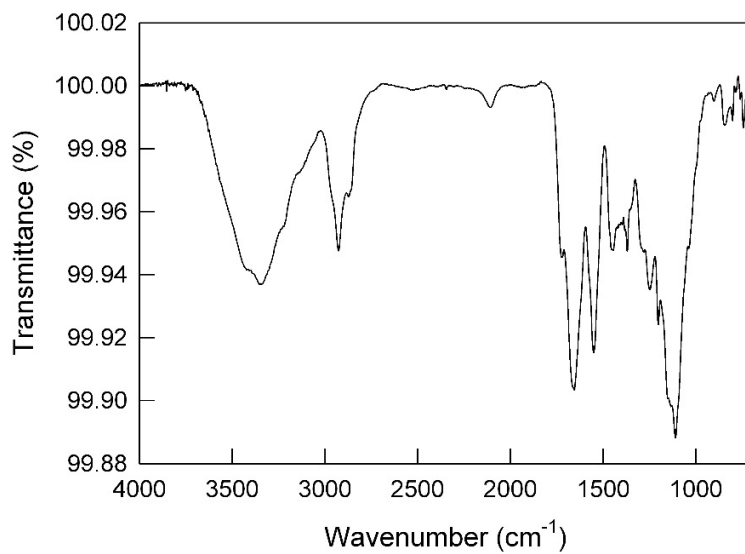


**Figure 5.5** IR spectrum of PG-RGD-AuNPs.

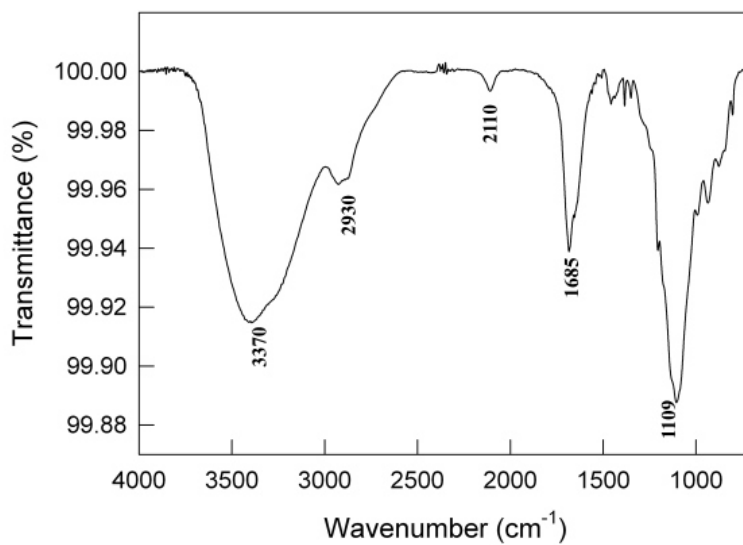


**Figure 5.6** IR spectrum of RGD-AuNPs.

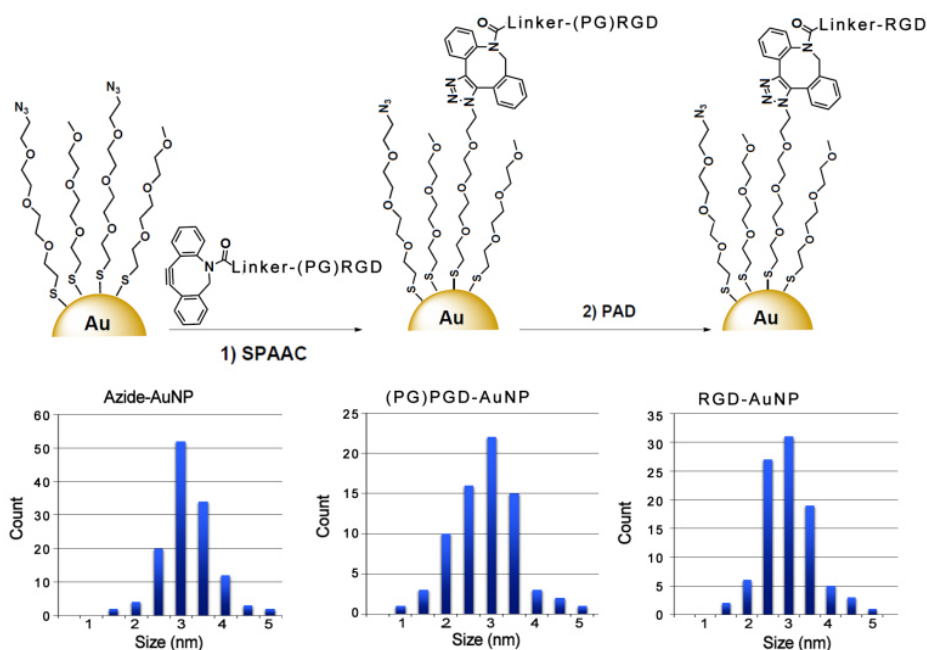


**Figure 5.7** Bioconjugation of AuNPs with RGD peptide via SPAAC-PAD, 1) acetonitrile, room temperature, 1 h; 2) 90% TFA/DCM, room temperature, overnight; and AuNP size distributions obtained from the corresponding TEM image of RGD-functionalized AuNPs via SPAAC-PAD.

To remove the protecting groups of the peptide, the AuNPs were then treated with 90% TFA/DCM at room temperature overnight to ensure complete deprotection. It is important to note that these small oligo-ethylene glycol-based AuNP are perfectly stable under these acidic conditions. TEM images recorded before and after this acidic treatment confirmed that the relatively harsh condition for PAD did not adversely affect the AuNP size distribution (Figure 5.7). The obtained RGD-AuNPs were then purified by dialysis using cellulose ester dialysis membranes (6-8 KDa MWCO).

To further confirm that the interfacial SPAAC reaction had proceeded, the deprotected RGD-AuNPs were reacted with molecular iodine. Oxidation of AuNPs with iodine

dissolved the gold into a mixture of Au(I) and Au(III) complexes and released the corona ligands as disulphides.<sup>44</sup> The structure of the most possible disulphide molecule produced by this reaction is shown in Figure 5.8. The mixture of disulphides was characterized by ESI-MS and the mass 1365.6084 [M+H]<sup>+</sup> *m/z* agrees well with the calculated mass of 1364.5992 for the proposed disulphide **1**. Importantly the mass for the corresponding disulphide with the protected peptide was not observed, indicating that the complete deprotection was achieved. This confirms the successful bioconjugation of AuNPs with a short oligopeptide via SPAAC-PAD without interference with side chains of the peptide. Moreover, efficient substitution was achieved on the surface of small size AuNPs with 31% of the azide groups reacting with the RGD peptide. This result is comparable with the reported conjugation of AuNPs with peptides via covalent bonding,<sup>20</sup> with the difference that this AuNP-bioconjugate was obtained through a simple and rapid pour-and-mix chemistry under ambient temperature and atmosphere while the purification only involved centrifugation and dialysis. The final calculated molecular raw formula of this AuNP is Au<sub>1000</sub>(RGD-linker-S)<sub>75</sub>(N<sub>3</sub>-EG<sub>4</sub>-S)<sub>170</sub>(MeEG<sub>3</sub>S)<sub>450</sub>.

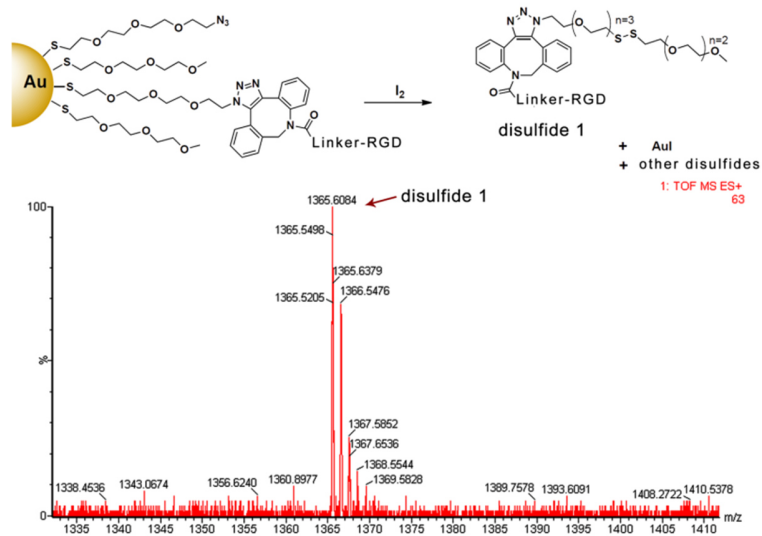
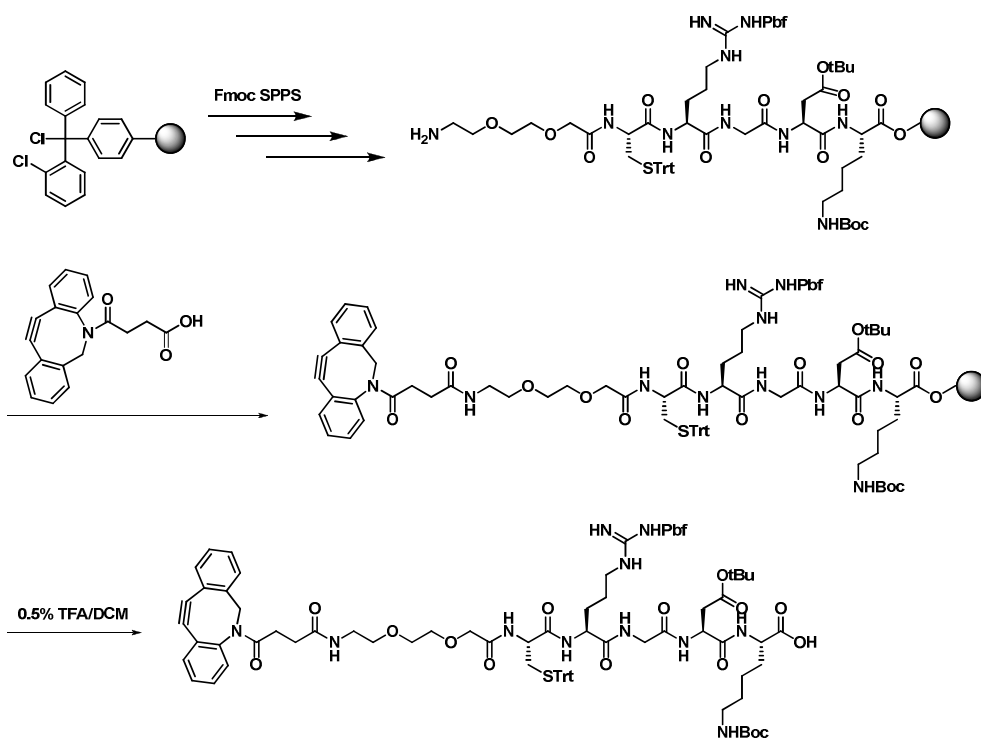


**Figure 5.8** Oxidative degradation of RGD-AuNPs by iodine. Disulfide 1 was characterized by ESI-MS. Calculated 1364.5992 and found 1365.6084 [1+] *m/z*.

To test the versatility of this method we employed a peptide with different nucleophilic residues. In particular, because it has been reported that in presence of reduced peptidylcysteine residues, strained cyclooctynes mainly react via thiol-yne addition instead of SPAAC reaction,<sup>33</sup> we decided to synthesize a CRGDK peptide and conjugate it to the azide-AuNPs via our SPAAC-PAD strategy (Scheme 5.4). This peptide has an additional interest because it is a neuropilin-1 (Nrp-1) receptor-targeted peptide for cancer treatment.<sup>32,45,46</sup>



**Scheme 5.4** Synthesis of DBCO-(PG)CRGDK peptide.

For these experiments, we followed the same procedure as previously discussed with the noted exception. The CRGDK peptide was synthesized via standard Fmoc SPPS method and DBCO acid was coupled to the N-terminus. A change in the acid strength for resin cleavage (0.5% TFA/DCM) was made to preserve the trityl thioether protecting group of cysteine. After SPAAC-PAD, the CRGDK-functionalized AuNPs were characterized by IR (Figure 5.9). The azide stretch in the IR spectrum became weaker compared to the azide-AuNPs before conjugation and the stretching at  $1685\text{ cm}^{-1}$  corresponded to the functional groups of peptide bond appeared, suggesting successful conjugation through the I-SPAAC-PAD. Also, a new absorbance at  $2692\text{ cm}^{-1}$  indicated the existence of the thiol group of cysteine and shows that the side chain of cysteine that would otherwise react with cyclooctyne via thiol-yne addition did not interfere with the I-SPAAC reaction with the aid

of PAD. Decomposition of the AuNPs by treatment with excess I<sub>2</sub> followed by ESI-MS analysis showed the two most possible disulfide molecules expected after a successful I-SPAAC-PAD, and no trace of protected peptide was found (Scheme 5.5). Therefore, our strategy showed to be also effective in creating small AuNP-oligopeptide bioconjugates in presence of nucleophilic residues that could otherwise attack the strained alkyne bond.

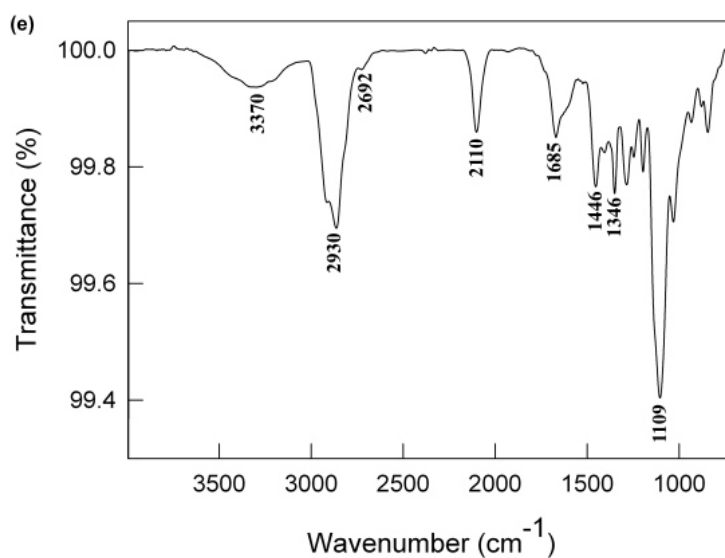


**Figure 5.9** IR spectrum of CRGDK-AuNPs.





incorporation of the interfacial biomolecule can be easily quantified. We anticipate that the demonstrated methodology for peptide-AuNP bioconjugation via the SPAAC-PAD will enable the fabrication of gold nanoparticles with a high degree of complexity with biomolecules for a variety of applications in targeted cancer diagnosis and therapies. Further modification and functionalization of AuNPs for better results of targeted CT imaging is currently underway.

## **5.4 Experimental**

### **Synthesis of “DBCO”-RGD peptide**

The “DBCO”-RGD peptide was synthesized manually via standard Fmoc SPPS procedure by using rink amide MBHA resin as solid support. Briefly, the peptide chain including RGD and a linker was grown on the resin and DBCO acid was coupled to terminate the peptide. The coupling of each residue used 5 equiv. (relative to the loading of resin) Fmoc-protected amino acids, 5 equiv. of HBTU and 10 equiv. of DIPEA in a DMF solution for 4 hours. During the synthesis, Fmoc protecting group was deprotected using 20% piperidine/DMF (v/v) for 15 minutes. At the end of the synthesis, DBCO acid was conjugated to the peptide following the above-mentioned procedure except that 1.1 equiv. DBCO acid, 1.1 equiv. HBTU and 2.2 equiv. DIPEA were used. After the completion of the synthesis, the resin was washed with DMF and DCM (each for four times) and dried under vacuum for 24 hours. Cleavage of the expected peptide and the removal of side chain protecting groups from the dried resin were performed by suspending the resin in cleavage cocktail containing TFA (95%) and TES (5%) for 1 hour. The filtration was concentrated to a viscous solution by flushing N<sub>2</sub>. After the precipitation in ice cold ether, the crude product was collected, dissolved in MQ water and freeze-dried. The characterization of

“DBCO”-RGD peptide with calculated mass 849.3657 [M+H]<sup>+</sup> was performed by Waters LCT Premier ESI-MS and found 849.3395 [M+H]<sup>+</sup>. Purity: 98.7% determined by HPLC with a C18 column and using a linear gradient of acetonitrile and MQ water containing 0.05% TFA.

### **Synthesis of DBCO-(PG)RGD peptide**

The DBCO-(PG)RGD peptide was synthesized manually via standard Fmoc SPPS procedure by using 2-chlorotrityl chloride resin as solid support. The coupling of the first residue used 1.5 equiv. Fmoc-protected amino acid and 4 equiv. of DIPEA in a DCM solution for 2 hours. Other amino acid couplings and DBCO acid coupling were carried out followed by the above-mentioned procedure. Cleavage of the protected peptide from the dried resin was performed by suspending the resin in cleavage cocktail containing TFA (5%), TES (5%) and DCM (90%) for 1 hour. The filtration was concentrated to a viscous solution by flushing N<sub>2</sub>. The crude product was dissolved in acetonitrile and purified by HPLC. The characterization of DBCO-(PG)RGD peptide with calculated mass 1259.5784 [M+H]<sup>+</sup> was performed by ESI-MS and found 1260.5776 [M+H]<sup>+</sup>. Purity: 96.5% determined by HPLC with a C18 column and using a linear gradient of acetonitrile and MQ water containing 0.05% TFA.

### **Synthesis of DBCO-(PG)CRGDK**

The synthesis was performed as described for DBCO-(PG)RGD. Cleavage of the protected peptide was performed by suspending the resin in cocktail containing 0.5% TFA/DCM for 15 min. The filtration was concentrated to a viscous solution by flushing N<sub>2</sub>. The crude product was dissolved in acetonitrile and purified by HPLC. The characterization of

DBCO-(PG)CRGDK with calculated mass 1659.7393 [M+H]<sup>+</sup> was performed by ESI-MS and found 1660.6294 [M+H]<sup>+</sup>. Purity: 94.8% determined by HPLC with a C18 column and using a linear gradient of acetonitrile and MQ water containing 0.05% TFA.

### **Synthesis of azide AuNPs**

In a typical synthesis, 50.0 mg of Me-EG<sub>3</sub>-AuNP were transferred into a clean 25 mL round bottom flask. This compound was dissolved in 10 mL of acetone. Then 10.0 mg (42.5 μmol) of N<sub>3</sub>-EG<sub>4</sub>-AuNP were transferred into this solution. The reaction was stirred vigorously for 20 min. After this time, the acetone was immediately evaporated off. The thin film of nanoparticles was washed first with hexanes (in which AuNP are not soluble) and the solvent was removed under vacuum. Subsequently the film was quickly rinsed with isopropanol three times. This entire washing procedure was repeated three times until the odour of the thiol was gone. 44.9 mg of nanoparticles were obtained. The nanoparticles were dissolved readily in H<sub>2</sub>O, acetone, acetonitrile, methanol, ethanol, DMF, DMSO and DCM with little to no aggregation and characterized by <sup>1</sup>H NMR and IR. <sup>1</sup>H NMR (CD<sub>3</sub>CN, 400 MHz): δ<sub>H</sub> (ppm): 3.60, 3.49, 3.39, 3.31. <sup>1</sup>H NMR (D<sub>2</sub>O, 400 MHz): δ<sub>H</sub> (ppm): 3.66, 3.57, 3.43, 3.32. IR (KBr disk, cm<sup>-1</sup>): 2921, 2871, 2101, 1443, 1349, 1292, 1244, 1198, 1119, 1033.

### **Bioconjugation of azide AuNPs with RGD peptide via SPAAC-PAD**

DBCO-(PG)RGD (1.2 equiv. of DBCO relative to azide substitution on AuNPs) and azide AuNPs were mixed in 3 mL acetonitrile at room temperature for 1 hour. After that, the AuNPs were purified by using centrifugal filter devices (10KDa MWCO) and washed with 60% MeOH/H<sub>2</sub>O until no unreacted peptide can be found by ESI-MS. The resulting AuNPs

were treated with 90% TFA/DCM at room temperature overnight and the solvent removed by flushing N<sub>2</sub>. The obtained AuNP-RGD were purified by dialysis against water using Cellulose ester dialysis membranes MWCO of 10 kDa for 2 days and characterized by IR, TEM and ESI-MS. IR (KBr disk, cm<sup>-1</sup>): 3370, 2930, 2110, 1685, 1109.

### **Bioconjugation of azide AuNPs with DBCO-(PG)CRGDK**

The bioconjugation was performed as described for AuNP-RGD. The obtained AuNP-CRGDK after SPAAC-PAD was characterized by IR and ESI-MS. IR (KBr disk, cm<sup>-1</sup>): 3370, 2930, 2692, 2110, 1685, 1446, 1346, 1109.

### **Calculation of nanoparticle formula**

Assuming that the AuNPs are spherical and that their size is monodisperse (3 nm) it is possible to calculate an approximate molecular formula for azide AuNPs. The number of gold atoms (N<sub>Au</sub>) can be calculated using the following formula:

$$N = \frac{\pi \rho d^3 N_A}{6 M_{Au}}$$

Where  $\rho$  is the density of the face centered cubic (fcc) gold lattice (19.3 g·cm<sup>-3</sup>),  $d$  is the average diameter of the nanoparticles in centimeters found from the TEM images,  $M_{Au}$  is the mole atomic weight of gold (196.9665 g mol<sup>-1</sup>), and  $N_A$  is Avogadro constant.

The number of thiol ligands surrounding the gold core (N<sub>L</sub>) can be calculated using the following formula:

$$N_L = \frac{N M_{Au} W_{\%}}{(1 - W_{\%}) [M W_{N_3-EG_4-S} M_{\%} + [M W_{Me-EG_3-S} (1 - W_{\%})]]}$$

Where W% is the percentage of mass loss due to the organic ligands found through TGA measurements,  $MW_{Me-EG3-S}$  is the molecular weight of the thiolate ligand,  $MW_{N3-EG4-S}$  is the molecular weight of the azide thiolates ligand, and M% is the mole percentage of azide ligand.

### 5.5 Supplementary Information

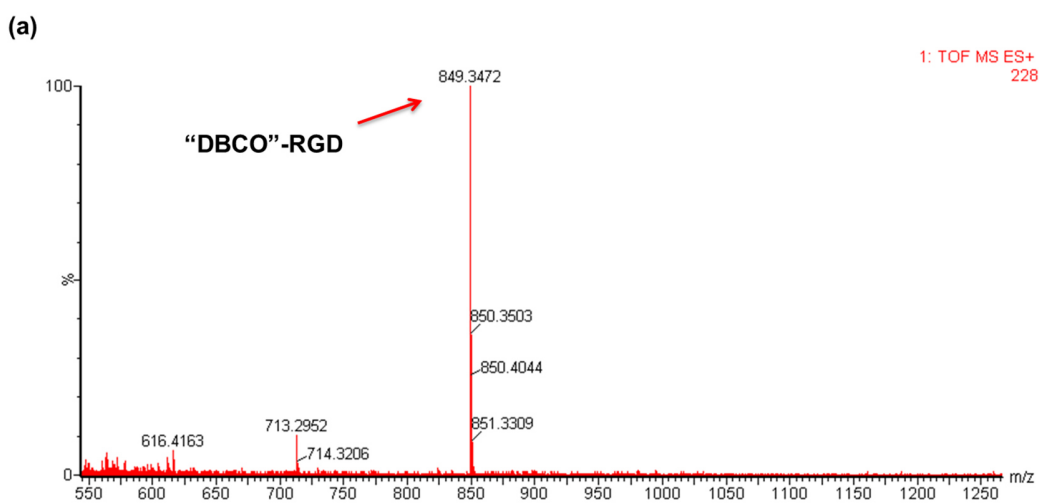


**Figure 5.10** ESI-MS analysis of “DBCO”-RGD. Calculated mass 849.3657  $[M+H]^+$  and found mass 849.3472  $[M+H]^+$ .

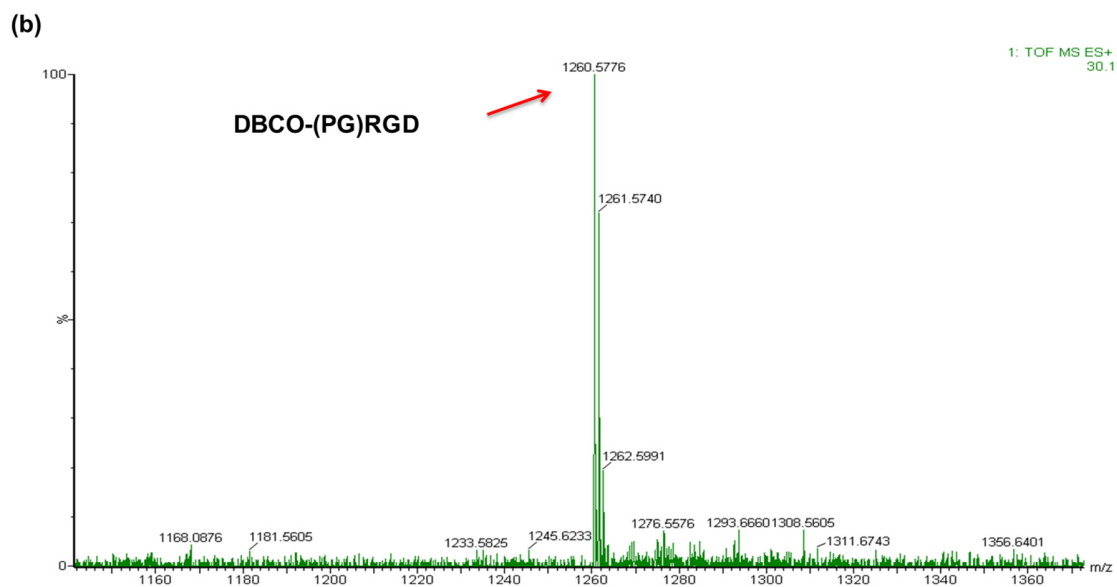


**Figure 5.11** ESI-MS analysis of DBCO-(PG)RGD. Calculated mass 1259.5784  $[M+H]^+$  and found mass 1260.5776  $[M+H]^+$ .

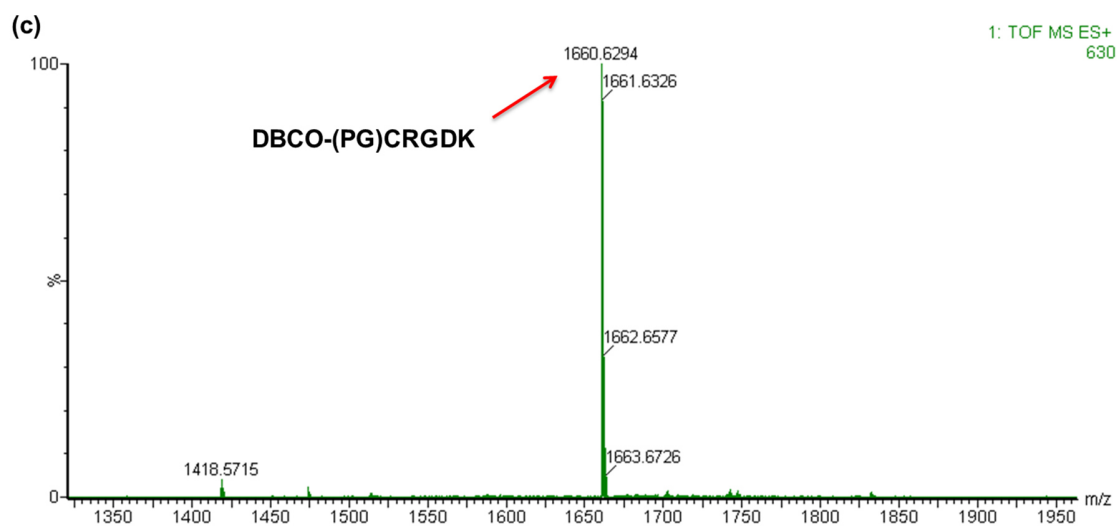


**Figure 5.12** ESI-MS analysis of DBCO-(PG)CRGDK. Calculated mass 1659.7393  $[M+H]^+$  and found mass 1660.6294  $[M+H]^+$ .

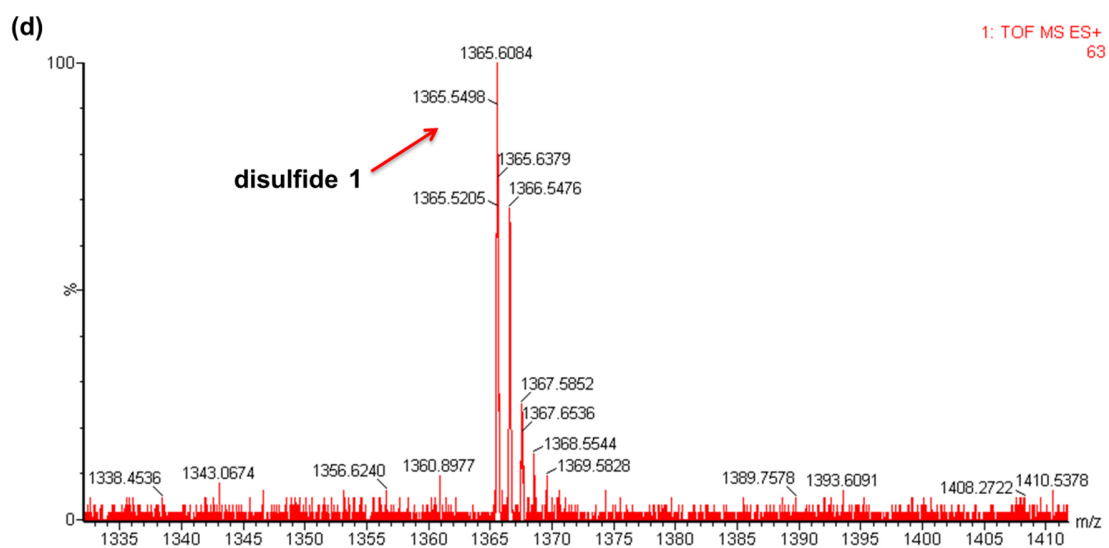


**Figure 5.13** ESI-MS analysis of disulfide **1** from re-oxidation of AuNP-RGD by iodine.

Calculated mass is 1364.5992 and found mass is 1365.6084  $[M+H]^+$  for Disulfide **1**.



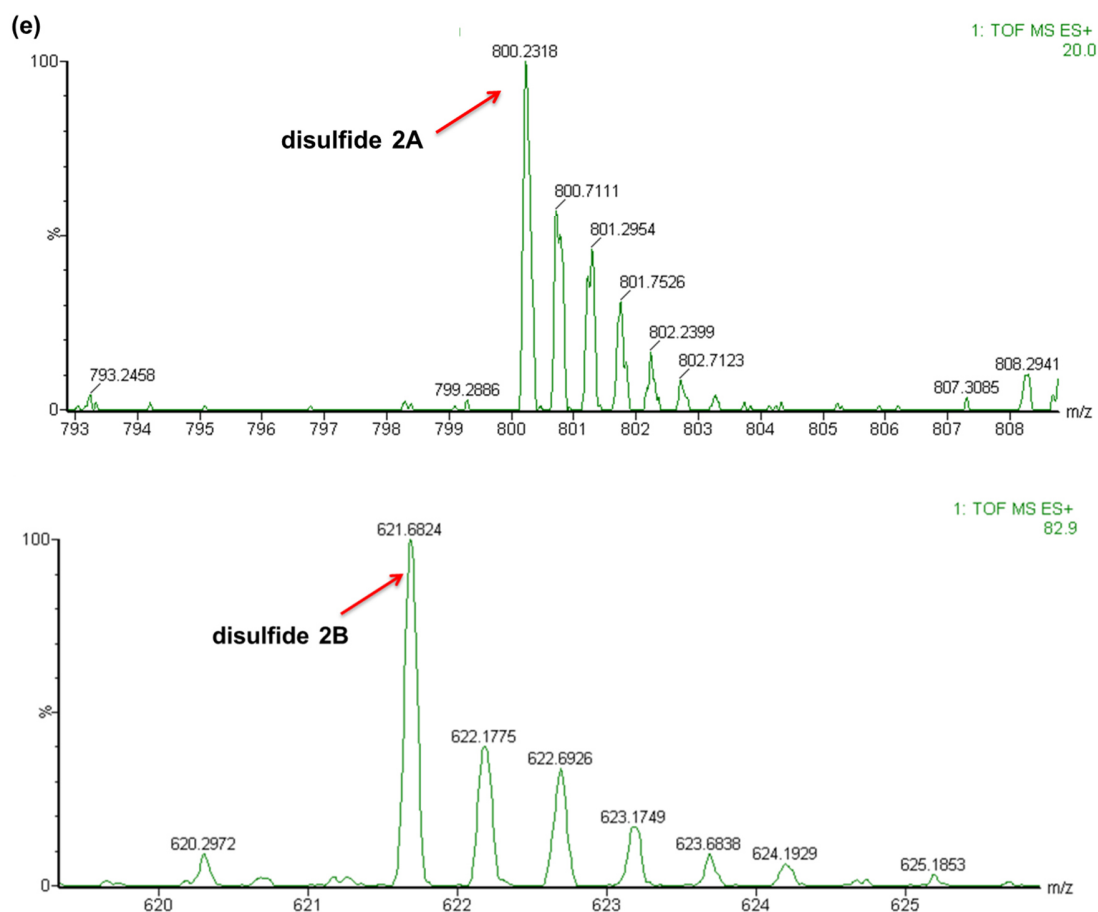


**Figure 5.14** ESI-MS analysis of disulfide **2A** (top) and **2B** (bottom) from re-oxidation of AuNP-CRGDK by iodine. Calculated mass is 1600.6645 and found mass 800.2318  $[M+2H]^{2+}$  for **2A**. Calculated mass is 1242.5162 and found mass 621.6824  $[M+2H]^{2+}$  for **2B**.

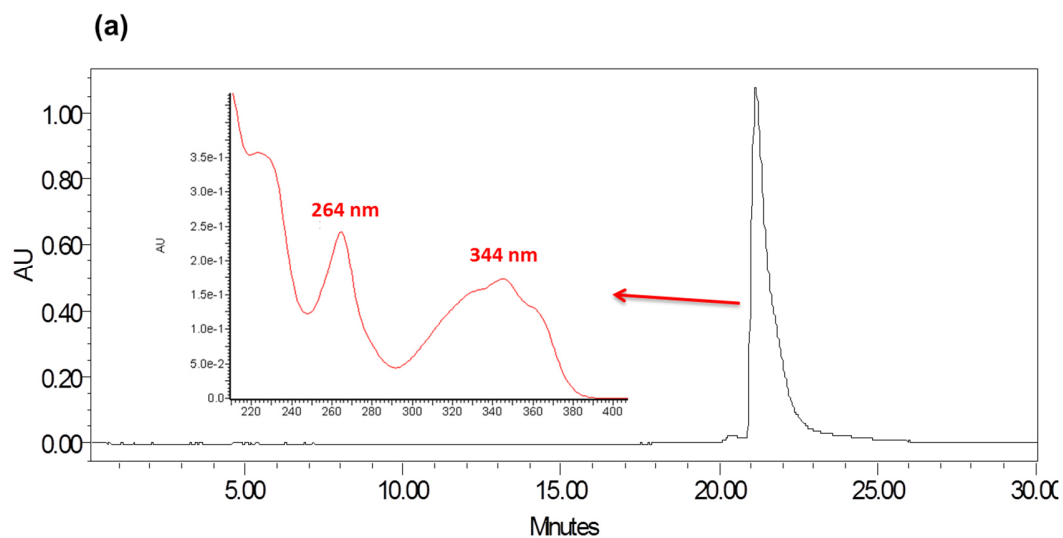


**Figure 5.15** HPLC-UV absorption analysis at 265 nm of “DBCO”-RGD.

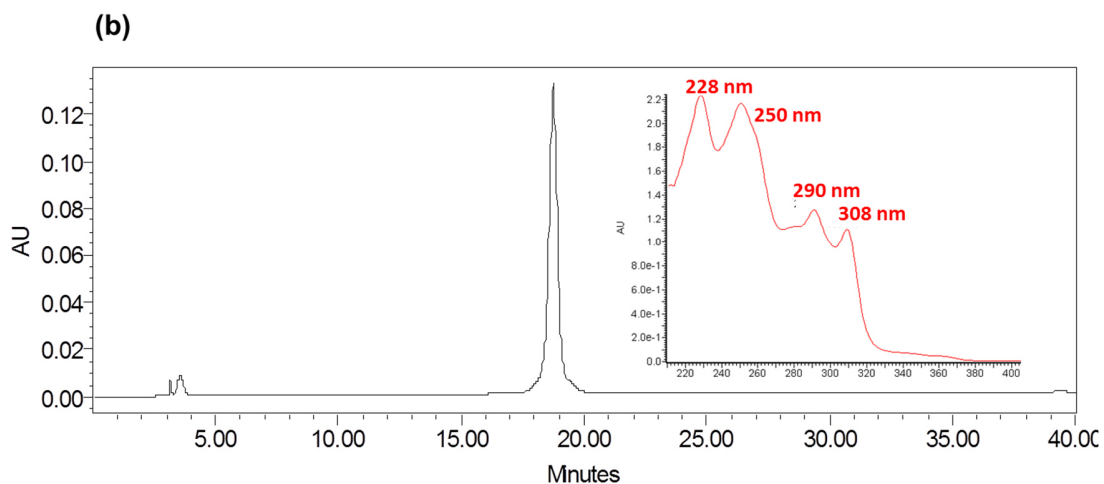


**Figure 5.16** HPLC-UV absorption analysis at 265 nm of DBCO-(PG)RGD.

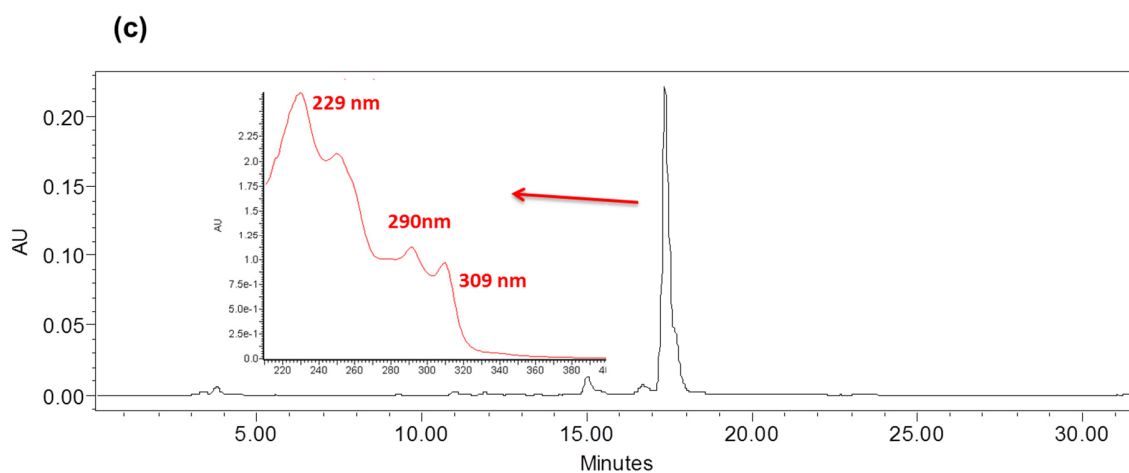


**Figure 5.17** HPLC-UV absorption analysis at 265 nm of DBCO-(PG)CRGDK.

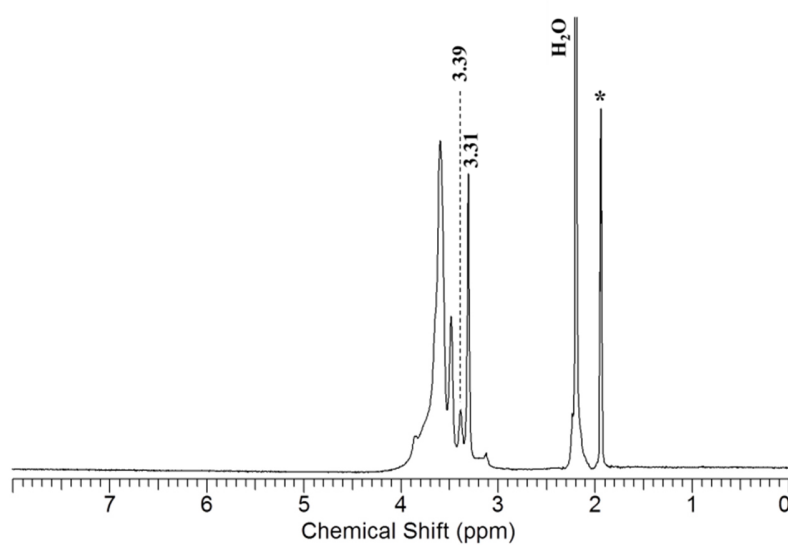


**Figure 5.18**  $^1\text{H}$  NMR spectrum of azide AuNP recorded in acetonitrile- $\text{d}_3$  and calibrated against residual acetonitrile (\*).

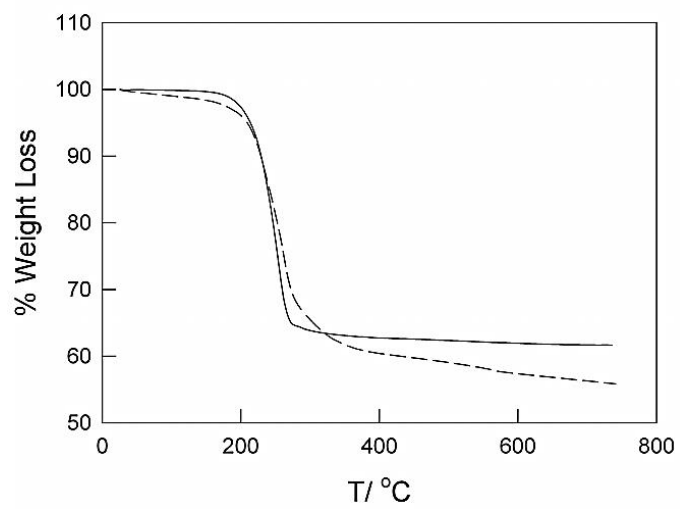


**Figure 5.19** TGA of control Me-EG<sub>3</sub>-AuNP (solid line) and of N<sub>3</sub>-EG<sub>4</sub>-AuNP (dashed line).

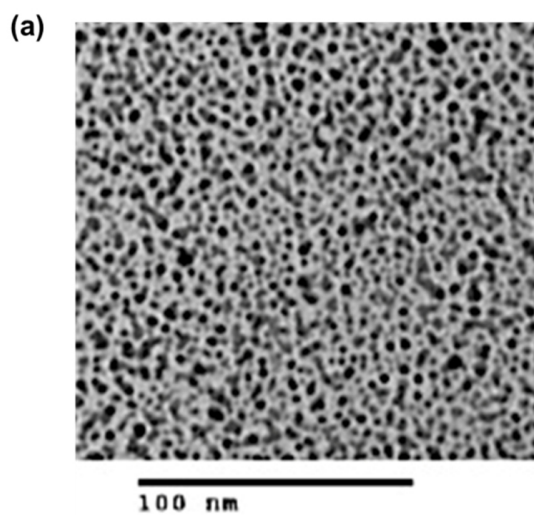


**Figure 5.20** TEM image of azide AuNPs.

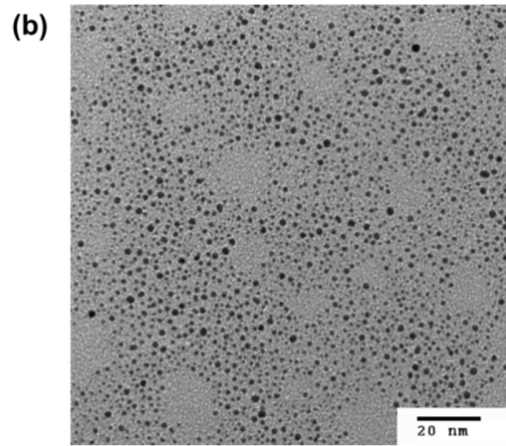


**Figure 5.21** TEM image of RGD-AuNPs.

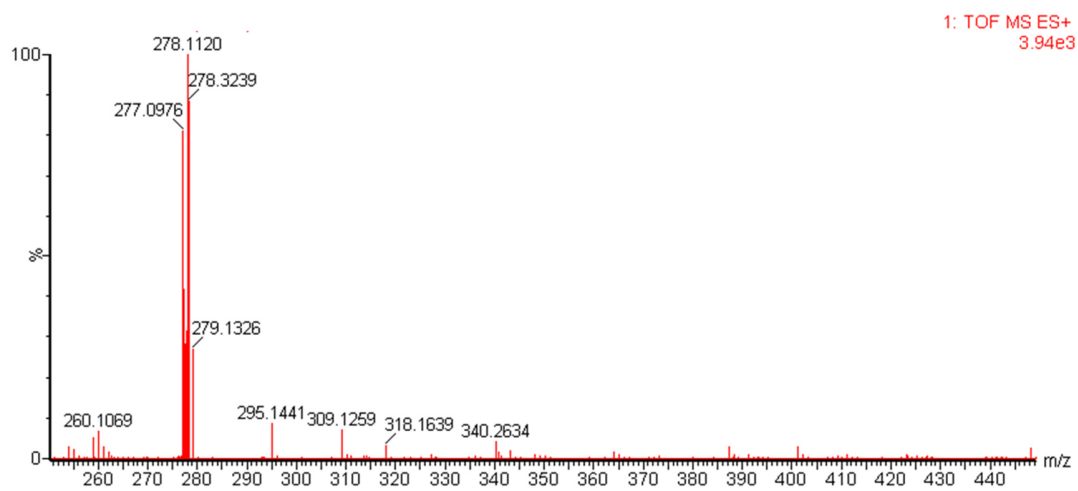
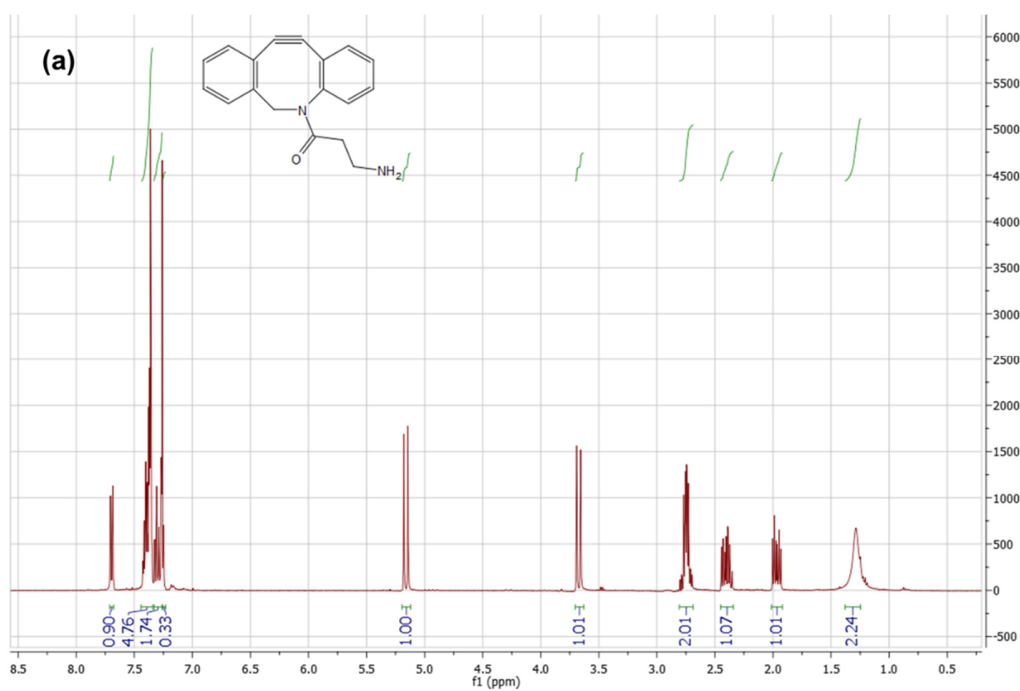


**Figure 5.22**  $^1\text{H NMR}$  (top) and ESI-MS (bottom) spectra of DBCO amine (found mass: 278.1120 [1+]).  $^1\text{H NMR}$  Spectra were recorded in  $\text{CDCl}_3$ .

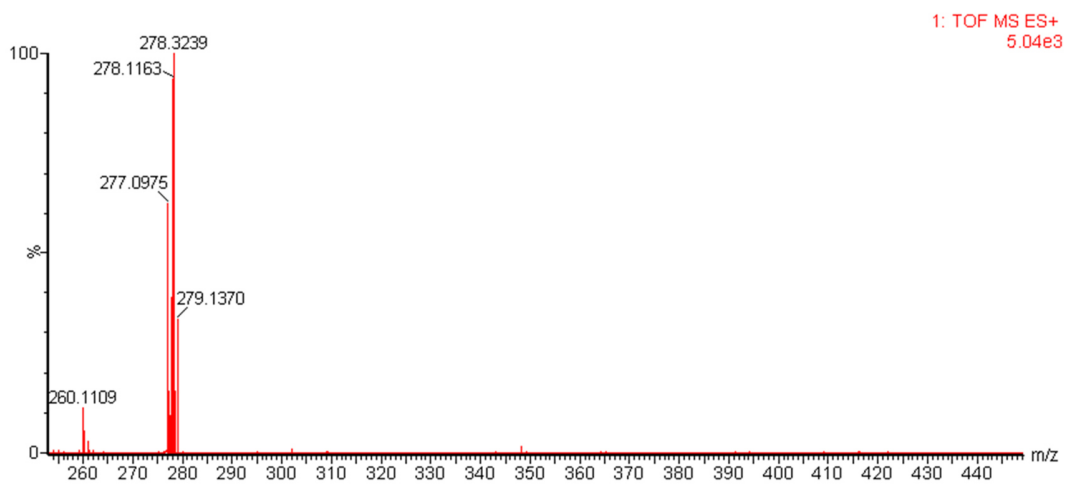
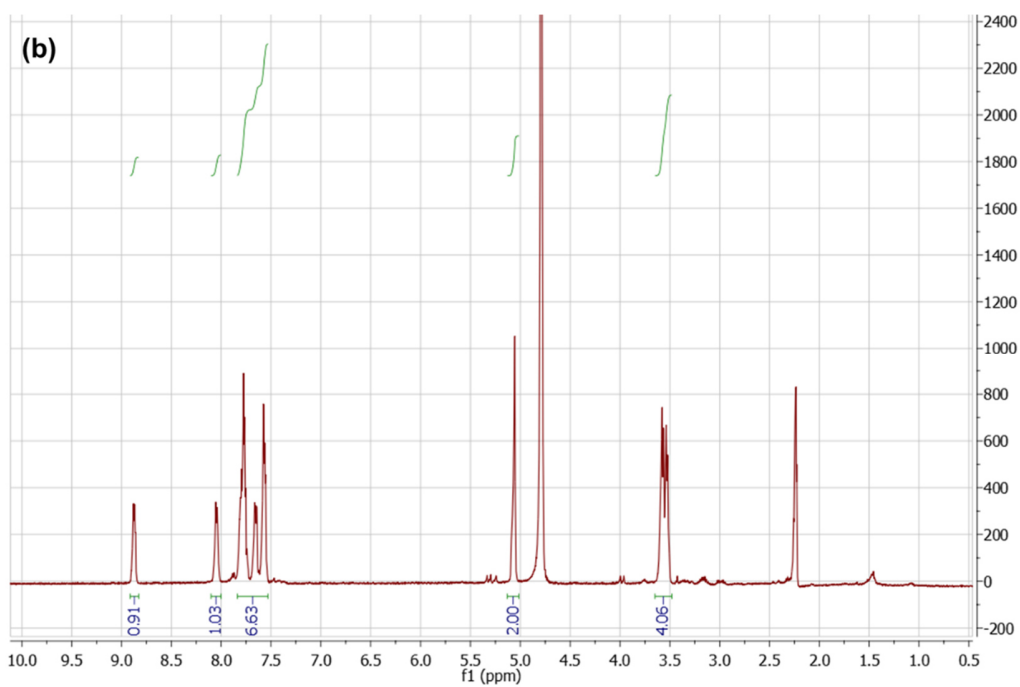


**Figure 5.23**  $^1\text{H}$  NMR (top) and ESI-MS (bottom) spectra of isolated compound (found mass: 278.3239 [1+]).  $^1\text{H}$  NMR Spectra were recorded in  $\text{D}_2\text{O}/\text{ACN}-\text{d}_3$  (2:1).

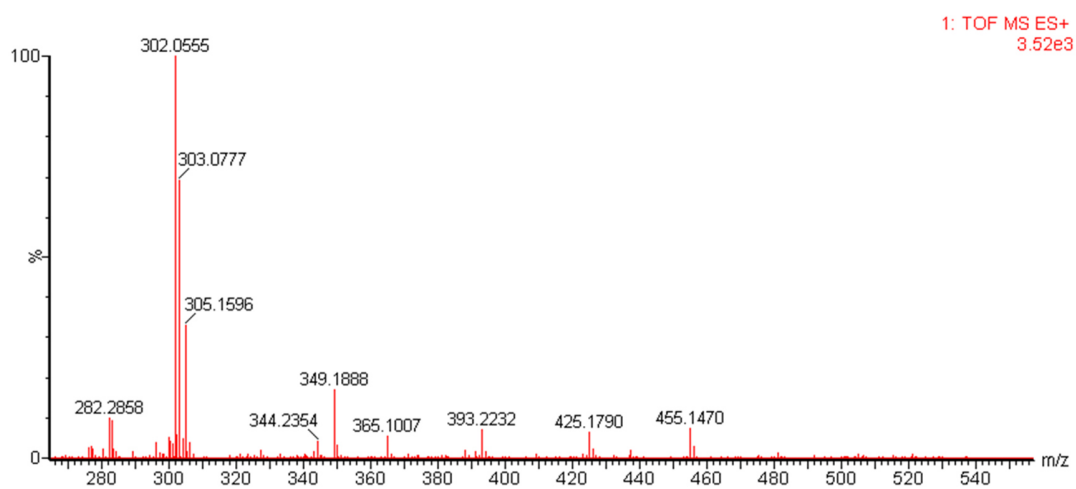
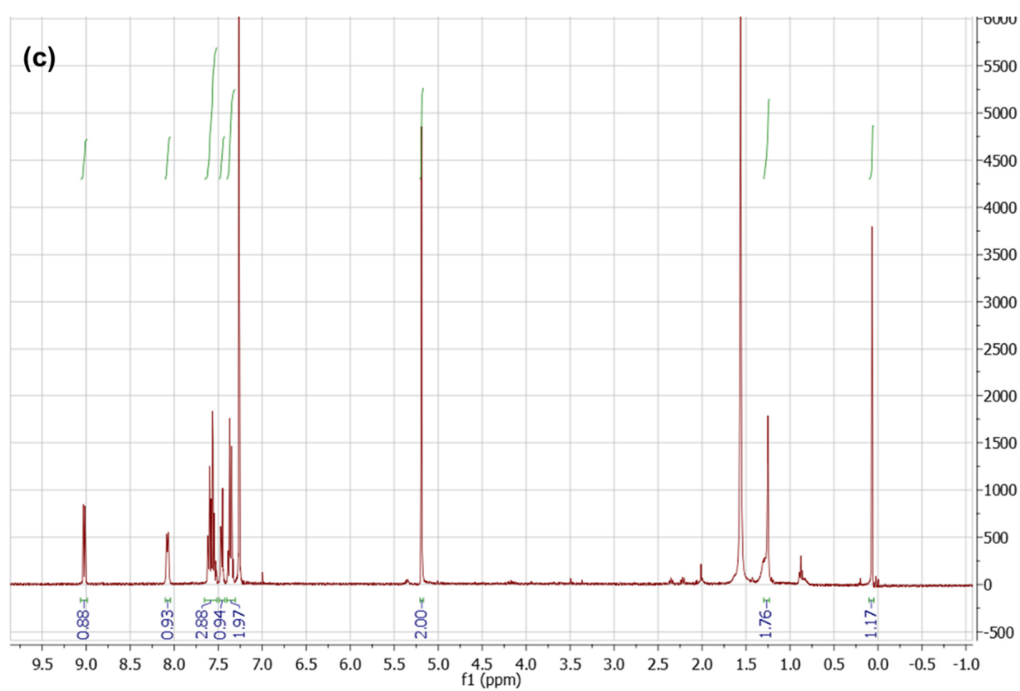


**Figure 5.24**  $^1\text{H}$  NMR (top) and ESI-MS (bottom) spectra of isolated compound (found mass: 302.0555 [1+]) after treatment of DBCO amine with concentrated TFA.  $^1\text{H}$  NMR Spectra were recorded in  $\text{CDCl}_3$ .



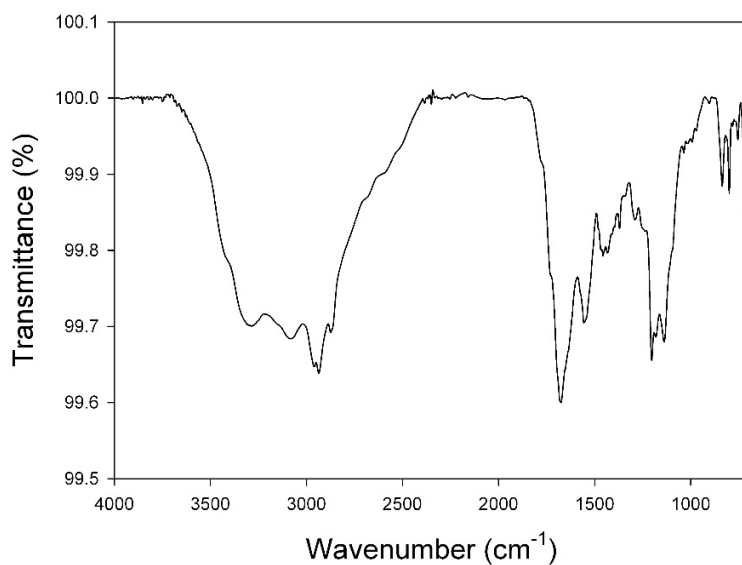


**Figure 5.25** IR spectrum of DBCO-PG-RGD.

## 5.6 References

- (1) Valden, M.; Lai, X.; Goodman, D. W. *Science* **1998**, *281*, 1647.
- (2) Chen, M. S.; Goodman, D. W. *Science* **2004**, *306*, 252.
- (3) Rayleigh, T. *Science* **2010**, *327*, 742.
- (4) Shaw, C. F. *Chem. Rev.* **1999**, *99*, 2589.
- (5) Dreaden, E. C.; Mackey, M. A.; Huang, X.; Kang, B.; El-sayed, M. A. *Chem. Soc. Rev.* **2011**, *40*, 3391.
- (6) Dreaden, E. C.; Alkilany. *Chem Soc Rev.* **2012**, *41*, 2740.
- (7) Hyafil, F.; Cornily, J.; Feig, J. E.; Gordon, R.; Vucic, E.; Amirbekian, V.; Fisher, E. A.; Fuster, V.; Feldman, L. J.; Fayad, Z. A. *Nat. Med.* **2007**, *13* (5), 636.
- (8) Lusic, H.; Grinsta, M. W. *Chem. Rev.* **2013**, *113*, 1641.

- (9) Haller, C.; Hizoh, I. *Invest. Radiol.* **2004**, *39* (3), 149.
- (10) Ai, K.; Liu, Y.; Liu, J.; Yuan, Q.; He, Y.; Lu, L. *Adv. Mater.* **2011**, *23* (42), 4886.
- (11) Fang, Y.; Peng, C.; Guo, R.; Zheng, L.; Qin, J.; Zhou, B.; Shen, M.; Lu, X.; Zhang, G.; Shi, X. *Analyst* **2013**, *138* (11), 3172.
- (12) Kinsella, J. M.; Jimenez, R. E.; Karmali, P. P.; Rush, A. M.; Kotamraju, V. R.; Gianneschi, N. C.; Ruoslahti, E.; Stupack, D.; Sailor, M. J. *Angew. Chem. Int. Ed.* **2011**, *50*, 12308.
- (13) Rabin, O.; Manuel Perez, J.; Grimm, J.; Wojtkiewicz, G.; Weissleder, R. *Nat. Mater.* **2006**, *5* (2), 118.
- (14) Liu, Z.; Ju, E.; Liu, J.; Du, Y.; Li, Z.; Yuan, Q.; Ren, J.; Qu, X. *Biomaterials* **2013**, *34* (30), 7444.
- (15) Liu, Z.; Dong, K.; Liu, J.; Han, X.; Ren, J.; Qu, X. *Small* **2014**, *10* (12), 2429.
- (16) Liu, Z.; Pu, F.; Liu, J.; Jiang, L.; Yuan, Q.; Li, Z.; Ren, J.; Qu, X. *Nanoscale* **2013**, *5* (10), 4252.
- (17) Liu, Y.; Ai, K.; Liu, J.; Yuan, Q.; He, Y.; Lu, L. *Angew. Chem. Int. Ed.* **2012**, *51*, 1437.
- (18) Oh, M. H.; Lee, N.; Kim, H.; Park, S. P.; Piao, Y.; Lee, J.; Jun, S. W.; Moon, W. K.; Choi, S. H.; Hyeon, T. *J. Am. Chem. Soc.* **2011**, *133*, 5508.
- (19) Jackson, P. A.; Rahman, W. N. W. A.; Wong, C. J.; Ackerly, T.; Geso, M. *Eur. J. Radiol.* **2010**, *75* (1), 104.

- (20) Hainfeld, J. F.; Slatkin, D. N.; Focella, T. M.; Smilowitz, H. M. *Br. J. Radiol.* **2006**, *79* (939), 248.
- (21) Peng, C.; Zheng, L.; Chen, Q.; Shen, M.; Guo, R.; Wang, H.; Cao, X.; Zhang, G.; Shi, X. *Biomaterials* **2012**, *33* (4), 1107.
- (22) Guo, R.; Wang, H.; Peng, C.; Shen, M.; Pan, M.; Cao, X.; Zhang, G.; Shi, X. *J. Phys. Chem. C* **2010**, *114* (1), 50.
- (23) Kim, D.; Park, S.; Jae, H. L.; Yong, Y. J.; Jon, S. *J. Am. Chem. Soc.* **2007**, *129* (24), 7661.
- (24) Page Faulk, W.; Malcolm Taylor, G. *Immunochemistry* **1971**, *8* (11), 1081.
- (25) Dykman, L.; Khlebtsov, N. *Chem. Soc. Rev.* **2012**, *41*, 2256.
- (26) Luo, Z.; Zheng, K.; Xie, J. *Chem. Commun.* **2014**, *50*, 5143.
- (27) Liu, H.; Xu, Y.; Wen, S.; Chen, Q.; Zheng, L.; Shen, M.; Zhao, J.; Zhang, G.; Shi, X. *Chem. - A Eur. J.* **2013**, *19* (20), 6409.
- (28) Aydogan, B.; Li, J.; Rajh, T.; Chaudhary, A.; Chmura, S. J.; Pelizzari, C.; Wietholt, C.; Kurtoglu, M.; Redmond, P. *Mol. Imaging Biol.* **2010**, *12* (5), 463.
- (29) Libutti, S. K.; Paciotti, G. F.; Byrnes, A. A.; Alexander Jr., H. R.; Gannon, W. E.; Walker, M.; Seidel, G. D.; Yuldasheva, N.; Tamarkin, L. *Clin Cancer Res.* **2010**, *16* (24), 6139.
- (30) Shirazi, A. N.; Mandal, D.; Tiwari, R. K.; Guo, L.; Lu, W.; Parang, K. *Mol. Pharm.* **2013**, *10* (2), 500.

- (31) Porta, F.; Speranza, G.; Krpetic, Z.; Dal Santo, V.; Francescato, P.; Scari, G. *Mater. Sci. Eng. B* **2007**, *140*, 187.
- (32) Kumar, A.; Ma, H.; Zhang, X.; Huang, K.; Jin, S.; Liu, J.; Wei, T.; Cao, W.; Zou, G.; Liang, X.-J. *Biomaterials* **2012**, *33* (4), 1180.
- (33) Bartczak, D.; Kanaras, A. G. *Langmuir* **2011**, *27* (16), 10119.
- (34) Zhang, M.-X.; Huang, B.-H.; Sun, X.-Y.; Pang, D.-W. *Langmuir* **2010**, *26* (12), 10171.
- (35) Wang, C.-F.; Mäkilä, E. M.; Kaasalainen, M. H.; Liu, D.; Sarparanta, M. P.; Airaksinen, A. J.; Salonen, J. J.; Hirvonen, J. T.; Santos, H. a. *Biomaterials* **2014**, *35* (4), 1257.
- (36) Agard, N. J.; Prescher, J. A.; Bertozzi, C. R. *J. Am. Chem. Soc.* **2004**, *126*, 15046.
- (37) Chigrinova, M.; McKay, C. S.; Beaulieu, L.-P. B.; Udachin, K. A.; Beauchemin, A. M.; Pezacki, J. P. *Org. Biomol. Chem.* **2013**, *11* (21), 3436.
- (38) Chang, P. V.; Prescher, J. A.; Sletten, E. M.; Baskin, J. M.; Miller, I. A.; Agard, N. J.; Lo, A.; Bertozzi, C. R. *Proc. Natl. Acad. Sci. U. S. A.* **2010**, *107* (5), 1821.
- (39) Beatty, K. E.; Fisk, J. D.; Smart, B. P.; Lu, Y. Y.; Szychowski, J.; Hangauer, M. J.; Baskin, J. M.; Bertozzi, C. R.; Tirrell, D. A. *ChemBioChem* **2010**, *11*, 2092.
- (40) van Geel, R.; Pruijn, G. J. M.; van Delft, F. L.; Boelens, W. C. *Bioconjug. Chem.* **2012**, *23* (3), 392.
- (41) Gobbo, P.; Novoa, S.; Biesinger, M. C.; Workentin, M. S. *Chem. Commun.* **2013**, *49*, 3982.

- (42) Pierschbacher, M. D.; Ruoslahti, E. *Proc. Natl. Acad. Sci. U. S. A.* **1984**, *81* (19), 5985.
- (43) Pierschbacher, M. D.; Ruoslahti, E. *Nature* **1984**, *309* (5963), 30.
- (44) Sun, L.; Crooks, R. M.; Chechik, V. *Chem. Commun.* **2001**, 359.
- (45) Kumar, A.; Huo, S.; Zhang, X.; Liu, J.; Tan, A.; Li, S.; Jin, S.; Xue, X.; Zhao, Y.; Ji, T.; Han, L.; Liu, H.; Zhang, X.; Zhang, J.; Zou, G.; Wang, T.; Tang, S.; Liang, X. *ACS Nano*. **2014**, *8* (5), 4205.
- (46) Wei, T.; Liu, J.; Ma, H.; Cheng, Q.; Huang, Y.; Zhao, J.; Huo, S.; Xue, X.; Liang, Z.; Liang, X.-J. *Nano Lett.* **2013**, *13* (6), 2528.

## CHAPTER VI: ONCLUSION AND OUTLOOK

With superior hybridization features, resistance to nucleases and proteases, chemical robustness and excellent sequence discrimination, PNA has become one of the most attractive artificial nucleic acids. PNA has demonstrated its utility as hybridization probes for molecular diagnostics, potential for antisense/antigene therapy as well as targeted imaging. However, the difficulties in preparing modified PNA probes remain in PNA chemistry, because it is usually expensive, time-consuming and labor-intensive to functionalize PNA. In order to prepare desired PNAs more efficiently and cost-effective, methodologies for the functionalization of PNA via post-synthetic click chemistry has been explored and discussed in this thesis. The developed approaches are convenient, simple and versatile, and provided a route to diverse PNA probes that have been evaluated.

Chapter II introduced the synthesis of quencher-free PNA molecular beacons by a simultaneous attachment of fluorophores via on-resin CuAAC for the first time. This easy, flexible method showed variability in development of single- or multiple-labeled PNAs. The pyrene-based stem-loop PNA beacon has shown its promise in the detection of cystic fibrosis genes and obviously could be extended to many target sequences or fluorophores.

Chapter III presented the development of conventional PNA molecular beacons via a "click-couple-click" strategy. A quencher and a fluorophore can be attached to a PNA oligomer sequentially without the need of complicated protection and deprotection of reactive sites of PNA. Microwave-assisted on-resin CuAAC has been applied for the first time to PNA, to the best of my knowledge, and the procedure of "click-couple-click" approach is fast, robust, efficient and operationally simple. Given that PNA probes are still

difficult and very expensive to be obtained, the presented method in this chapter will be of great help in rapidly and easily synthesizing various PNAs. A series of PNA beacons have been successfully synthesized and characterized. This methodology complements the one presented in Chapter II for the synthesis of homo-dimer MBs. Thus, this method gives more synthetic variability in the choice of fluorophore-quencher or donor-acceptor pairs for customized MB construction.

Expanding on the aforementioned click chemistry, Chapter IV showed the preparation of a Gd(III)-containing PNA hybridization probe as a potential MRI contrast agent. Four units of alkynyl Gd(III)-DOTA were clicked to a PNA simultaneously and the resulting oligomer has been demonstrated useful in binding with the poly(rA) tail. This method significantly simplifies the procedure for the conjugation of a PNA probe with Gd chelators which generally requires coupling of chelators like DOTA, protection and/or deprotection of nucleobases as well as Gd chelation. By binding to poly(rA) to form a triplex, the probe, (Gd(III)-DOTA)<sub>4</sub>-PNA, would concentrate and deliver a high load of Gd ions in a microenvironment.

As AuNPs are promising CT contrast agents, bioconjugation of PNAs to AuNPs for targeted CT imaging would also be of great interest. The use of a peptide would be a good start for investigation of the conjugation methods. In chapter V, peptide-decorated AuNPs via strain-promoted azide-alkyne cycloaddition and post assembly deprotection (SPAAC-PAD) is presented. SPAAC was applied for the bioconjugation of AuNPs because of the benefits of copper-free click chemistry. Due to the possible decomposition of cyclooctyne under regular conditions for peptide cleavage, post assembly deprotection has been proposed and proven to be helpful for the conjugation. This method has been demonstrated

useful and convenient for functionalization of small, water-soluble gold nanoparticles with oligopeptides. Future studies on decoration of AuNPs with PNAs by using SPAAC-PAD should be performed.

To expand the application of PNA and thoroughly investigate the properties of PNA probes, synthetic protocols which are more cost-effective, robust, convenient and versatile for are needed. Therefore, with the chemistry and procedure developed during this thesis, rapid preparation of various PNA probes is made possible, which may reduce the difficulties in functionalization of PNAs as performed in research laboratories and commercial companies.



# Appendices

## Appendix I Copyright Clearance

2/1/2017

Rightslink® by Copyright Clearance Center



# RightsLink®

Home

Account Info

Help



**Title:** Olefinic Peptide Nucleic Acids (OPAs): New Aspects of the Molecular Recognition of DNA by PNA

**Author:** Rolf Schütz, Michel Cantin, Christopher Roberts, Beate Greiner, Eugen Uhlmann, Christian Leumann

**Publication:** Angewandte Chemie International Edition

**Publisher:** John Wiley and Sons

**Date:** Apr 3, 2000

© 2000 WILEY-VCH Verlag GmbH, Weinheim, Fed. Rep. of Germany

Logged in as:  
Xiaoxiao Wang  
Account #:  
3001103938

LOGOUT

### Order Completed

Thank you for your order.

This Agreement between Xiaoxiao Wang ("You") and John Wiley and Sons ("John Wiley and Sons") consists of your license details and the terms and conditions provided by John Wiley and Sons and Copyright Clearance Center.

Your confirmation email will contain your order number for future reference.

## JOHN WILEY AND SONS LICENSE TERMS AND CONDITIONS

Jan 23, 2017

This Agreement between Xiaoxiao Wang ("You") and John Wiley and Sons ("John Wiley and Sons") consists of your license details and the terms and conditions provided by John Wiley and Sons and Copyright Clearance Center.

License Number	4034891008705
License date	Jan 23, 2017
Licensed Content Publisher	John Wiley and Sons
Licensed Content Publication	European Journal of Organic Chemistry
Licensed Content Title	A Template-Mediated Click–Click Reaction: PNA–DNA, PNA–PNA (or Peptide) Ligation, and Single Nucleotide Discrimination
Licensed Content Author	Xiaohua Peng,Hong Li,Michael Seidman
Licensed Content Date	Jun 17, 2010
Licensed Content Pages	4
Type of Use	Dissertation/Thesis
Requestor type	University/Academic
Format	Electronic
Portion	Figure/table
Number of figures/tables	1
Original Wiley figure/table number(s)	Figure 1
Will you be translating?	No
Title of your thesis / dissertation	Functionalization of peptide nucleic acids via post-synthetic click chemistry
Expected completion date	Apr 2017
Expected size (number of pages)	170



RightsLink®

[Home](#)[Account Info](#)[Help](#)ACS Publications  
Most Trusted. Most Cited. Most Read.**Title:**Reductive Alkylation and  
Sequential Reductive Alkylation-  
Click Chemistry for On-Solid-  
Support Modification of  
Pyrrolidiny Peptide Nucleic AcidLogged in as:  
Xiaoxiao Wang  
Account #:  
3001103938[LOGOUT](#)**Author:**Boonsong Ditmangklo,  
Chalothorn Boonlua, Chaturong  
Suparpprom, et al**Publication:** Bioconjugate Chemistry**Publisher:** American Chemical Society**Date:** Apr 1, 2013

Copyright © 2013, American Chemical Society

**PERMISSION/LICENSE IS GRANTED FOR YOUR ORDER AT NO CHARGE**

This type of permission/license, instead of the standard Terms & Conditions, is sent to you because no fee is being charged for your order. Please note the following:

- Permission is granted for your request in both print and electronic formats, and translations.
- If figures and/or tables were requested, they may be adapted or used in part.
- Please print this page for your records and send a copy of it to your publisher/graduate school.
- Appropriate credit for the requested material should be given as follows: "Reprinted (adapted) with permission from (COMPLETE REFERENCE CITATION). Copyright (YEAR) American Chemical Society." Insert appropriate information in place of the capitalized words.
- One-time permission is granted only for the use specified in your request. No additional uses are granted (such as derivative works or other editions). For any other uses, please submit a new request.

If credit is given to another source for the material you requested, permission must be obtained from that source.

[BACK](#)[CLOSE WINDOW](#)

Copyright © 2017 [Copyright Clearance Center, Inc.](#) All Rights Reserved. [Privacy statement.](#) [Terms and Conditions.](#)  
Comments? We would like to hear from you. E-mail us at [customercare@copyright.com](mailto:customercare@copyright.com)



RightsLink®

[Home](#)[Account Info](#)[Help](#)

**Title:** Clickable Cy-Azido(methylene/butylene) Peptide Nucleic Acids and Their Clicked Fluorescent Derivatives: Synthesis, DNA Hybridization Properties, and Cell Penetration Studies

**Author:** Deepak R. Jain, Krishna N. Ganesh

**Publication:** The Journal of Organic Chemistry

**Publisher:** American Chemical Society

**Date:** Jul 1, 2014

Copyright © 2014, American Chemical Society

Logged in as:

Xiaoxiao Wang

Account #:

3001103938

[LOGOUT](#)

#### PERMISSION/LICENSE IS GRANTED FOR YOUR ORDER AT NO CHARGE

This type of permission/license, instead of the standard Terms & Conditions, is sent to you because no fee is being charged for your order. Please note the following:

- Permission is granted for your request in both print and electronic formats, and translations.
- If figures and/or tables were requested, they may be adapted or used in part.
- Please print this page for your records and send a copy of it to your publisher/graduate school.
- Appropriate credit for the requested material should be given as follows: "Reprinted (adapted) with permission from (COMPLETE REFERENCE CITATION). Copyright (YEAR) American Chemical Society." Insert appropriate information in place of the capitalized words.
- One-time permission is granted only for the use specified in your request. No additional uses are granted (such as derivative works or other editions). For any other uses, please submit a new request.

If credit is given to another source for the material you requested, permission must be obtained from that source.

[BACK](#)[CLOSE WINDOW](#)

Copyright © 2017 [Copyright Clearance Center, Inc.](#) All Rights Reserved. [Privacy statement](#). [Terms and Conditions](#).  
Comments? We would like to hear from you. E-mail us at [customer-care@copyright.com](mailto:customer-care@copyright.com)



RightsLink®

[Home](#)[Account Info](#)[Help](#)

**Title:** New cyanine dyes as base surrogates in PNA: Forced intercalation probes (FIT-probes) for homogeneous SNP detection

**Author:** Lucas Bethge, Dilip Venkatrao Jarikote, Oliver Seitz

**Publication:** Bioorganic & Medicinal Chemistry

**Publisher:** Elsevier

**Date:** 1 January 2008

Copyright © 2007 Elsevier Ltd. All rights reserved.

Logged in as:  
Xiaoxiao Wang  
Account #:  
3001103938

[LOGOUT](#)**Order Completed**

Thank you for your order.

This Agreement between Xiaoxiao Wang ("You") and Elsevier ("Elsevier") consists of your license details and the terms and conditions provided by Elsevier and Copyright Clearance Center.

Your confirmation email will contain your order number for future reference.



RightsLink®

[Home](#)[Account Info](#)[Help](#)

**Title:** Peptide nucleic acid fluorescence in situ hybridization for identification of Listeria genus, Listeria monocytogenes and Listeria ivanovii

**Author:** Xiaofeng Zhang, Shan Wu, Ke Li, Jiangbing Shuai, Qiang Dong, Weihuan Fang

**Publication:** International Journal of Food Microbiology

**Publisher:** Elsevier

**Date:** 2 July 2012

Copyright © 2012 Elsevier B.V. All rights reserved.

Logged in as:  
Xiaoxiao Wang  
Account #:  
3001103938

[LOGOUT](#)**Order Completed**

Thank you for your order.

This Agreement between Xiaoxiao Wang ("You") and Elsevier ("Elsevier") consists of your license details and the terms and conditions provided by Elsevier and Copyright Clearance Center.

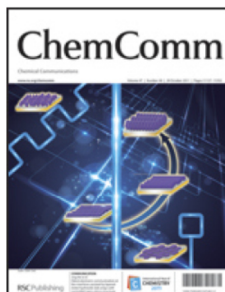
Your confirmation email will contain your order number for future reference.

1/24/2017

Rightslink® by Copyright Clearance Center



# RightsLink®

[Home](#)[Account Info](#)[Help](#)

**Title:** BNAs: novel nucleic acid analogs with a bridged sugar moiety

**Author:** Takeshi Imanishi, Satoshi Obika

**Publication:** Chemical Communications (Cambridge)

**Publisher:** Royal Society of Chemistry

**Date:** Apr 24, 2002

Copyright © 2002, Royal Society of Chemistry

Logged in as:  
Xiaoxiao Wang  
Account #:  
3001103938

[LOGOUT](#)

### Order Completed

Thank you for your order.

This Agreement between Xiaoxiao Wang ("You") and Royal Society of Chemistry ("Royal Society of Chemistry") consists of your license details and the terms and conditions provided by Royal Society of Chemistry and Copyright Clearance Center.

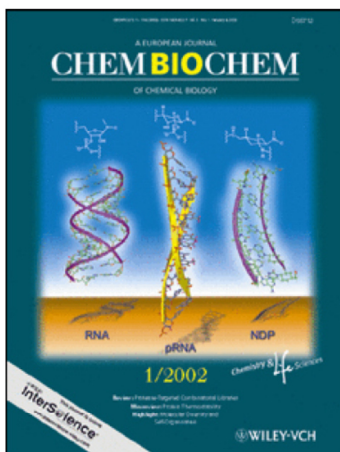
Your confirmation email will contain your order number for future reference.

1/26/2017

Rightslink® by Copyright Clearance Center



# RightsLink®

[Home](#)[Account Info](#)[Help](#)

**Title:** PNA Molecular Beacons Assembled by Post-Synthetic Click Chemistry Functionalization

**Author:** Xiaoxiao Wang, Robert H. E. Hudson

**Publication:** ChemBioChem

**Publisher:** John Wiley and Sons

**Date:** Sep 3, 2015

© 2015 WILEY-VCH Verlag GmbH & Co. KGaA, Weinheim

Logged in as:  
Xiaoxiao Wang  
Account #:  
3001103938

[LOGOUT](#)

### Order Completed

Thank you for your order.

This Agreement between Xiaoxiao Wang ("You") and John Wiley and Sons ("John Wiley and Sons") consists of your license details and the terms and conditions provided by John Wiley and Sons and Copyright Clearance Center.

Your confirmation email will contain your order number for future reference.



# RightsLink®

[Home](#)
[Account Info](#)
[Help](#)


**Title:** Using tRNA-linked molecular beacons to image cytoplasmic mRNAs in live cells

**Author:** Musa M Mhlanga, Sanjay Tyagi

**Publication:** Nature Protocols

**Publisher:** Nature Publishing Group

**Date:** Nov 2, 2006

Logged in as:  
Xiaoxiao Wang  
Account #:  
3001103938

[LOGOUT](#)

Copyright © 2006, Rights Managed by Nature Publishing Group

## Review Order

Please review the order details and the associated [terms and conditions](#).

No royalties will be charged for this reuse request although you are required to obtain a license and comply with the license terms and conditions. To obtain the license, click the Accept button below.

Licensed Content Publisher	Nature Publishing Group
Licensed Content Publication	Nature Protocols
Licensed Content Title	Using tRNA-linked molecular beacons to image cytoplasmic mRNAs in live cells
Licensed Content Author	Musa M Mhlanga, Sanjay Tyagi
Licensed Content Date	Nov 2, 2006
Licensed Content Volume	1
Licensed Content Issue	3
Type of Use	reuse in a dissertation / thesis
Requestor type	academic/educational
Format	electronic
Portion	figures/tables/illustrations
Number of figures/tables/illustrations	1
High-res required	no
Figures	Figure 1
Author of this NPG article	no
Your reference number	
Title of your thesis / dissertation	Functionalization of peptide nucleic acids via post-synthetic click chemistry
Expected completion date	Apr 2017
Estimated size (number of pages)	170

**RightsLink®**[Home](#)[Account Info](#)[Help](#)**ACS Publications**  
Most Trusted. Most Cited. Most Read.**Title:** Unambiguous Detection of Target DNAs by Excimer–Monomer Switching Molecular Beacons**Author:** Kazuhisa Fujimoto, Hisao Shimizu, Masahiko Inouye**Publication:** The Journal of Organic Chemistry**Publisher:** American Chemical Society**Date:** May 1, 2004

Copyright © 2004, American Chemical Society

Logged in as:  
Xiaoxiao Wang  
Account #:  
3001103938[LOGOUT](#)**PERMISSION/LICENSE IS GRANTED FOR YOUR ORDER AT NO CHARGE**

This type of permission/license, instead of the standard Terms & Conditions, is sent to you because no fee is being charged for your order. Please note the following:

- Permission is granted for your request in both print and electronic formats, and translations.
- If figures and/or tables were requested, they may be adapted or used in part.
- Please print this page for your records and send a copy of it to your publisher/graduate school.
- Appropriate credit for the requested material should be given as follows: "Reprinted (adapted) with permission from (COMPLETE REFERENCE CITATION). Copyright (YEAR) American Chemical Society." Insert appropriate information in place of the capitalized words.
- One-time permission is granted only for the use specified in your request. No additional uses are granted (such as derivative works or other editions). For any other uses, please submit a new request.

If credit is given to another source for the material you requested, permission must be obtained from that source.

[BACK](#)[CLOSE WINDOW](#)



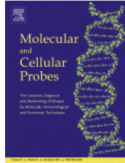


RightsLink®

Home

Account  
Info

Help



**Title:** PNA molecular beacons for rapid detection of PCR amplicons  
**Author:** E Ortiz,G Estrada,P,M Lizardi  
**Publication:** Molecular and Cellular Probes  
**Publisher:** Elsevier  
**Date:** August 1998  
 Copyright © 1998 Academic Press. All rights reserved.

Logged in as:  
Xiaoxiao Wang  
Account #:  
3001103938

LOGGOUT

### Order Completed

Thank you for your order.

This Agreement between Xiaoxiao Wang ("You") and Elsevier ("Elsevier") consists of your license details and the terms and conditions provided by Elsevier and Copyright Clearance Center.

Your confirmation email will contain your order number for future reference.

[Printable details.](#)

License Number	4043101308065
License date	Feb 06, 2017
Licensed Content Publisher	Elsevier
Licensed Content Publication	Molecular and Cellular Probes
Licensed Content Title	PNA molecular beacons for rapid detection of PCR amplicons
Licensed Content Author	E Ortiz,G Estrada,P,M Lizardi
Licensed Content Date	August 1998
Licensed Content Volume	12
Licensed Content Issue	4
Licensed Content Pages	8
Type of Use	reuse in a thesis/dissertation
Portion	figures/tables/illustrations
Number of figures/tables/illustrations	2
Format	electronic
Are you the author of this Elsevier article?	No
Will you be translating?	No
Order reference number	
Original figure numbers	Fig. 2, Fig. 3
Title of your thesis/dissertation	Functionalization of peptide nucleic acids via post-synthetic click chemistry
Expected completion date	Apr 2017
Estimated size (number of pages)	170



# RightsLink®

[Home](#)
[Account Info](#)
[Help](#)


**Title:** Low-Noise Stemless PNA Beacons for Sensitive DNA and RNA Detection

**Author:** Elke Socher, Lucas Bethge, Andrea Knoll, Nadine Jungnick, Andreas Herrmann, Oliver Seitz

**Publication:** Angewandte Chemie International Edition

**Publisher:** John Wiley and Sons

**Date:** Oct 23, 2008

Copyright © 2008 WILEY-VCH Verlag GmbH & Co. KGaA, Weinheim

Logged in as:  
Xiaoxiao Wang  
Account #:  
3001103938

[LOGOUT](#)

### Order Completed

Thank you for your order.

This Agreement between Xiaoxiao Wang ("You") and John Wiley and Sons ("John Wiley and Sons") consists of your license details and the terms and conditions provided by John Wiley and Sons and Copyright Clearance Center.

Your confirmation email will contain your order number for future reference.



# RightsLink®

[Home](#)
[Account Info](#)
[Help](#)


**Title:** Solid-Phase Synthesis of Doubly Labeled Peptide Nucleic Acids as Probes for the Real-Time Detection of Hybridization

**Author:** Oliver Seitz

**Publication:** Angewandte Chemie International Edition

**Publisher:** John Wiley and Sons

**Date:** Sep 13, 2000

© 2000 WILEY-VCH Verlag GmbH, Weinheim, Fed. Rep. of Germany

Logged in as:  
Xiaoxiao Wang  
Account #:  
3001103938

[LOGOUT](#)

### Order Completed

Thank you for your order.

This Agreement between Xiaoxiao Wang ("You") and John Wiley and Sons ("John Wiley and Sons") consists of your license details and the terms and conditions provided by John Wiley and Sons and Copyright Clearance Center.

Your confirmation email will contain your order number for future reference.

2/6/2017

Rightslink® by Copyright Clearance Center

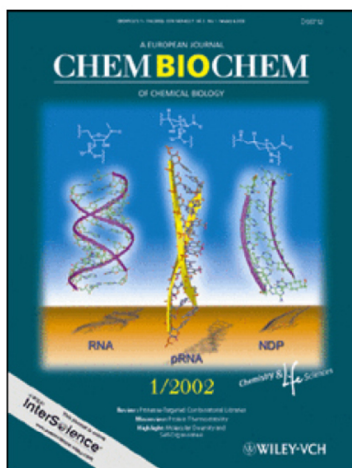


RightsLink®

Home

Account Info

Help



**Title:** Forced Intercalation Probes (FIT Probes): Thiazole Orange as a Fluorescent Base in Peptide Nucleic Acids for Homogeneous Single-Nucleotide-Polymorphism Detection

**Author:** Olaf Köhler, Dilip Venkatrao Jarikote, Oliver Seitz

**Publication:** ChemBioChem

**Publisher:** John Wiley and Sons

**Date:** Dec 7, 2004

Copyright © 2005 WILEY-VCH Verlag GmbH & Co. KGaA, Weinheim

Logged in as:  
Xiaoxiao Wang  
Account #:  
3001103938

LOGOUT

### Order Completed

Thank you for your order.

This Agreement between Xiaoxiao Wang ("You") and John Wiley and Sons ("John Wiley and Sons") consists of your license details and the terms and conditions provided by John Wiley and Sons and Copyright Clearance Center.

Your confirmation email will contain your order number for future reference.

2/1/2017

Rightslink® by Copyright Clearance Center



RightsLink®

Home

Account Info

Help



WILEY

**Title:** Gadolinium-based contrast agents for magnetic resonance cancer imaging

**Author:** Zhuxian Zhou, Zheng-Rong Lu

**Publication:** Wiley Interdisciplinary Reviews - Nanomedicine and Nanobiotechnology

**Publisher:** John Wiley and Sons

**Date:** Oct 9, 2012

Copyright © 2012 Wiley Periodicals, Inc.

Logged in as:  
Xiaoxiao Wang  
Account #:  
3001103938

LOGOUT

### Order Completed

Thank you for your order.

This Agreement between Xiaoxiao Wang ("You") and John Wiley and Sons ("John Wiley and Sons") consists of your license details and the terms and conditions provided by John Wiley and Sons and Copyright Clearance Center.

Your confirmation email will contain your order number for future reference.



[Home](#)

[Account Info](#)

[Help](#)



**Title:** Gadolinium-based contrast agents for magnetic resonance cancer imaging

**Author:** Zhuxian Zhou,Zheng-Rong Lu

**Publication:** Wiley Interdisciplinary Reviews - Nanomedicine and Nanobiotechnology

**Publisher:** John Wiley and Sons

**Date:** Oct 9, 2012

Copyright © 2012 Wiley Periodicals, Inc.

Logged in as:  
Xiaoxiao Wang  
Account #:  
3001103938

[LOGOUT](#)

### Order Completed

Thank you for your order.

This Agreement between Xiaoxiao Wang ("You") and John Wiley and Sons ("John Wiley and Sons") consists of your license details and the terms and conditions provided by John Wiley and Sons and Copyright Clearance Center.

Your confirmation email will contain your order number for future reference.

## Peptide-decorated gold nanoparticles *via* strain-promoted azide–alkyne cycloaddition and post assembly deprotection

X. Wang, P. Gobbo, M. Suchy, M. S. Workentin and R. H. E. Hudson, *RSC Adv.*, 2014, 4, 43087  
DOI: 10.1039/C4RA07574A

If you are not the author of this article and you wish to reproduce material from it in a third party non-RSC publication you must [formally request permission](#) using RightsLink. Go to our [Instructions for using RightsLink page](#) for details.

Authors contributing to RSC publications (journal articles, books or book chapters) do not need to formally request permission to reproduce material contained in this article provided that the correct acknowledgement is given with the reproduced material.

Reproduced material should be attributed as follows:

- For reproduction of material from NJC:  
Reproduced from Ref. XX with permission from the Centre National de la Recherche Scientifique (CNRS) and The Royal Society of Chemistry.
- For reproduction of material from PCCP:  
Reproduced from Ref. XX with permission from the PCCP Owner Societies.
- For reproduction of material from PPS:  
Reproduced from Ref. XX with permission from the European Society for Photobiology, the European Photochemistry Association, and The Royal Society of Chemistry.
- For reproduction of material from all other RSC journals and books:  
Reproduced from Ref. XX with permission from The Royal Society of Chemistry.

If the material has been adapted instead of reproduced from the original RSC publication "Reproduced from" can be substituted with "Adapted from".

In all cases the Ref. XX is the XXth reference in the list of references.

If you are the author of this article you do not need to formally request permission to reproduce figures, diagrams etc. contained in this article in third party publications or in a thesis or dissertation provided that the correct acknowledgement is given with the reproduced material.

Reproduced material should be attributed as follows:

- For reproduction of material from NJC:  
[Original citation] - Reproduced by permission of The Royal Society of Chemistry (RSC) on behalf of the Centre National de la Recherche Scientifique (CNRS) and the RSC
- For reproduction of material from PCCP:  
[Original citation] - Reproduced by permission of the PCCP Owner Societies
- For reproduction of material from PPS:  
[Original citation] - Reproduced by permission of The Royal Society of Chemistry (RSC) on behalf of the European Society for Photobiology, the European Photochemistry Association, and RSC
- For reproduction of material from all other RSC journals:  
[Original citation] - Reproduced by permission of The Royal Society of Chemistry

If you are the author of this article you still need to obtain permission to reproduce the whole article in a third party publication with the exception of reproduction of the whole article in a thesis or dissertation.

## Curriculum Vitae

<b>Name</b>	Xiaoxiao Wang
<b>Post-secondary Education and Degrees:</b>	Nankai University Tianjin, China 2005-2009 BSc. in Materials Chemistry
	Sun Yat-sen University Guangzhou, Guangdong, China 2009-2011 Graduate studies in Medicinal Chemistry
	The University of Western Ontario London, Ontario, Canada 2011-2017 Ph.D. candidate in Organic Chemistry Western Graduate Research Scholarship 2011-2017
<b>Honours and Awards:</b>	
<b>Related Work Experience</b>	Teaching Assistant The University of Western Ontario 2011-2016
	Research Assistant The University of Western Ontario 2011-2017

### Publications:

- [1] **Xiaoxiao Wang**, Robert H. E. Hudson, “*PNA Molecular Beacons Assembled by Post-Synthetic Click Chemistry Functionalization.*”, **ChemBioChem**, 2015, 16, 2156.
- [2] Pierangelo Gobbo, Wilson Luo, Sung Ju Cho, **Xiaoxiao Wang**, etc. “*Small gold nanoparticles for interfacial Staudinger-Bertozzi ligation.*”, **Org. Biomol. Chem.**, 2015, 13, 4605.
- [3] **Xiaoxiao Wang**, Pierangelo Gobbo, Mojmir Suchy, etc., “*Peptide-decorated gold nanoparticles via strain promoted azide-alkyne cycloaddition and post assembly deprotection.*”, **RSC Advances**, 2014, 4, 43087.
- [4] **Xiao-Xiao Wang**, Chen-Xi Zhou, Jin-Wu Yan, etc., “*Synthesis and evaluation of quinazolone derivatives as a new class of c-KIT G-quadruplex binding ligands.*”, **ACS Med. Chem. Lett.**, 2013, 4(10), 909.

[5] Wei-Jia Chen, Chen-Xi Zhou, Pei-Fen Yao, **Xiao-Xiao Wang**, etc., “Disubstituted 1,8-dipyrazolcarbazole derivatives as a new type of c-myc G-quadruplex binding ligands.”; **Bioorg. Med. Chem.**, 2012, 20(9), 2829.

[6] Zhi-Shu Huang, Lian-Quan Gu, Jia-Heng Tan, **Xiao-Xiao Wang**; “Synthetic Methodology of Quinazolone Derivatives and Their Application in Cancer Research.”, **Patent of State Intellectual Property Office of P. R. China**, Publication No. CN102382064B.

[7] Jin-Qiang Hou, Jia-Heng Tan, **Xiao-Xiao Wang**, etc., “Impact of planarity of unfused aromatic molecules on G-quadruplex binding: learning from isaindigotone derivatives.”; **Org. Biomol. Chem.** 2011, 9(18), 6422.

[8] Zhijie Wu, Yuzhen Mao, **Xiaoxiao Wang**, Minghui Zhang, “Preparation of a Cu-Ru/carbon nanotube catalyst for hydrogenolysis of glycerol to 1,2-propanediol via hydrogen spillover.”, **Green Chemistry**, 2011, 13(5), 1311.

#### **Academic Conferences:**

[1] Poster Presentation, **Xiaoxiao Wang**, Robert H. E. Hudson, “Versatile synthesis of PNA molecular beacons via on-resin click chemistry”, 2nd Fluorescent Biomolecules and their Building Blocks: Design and Applications (FB3), San Diego, USA, August 2014.

[2] Oral Presentation, **Xiaoxiao Wang**, Pierangelo Gobbo, Mark S. Workentin and Robert H. E. Hudson, “Bioconjugation of a Receptor-Avid Peptide to Gold Nanoparticles for Cancer Imaging”, CAMBR Distinguished Lecture and Research Day, London, Canada, November 2013.

[3] Oral Presentation, **Xiaoxiao Wang**, Pierangelo Gobbo, Mark S. Workentin and Robert H. E. Hudson, “Oligopeptide Decorated Gold Nanoparticles via Post Assembly Deprotection”, Western Research Forum, London, Canada, March 2013.

[4] Poster Presentation, **Xiaoxiao Wang**, Robert. H. E. Hudson, “Facile Derivatization of PNA Oligomers by on-resin click chemistry”, XX International Round Table Conference on Nucleosides, Nucleotides and Nucleic Acids, Montréal, Canada, August, 2012.